UNIVERSITY OF SOUTHAMPTON

FACULTY OF NATURAL & ENVIRONMENTAL SCIENCES

School of Biological Sciences

INVESTIGATIONS INTO THE IMMUNE MODULATORY ROLE OF HSPB5

by

Nyasha Jermaine Matinyarare

Thesis for the degree of Doctor of Philosophy

September 2014

UNIVERSITY OF SOUTHAMPTON

ABSTRACT

FACULTY OF NATURAL & ENVIRONMENTAL SCIENCES

School of Biological Sciences

Thesis for the degree of Doctor of Philosophy

INVESTIGATIONS INTO THE IMMUNE MODULATORY ROLE OF HSPB5

Nyasha Jermaine Matinyarare

Small heat-shock proteins are conserved molecular entities present in all mammalian cells. They have historically been studied in the context of being intracellular molecular chaperones that are constitutively expressed, with a capacity to be induced by cellular stress, in order to promote and remediate protein folding. More recently however, growing evidence suggests that the action of small heat-shock proteins is not limited to protein folding but also extends to a wider range of important cellular roles.

Of the 11 small heat-shock proteins that are expressed in mammalian cells, only 4, HSPB1, HSPB5, HSPB6 and HSPB8, are expressed in the central nervous system (CNS). The role of these small heat-shock proteins in the CNS is thought to be protective as they show widespread upregulation during several neurological conditions. Confoundingly however, studies from R6/2 animal models of Huntington's disease show a selective reduced expression of HSPB5 in these animals, raising pertinent questions as to whether this reduction is cause or effect of the condition.

Here, we have investigated whether reduced expression of HSPB5 has a detrimental effect, focussing specifically on HSPB5's proposed immune modulatory role. Using mice inoculated with *S. typhimurium*, we found that, in our hands, mice lacking HSPB5 did not appear to be phenotypically different from wild type animals and equally, the reduced expression of HSPB5 did not exacerbate systemic inflammation or potentiate disease progression. Furthermore, to investigate HSPB5's role in the CNS, we inoculated animals with ME7 Prion and also found that deficiency in HSPB5 did not alter phenotype or behaviour and did not negatively influence disease progression. Lastly, we investigated whether the reduced expression of HSPB5 as observed in R6/2 animals was reciprocated in humans. Our findings show that in humans disease, there is no reduction of HSPB5. Our findings suggests that in C57BL/6 animals, HSPB5 does not appear to have an immune modulatory role; they also highlight how data obtained from animal models should be taken tentatively.

TABLE OF CONTENTS

LIST OF FIGURES

LIST OF TABLES

ACKNOWLEDGEMENTS

Firstly I would like to thank my supervisors Dr Andreas Wyttenbach, Professor Hugh Perry and Professor Vincent O'Connor for giving me the opportunity to pursue this project. A very special thanks to Professor Vincent O'Connor who, following Dr Wyttenbach's departure, adopted me under his guidance and counsel and provided a proactive mentoring role that I have little doubt has irrevocably shaped my thoughts and attitudes, scientifically and personally, for the rest of my life. Like the deep reverence John H Watson (Dr Watson) has for Sherlock Holmes, I will forever be thankful and indebted to Professor O'Connor's critical eye to detail and special skills of scientific deduction, reasoning and inference, some of which I have assimilated. For this, I thank you.

I would also like to thank Dr Jessica Teeling, Dr Delphine Boche, Dr Ursula Puntener, Dr Diego Nicola-Gomez, Dr Patrick Garland, Dr Ayodeji Asuni and Dr Dieter Riethmacher in no little part for the countless help they have offered me even with their ever limited time schedules. Special thank you to Dr Joanne Bailey, Dr Shmma Quraishe and (soon to be Dr) Matthew Davies for their friendship and extraordinary professional capacity; you have been instrumental in the development and culmination of this project. I would also like to thank all the people that worked "behind the scene" and allowed this project to go forward, namely, Ms Lorraine Prout, Ms Caroline Smith, Mr Andrew Crocker, Ms Leslie Lawes, Mr Mike Broome, Mr Bob Churcher and Mr Mark Gowland-Pryde.

Naturally, I also would not have been able to complete this project without the support and encouragement from my family and friends. Mum and Dad, thank you for your prayers and thank you for believing in me. I am grateful for the sacrifices you made in order to provide this opportunity for me. Benson, thanks for the countless discussions we had; I found tremendous inspiration from them. Victor, thanks for being the first in our family to go to university and setting the benchmark very high.

Lastly, I would like to thank my friends for supporting me through the good times and the bad. It is possible for me to list everyone on of you but you know who you are. Thank you.

DECLARATION OF AUTHORSHIP

I, Nyasha J Matinyarare declare that this thesis and the work presented in it are my own and has been generated by me as the result of my own original research.

I confirm that:

1. This work was done wholly or mainly while in candidature for a research degree at this University;

2. Where any part of this thesis has previously been submitted for a degree or any other qualification at this University or any other institution, this has been clearly stated;

3. Where I have consulted the published work of others, this is always clearly attributed;

4. Where I have quoted from the work of others, the source is always given. With the exception of such quotations, this thesis is entirely my own work;

5. I have acknowledged all main sources of help;

6. Where the thesis is based on work done by myself jointly with others, I have made clear exactly what was done by others and what I have contributed myself;

7. Either none of this work has been published before submission, or parts of this work have been published as: [please list references below]:

Signed:
.....
....

Date:
.....
.....

ABBREVIATIONS

ABC	Avidin biotin complex
Aβ	Amyloid beta
AD	Alzheimer's disease
ALS	Amyotrophic lateral sclerosis
ANOVA	Analysis of variance
ATP	Adenosine-5'-triphosphate
AU	Arbitrary units
β2M	Beta 2 microglobulin
BLAST	Basic local alignment search tool
Bfsp1	Filensin
Bfsp2	Phakinin
BSE	Bovine spongiform encephalopathy
CA1	Cornu Ammonis 1
CA2	Cornu Ammonis 2
Ca2+	Calcium ions
CA3	Cornu Ammonis 3
CaCl2	Calcium chloride
Casp3	Caspase 3
CC	Corpus callosum
CD11b	Cluster of differentiation molecule 11B
CD3+	Cluster of differentiation molecule 3 positive
CD4+	Cluster of differentiation molecule 4 positive
CD68	Cluster of differentiation molecule 68
CD8+	Cluster of differentiation molecule 8 positive
Cdh16	Cadherin 16
cDNA	complementary DNA
cfu	Colony forming units
CjD	Creutzfeldt-Jakob disease

CNP	2'-3'-cyclic nucleotide 3'phosphodiesterase
CNS	Central nervous system
Cryab	HSPB5
Crybb2	Beta 2 crystallin
Crygc	Gamma-c crystallin
Csn3	Kappa casein
Ctx	Cortex
Cu2+	Copper ions
CWD	Chronic wasting disease
Cyc1	Cyclin D1
DAB	Diaminibenzidine
DAPI	4',6-diamidino-2-phenylindole
DG	Dentate gyrus
DNA	Deoxyribonucleic acid
DPX	Distrine Plastizier Xylene
DRM	Desmin related myopathy
DTI	Diffuse tensor imaging
EAE	Experimental autoimmune encephalomyelitis
EDTA	Ethylene-diamine-tetra-acetic acid
ER	Endoplasmic reticulum
Fbx4	F-box protein 4
Fe2+	Iron ions
FGF-2	Basic fibroblast growth factor
GALT	Gut associated lymphoid tissue
GAPDH	Glyceraldehyde 3-phosphate dehydrogenase
GFAP	Glial fibrillary acidic protein
H2O2	Hydrogen peroxide
HCl	Hydrochloric acid
HD	Huntington's disease
HET	Heterozygous

HRP	Horse radish peroxidase
HSP	Heatshock protein
HSPB5 -/-	HSPB5 knockout
HSPB5 +/-	HSPB5 heterozygous
HSPB5 +/+	HSPB5 wildtype
HTT	Huntingtin protein
I.C	Intracranial
I.P	Intraperitoneal
I.V	Intravenous
IBA1	Ionized calcium binding adaptor molecule 1
ICAM1	Intercellular adhesion molecule 1
IFN-γ	Interferon gamma
IKκB	Inhibitor of nuclear factor kappa-B kinase subunit beta
IL-10	Interleukin-10
IL-12	Interleukin 12
IL-12p70	Interleukin 12 (active form)
IL-17	Interleukin 17
IL-18	Interleukin-18
IL-1β	Interleukin 1 beta
Ins1	Insulin
IκBα	Nuclear factor of kappa light polypeptide gene enhancer in B-cells inhibitor, alpha
kDa	kiloDalton
KO	Knockout
LPS	Lipopolysaccharide
MAP	Microtuble associated protein
MBP	Myelin basic protein
ME7	Mouse adapted prion strain- ME7
MgCl2	Magnesium chloride
MHCI	Major histocompatibility complex 1

MHCII	Major histocompatibility complex 2
mHTT	mutant Huntingtin protein
mRNA	Messenger RNA
MS	Multiple sclerosis
Na2CO3	Sodium carbonate
NBH	Normal brain homogenate
NFKβ	Nuclear factor kappa-light-chain-enhancer of activated B cells
NFT	Neurofibrillary tangles
NGF-2	Nerve growth factor 2
nvCJD	new variant Creutzfeldt-Jakob disease
PBS	Phosphate-buffered saline
PCR	Polymerase chain reaction
PD	Parkinson's disease
PM	Post mortem
PNS	Peripheral nervous system
PrD	Prion disease
PrPc	Prion protein (cellular)
Prph	Peripherin
Prpn	Prion protein
PrPSc	Prion protein (scrapie)
R6/2	Huntington's disease animal model expressing mHTT exon 1
RNA	Ribonucleic acid
ROS	Reactive oxygen species
rt-PCR	real-time polymerase chain reaction
SCA3	Spinocerebellar ataxia 3
SDS	Sodium dodecyl sulfate
SEM	Standard error of the mean
sHSP	small Heatshock protein
SN	Substantia nigra
Snca	Alpha synuclein gene

SOD1	Superoxide dismutase 1
SOr	Stratum oriens
SPy	Stratum pyramidale
SRad	Stratum radiatum
TEMED	N,N,N',N'-tetramethyl-ethylenediamine
TGFβ1	Transforming growth factor beta 1
TNF-α	Tumour necrosis factor alpha
Tubu1a	Tubulin
VCAM1	Vascular cell adhesion protein 1
VEGF	Vascular endothelial growth factor
Vim	Vimentin
WM	White matter
WT	Wildtype
Zn2+	Zinc ions

1. CHAPTER 1

GENERAL INTRODUCTION

The following chapter is a literature review. The review provides an introduction into protein misfolding and neurodegeneration and concludes with the role of specific heatshock proteins during neurodegeneration. It aims to provide the reader with the underlying scientific background to the project and highlights the current thinking in the scientific community and the basis of our investigation.

1.1 The global burden of neurodegenerative conditions

Neurodegenerative diseases, which include conditions such as Alzheimer's disease, Parkinson's disease, Huntington's disease and multiple sclerosis, are a diverse set of conditions that are characterised by selective and progressive neuronal loss in the nervous system (see table 1 for an example of common neurodegenerative conditions in the UK). Currently, neurodegenerative conditions affect 22 million individuals worldwide (Jack et al., 2009); and as there is a strong link between advanced age and the likelihood of developing a neurodegenerative disease. The World Health Organisation (WHO) estimates that by 2040, neurodegenerative conditions will have overtaken cancer as the 2nd leading cause of death, after cardiovascular disease (Jack et al., 2009).

Although neurodegenerative diseases have been studied since the late 19th century, the processes that underpin the conditions are still not fully understood. As a result, none of these conditions are curable: current therapeutics target the symptoms and not the cause. Significant progress has however been made in trying to understand the molecular mechanisms that underpin these conditions: for example, we now know that for many neurodegenerative conditions, including Alzheimer's, Parkinson's and Huntington's disease, they are all characterised by the misfolding and aggregation of otherwise normal cellular proteins. Such similarity between different conditions offers hope for therapeutic advances that could ameliorate many diseases simultaneously. As protein misfolding is implicated as a cause of neurodegeneration, the concept of pharmacologically inducing/modulating protein (re)folding has gained significant traction in recent years (Clark et al., 2000; Muchowski et al., 2005; Sajjad et al., 2010). This thesis will focus on the role of specific protein-folding molecular chaperones, known as heatshock proteins, in two contexts: their role in neurodegeneration and their role in modulating inflammation.

Neurodegenerative condition	Number of people with the condition (UK)	Number of deaths from the condition (UK)	Age of onset (years old)	Life expectancy after diagnosis
Alzheimer's disease	800,000	60,000	>65	7-9 years
Huntington's disease	6,000-10,000	230	30-50	10-30 years
Motor neuron disease	5,000	1,500	40-60	3-5 years
Multiple sclerosis	100,000	1500	20-50	25-35 years
Multiple system atrophy	3,000	200	38-75	<10 years
Parkinson's disease	120,000	7700	>50	2-37 years
Progressive supranuclear palsy	4,000-10,000	300	>40	<10 years

Table 1.1 List of major neurodegenerative conditions in the UK.

Whilst the list is by no means exhaustive, it illustrates that large numbers of the population that are affected by neurodegenerative conditions. As neurodegenerative conditions are more prevalent mid-to-late stage of life, increased life expectancy means more individuals are likely to become afflicted by these conditions; as these conditions tend to be chronic conditions requiring significant human and economic cost from families and public health services, they have become a major health priority. Source: office for national statistics (ONS), annual mortality extracts and the national end of life care intelligence network (NEoLCIN) bulletin (Maxwell, 2010).

1.2 Proteins, protein homeostasis and disease

All living cells contain encoded information in the form of ribonucleic acid (RNA) that, when decoded at the ribosome, provides direction for the synthesis of proteins (Dobson et al., 1999). Proteins are crucial to living cells because they mediate virtually all biological processes. As macromolecules, proteins are synthesised, firstly, from single amino-acids into nascent polypeptide chains, and secondarily, folded into intermediate structures that can adopt tertiary and quaternary 3-dimensional conformations (see figure 1.1) (Horwich, 2002). The 3-dimensional arrangement of a protein is important for function (Dobson, 2004). Adoption and maintenance of this functional 3-dimensional structure is influenced by intra-molecular covalent and non-covalent bonds that are sensitive to disruption from several physiological, chemical and environmental factors (Dobson, 2004). If left unchecked, such disruptions promote unravelling and, subsequently, misfolding of proteins (Outeiro et al., 2007).

Protein misfolding is detrimental to cells because misfolded proteins tend to expose hydrophobic regions that have a propensity to aggregate; aggregation hinders normal protein function and increases the likelihood of cell malfunction and disease (Dobson et al., 1999). The list of conditions that are caused by protein-misfolding is extensive: for example, systemic conditions include sickle cell anaemia (Perutz, 1992) and cystic fibrosis (Johnston et al., 1998), whilst protein aggregation in neurons tends to induce one of several neurodegenerative conditions (Outeiro et al., 2007) (see section 1.2.2).

Prokaryotic and eukaryotic cells have evolved extensive mechanisms to ensure correct protein folding and limit protein misfolding (Lindquist et al., 1988). Perhaps the most specialised mechanism used by cells to promote correct protein folding and circumvent protein misfolding is the heat-shock response (HSR) (Lindquist, 1986). This stress-response is characterised by the upregulation of genes that encode a family of proteins known as heat-shock proteins (HSPs) (for major properties of HSPs, see table 1.2, and for a mechanistic illustration, see figure 1.1).

HSP Family	Number of members	Relative molecular weight (kDa)	Main properties
Small HSP	11[1]	12-30[2]	-Constitutively expressed[3] -Induced during cellular stress[3] -ATP-independent[4] -Prevents aggregation of proteins[3]
HSP40	41[5]	≈ 40[6]	-Constitutively expressed[6] -ATP-dependent[7] -Co-chaperone to HSP70[8]
HSP60	11[5]	≈ 60[6]	-Constitutively expressed[6] -ATP-dependent[9] -Folds proteins into globular structure[9]
HSP70	13[10]	68-78[6]	-Constitutively expressed[6] -Some members induced during cell stress[6] -ATP-dependent[11] -Folds linear polypeptides into proteins[11]
HSP90	5[5]	84-90[6]	-Constitutively expressed[12] -Induced during cellular stress[12] -ATP-dependent[12] -Folds nearly-mature proteins[13] -Involved in signal transduction[14]
HSP100	2[5]	100-110[6]	-Induced during cellular stress[15] -ATP-dependent[15] -Solubilises aggregated proteins[16]

Table 1.2 Heatshock protein sub-families, properties and main functions.

The HSP super-family can be sub-divided into 6 sub-families: small HSPs, HSP40, HSP60, HS60, HSP90 and HSP100. Each member family is classed based on structural and functional similarities. References: 1 (Kirbach et al., 2011); 2 (Ganea, 2001); 3 (Jakob et al., 1993); 4 (Gusev et al., 2002); 5 (Kampinga et al., 2009); 6 (Ellis, 2011); 7 (Ellis, 2006); 8 (Craig et al., 2006); 9 (Ranford et al., 2004); 10 (Brocchieri et al., 2008); 11 (Mayer et al., 2005); 12 (Csermely et al., 1998); 13 (Young et al., 2001); 14 (Echeverria et al., 2010); 15 (Doyle et al., 2009); 16 (Doyle et al., 2013).

The role of heatshock proteins in protein folding

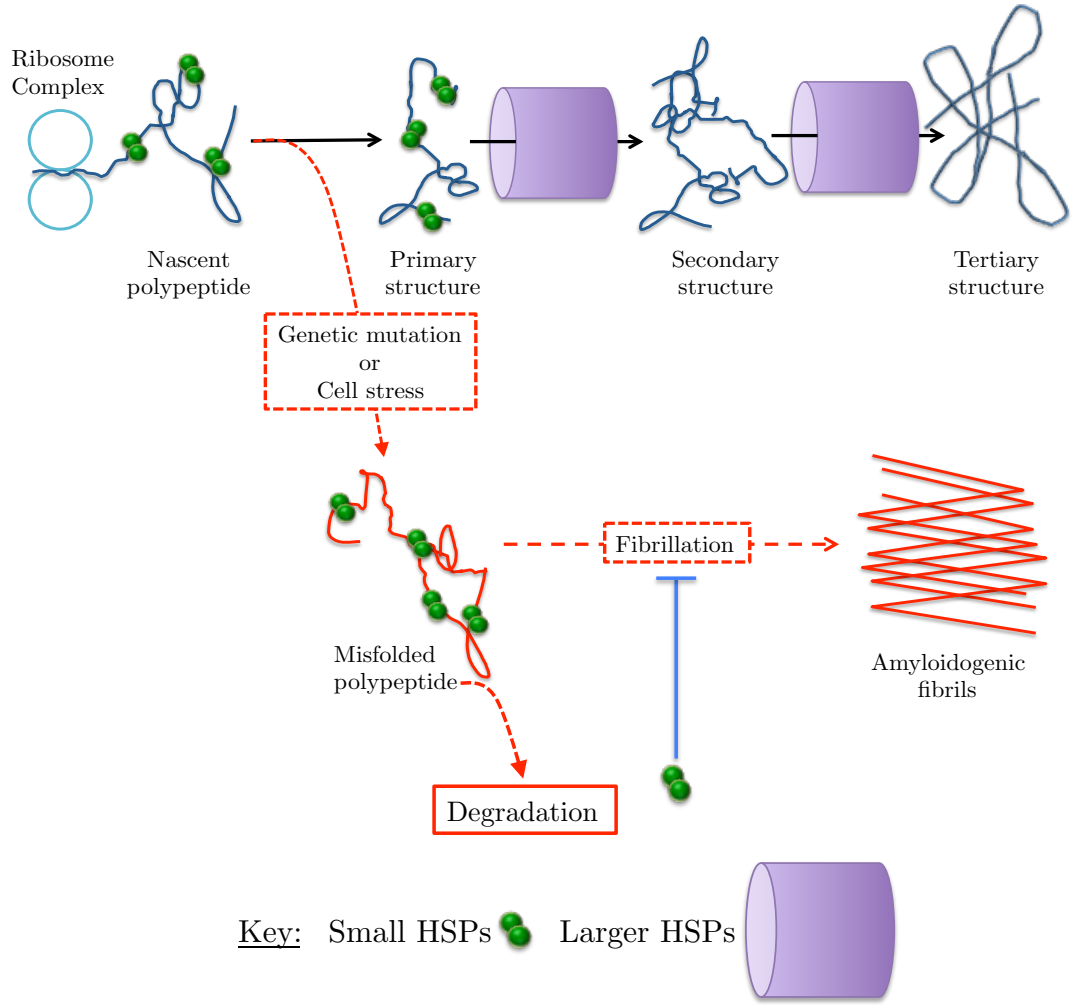

Figure 1.1 Role of heatshock proteins in protein folding.
Nascent polypeptides are translated at ribosomal structures in the cytosol and/or on rough endoplasmic reticulum (ER). Small HSPs facilitate the process by transiently binding to nascent polypeptides and chaperoning them to larger HSPs. Larger HSPs, like HSP60, HSP70 and HSP90, are ATPase-dependant, and fold polypeptides into secondary and tertiary structures. Correctly folded polypeptides can successfully adopt a 3-dimensional conformation that is crucial for protein function (black pathway). Genetic mutations and/or cellular stress, however, can disrupt protein folding (red pathway). Genetic mutations can alter a polypeptide's primary sequence, which can result in protein misfolding. Cellular stressors, such as excessive heat or oxidative stress, can also prompt protein misfolding by disrupting intra-molecular covalent and non-covalent interactions. Misfolded proteins are detrimental because they have the propensity to interact with other misfolded proteins, which promotes protein aggregation and fibrillation (see figure 1.3 for in-depth schematic). To circumvent aggregation and fibrillation, sHSPs have been shown to bind to misfolded polypeptides as well as oligomeric aggregates, thereby inhibiting fibrillation (see figure 1.3). Small HSPs also show the capacity to off-load misfolded proteins for degradation. Protein misfolding can occur at several points in a protein's life-cycle; for simplicity, only one misfolding pathway has been illustrated (i.e. red pathway).

1.2.1 Heat-shock proteins (HSPs)

The HSP super-family is structurally and functionally diverse (see table 1.2). The physiological role of HSPs is to facilitate protein folding, and during cellular stress, some HSPs are induced to promote protein re-folding (table 1.2). Furthermore, if proteins are damaged beyond repair, HSPs can also expedite protein degradation (see figure 1.1) (Ellis, 2006). HSPs are therefore involved in all aspects of a protein's life-cycle, from synthesis to degradation, and thus, are crucial components of protein homeostasis. This thesis focuses on the small heatshock protein (sHSP) family and their role in the protein misfolding associated with neurodegenerative diseases.

1.2.1.1 Small HSPs (sHSPs)

The sHSP sub-family comprises of 11 structurally and functionally similar protein members, HSPB1-HSPB11 (Kirbach et al., 2011) (summarised in figure 1.2). This sub-family of proteins is described as "small" because all the members of the family have molecular weights ranging between 12kDa and 30kDa (Jakob et al., 1993), which is in stark contrast to the other HSP sub-families that range from 40kDa to 110kDa (Lindquist et al., 1988) .

Small HSP are also distinguished from other HSPs by a conserved 80-100 amino-acid sequence known as the alpha-crystallin domain (Ganea, 2001). This domain confers sHSPs their chaperone capabilities, however, as the domain lacks ATPase activity, sHSPs are incapable of actively folding polypeptides into mature proteins (Gusev et al., 2002); instead, sHSPs mediate protein-folding by transiently binding to unfolded polypeptides and chaperoning them to larger, more competent, ATPase-containing HSPs, such as HSP60, HSP70 and HSP90, which have refoldase machinery (see figure 1.1) (Horwitz, 1992; Jakob et al., 1993; Carra et al., 2008; Ellis, 2011). The functional capacity of sHSPs is determined by phosphorylation of key residues: phosphorylation promotes the formation of large oligomeric complexes of between 15 to 50 mono- or heteromeric subunits (Horwitz, 1992; Jakob et al., 1993) (see figure 1.3).

Structural organisation of small heatshock protein (sHSP) family members

Name	Other names	Organisation of sHSP
HSPB1	HSP25/HSP27/HSP28	
HSPB2	MKBP	
HSPB3	HSP17	
HSPB4	αA-crystallin	
HSPB5	αB-crystallin	
HSPB6	HSP20	
HSPB7	cvHSP	
HSPB8	HSP22	
HSPB9	Ct51	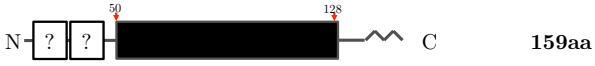
HSPB10	ODF1	
HSP11	PP25	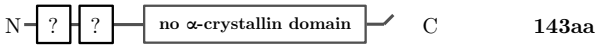

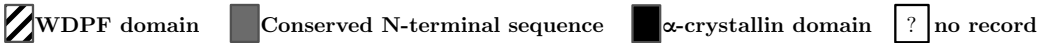

Figure 1.2 Structure and functional properties of small heatshock proteins (sHSPs).

(A) Sequence alignment of all sHSP family members, illustrating the amino-acid length as well as location of conserved WDPF sequence and the α-crystallin domain. Small HSPs share between 24-65% sequence homology. The WDPF domain is a conserved N-terminal domain with the primary sequence PSRLFDQXFGEXLL. The α-crystallin domain is a conserved 80-100 amino acid sequence present in all sHSPs; as HSPB11 lacks an α-crystallin domain, it's assignation as a sHSP has been questioned (Kappé et al., 2010). Amino acid sequences of sHSPs and conserved domains were identified through a systematic search through the National Centre for Biotechnology Information's (NCBI) Conserved Domains Database (CDD v3.11-45746PSSMs) and supported by literature (Lambert et al., 1999; Gusev et al., 2002).

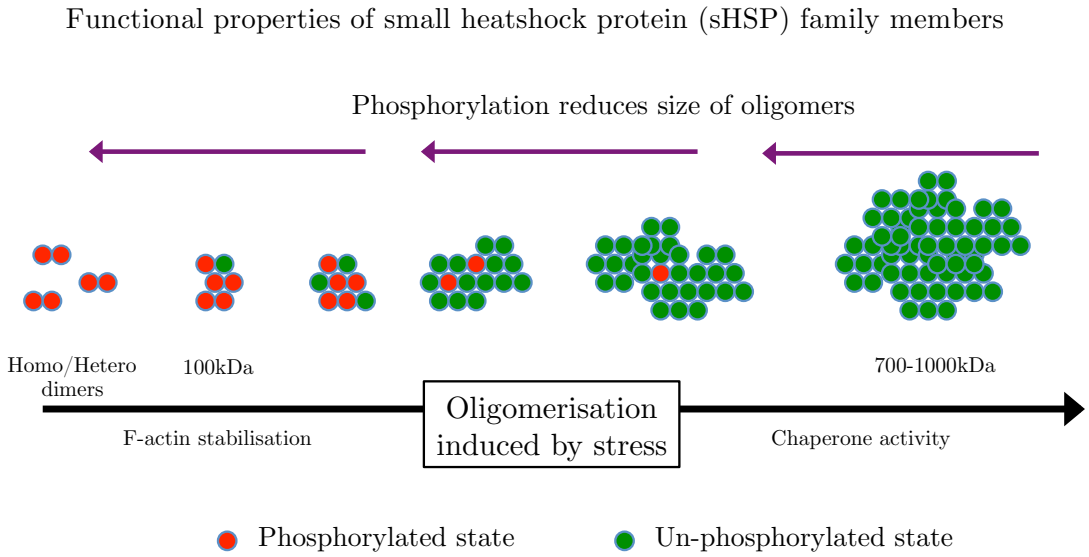

Figure 1.3 Functional properties of sHSPs.

Functional properties of sHSPs. Cellular stress induces oligomerisation and facilitates chaperone activity; the WDPF domain mediates oligomerisation, whilst the α-crystallin domain mediates chaperone activity. The phosphorylation state dictates oligomerisation.

Oligomerisation of sHSPs increases their chaperone activity and is mediated by a conserved domain known as the WDPF domain (see figure 1.3). This domain also confers additional functional capacity to sHSPs by allowing sHSPs to interaction with a diverse range of effector proteins (including other sHSPs) (Fontaine et al., 2005; Arrigo et al., 2007). As a result, sHSPs can mediate a plethora of functions unrelated to protein folding, including roles in cytoskeleton stabilisation, cell cycle regulation, apoptosis regulation, as well as, intracellular signalling (Arrigo et al., 2007) (see table 1.5). Small HSPs are therefore indispensible to cellular function.

Although sHSPs share significant structural and functional characteristics, they show differential tissue distribution and cellular expression -perhaps suggesting specialist functions in different compartments. In humans and rodents, for example, HSPB1, HSPB5, HSPB6 and HSPB8 show ubiquitous protein expression systemically (Tallot et al., 2003; Verschuure et al., 2003) and also in the CNS (Quraishe, 2010; Kirbach et al., 2011). HSPB2, HSPB3, and HSPB7 show localisation only in cardiac and skeletal muscle (Sugiyama et al., 2000). HSPB4 is exclusively expressed in the eye (Brady et al., 1997). HSPB9 and HSPB10 are expressed only in the testes (Verschuure et al., 2003). HSPB11 has only recently been identified as a sHSP, therefore there is limited protein-expression data available (see summary in table 1.3).

In the CNS, constitutive cellular expression of HSPB1 is observed in neuronal cells with some occasional non-neuronal staining in astrocytes, ependymal cells and cells of the choroid plexus (Plumier et al., 1997; Armstrong et al., 2001). Induced expression is ubiquitous (section 1.4.1). HSPB5 is constitutively expressed in white-matter-rich areas, with a specific oligodendrocyte localisation (Klemenz et al., 1991; Iwaki et al., 1992; Quraishe, 2010). Induced expression can be observed in astrocytes and neurons (section 1.4.1). Limited literature is available on the constitutive cellular expression of HSPB6; anatomical characterisation however, shows high expression in cerebellum, cortex and hippocampus (Verschuure et al., 2003). For HSPB8, cellular localisation is observed in motor neurons of the ventral horn (Irobi et al., 2004; Quraishe, 2010).

Small HSP	Protein expression	Inducible	Capacity to reduce aggregates
HSPB1	Ubiquitous (incl. CNS)	Yes[1,2]	Yes[3,4]
HSPB2	Cardiac and Skeletal muscle	No[1,2]	Yes[3]
HSPB3	Cardiac and Skeletal muscle	No[1,2]	Yes[3]
HSPB4	Eye lens	No[1,2]	Yes[5]
HSPB5	Ubiquitous (incl. CNS)	Yes[1,2]	Yes[3,4,6,7,8,9]
HSPB6	Ubiquitous (incl. CNS)	No[1,2]	Yes[3]
HSPB7	Cardiac and Skeletal muscle	No[1,2]	Yes[10]
HSPB8	Ubiquitous (incl. CNS)	Yes[1,2]	Yes[3]
HSPB9	Testes	No[1,2]	Yes[12]
HSPB10	Testes	No[1,2]	No studies
HSPB11	Limited protein data (*mRNA ubiquitous)	No[1,2]	No studies

Table 1.3 Anatomical localisation and functional properties of small HSPs.

Small HSPs are constitutively expressed; only HSPB1, HSPB5 and HSPB8 appear to be induced by various different stressors. In vitro, HSPB1-HSPB9 have been shown to have the capacity to reduce aggregation of several different proteins. References: 1 (Morimoto et al., 1998); 2(Zhang et al., 2002); 3 (Bruinsma et al., 2011); 4 (Yerbury et al., 2013); 5 (Brady et al., 1997); 6 (Ghosh et al., 2008); 7 (Robertson et al., 2010); 8 (Shammas et al., 2011); 9 (Sun et al., 2005b); 10 (Vos et al., 2010); 11 (Vos et al., 2011).

Regardless of cellular localisation, sHSP are induced in several protein-misfolding conditions (see table 1.4) and are thought to mediate a protective role.

1.2.2 Expression of Small HSPs during protein-misfolding disease

1.2.2.1 Expression of sHSPs during Alzheimer's disease

Alzheimer's disease (AD), like other Tauopathy conditions, is characterised by misfolding and intracellular aggregation of tau protein into neurofibrillary tangles (NFTs) (Selkoe et al., 1999). Unlike other Tauopathies however, AD is also characterised by extracellular accumulation of Aβ protein (Mudher et al., 2002). NFTs and Aβ aggregates are implicated in the death of cortical neurons (Wenk, 2003). Both *in vitro* and *in vivo* models show that all 4 CNS-expressed-sHSPs (see table 1.3) colocalise with Aβ aggregates and are induced in both neuronal and glial cells (Lowe et al., 1990; Shinohara, 1993; Renkawek et al., 1994b; Wilhelmus et al., 2006a; 2006b). HSPB1 and HSPB5 show the most significant induction (Björkdahl et al., 2008). There are currently no studies investigating the effect of sHSP over-expression in AD, however, based on results from other conditions (see below), it is likely that induction is protective.

1.2.2.2 Expression of sHSPs during Parkinson's disease

Parkinson's disease (PD) is caused by misfolding and aggregation of α-synuclein protein (Bruinsma et al., 2011). Small HSPs appear to colocalise with α-synuclein aggregates with HSPB1 and HSPB5 being induced in neurons and glia in cortical and hippocampal tissue (Renkawek et al., 1994a; 1999; Outeiro et al., 2007) (summarised table 1.3). This induction is mirrored in transgenic PD animal models (α-synA53T) (Wang et al., 2008). *In vitro* studies show overexpression of HSPB1, but surprisingly, not overexpression of HSP70, to suppress α-synuclein fibrillation, suggesting that the *in vivo* induction of sHSPs in PD is likely to be protective (Zourlidou et al., 2004). *In vitro,* HSPB5 interacts with α-synuclein and inhibits aggregate formation (see section 1.4.2.1). These results would suggest a protective role for HSPB5 during PD.

Disease	sHSP	State of expression
Amyotrophic lateral sclerosis	HSPB1	Upregulated: Mouse (Vleminckx et al., 2002; Wang et al., 2008)
	HSPB5	Upregulated: Mouse (Vleminckx et al., 2002; Wang et al., 2008) Upregulated: Human (Iwaki et al., 1992)
Alexander's disease	HSPB1	Upregulated: Human (Head et al., 1993; Iwaki et al., 1993)
	HSPB5	Upregulated: Human (Iwaki et al., 1989; 1992; Head et al., 1993; Iwaki et al., 1993)
Alzheimer's disease	HSPB1	Upregulated: Human (Shinohara, 1993; Renkawek et al., 1994b)
	HSPB5	Upregulated: Human (Lowe et al., 1990; Shinohara, 1993)
	HSPB6	Upregulated: Human (Wilhelmus et al., 2006a; 2006b)
	HSPB8	Upregulated: Human (Wilhelmus et al., 2006a; 2006b)
Epilepsy	HSPB1	Upregulated: Human (Bidmon et al., 2004)
Huntington's disease	HSPB5	Downregulated: Mouse (Zabel et al., 2002*; Quraishe, 2010**) *Zabel et al., 2002: Down-regulation, whole brain lysate, 12weeks **Quraishe, 2010: Down-regulation, Striatum, Frontal cortex, Cerebellum, 9weeks and 17weeks
Multiple Sclerosis	HSPB1	Upregulated: Human (Aquino et al., 1997)
	HSPB5	Upregulated: Human (Han et al., 2008)
Other Tauopathies	HSPB1	Upregulated: Human (Dabir et al., 2004)
	HSPB5	Upregulated: Human (Lowe et al., 1992b; Dabir et al., 2004)
Parkinson's disease	HSPB1	Upregulated: Human (Renkawek et al., 1992; 1994a) Upregulated: Mouse (Wang et al., 2008)
	HSPB5	Upregulated: Human (Iwaki et al., 1992; Renkawek et al., 1994b) Upregulated: Mouse (Wang et al., 2008)
Prions disease	HSPB1	Upregulated: Mouse (Tortosa et al., 2008) Upregulated: Sheep (Vidal et al., 2008)
	HSPB5	Upregulated: Human (Iwaki et al., 1992; Renkawek et al., 1992)
Spinocerebellar ataxia	HSPB1	Upregulated: Mouse (Chang et al., 2005) Upregulated: Human (Chang et al., 2005)

Table 1.4 Expression of small heatshock proteins (sHSPs) during major neurological conditions.

HSPB1 and HSPB5 appear to be induced most frequently. The majority of conditions, except Huntington's disease, show increased expression of sHSPs.

1.2.2.3 Expression of sHSPs during Prion diseases

Prion diseases are a unique set of neurodegenerative conditions that affect humans as well as a wide range of animals (Collinge, 2005): in humans, versions of the disease include Creutzfeldt-Jakob disease (CJD), new variant CJD (nvCJD) and Kuru. In animals, versions include bovine spongiform encephalopathy (BSE) in cattle, scrapie in sheep and chronic wasting disease (CWD) in elk deer.

Regardless of species, prion pathogenesis is initiated by the introduction of misfolded prion protein (PrP^{Sc}) into a host's proteome either by genetic, sporadic or transmissible means (Brown et al., 2000). Introduction of PrP^{Sc} into the proteome initiates pathogenic interaction of PrP^{Sc} with normal prion protein (PrP^{C}) that then results in extra-cellular aggregate deposits and eventually neuronal degeneration and animal death (Prusiner, 2001). The precise mechanisms underlying prion propagation are not understood: it has been proposed that prion propagation may occur through PrP^{Sc} acting as a template that promotes autocatalytic conversion of PrP^{C} (Caughey, 2003), or that PrP^{Sc} acts as a seed that promotes accumulation of further PrP^{Sc} (Soto et al., 2006) (see figure 1.4 for an illustration of models of prion pathogenesis).

Regardless of the model of prion propagation, aggregates of PrP^{Sc} significantly induce HSPB1 and HSPB5: HSPB1 is found significantly induced in sheep and mice expressing bovine PrP^{Sc} (Tortosa et al., 2008; Vidal et al., 2008), whilst HSPB5 shows significant induction in neurons and glia of diseased human and ME7-Prion mice (Kato et al., 1992; Renkawek et al., 1992; Quraishe, 2010). Studies in yeast suggest that over-expression of yeast HSP104/HSP70/HSP40 complex reduces highly ordered aggregates and thus limits the ability for PrP^{Sc} to interact with PrP^{C} and initiate self-perpetuating conversion of normal prion protein (Moriyama et al., 2000; Romanova et al., 2009; Doyle et al., 2013). This data therefore suggests a protective role for HSPs during prion disease; however investigations on the contribution of sHSPs have not yet been done. This aspect will be discussed further in chapter 4.

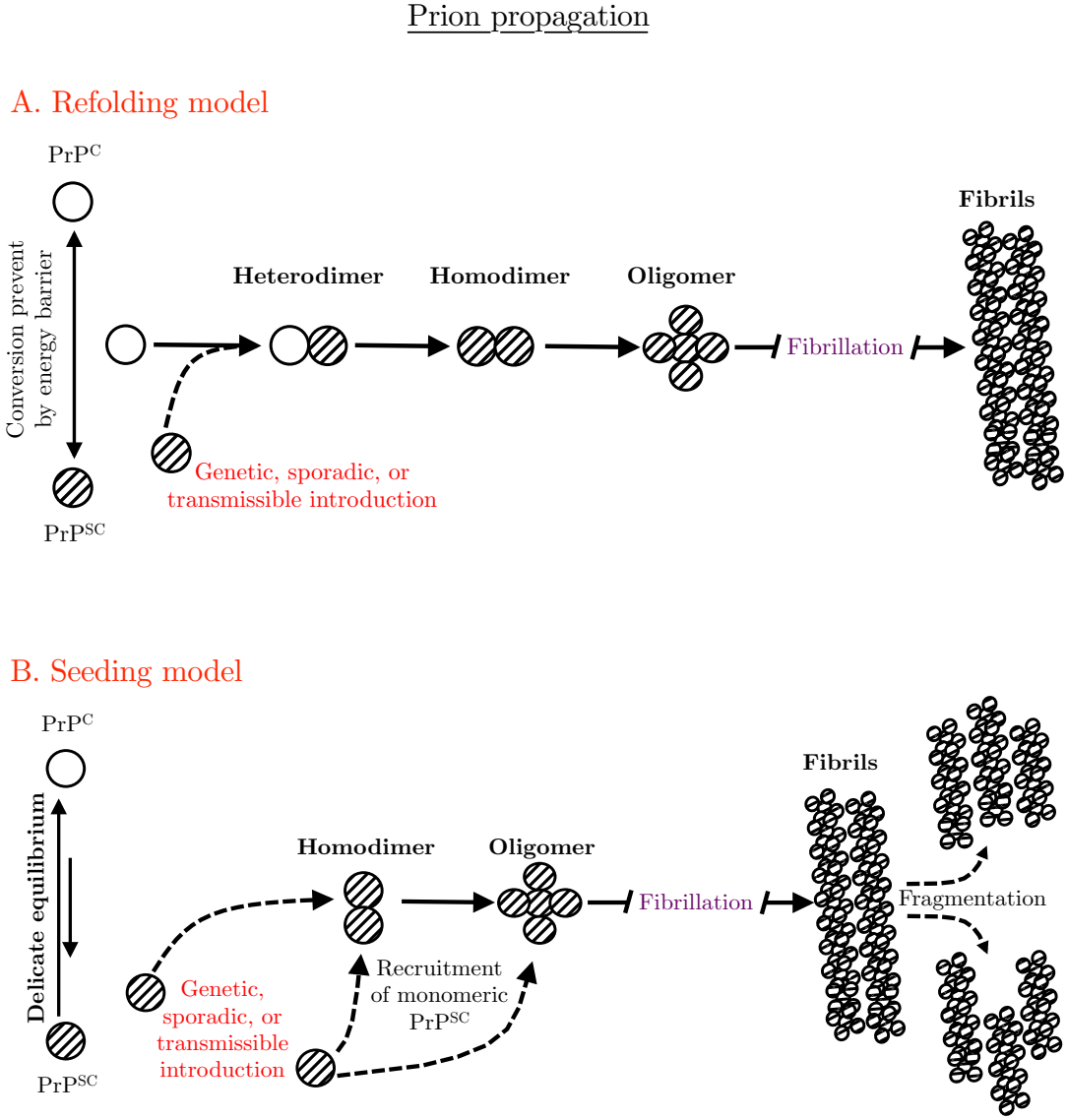

Figure 1.4 Schematic representation of models for the conformational conversion of PrP^{C} to PrP^{Sc}.

(A) Refolding model. This model is also known as template-assisted refolding because it predicts that PrP^{Sc} acts as pathogenic template that promotes PrP^{C} to misfold and refold as PrP^{Sc}. In this model, spontaneous conversion of PrP^{C} to PrP^{Sc} does not occur because of a high-energy thermodynamic barrier. However, introduction of PrP^{SC} into the proteome by genetic, sporadic or transmissible means initiates the template-based conversion of PrP^{C} to PrP^{Sc}. The precise mechanisms underlying how PrP^{Sc} converts a predominantly α-helical PrP^{C} to the β-sheet-rich PrP^{SC} conformation is not known. Interaction of PrP^{SC} with other PrP^{Sc} monomers prompts formation of PrP^{SC} oligomeric structures that promote fibrillation and formation of amyloidogenic fibrils (for mechanism, see figure 1.5). (B) Seeding model. In this model, it is proposed that PrP^{C} and PrP^{Sc} are constitutively expressed and exist in a delicate equilibrium. However, increased introduction of PrP^{Sc} by genetic, sporadic or transmissible means skews the equilibrium and results in dimerisation of PrP^{Sc} to form oligomers. Oligomers, with their higher association constants (see figure 1.5), recruit more PrP^{Sc} at a faster rate. This effect is regarded as the seeding phase and promotes fibrillation of oligomers into amyloidogenic fibrils. This model concludes with suggestion that fibrils fragment into smaller units that "seed" further autocatalytic conversion of PrP^{C} to PrP^{Sc}.

1.2.2.4 Expression of sHSPs during Huntington's disease

Huntington's disease (HD) is 1 of 9 conditions that are characterised by genetic mutations that promote the uninterrupted genetic addition of glutamine residues to a protein's sequence (Todd et al., 2013); excessive expansion of glutamine residues past a critical stable threshold results in protein misfolding and aggregation. In HD, polyglutamine (polyQ) expansion occurs at the N-terminus of the Huntingtin (HTT) protein to create an extended polyQ tract: tracts beyond 36 glutamine-repeats result in protein misfolding, aggregation and disease (figure 1.5) (Ross et al., 2011). Longer polyQ tracts predict earlier onset and more severe disease (Langbehn et al., 2004).

Misfolded HTT protein, referred to as mutant HTT (mHTT), pathologically aggregates as intra-nuclear inclusions (Ross et al., 2011). Whilst the physiological role of HTT is currently unknown, the misfolding of HTT protein is thought to disrupt HTT-mediated processes and contribute to disease (Cattaneo et al., 2005) and to a larger extent, mHTT is also thought to gain toxic function and sequester other proteins, thereby further contributing to pathology (Tobin et al., 2000; Shao et al., 2007). The loss of normal HTT function and mHTT's toxic gain of function cumulatively results in significant loss of striatal neurons, with as much as 95% of GABAergic medium spiny neurons being lost (Halliday et al., 1998; Vonsattel et al., 1998). To a lesser extent, atrophy of other brain regions, including the cerebral cortex, subcortical white-matter, thalamus and areas of the hypothalamus, is also observed (Vonsattel, 2008).

Contrary to findings from other protein misfolding diseases (see comparison in table 1.4), induction of sHSPs is not observed during HD. Results from HD animal models (R6/2 mice) show a reduced expression of HSPB5 during disease progression (Zabel et al., 2002; Quraishe, 2010) (discussed further in chapter 2 and 5). In both studies, the reduced expression was only observed at the protein level and not the transcript level, suggesting mHTT may influence HSPB5 turnover and/or that mHTT sequesters HSPB5. Regardless of the specific nature of the reduced expression, this raises important question as to whether reduced expression of HSPB5 is pathological.

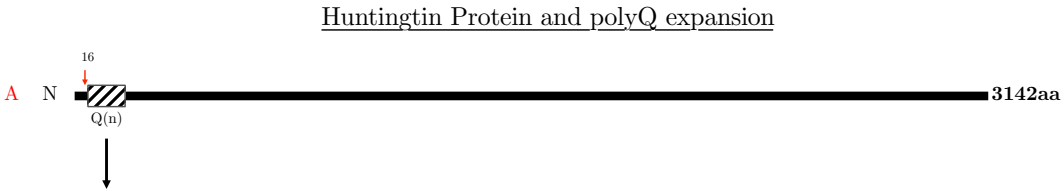

B

PolyQ Count	Classification	Disease status	Disease onset
<26	Normal	Will no be affected	-
27-35	Intermediate	Will no be affected	-
36-39	Reduced Penetrance	Elevated Risk	35-44
>40	Full Penetrance	Will be affected	35-44
>60	Juvenile Onset	Will be affected	<21

Figure 1.5 Huntingtin protein, polyQ expansion, and disease state.

(A) Simplified schematic of huntingtin protein highlighting the N-terminal segment where polyQ expansion occurs. (B) PolyQ lengths and their resulting phenotypes: less than 35 repeats lead to normal phenotype, however, the closer the number is to 35, the chance for genetic slippage and therefore the greater the likelihood to pass on more than 35 polyQ to offspring. 36-39 polyQs result in an elevated risk of developing HD with the key determinant as to whether an individual develops the condition being environmental factors/diet/lifestyle. If an individual develops the condition, the average disease onset will be 35-44 years of age. 40 or more polyQ repeats lead to fully penetrant disease with an average onset of 35-44 years of age. Greater than 60 polyQ expansions lead to an accelerated form of HD that is referred to as juvenile onset because disease onset is often below 21 years of age.

Given that HSPB5 has pleiotropic roles (see table 1.5) and that *in vitro* studies show over-expression of HSPB5 to be protective against various cellular stressors including heat stress, protein misfolding and administration of prostaglandins and interferon-gamma (Kamradt et al., 2001a; Arrigo et al., 2005; Kamradt et al., 2005; Hagemann et al., 2009), the reduced expression of HSPB5, as observed in R/2 animals (see table 1.4) likely contributes significantly to pathology. In addition, the observed reduced expression of HSPB5 in the animal model raises questions as to whether this effect is mirrored in human disease. This thesis will therefore aim to investigate both these questions: is the reduced expression of HSPB5 detrimental to disease progression and is the reduced expression mirrored in human disease? To understand the consequences of HSPB5's reduced expression in R6/2 animals, it is necessary to firstly dissect HSPB5's role(s) during health and also during disease.

1.3 Cellular role of HSPB5 during neurodegeneration

HSPB5 is expressed ubiquitously (see table 1.3). In the CNS, constitutive expression of HSPB5 is observed in oligodendrocytes (Renkawek et al., 1992; Quraishe, 2010) and during disease-state, HSPB5 can be induced in astrocytes (Iwaki et al., 1992; Renkawek et al., 1992) and neurons (Iwaki et al., 1992; Lowe et al., 1992a). Induction of HSPB5 in astrocytes and neurons during disease-state suggests HSPB5 mediates protective roles within these cell-types (discussed further in section 1.4.2.1 and 1.4.3).

Phosphorylation of either 1 or a combination of serine-19, serine-45 and serine-59 residues is crucial for HSPB5's functionality (Kato et al., 1994) as it allows HSPB5 to form oligomeric structures (Simon et al., 2013). Like other sHSPs, the oligomerisation of HSPB5 improves its chaperone activity and also confers additional functional capacity for the sHSP to interact with a diverse range of protein partners (Arrigo, 2013; Ciocca et al., 2013). As a result, HSPB5 is capable of overseeing several cellular roles above and beyond protein folding, including inhibiting protein aggregation, cytoskeleton stabilisation, cell-cycle regulation and inhibiting apoptosis (table 1.5).

1.3.1 HSPB5 inhibits protein aggregation and fibrillation

In vitro evidence shows that HSPB5 interacts with and inhibits fibril formation of several neurodegenerative disease-causing proteins, including the proteins that are implicated in AD, PD, PrD and spinocerebellar ataxia 3 (SCA-3) (Sun et al., 2005a; Robertson et al., 2010; Bruinsma et al., 2011; Shammas et al., 2011; Yerbury et al., 2013). In each case, although induced by the misfolding of different proteins, aberrant proteins aggregate and form highly ordered, β-sheet-rich conformations that are known as amyloidogenic aggregates (Dobson, 2004) (see figure 1.6). Formation of these SDS-insoluble, β-sheet-rich conformations can be tracked experimentally by fluorescent-dye Thioflavin T, and it appears that formation of amyloidogenic aggregates occurs in 2 kinetic phases: nucleating phase and an elongation phase (Kim et al., 2002). HSPB5 inhibits both nucleating and elongation phases (see figure 1.6).

In vitro evidence suggests that HSPB5 can inhibit the nucleation phase of protein fibrillation: Robertson et al., (2010), show that with Ataxin-3, a poly-Q-addition-prone protein, HSPB5 binds to a conserved Josephine domain and thus inhibits nucleation. In most other cases, HSPB5 inhibits the elongation phase: with Aβ42, one of the proteins implicated in AD, immuno-electron microscopy shows that HSPB5 associates with the entire length of Aβ42 protein, including the terminal ends, and inhibits the elongation phase of fibril formation (Shammas et al., 2011). Similarly, surface plasmon resonance, highlights that although there is a weak and transient interaction of HSPB5 with α-synuclein, this interaction is sufficient to inhibit elongation and fibril formation (Bruinsma et al., 2011). Studies with SOD1, a protein implicated for causing amyotrophic lateral sclerosis (ALS), also show that HSPB5 inhibits the elongation phase of fibril formation (Yerbury et al., 2013). Taken together, this data highlight that HSPB5 can supress fibrillation at multiple stages of aggregation. It is likely therefore that reduced expression of HSPB5, as observed in R6/2 mice, may contribute to pathology as it allows fibrillation of mHTT to go unhindered (summarised figure 1.6).

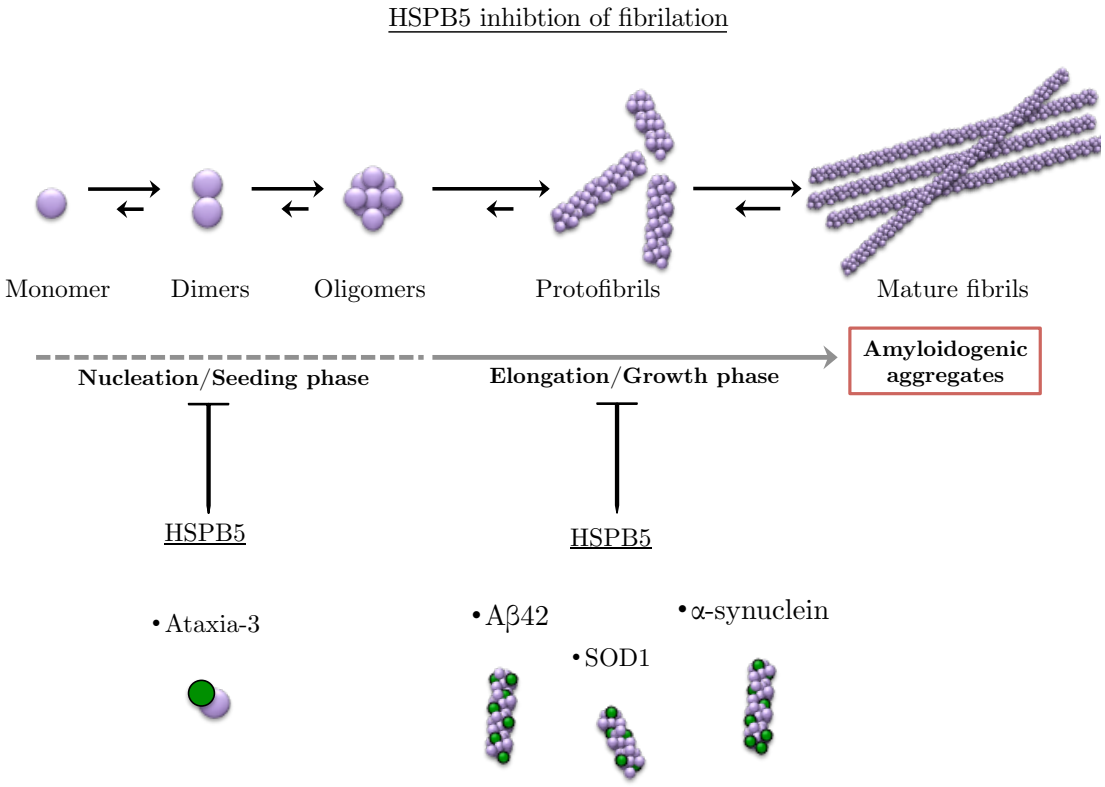

Figure 1.6 Schematic diagram showing the aggregation characteristics of amyloidogenic aggregates.

Most proteins that cause neurodegenerative diseases aggregate to form insoluble aggregates that are known as amyloidogenic aggregates. Amyloidogenic aggregates are β-sheet-rich and experimentally measured by fluorescent-dye Thioflavin T or diazo-dye Congo Red. The kinetics of amyloidogenic aggregate formation can be seen to occur in 2 phases: a nucleation/seeding phase and an elongation/growth phase (Kim et al., 2002). The nucleation phase is the slowest phase and is characterised by monomeric misfolded proteins binding to other misfolded proteins to make dimers and eventually oligomers of misfolded protein. As oligomers become larger, their association constant also increases, which means that it becomes easier for other proteins to associate with the oligomers (Ellis, 2011). This effect is synonymous to the colloquialism "snowball effect" and is referred to, here, as nucleation. Once nucleation occurs, oligomers associate with other oligomers to form protofibrils. This phase is known as the elongation/growth phase. Protofibrils associate together to form highly ordered mature fibrils. HSPB5 appears to interact and inhibit fibril formation via one of two ways: it can inhibit the nucleation phase (e.g. Ataxia-3), or it can inhibit the elongation phase (e.g. Aβ42, SOD1, α-synuclein) of fibril aggregation. It is not certain if formation of amyloidogenic aggregates is pathogenic or protective. Some consider amyloidogenic aggregates to be cytotoxic and a key pathological hallmark of neurodegenerative conditions (Ellis et al., 2006), whilst others believe that misfolded oligomeric proteins are toxic to cells and thus formation of mature fibrils acts as a sink that sequesters and attenuates toxicity (Zhao et al., 2012). It is uncertain if HSPB5-mediated inhibition of amyloidogenic aggregates is protective or pathogenic.

1.3.2 HSPB5 mediates cytoskeleton stabilisation, cell adhesion and tissue integrity

Cytoskeletal dysfunction is implicated in a wide range of neurodegenerative conditions (McMurray, 2000). HSPB5 helps the assembly of cytoskeletal elements (Gopalakrishnan et al., 1992; Benndorf et al., 1994) and during thermal or oxidative stress, HSPB5 stabilises and protects the cytoskeleton from unfolding (Liang et al., 1997; Mounier et al., 2002). HSPB5's cytoskeleton stabilisation role involves chaperoning and stabilising intermediate filaments (desmin (Ghosh et al., 2007b), vimentin, peripherin (Djabali et al., 1997; 1999) and GFAP (Ghosh et al., 2007b)) and microfilament F-actin (Singh et al., 2007) and tubulin (Ohto-Fujita et al., 2007).

The importance of HSPB5 in cytoskeletal stabilisation can be illustrated by that reduced function of HSPB5, due to mutations, leads to the development of a number of congenital conditions. For example, an R120G point mutation in human HSPB5 contributes to an inability of HSPB5 to interact with desmin, which leads to misfolding and aggregation of the protein, resulting in either a muscular condition known as desmin-related myopathy (DRM) (Wang et al., 2001) or cardiomyopathy and congenital cataract (Vicart et al., 1998). In terms of HSPB5's interaction with F-actin, and tubulin, reduced expression of HSPB5 has been shown to result in abnormal mitotic spindle formation in lens epithelial cells (Nicholl et al., 1994) and to impair cytoskeletal organisation and MCF-7 cell growth (Mairesse et al., 1996). These data highlight the important role mediated by HSPB5 in cytoskeleton stabilisation and imply detrimental effects as due to reduced expression of HSPB5.

HSPB5 also interacts with β-catenin and cadherin-16 and thus appears to have an indirect role in facilitating cell-cell adhesion and maintaining tissue integrity (Thedieck et al., 2008). It appears that HSPB5 is important in helping β-catenin and cadherin-16 attach to cytoskeletal components. Thedieck et al., (2008) did not study the effect of β-catenin and cadherin-16 dynamics in the absence of HSPB5; reduced expression of HSPB5 would likely negatively influence cell-cell adhesion dynamics.

	Interacting protein	Functional role of HSPB5	Cellular process modified
HSPB5:	β-Catenin	Cell adhesion[1]	HSPB5 facilitates cytoskeleton stabilisation, cell adhesion and tissue integrity
	Cadherin-16	Stabilisation[2]	
	Desmin	Chaperoning[3]	
	F-actin	Protein integrity[4,5,6]	
	GFAP	Stabilisation[7,8]	
	Peripherin	Chaperoning[9,10]	
	Tubulin	Chaperoning[3,11]	
	Vimentin	Chaperoning[9,10,12]	
HPB5:	α-synuclein	Inhibits fibrillation[13,14]	HSPB5 inhibits protein fibrillation/aggregation
	Aβ-amyloid	Inhibits fibrillation[13,15]	
	Apo-lipoprotein	Inhibits aggregation[16]	
	K-casein	Inhibits aggregation[17]	
	PolyQ proteins	Inhibits aggregation[17]	
	PrP^C	Inhibits aggregation[18]	
	SOD1	Inhibits aggregation[19]	
HSPB5:	Bax	Inhibits translocation to mitochondria[20]	HSPB5 inhibits apoptosis pathways
	Bcl-Xs	Inhibits translocation to mitochondria[20]	
	Caspase-3	Negative regulator of activity[21]	
	p-53	Inhibits translocation to mitochondria[22]	
HSPB5:	FGF-2	Chaperone FGF-2[3]	HSPB5 facilitates growth factors and transduction pathways
	NGF-β	Chaperone NGF-β[3]	
	VEGF	Chaperone VEGF[3]	

Continued next page...

	Interacting protein	Functional role of HSPB5	Cellular process modified
HSPB5:	C8/α7 proteasome	Degradation of HSPB5 interacting proteins[23]	HSPB5 helps regulation of protein degradation
	Fbx4	Cyclin D1 ubiquitination/degradation[24]	
HSPB5:	Cyclin D1	Ubiquitinated by HSPB5-fbx4[24]	HSPB5 helps cell cycle regulation
HSPB5	IKKβ	Stimulate kinase activity[25]	HSPB5 interacts with protein kinases

Table 1.5 Proteins that are known to interact with HSPB5.

Using its WDPF domain, HSPB5 interacts with several protein partners and thus facilitates several cellular processes including, cytoskeleton and tissue stabilisation, inhibition of protein fibrillation and aggregation, inhibition of apoptotic pathways, facilitation of cell-cycle regulation, survival and signal transduction, as well as, protein degradation. The table shows what the perceived role of HSPB5 in that interaction. References: 1 (Fanelli et al., 2008); 2 (Thedieck et al., 2008); 3 (Ghosh et al., 2007a); 4 (Del Vecchio et al., 1984); 5 (Wang et al., 1996); 6 (Singh et al., 2007); 7 (Wettstein et al., 2012); 8 (Hagemann et al., 2009); 9 (Djabali et al., 1997); 10 (Djabali et al., 1999); 11 (Ohto-Fujita et al., 2007); 12 (Perng et al., 1999); 13 (Ghosh et al., 2008); 14 (Bruinsma et al., 2011); 15 (Shammas et al., 2011); 16 (Hatters et al., 2001); 17 (Robertson et al., 2010); 18 (Sun et al., 2005b); 19 (Yerbury et al., 2013); 20 (Mao et al., 2004); 21 (Hu et al., 2012); 22 (Liu et al., 2007); 23 (Boelens et al., 2001); 24 (Lin et al., 2006); 25 (Adhikari et al., 2011).

1.3.3 HSPB5 mediates a role in cell growth, cell-cycle regulation and signal transduction pathways

HSPB5 not only facilitates the afore-mentioned roles, but also interacts and modulates the activity of proteins involved in cell growth, cell-cycle regulation and signal transduction. The sHSP has been shown to have strong chaperoning interactions with basic fibroblast growth factor (FGF-2), nerve growth factor beta (NGF-β) and vascular endothelial growth factor (VEGF) (Ghosh et al., 2007b). HSPB5 appears to protect these proteins from unfolding during cellular stress and therefore indirectly promotes cell growth and differentiation (Ghosh et al., 2007b).

Using its WDPF domain, HSPB5 can also interact with FBX4 protein, an F-box-containing protein that is a crucial component of the ubiquitin- ligase SCF complex (SKP1/CUL1/F-box) (den Engelsman et al., 2003). This complex regulates the cell cycle. HSPB5's role in this complex is thought to increase substrate specificity of FBX4, which results in targeted ubiquitination of phosphorylated cyclin-D1 (Lin et al., 2006). Phosphorylation of ubiquitinated cyclin-D1 leads to proteasomal degradation of cyclin-D1 and results in slower cell-cycle progression (Lin et al., 2006). HSPB5 expression has therefore been implicated as a therapeutic substrate for various cancers. Impairment of HSPB5's interaction with FBX4 reduces cyclin-D1 ubiquitination and accelerates cell-cycle progression in several tumour cell lines (Lin et al., 2006). Reduced expression of HSPB5 is therefore likely to increase cell-cycle progression in R6/2 animals, although it is unclear which cells or which organs.

HSPB5 is also involved in signal transduction; HSPB5 stimulates inhibitor of nuclear factor kappa-B, subunit beta (IKK-β) kinase activity (Adhikari et al., 2011). Activated IKK-β phosphorylates and thus initiates the degradation of nuclear factor of kappa light polypeptide gene enhancer in B-cells inhibitor, alpha (IκBα); this liberates nuclear factor kappa-B transcription factor (NF-κβ), allowing wide modulation of cell function. These data highlight HSPB5's crucial physiological roles.

1.3.4 HSPB5 negatively regulates apoptotic pathways

Finally, HSPB5 appears to be a negative regulator of apoptosis (table 1.5). Apoptosis is a key feature in neurodegenerative conditions and can be induced by misfolded proteins, oxidative stress, and even excessive cytokine stimulation (Thompson, 1995). Misfolded proteins and oxidative stress induce apoptosis via the mitochondrial apoptotic pathway whilst extracellular insults, such as cytokines, induce apoptosis via death receptors that belong to the tumour necrosis factor receptor superfamily (Green, 2011). Both these pathways coalesce at the activation of executioner caspase-3. HSPB5 appears to be a potent inhibitor of apoptosis by inhibiting activation of this executioner caspase (Mao et al., 2004; Liu et al., 2007; Hu et al., 2012).

In vitro and *in vivo* evidence shows HSPB5 to suppress procaspase-3, the pro-enzyme responsible for the synthesis of caspase-3, thereby inhibiting the downstream effects of caspase-3 activation and thus apoptosis (Mao et al., 2001; Kamradt et al., 2001b). More recent evidence further shows that HSPB5 also inhibits apoptosis further upstream to caspase-3 activation by binding to and inhibiting pro-apoptotic proteins Bax, Bcl-Xs (Mao et al., 2004; Hu et al., 2012) and p53 (Liu et al., 2007). The binding of HSPB5 to these proteins sequesters them in the cytoplasm and prevents their translocation to the mitochondria where they would normally induce the release of cytochrome c and DIABLO proteins that form the apoptosome and promote apoptosis.

It is therefore evident that HSPB5 can facilitate several important physiological roles during health and also disease (summarised in table 1.5). However, it is important to note that many of these interactions are deduced from *in vitro* studies; extrapolation of the protective capacity of HSPB5 therefore remains theoretical. Perhaps the most direct *in vivo* evidence for the protective role of HSPB5 can be gleaned from animal and human experiments of multiple sclerosis and stroke; in both conditions, there is compelling evidence for HSPB5 mediating a robust anti-inflammatory role (Ousman et al., 2007; Arac et al., 2011; Rothbard et al., 2011; 2012).

1.3.5 HSPB5 as an inflammatory mediator

1.3.5.1 HSPB5 is protective in multiple sclerosis

The first evidence for HSPB5 being a potent immune modulator stems from studies of multiple sclerosis (MS) (Ousman et al., 2007; Rothbard et al., 2011; 2012). MS is an autoimmune condition that is characterised by T-cell-mediated inflammatory response against the myelin sheath that encapsulates neurons (Nataf, 2009). Although MS is not a protein-misfolding disease, HSPB5 is found significantly upregulated in MS lesions (van Noort et al., 1995; Chabas et al., 2001). Due to this induction, HSPB5 was initially thought to be an auto-antigen for T-cells (van Noort et al., 1995). More recently, however, following failed attempts to induce MS by immunising mice with HSPB5 (Verbeek et al., 2007), it has become widely accepted that the induction of HSPB5 that is observed during MS in not pathological and has instead been suggested to be protective (Ousman et al., 2007; Rothbard et al., 2011; 2012).

This conclusion is based on that during experimentally induced MS, mice deficient of HSPB5 showed significantly exaggerated activation of T-cells and had increased levels of pro-inflammatory cytokines, which led to worse disease progression (Ousman et al., 2007). In addition, intravenous (I.V) addition of HSPB5 to the deficient animals resulted in reduced amount of pro-inflammatory mediators and improved the clinical progression of disease. Altogether, these findings suggest HSPB5 to have an immune modulatory role (characterised further in chapter 3 and 4).

The precise mechanism by which HSPB5 modulates the immune system is uncertain, however, there is some evidence that HSPB5 may have the capacity to modulate the proliferative capacity of immune cells and modulate pro-inflammatory cytokine production (Arac et al., 2011); evidence from astrocytes suggests that the molecular basis to HSPB5's immune-modulatory action appears to be founded on HSPB5 acting as a pro-inflammatory transcription repressor (Shao et al., 2013) (discussed in further detail in chapter 3). Whether this applies to other cell-types is uncertain. As HSPB5 does not

possess a secretion signal sequence, in somewhat an unorthodox manner, HSPB5 is also thought to mediate its immune-modulatory role by extracellularly binding to circulating pro-inflammatory molecules (Rothbard et al., 2012). The evidence shows elevated levels of HSPB5 in MS patients' plasma; precipitation of-which shows HSPB5 bound to acute phase proteins, complement and coagulation proteins. There is some evidence for the extracellular release of other HSPs, such as HSP70, via a non-classical secretory pathway that does not include cell-death-mediated release (Hightower et al., 1989; Mambula et al., 2007; Vega et al., 2008). For HSPB5, evidence suggests exosomal release (Gangalum et al., 2011). This data therefore highlight an intra and extra-cellular anti-inflammatory role for HSPB5.

1.3.5.2 HSPB5 is protective in stroke

In addition, there is compelling evidence that HSPB5's induction during stroke mediates an immune modulatory role. HSPB5 is found upregulated in 68% of human stroke brains (Minami et al., 2003). Stroke is a neurological condition that is caused by the focal interruption of blood-flow to the brain, either through blockage of blood vessels (thrombotic) or rupture of blood vessels (haemorrhagic) (Piao et al., 2005). Regardless of the cause, the resulting disruption of blood-flow leads to localised hypoxia that, if not rectified quickly, leads to hypoxic stress and the initiation of a cascade of cellular events that culminate in tissue death (see figure 1.7) (Piao et al., 2005). One important element observed during ischaemic cascade is microglial activation; microglia, the immune cells of the brain, are important during stroke because they phagocytose dead cells and "mop-up" cytotoxic compounds (Wood, 1995). However, microglia also produce copious amounts of pro-inflammatory cytokines that, in itself, can damage tissue, and to a larger extent, promote peripheral leukocyte infiltration that exacerbates inflammation and results in additional tissue damage (Patel et al., 2013). Balancing the protective aspects and the detrimental effects of microglial activation is therefore a tricky homeostatic act.

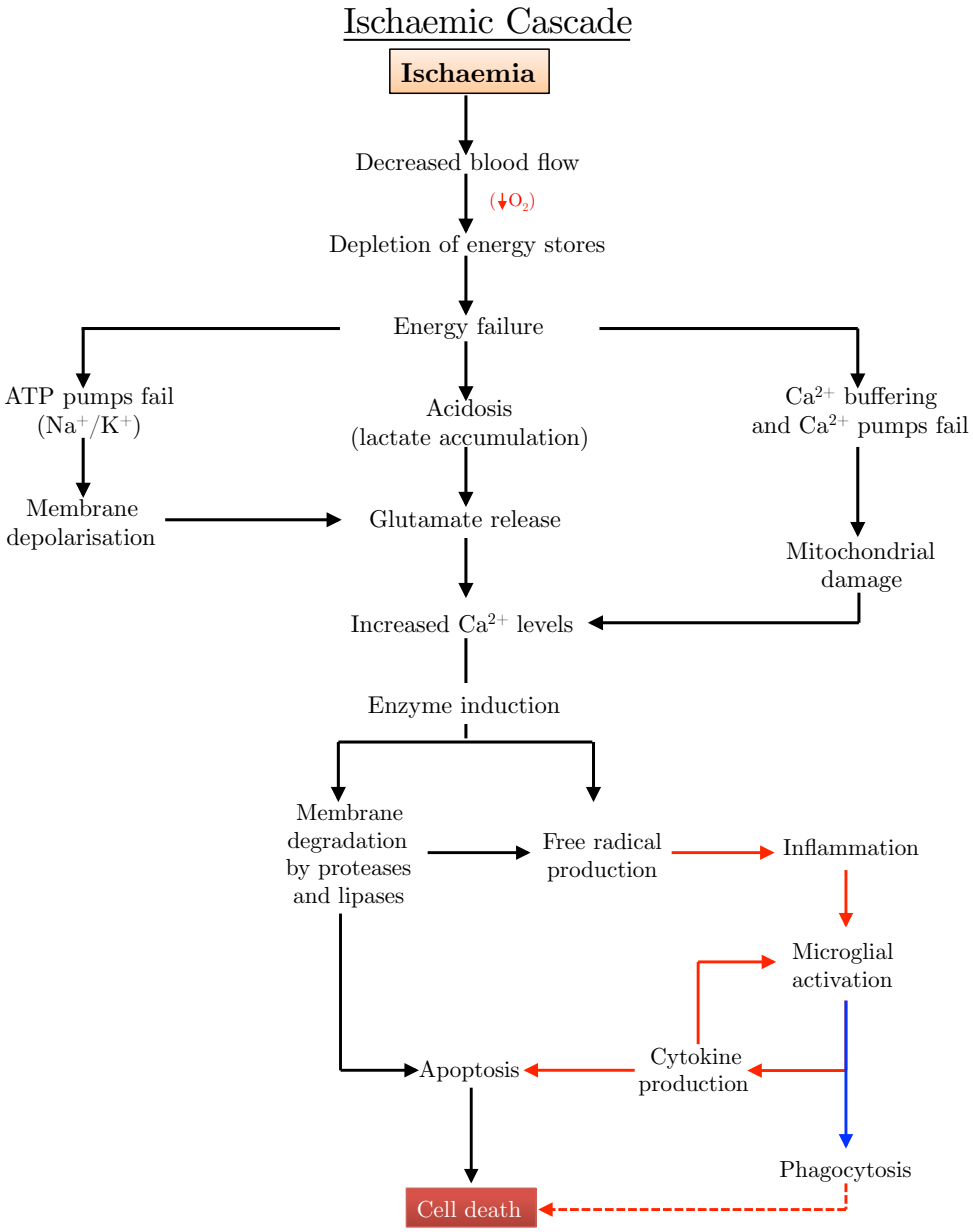

Figure 1.7 Schematic of the molecular events that occur during ischaemic stroke.

Ischaemic stroke is caused by the blockage of blood vessels that results in decreased blood flow to a focal area of the brain. Decreased blood flow results in reduced oxygen to brain tissue; brain tissue ceases to function adequately if deprived of oxygen for 60-90seconds. Insufficient aerobic respiration leads to depletion of intra-cellular energy stores and thus failure of the ATP and Ca^{2+}-pump as well as increased anaerobic respiration and lactate accumulation. Failure of the ATP-pump results in dis-equilibration of the Na^{+} and K^{+} gradient and results in membrane depolarisation, whilst failure of the Ca^{2+}-pump results in mitochondrial damage and release of Ca^{2+} from mitochondrial stores. Increase in cytosolic Ca^{2+} initiates a cascade of events, one of which is the induction of several enzymes that initiate apoptosis. This process leads to free-radical production and cell death, both of which activate microglia. Activated microglia phagocytose cell debris but also produce further cytokines that can promote further apoptosis and cell death. Microglial cytokines are thought to result in a "leaky" blood-brain-barrier that, during reperfusion, results in an influx of peripheral leukocytes and an exaggerated inflammatory response that is detrimental. HSPB5 is thought to modulate aspects of this immune response. Pathway adapted from (De Keyser et al., 1999)

Studies investigating HSPB5's immune-modulatory role show that I.V administration of HSPB5 12hrs after stroke results in significantly reduced infarct/lesion sizes and better prognosis for affected animals (Arac et al., 2011). The reason for the reduced lesion size is thought to be due to HSPB5's immune modulatory effects: Arac et al., (2011) illustrated how mice deficient of HSPB5 showed significantly increased infiltration of $CD3^+$ and γδ-T-cells, and had larger lesion sizes following stroke. In addition to this, they also showed that exogenous addition of HSPB5 to mice deficient of HSPB5, as well wild-type mice, results in smaller lesion sizes as due to reduced proliferative capacity of $CD3^+$ $CD4^+$, $CD8^+$ and γδ-T-cells as well as reduced production of pro-inflammatory cytokines interleukin-17 (IL-17) and interferon gamma (IFN-γ) (Arac et al., 2011). These findings suggest that HSPB5 attenuates the inflammatory response and reduces aberrant immune activation.

1.4 Concluding remarks

Cumulatively, the data from MS and stroke studies provides strong *in vivo* evidence for HSPB5's capacity to modulate the immune response. This raises questions as to the impact of the reduced expression of HSPB5 observed by Zabel (2002) and Quraishe (2010) in R6/2 mice. Given that aberrant innate and adaptive immune response have been implicated during HD (Ellrichmann et al., 2013), an investigation into HSPB5's role as an immune modulator becomes quite interesting, not only in the context of R6/2 animals but also in the context of HD patients.

This thesis will therefore aim to provide some insight into HSPB5's immune modulatory role. We will use HSPB5 transgenic mice that do not express the gene (HSPB5 knockout (KO) animals) to investigate the absence of HSPB5 and its effect on basal phenotype (chapter 2), peripheral immune system (chapter 3) and the central immune system (chapter 4). The thesis will conclude with a comparative study between R6/2 mice and human HD tissue to evaluate if the observations made in the animal model extrapolate to the human disease (chapter 5).

2. CHARACTERISATION OF HSPB5-DEFICIENT ANIMALS

This chapter provides a baseline characterisation of HSPB5 KO animals. Such characterisation is important to understand the phenotype (cellular, morphological and behavioural) of animals lacking HSPB5. This characterisation will inform subsequent experiments by identifying potential confounding variables that may be apparent in mice lacking HSPB5.

2.1 Introduction

Small heat shock proteins (sHSPs) mediate crucial homeostatic roles in all living cells (see chapter 1); they not only facilitate protein folding and re-folding (Haslbeck et al., 2002) but they also negate apoptosis (Mao et al., 2004; Hu et al., 2012), stabilise actin and intermediate filaments (Hagemann et al., 2009; Wettstein et al., 2012) and promote cell survival, growth and differentiation (Djabali et al., 1999; Goldbaum et al., 2001). Whilst the majority of sHSPs show upregulation in the CNS during several neurodegenerative conditions (table 1.4), in the R6/2 animal model of Huntington's disease (HD), there is a selective reduced expression of HSPB5 (chapter 1). Given HSPB5's pleiotropic roles (see section 1.3), we hypothesise that the reduced expression observed in R6/2 animals impinges several cellular processes and thus may be detrimental/pathological. As HSPB5 appears to have a potent negative regulatory capacity on inflammatory processes, which are implicated in many neurodegenerative conditions, its reduced expression raises important questions. This thesis will therefore investigate HSPB5's immune modulatory role in more detail.

This chapter will firstly characterise behavioural parameters, cellular profiles and morphological features of HSPB5 KO mice as compared to wild type animals. This comparison is useful as subsequent experiments (chapter 3 and chapter 4) use behavioural, cellular and morphological parameters to characterise the impact of reduced HSPB5 expression. A caveat to this investigation, however, is that HSPB5 KO mice also inadvertently carry a deletion for another sHSP, HSPB2, thereby creating a double mutant ($HSPB5^{-/-}$, $HSPB2^{-/-}$); as these animals are double mutants, it is necessary to investigate whether the erroneous deletion of HSPB2 has any confounding effects.

Previous characterisation of HSPB5 KO animals under a 129Sv background suggests that the inadvertent deletion of HSPB2 has negative effects: results show that although the double mutants are viable, they suffer from muscular dystrophy, kyphosis and die prematurely, ca. 10-12months of age (Brady et al., 2001).

These effects are caused because both HSPB2 and HSPB5 are expressed in skeletal muscle (see table 1.2); their absence in KO animals, therefore, compromises the musculature. As some of our subsequent characterisations will rely on behavioural analyses that are influenced by muscular exertion, characterisation of behavioural aspects of these mice is necessary. Whilst Brady et al., (2001) studied the effect of knocking out HSPB2 and HSPB5 on the musculature, they did not investigate the effects of knocking out HSPB2 and HSPB5 on the CNS. Whilst we do not envision the lack of HSPB2 to have an effect in the CNS (as HSPB2 is not expressed there) this chapter will also characterise the effect of lack of HSPB2 and HSPB5 on cellular and morphological aspects of cells in the CNS. These findings will provide a baseline that will inform subsequent experiments and eliminate extraneous variables. To simplify, although the animals are double mutants ($HSPB2^{-/-}$/$HSPB5^{-/-}$), they will simply be referred to from now as HSPB5 KO mice.

2.2 Aims

As HSPB2 and HSPB5 are expressed in muscle cells, this chapter will:

1. Determine whether the knockout mice show any physical/behavioural differences to wild type animals.
2. As subsequent work will focus on the CNS, we will characterise whether HSPB5 KO mice show any cellular or morphological differences as compared to animals that express HSPB5.

These measurements will provide a baseline for subsequent experiments and will eliminate confounding variables.

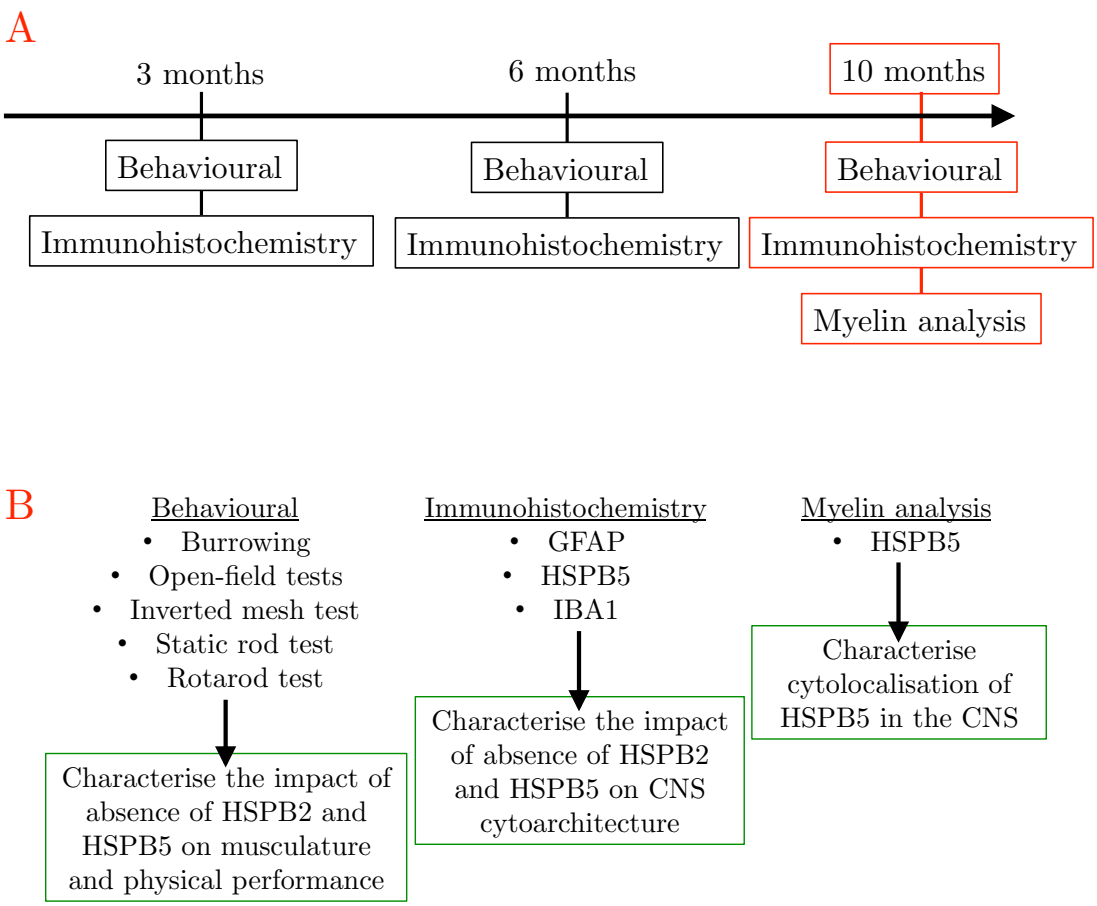

Figure 2.1 Time line showing experimental set-up and experimental procedues.

(A) Time-line showing the 3 time-points behavioural experiments were done and tissue was collected for analysis. To investigate the impact of knocking out HSPB2 and HSPB5, behavioural analysis was done at 3, 6 and 10months of age; immunohistochemical analysis was also done at the same time-points. The 10-month time-point is a critical time-point as previous experiments suggest that HSPB5 KO do not survive past this point (Brady et al., 2001). (B) Experimental procedures utilised and the reason why they were done. Behavioural tests used to characterise the HSPB5 KO mice are burrowing (2.3.3.1), open-field (2.3.3.2), inverted mesh (2.3.3.3), static rod (2.3.3.4) and rotarod tests (2.3.3.5). These tests were done to try and characterise the impact of the absence of both HSPB2 and HSPB5 on musculature and physical performance. Immunohistochemical analysis involved staining for HSPB5, GFAP, the astrocyte marker and IBA1, the microglial marker (2.3.4.1). These investigations provide understanding of whether HSPB5 KO animals show different cellular composition to wild type animals. Myelin analysis of wild type animals was done at the 10-month time-point (2.3.5). This analysis was done to provide better understanding of HSPB5's localisation in oligodendrocytes.

2.3 Materials and methods

2.3.1 Generation of HSPB5$^{-/-}$ mice

HSPB5 KO mice (HSPB2$^{-/-}$/HSPB5$^{-/-}$) were generated by the Wawrousek lab (N.I.H, Bethesda, Maryland) and backcrossed for several generations onto a C57Bl/6 background in the Muchowski lab (University of California San Francisco, California) and then passed on as a gift to our lab (BRF, University of Southampton). In our lab, the mice colony was expanded as follows: HSPB5 heterozygous (HSPB5$^{+/-}$) mice were crossed with HSPB5 heterozygous (HSPB5$^{+/-}$) mice to generate $\frac{1}{4}$ wild type, $\frac{1}{2}$ heterozygous, and $\frac{1}{4}$ knock out littermate mice. Genotype was confirmed by polymerase chain reaction (PCR). The breeding cross did not generate these Mendelian ratios, which, as observed later, imposed a difficulty to a perfectly controlled experiment.

2.3.2 Animals and animal husbandry

Littermate animals were separated by sex and housed in groups of 5 in plastic cages with sawdust bedding. Mice were fed on an RM-1 Standard laboratory chow diet and had access to food and water *ad libitum*. The holding room was temperature controlled (21 – 23^{o}C) with a 12hr:12hr light dark cycle (lights on at 07:00). All procedures were performed in accordance with the UK animals (Scientific Procedures) Act 1986 under personal license and ethical approval obtained from the University of Southampton and the UK Home Office.

2.3.3 Behavioural Analyses

2.3.3.1 Burrowing test

Mice were placed in individual cages that had a 20cm long opaque, plastic tube with an opening diameter of 6.8cm. The tubes were filled with 200g of standard laboratory chow pellets and positioned in a 3cm-high elevated position. Mice were left in in cage in a semi-lit, quiet environment initially for 2 hours and then overnight (*ca.* 16hrs). The amount of pellets dug out (left in the tube) were weighed and recorded for both the 2hr and overnight condition. The mice were not under dietary restriction.

2.3.3.2 Open-field test

Mice were placed in the centre of individual Perspex boxes of 27cm L x 27cm W x 20.3cm H that was lined with infrared optics to measure animal movement over a period of 3 minutes. Distance travelled by the mice, average velocity, and time spent resting during the 3-minute test period were recorded. Data was processed and analysed by activity monitor software (Med associates Inc., USA). In-between tests, the boxes were cleaned with Virkon® disinfectant (Anachem, UK) and allowed to dry before introduction of a new animal.

2.3.3.3 Inverted mesh test

Mice were placed individually on a wire mesh measuring 40cm x 40cm. The mesh was mounted approximately 1m above the ground over soft cushioning and was inverted. Upon inversion, the timer was started, and the time it took for the mice to fatigue and fall off was recorded. A cut-off time of 2 minutes was implemented.

2.3.3.4 Static rod test

A wooden rod measuring 60cm L x 2.8cm D was affixed to a table at a 90^{O} protruding angle off the surface of a table. The rod was positioned over soft cushioning approximately 1m from the ground. Mice were placed at the furthest end of the rod away from the table facing away from the table and the timer was started. The mice were expected to turn around 180^{O} so as to face the table and then they were expected to navigate to "safety". The timer was stopped upon successful completion of the task.

2.3.3.5 Rotarod

Mice were placed on an automated rotating cylinder and allowed to find their balance. The machine was turned on and speed incrementally increased. The total time it took for the mice to stay on the apparatus was measured and recorded.

2.3.3.6 Statistical analysis

Values obtained from behavioural tests were compiled and statistically analysed using GraphPad Prism v6 (GraphPad Software, US). For group data, which was analysing the effect of genotype as well as age on the mice, data was statistically analysed using an two-way analysis of variance (2-way ANOVA); Tukey post-hoc test was done to compare multiple comparisons. When comparing difference between male and female mice, an unpaired T-test was used and as the sample sizes were very small, Welch's correction was applied to the data in order to take into account differences in standard deviation.

2.3.4 Tissue collection and processing

2.3.4.1 Brains

At the end of the experiment (see figure 2.1), animals were terminally anaesthetised with 10µl/g Sodium Pentobarbital (Sigma, UK). Death was confirmed by pedal reflex loss. Mice were perfused with heparinised saline and then 10% formalin. The brain was removed and placed in 10% formalin overnight at 4°C for immunohistochemistry processing

2.3.4.1.1 Immunohistochemistry

Formalin-fixed brains were de-hydrated by immersion in a series of increasing concentration alcohols from 70% ethanol to 80%, 90%, 100% and, lastly, immersion into Histoclear (Sigma Aldrich, UK) (see table 2.2); this process was automated by a Leica-TP 1020 tissue processor (Leica Biosystems, UK). Following the Histoclear step, tissue was placed in plastic cassettes (Fisher Scientific, UK) and submerged in molten (40°C) paraffin wax (Polywax, UK) and allowed to solidify. Wax blocks were stored at room temperature. The wax-blocks were cut into 10µm sections on a Leica RM2255 rotary microtome (Leica Biosystems, UK) and tissue was floated on 40°C dH_2O in a tissue floatation bath (LAMB, UK). The resulting sections were mounted on SuperFrost™ microscope slides (Fisher Scientific, UK) and dried overnight at 37°C. Slides were stored at room temperature.

2.3.4.1.1.1 Immunostaining

Sections were heated at 60ºC for 30 minutes and then de-waxed in xylene (Fisher Scientific, UK) before being re-hydrated by immersion in a series of decreasing alcohol concentrations (see table 2.3). Endogenous peroxidase activity was blocked with a solution of 1% hydrogen peroxide (H_2O_2) for 3 minutes and subsequent antigen retrieval was done for 5 minutes by heating in citrate buffer (10mM citric acid (pH6)) in a 700W microwave. Non-specific binding was prevented by incubating sections in goat serum (GIBCO life technologies, UK). Sections were incubated with primary antibodies (see table 2.4). Appropriate biotinylated secondary antibody (see table 2.4) was applied for 1hr and then sections were incubated in ABC complex (Vector Laboratories, UK) for 45 minutes. Immunoreactivity was determined by immersion in diaminobenzidine (DAB) solution (Sigma Aldrich, UK). Sections were counterstained with Harris haematoxylin (VWR, UK) and de-hydrated by immersing in a series of increasing concentration alcohols (reversal of table 2.3) and, lastly, by immersion into xylene (Fisher Scientific, UK). Coverslips were applied with Distrene-Plasticiser-Xylene (DPX) combined-mountant (VWR, UK). All images were taken using a Zeiss Axio Observer Z1 inverted microscope (Zeiss, UK).

2.3.5 In silico microarray analysis of HSPB5 expression

The tissue-specific pattern of mRNA expression can indicate important clues about gene function. Using the GeneAtlas MOE430 gcrma (Su et al., 2004), the raw data pertaining to HSPB5 high-density oligonucleotide arrays was downloaded from www.biogps.com and plotted graphically to determine the tissue and cells that show the highest expression of HSPB5. The original data had been obtained from 191 mice using a vast array of high-density Affymetrix probes and had been GCRMA summarised i.e. processed through an algorithm that removes background noise, normalises the probes to allow comparison between multiple chips and summarised in expression values that are robust and outlier resistant (Su et al., 2004).

Treatment	Duration
70% ethanol	2 hours
70% ethanol	2 hours
80% ethanol	1 hour
90% ethanol	1 hour
Absolute ethanol I	1 hour
Absolute ethanol II	10 hours
Histoclear I	4 hours
Histoclear II	2 hours

Table 2.1 Automated settings for the dehydration of tissue using the Leica-TP 1020 tissue

Treatment	Duration
Xylene I	10 minutes
Xylene II	10 minutes
100% ethanol	3 minutes
90% ethanol	3 minutes
80% ethanol	3 minutes
70% ethanol	3 minutes

Table 2.2 Tissue rehydration for immunohistochemistry.

1^{O} antibody	Species	Dilution	Incubation	Biotinylated antibody	Dilution
GFAP (DAKO, US)	Mouse	1:5000	Over-night	Goat anti mouse-HRP	1:250
HSPB5 (Abcam, UK)		1:250			
IBA1 (Abcam, UK)		1:500			

Table 2.3 Primary and secondary antibodies used for immunohistochemistry analysis.

2.3.6 Myelin analysis

Biochemical analysis of white-matter was achieved by sub-fractionation of brain homogenates to enrich for myelin fraction relative to non-myelin fractions. The sub-fractionation was done using a modified protocol from a paper by Kim and Pfeiffer (2000) (see figure 2.2). All steps were carried out at 4^0C. Two wild-type adult mice brains (cortex, cerebellum, brain-stem) (≈1g) were homogenised in a glass Teflon homogeniser in 5 ml homogenisation buffer (0.32M Sucrose, 0.1mM $CaCl_2$, 1mM $MgCl_2$, Protease inhibitor cocktail). The homogenate was brought to a final sucrose concentration of 1.25M by adding 9.5ml 2M Sucrose and 4.11ml 0.1mM $CaCl_2$ and then overlaid with 1M sucrose 0.1mM $CaCl_2$. The 1M sucrose was overlaid with homogenisation buffer and the resulting sucrose gradient was carefully balanced and ultra-centrifuged at 24 000 rpm (SW-28, 141 000g; Beckman) for 3 hours. Floating myelin was collected at the top phase of the homogenisation buffer. To wash off sucrose the myelin fraction was re-suspended in phosphate-buffered saline (PBS) and ultra-centrifuged at 19 000 rpm (SW-28, 30 000g; Beckman) for 30 minutes. The pellet was collected and re-suspended in 2ml PBS, sub-aliquoted into 200µl portions and stored at -20^0C. See figure 2.2 for illustration.

2.3.6.1 Detergent extraction of intra-membrane proteins

200µl crude myelin from 2.3.6 was extracted in 500µl 1% Trition-TX100 TNE buffer (25mM Tris HCl, 0.15M NaCl, 5mM EDTA, protease inhibitor cocktail). The mixture was then sub-aliquoted equally into three parts: one aliquot was retained as a representation "total protein" whilst the other two were incubated at either 4^0C or 37^0C for 30 minutes. The incubated extracts were then centrifuged at 13 000 x g (Heraeus #7593, Sorval) at 4^0C for 10 minutes to produce a detergent insoluble pellet and a detergent soluble fraction. The detergent insoluble pellet was re-suspended in equal volume 2% SDS to that of the soluble fraction, so as to allow comparison of the relative protein amounts in each sample. All samples were then stored in sample buffer (62.5mM Tris-HCl (ph6.8), 2% SDS, 10% glycerol, 5% 2-mercaptoethanol, 0.000625% Bromophenol Blue) (see figure 2.3A).

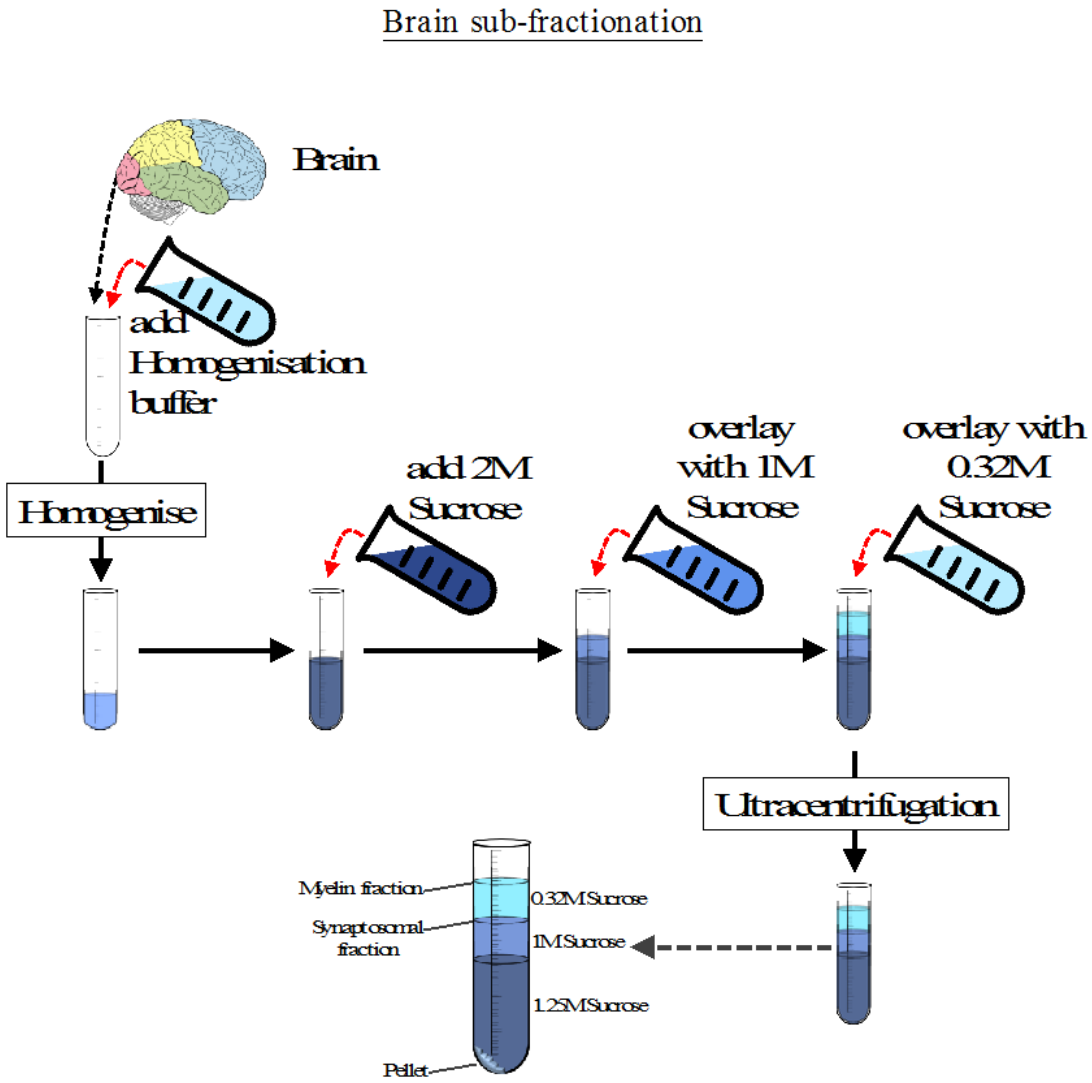

Figure 2.2 Brain sub-fractionation.

Schematic of brain sub-fractionation to enrich for myelin. 2 wild type brains (cortex, cerebellum, brain-stem) were pooled and homogenised in 5ml of homogenisation buffer. 9.5ml of 2M sucrose were added to the mixture to bring the sucrose to a final concentration of 1.25M sucrose. The 1.25M sucrose solution was overlaid with 1M sucrose solution, following which; the 1.25M sucrose solution was overlaid with 0.32M sucrose. The gradient was ultracentrifuged to create a pellet, synaptosomal and myelin fraction. Modified from Kim and Pfeiffer (2000).

2.3.6.2 pH partitioning of cytoskeletal proteins

200µl crude myelin from 2.3.6 was thawed and sub-aliquoted equally into three parts: one aliquot was retained as a representation of "total protein" and was re-suspended in 1% Trition-TX100 TNE buffer (pH 7.2) (see illustration in figure 2.3B). The other two aliquots were extracted in TNE buffered either at pH6 or at pH8 and incubated at 4^0C for 1 hour. Samples were then centrifuged at 100 000 x g (TLA-55, Beckman) for 1 hour to produce a detergent insoluble pellet and a detergent soluble fraction. The detergent insoluble pellet was re-suspended in equal volume PBS to that of the soluble fraction, and then all three samples were solubilised in sample buffer (see figure 2.3B).

2.3.6.3 High salt protein extraction of membrane proteins

200µl crude myelin was thawed and extracted by alkaline or high-salt extraction with either 100mM Na_2CO_3 ((pH11.5) (+ protease inhibitor cocktail)) or 1M NaCl ((pH7.4) + protease inhibitor cocktail), respectively (see illustration in figure 2.3C). Mixtures were sub-aliquoted equally into three parts: one aliquot was retained as a measure of total protein, the other aliquot was used to extract soluble and insoluble components by incubating at 4^0C for 1 hour and centrifuging at 100 000 x g (TLA-55, Beckman) for 1 hour to produce an insoluble pellet and a soluble fraction. The third aliquot (only present in NaCl treated condition) was subjected to proteinase K (2 µg/ml) treatment at 37^0C for 1 hour and then was centrifuged at 100 000 x g (TLA-55, Beckman) for 1 hour to produce an insoluble pellet and a soluble fraction. All samples were re-suspended in equal volumes of 2%SDS. Samples were stored in sample buffer. See figure 2.3C for illustration.

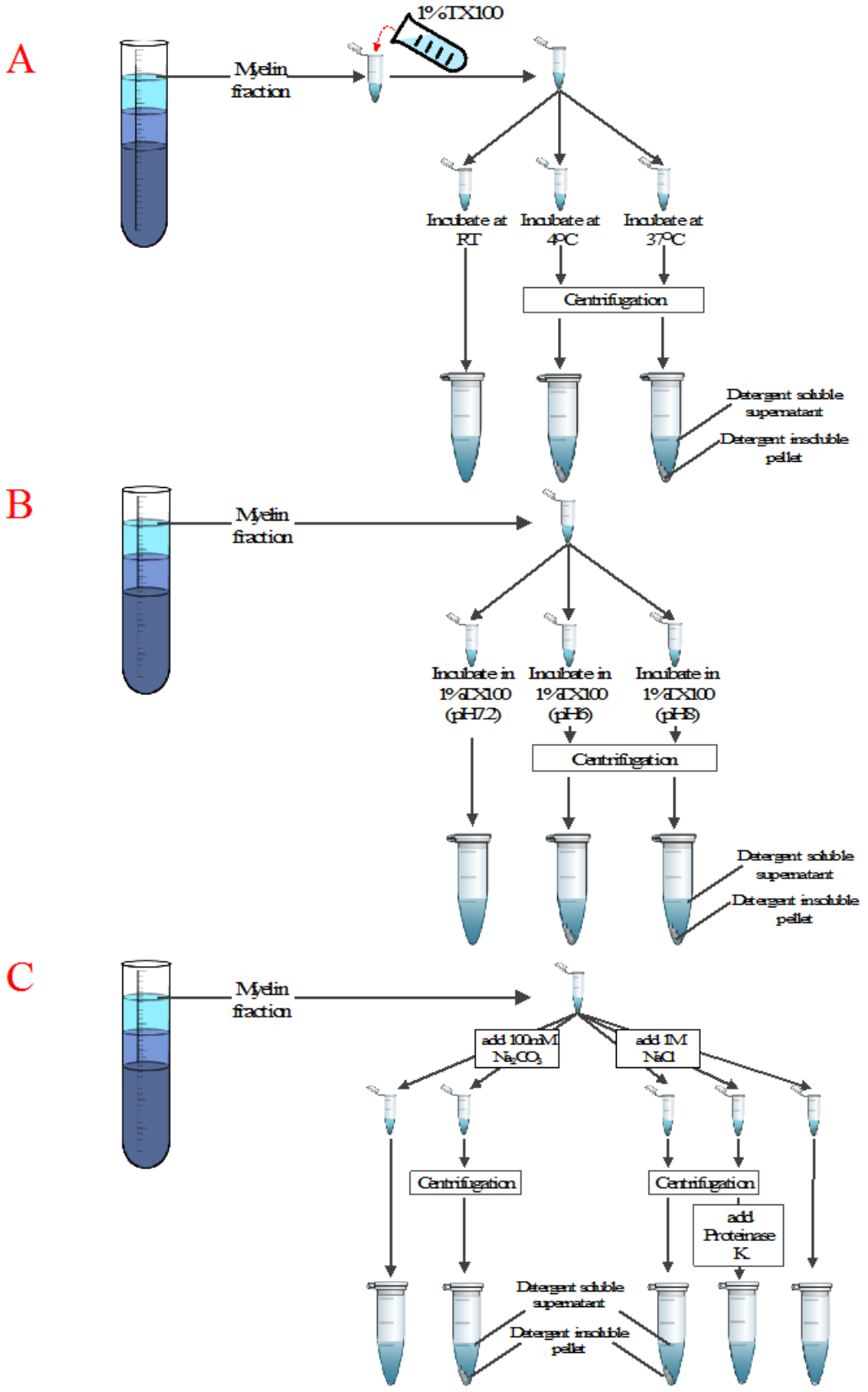

Figure 2.3 Schematic of myelin analysis experiments.
(A) Detergent extraction of intra-membrane proteins (2.3.6.1), modified from Kim et al (2000) (B) pH partitioning of cytoskeletal elements (2.3.6.2), modified from Phillips (2001). (C) High-salt extraction of membrane proteins (2.5.6.3).

2.3.7 SDS-PAGE and Western Blotting

Total protein concentration was assessed using a Bio-Rad D_C protein assay kit (Bio-Rad, UK), as per manufacturer's instruction. All samples were diluted to a final concentration of 4mg/ml in 5x sample buffer (250mM TRIS-HCl (pH6.8), 10% SDS, 30% Glycerol, 5% β-mercapto-ethanol, 0.02% bromo-phenol blue) and run on a polyacrylamide gel composed of 5% stacking gel and 12.5% resolving gel in 1x Laemmli buffer (5mM TRIS (pH8.3), 192mM Glycine, 0.1% SDS) using the Bio-Rad protein gel system (Bio-Rad, UK). Equivalent loading was checked by coomassie staining (Sigma Aldrich, UK), as per manufacturer's instructions. Coomassie membranes were scanned at 700nm using the Odyssey infrared imaging scanner (LiCOR, UK) and quantified using Odyssey software v1.2 (LiCOR, UK). Proteins were transferred to nitrocellulose membrane (Amersham, UK) overnight (16-18hrs) at 4°C in transfer buffer (1x Laemmli buffer, 20% (v/v) Methanol). Membranes were blocked with 4% non-fat milk (TESCO, UK) and incubated in primary antibodies (table 2.3). Membranes were washed in TRIS-buffered saline with 0.05% tween (TBS-T) (pH7.2) and incubated in secondary antibodies (table 2.5). Membranes were visualised using the Odyssey infrared imaging scanner (LiCOR, UK), as per manufacturer's instructions.

2.3.7.1 Statistical analysis

Immunoreactivity was measured by quantifying pixel intensity using Odyssey software v1.2 (LiCOR, UK). The immunoreactivity observed on each nitrocellulose membrane was normalised to counterpart coomassie gels that were loaded and run concurrently. Values and graphs were compiled and statistically analysed using GraphPad Prism v6 (GraphPad Software, US). Data was statistically analysed using an unpaired T-test and as the sample sizes were very small, Welch's correction was applied to the data in order to take into account differences in standard deviation.

Primary antibody	Originating species	Dilution	Secondary antibody	Dilution
CNP (Abcam, UK)		1:1000		
MBP (Abcam, UK)	Mouse	1:500	anti-mouse IR (Invitrogen, UK)	1:1000
HSPB5 (Abcam, UK)		1:500		

Table 2.4 Primary and secondary antibodies used to analyse extracted myelin.

2.4 Results

2.4.1 HSPB5 expression

2.4.1.1 *In silico* analysis of HSPB5 cellular localisation

High-throughput gene expression profiling data from an mRNA microarray database shows the tissue-specific pattern of HSPB5 mRNA expression in mice (figure 2.4). The data shows that in the peripheral nervous system (PNS), the predominant anatomical expression of HSPB5 mRNA is in cardiac, placenta and skeletal muscle tissue (figure 2.4A). There is also a high expression of HSPB5 in the lens of the eye, the iris and the eye-cup (figure 2.4B). Regions of the brain that showed high expression of HSPB5 mRNA were the cerebellum, hippocampus and the hypothalamus (figure 2.4B). Out of the immune cells measured, mRNA expression shows microglia express almost 100fold more HSPB5 mRNA than B-cells or $CD4^+$ and $CD8^+$ T-cells (figure 2.4B). The database did not have microarray data on astrocyte or oligodendrocyte expression of HSPB5.

2.4.1.2 Biochemical analysis of HSPB5 localisation

Protein expression of HSPB5 in the CNS was assessed by sub-cellular fractionation of brain homogenate across a sucrose gradient and western blotting. Centrifugation of brain homogenate led to fractionation of the homogenate into separate fractions, namely, myelin, synaptosomal, and pellet fractions (see figure 2.2). Western blot analysis of the subsequent brain fractions highlights enrichment of CNP and HSPB5 in the myelin fraction, whilst non-myelin proteins such as GFAP are de-enriched in the myelin fraction (figure 2.5A). Detergent extraction has been used to operationally define sub-membranous proteins, membrane-bound and scaffold-bound proteins. Extraction of the myelin fraction at either pH6 or pH8 reveals whether HSPB5 is associated with cytoskeletal proteins, at pH6 cytoskeletal associated proteins are insoluble, at pH8 they are soluble (figure 2.5B). The results show that HSPB5 is found equally partitioned in both the pH6 and the pH8 fractions, suggesting two pools of HSPB5 exist- an insoluble faction (associated with cytoskeletal components) and a soluble fraction (cytosolic localisation) (figure 2.5B).

Washing myelin with sodium bicarbonate (Na_2CO_3) or sodium chloride (NaCl) disrupts non-covalent, electrostatic interactions that associate peripheral membrane proteins to the membrane: if HSPB5 is associated to such a protein, the wash will strip the protein off the membrane, resulting in HSPB5 immuno-reactivity in the supernatant. If HSPB5 is not bound to a membrane protein, the washes will not have an effect, and thus, HSPB5 immuno-reactivity will be found in the pellet fraction. The results from the Na_2CO_3 wash support the presence of two pools of HSPB5 by showing immunoreactivity in both the pellet fraction and the supernatant fraction i.e. there is a pool of HSPB5 that is not attached to membrane proteins (pellet) and there is another pool that is stripped from membrane protein and ends up in the supernatant; this signature is similar to compact myelin protein CNP (figure 2.5C).

The 1M NaCl wash, which is much "harsher" than the Na_2CO_3 wash, shows increased HSPB5 immuno-reactivity in the supernatant fraction and no change in the pellet fraction (figure 2.5C). Both results suggest that there is a pool of HSPB5 that is attached to elements of membrane-bound proteins (supernatant) and there is another pool of HSPB5 that is not attached to such proteins (pellet).

To add further insight to these distinct pools of HSPB5, we extracted the myelin proteins with Triton (TX-100) at either 4^0C or 37^0C. At 4^0C, lipid raft associated proteins are insoluble, whilst at 37^0C they become soluble. HSPB5 does not show the characteristic of lipid-raft associated proteins and shows similar characteristics to CNP (figure 2.5D) in that at 40^0C, 69% of CNP, a cytoplasmic peripheral membrane protein, is found in the detergent soluble fraction whilst 16% is found in the insoluble fraction. The remaining 15% of total protein is unaccounted for and can potentially be explained by protein loss during experimental steps. At 37^OC, the detergent soluble fraction increases by 12%; an insoluble fraction however, still remains, thus suggesting two pools of CNP. For HSPB5, at 4^OC, 52% of HSPB5 was detected in the soluble fraction whilst 14% was located in the insoluble fraction. At 37^0C, there is an increased immunoreactivity of HSPB5 in the soluble fraction.

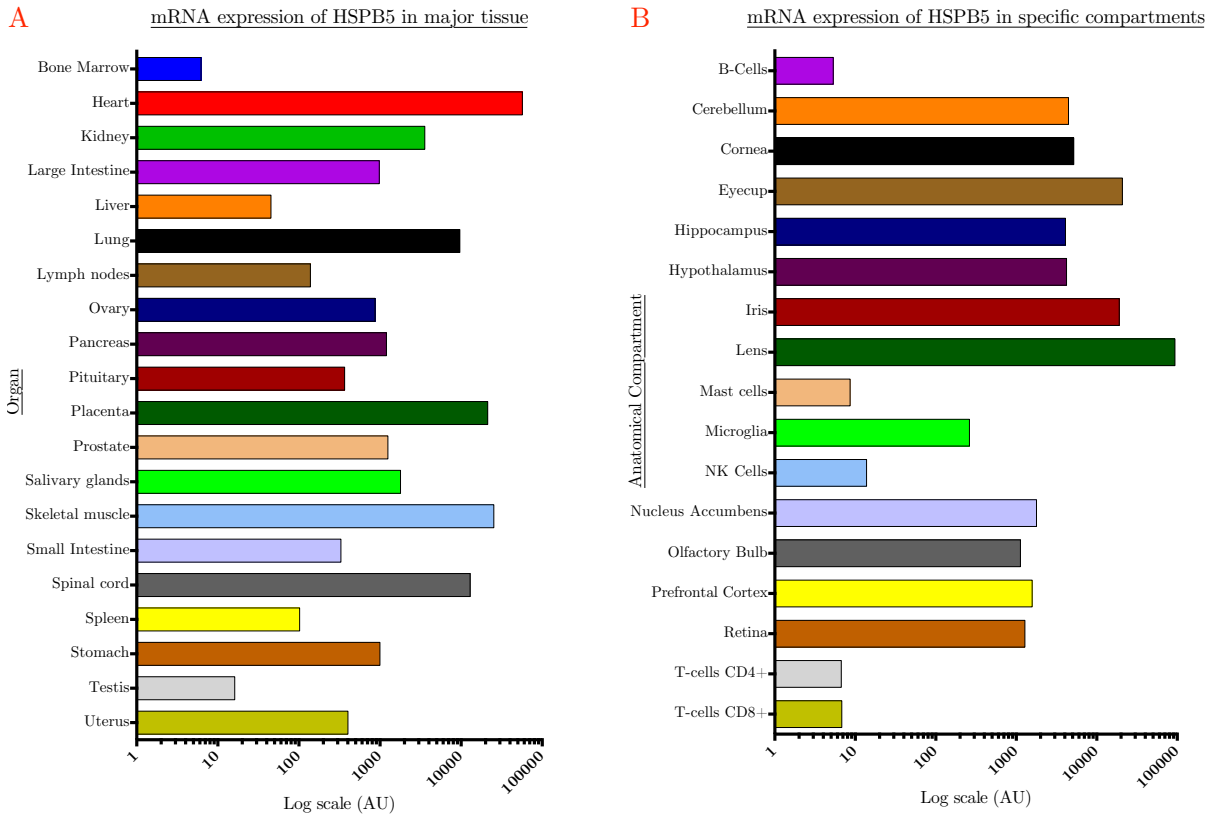

Figure 2.4 High-density oligonucleotide array, high-throughput gene expression of HSPB5 expression.

Affymetrix GeneChip microarray analysis of HSPB5 expression in major tissue profiled from 191 mice. (A) HSPB5 mRNA expression in major tissue in the PNS. (B) HSPB5 mRNA expression in specific compartments. For the probe-level data obtained from GeneChips, the perfect-match values were background-corrected and then normalized by the GCRMA method (see methods). Raw data was obtained from GeneAtlas MOE430 gcrma (Su et al., 2004).

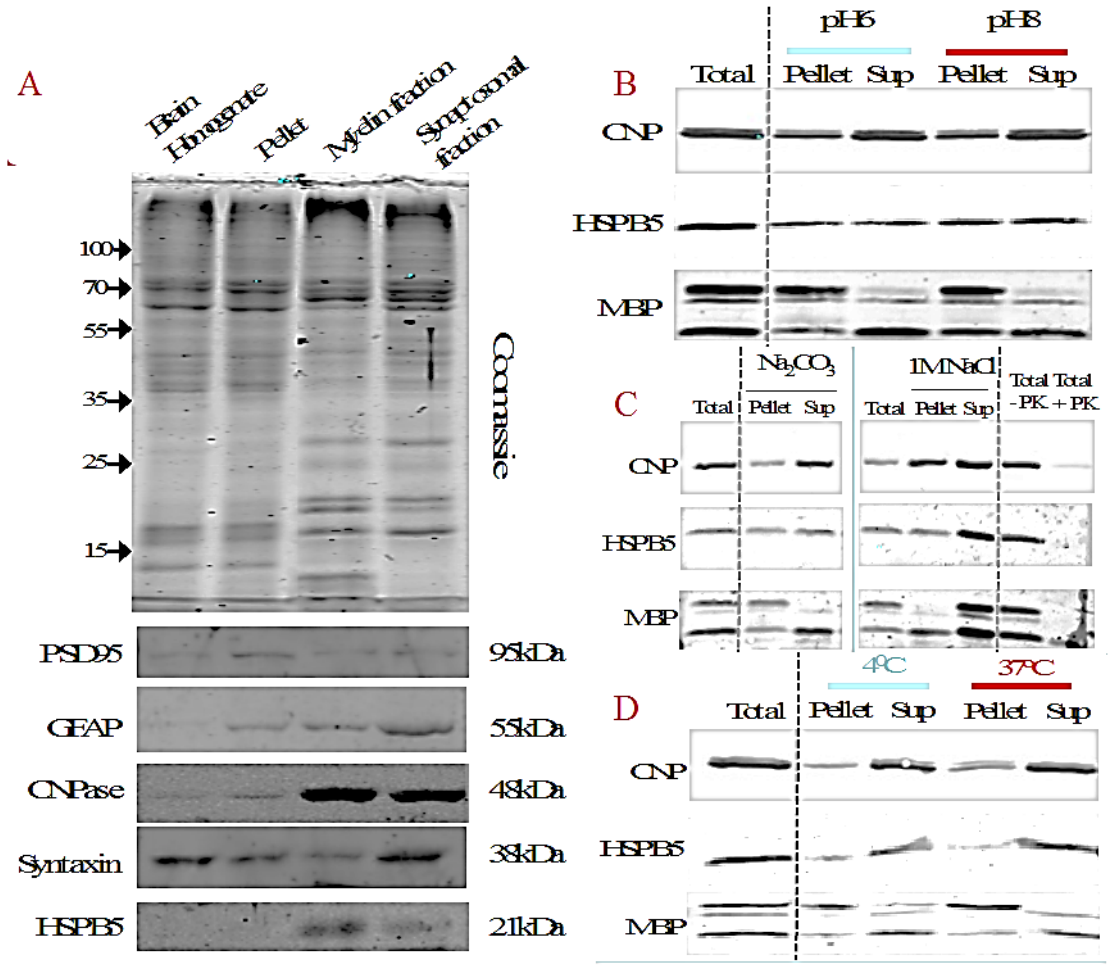

Figure 2.5 Biochemical analysis of HSPB5 localisation.
(A) Coomassie gel showing equally loaded samples (20µg) of brain homogenate, pellet, myelin and synaptosomal fractions. Western blots show the enrichments of certain proteins in specific compartments: as compared to "brain homogenate", PSD95 and Syntaxin are de-enriched in the myelin fraction and are enriched in the synaptosomal fraction (as expected). GFAP, CNPase and HSPB5 show enrichment in the myelin fraction. CNP and HSPB5 are localised in myelin and therefore should be enriched in this compartment; GFAP however should not be enriched in this compartment. GFAPs enrichment in the myelin fraction is likely due to contamination of that that fraction during pipetting due to close proximity of myelin fraction and synaptosomal fraction (see figure 2.2); similarly, the enrichment of CNPase in the synaptosomal fraction is also due to contamination as CNPase should not be enriched in this compartment. (B) pH partitioning of cytoskeletal elements/specialisation (see 2.4.1.2 for biochemical explanation). (C) High salt wash to determine whether HSPB5 is attached to membrane bound proteins (see 2.4.1.2 for biochemical explanation). (D) Triton extraction of soluble proteins at different temperatures to determine whether HSPB5 is incorporated in lipid rafts.

2.4.2 Behavioural characterisation of HSPB5 knock out mice

In the 129Sv mouse background, HSPB5 KO mice show phenotypic differences from wild type mice from 40 weeks of age (Brady et al., 2001). In our laboratory we use C57Bl/6 mice; we therefore investigate whether there are any phenotypic differences of HSPB5 KO mice in this background. Although our breeding plan was set up to generate 1:2:1 ratio of wild type (WT), heterozygous (HET) and knock out (KO) mice, the breeding plan did not generate this ratio: there was a distinct shortage of WT littermates. Instead of using non-littermate WT animals, our comparison is done with littermate HET animals, which show ≈50% HSPB5 expression (figure 2.5 supplementary). As these animals have ≈50% the amount of HSPB5 and they do not appear to suffer from haploid insufficiency, we decided that they would be sufficient to discriminate any phenotypic change from the HSPB5 KO mice, and therefore we used the HET animals as a suitable internal control.

2.4.2.1 Total cohort analysis

Analysis of HSPB5 KO mice across a 10-month time course shows that the animals do not differ significantly from HET animals in key tasks examined (figure 2.6 and 2.7). Animal weight shows that all the animals, regardless of genotype, gain weight as they age (figure 2.6A). There is also no significant difference ($p>0.05$) between the HET and KO mice at all the time points observed (figure 2.6A), however at the 10 month time-point, there appears to be a trend towards lower weight in KO animals ($p>0.05$). It is important to be mindful that given larger n-numbers, KO animals may have exhibited significantly less weight at this time-point.

During the open-field test, the results show that there are no significant differences ($p>0.05$) in the distance traveled by the animals across different ages and between genotypes (figure 2.6B). Similarly, the time spent resting during the open-field exercise does not show significant difference ($p>0.05$) across different ages and between genotypes (figure 2.6C).

Several other behavioural tests showed no significant difference in the performance of KO animals as compared to HET animals across different ages (data not shown). Although no differences were observed between genotypes, what is increasingly apparent when data-points are plotted individually, is that gender-linked differences may affect performance: focusing specifically on the oldest group of mice (as this age group encompasses our subsequent experimental timeline), it is evident that there is a bimodal distribution in how the animals perform key tests (figure 2.7). In open field tests, distance travelled and time spent resting, there is a trend for female mice to travel the least distance and to spend the most time resting ($p>0.05$) (figure 2.7B, C). In the inverted mesh test, a strength test, there is also discernible gender bias ($p>0.05$) with female animals holding on longer than male animals (figure 2.7D). These results therefore highlight the need to segregate animals on the basis of gender for subsequent experiments.

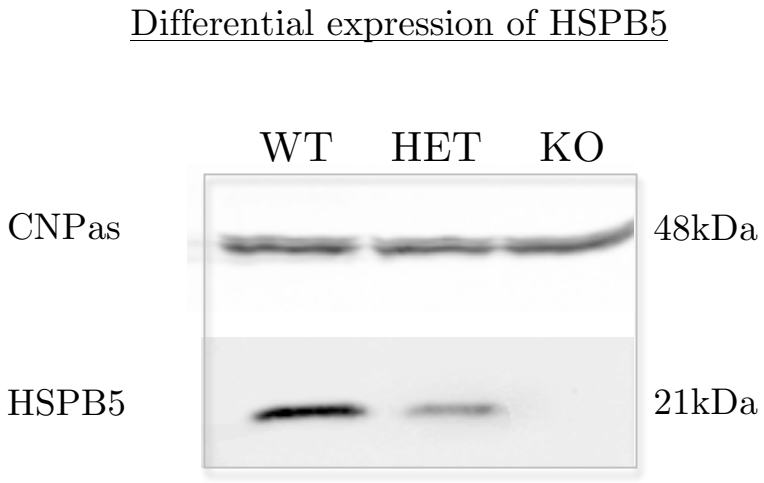

Figure 2.5 Supplementary: Western blots of myelin from WT, HET and KO animals. Equal loading confirmed with CNPase blot. Robust HSPB5 immunoreactivity in WT. HET animals show modest HSPB5 immunoreactivity. There is no immunoreactivity in KO animals.

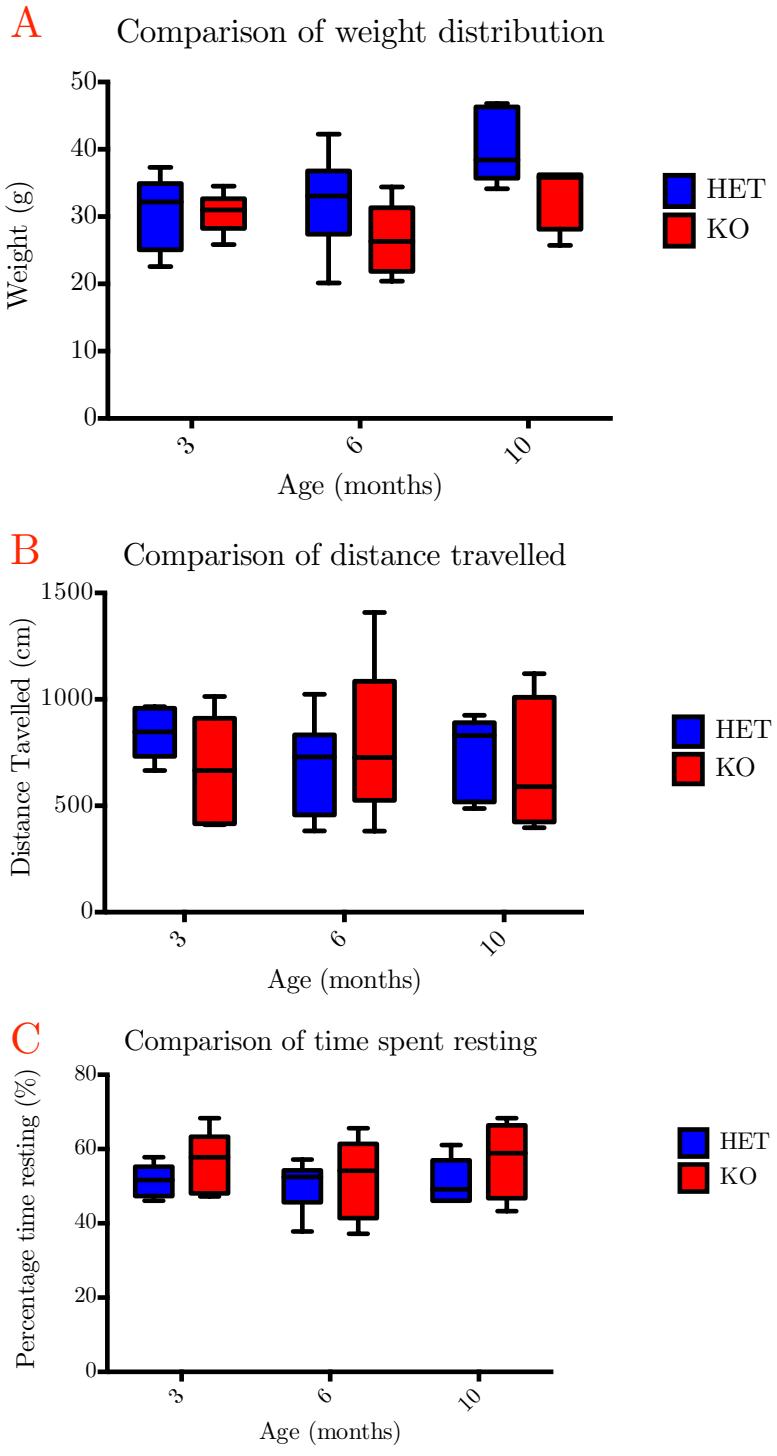

Figure 2.6 Weight characterisation of heterozygous and knock out mice across 3 different time points.

(A) Assessment of weight distribution between the different genotypes. (B) Open field test assessing the total distance travelled over 3 minutes. (C) Evaluation of the time spent resting as a percentage of 3 minutes. n=6 for HET animals and n=4 for KO animals. Abbreviations: HET, heterozygous; KO, knock out.

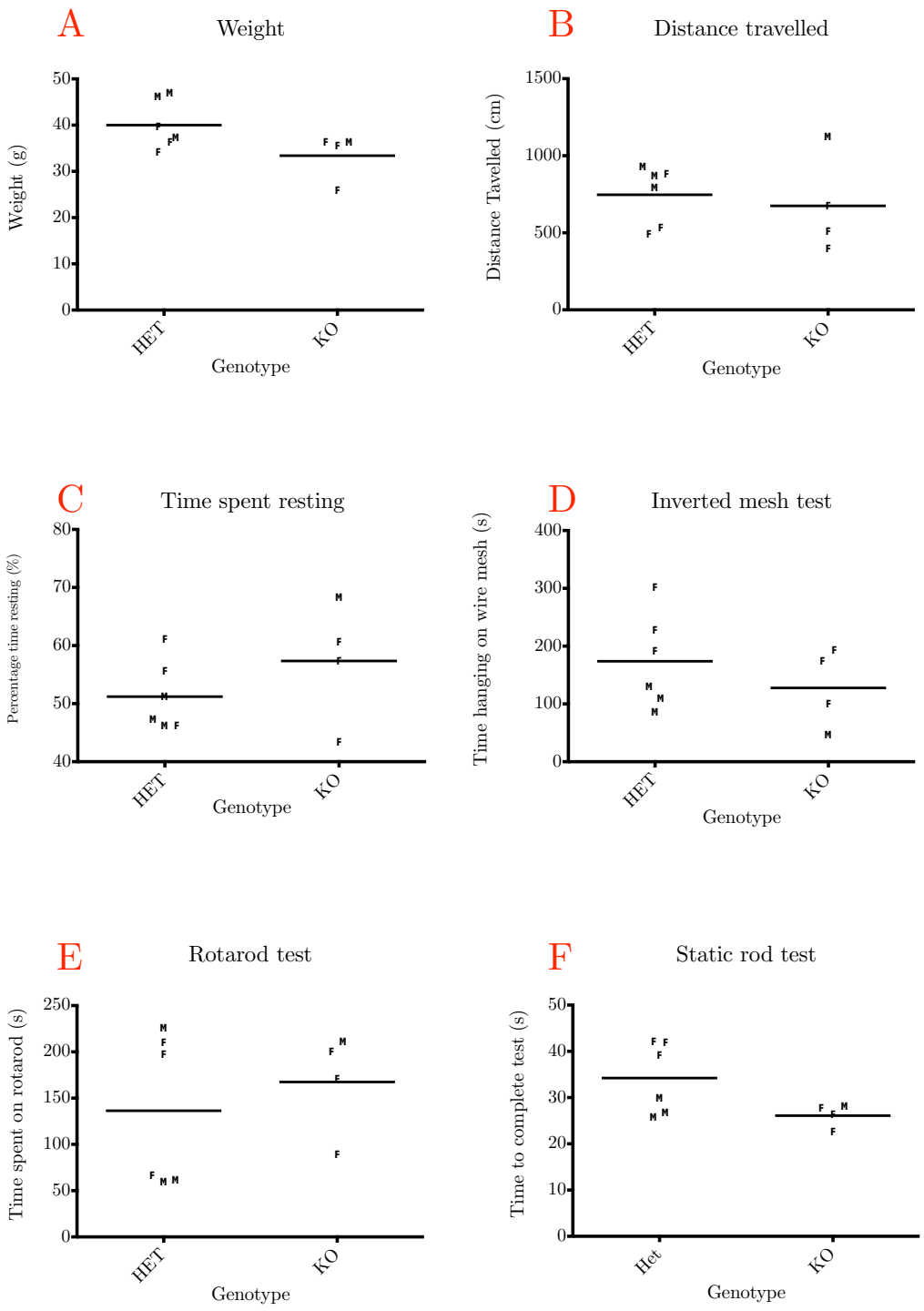

Figure 2.7 Characterisation of gender bias in behavioural tasks. "F" denotes Female animals and "M" denotes Male animals. (A) Characterisation of weight distribution. (B) Characterisation of total distance travelled over 3 minutes. (C) Evaluation of the time spent resting as a percentage of 3 minutes. (D) Characterisation of time spent hanging upside-down on wire mesh. (E) Time spent on rotarod machine. (F) Time spent to complete static rod test. n=6 for HET animals and n=4 for KO animals. Abbreviations: HET, heterozygous; KO, knock out.

2.4.2.2 Immunohistochemical characterisation of HSPB5 knock out mice

In silico microarray data showed high HSPB5 expression in the cerebellum, hippocampus and hypothalamus (figure 2.4). Immunohistochemical analysis of HSPB5 will focus only on the hippocampus, primarily because this region is a key region analysed in subsequent experiments (chapter 4).

2.4.2.3 Localisation of HSPB5 in the hippocampus

Following extensive titration and optimisation of the HSPB5 antibody (data not shown), Hippocampal sections from HSPB5 HET and KO mice at 3, 6, and 10 months of age were stained with HSPB5. The sections show discrete HSPB5 staining in the corpus callosum and the fimbria (black arrows) of HET animals but no staining in the KO mice (figure 2.8A). Both the corpus callosum and the fimbria are rich in white-matter i.e. oligodendrocytes; there is very little HSPB5 staining in areas with high neuronal counts such as the stratum oriens (SOr), stratum pyramidale (SPy), or the stratum radiatum (SRad) (figure 2.8A), suggesting little or no HSPB5 localisation in cells other than oligodendrocytes. In the HET animals, a magnified view of the corpus callosum shows HSPB5 staining in cells that are arranged in rows/tandem (black arrows) (figure 2.8B), with the cytology of oligodendrocytes (Cerghet et al., 2006). There is also some staining of cells that are not arranged in rows/tandem which could either be isolated oligodendrocytes or astrocytes (figure 2.8B).

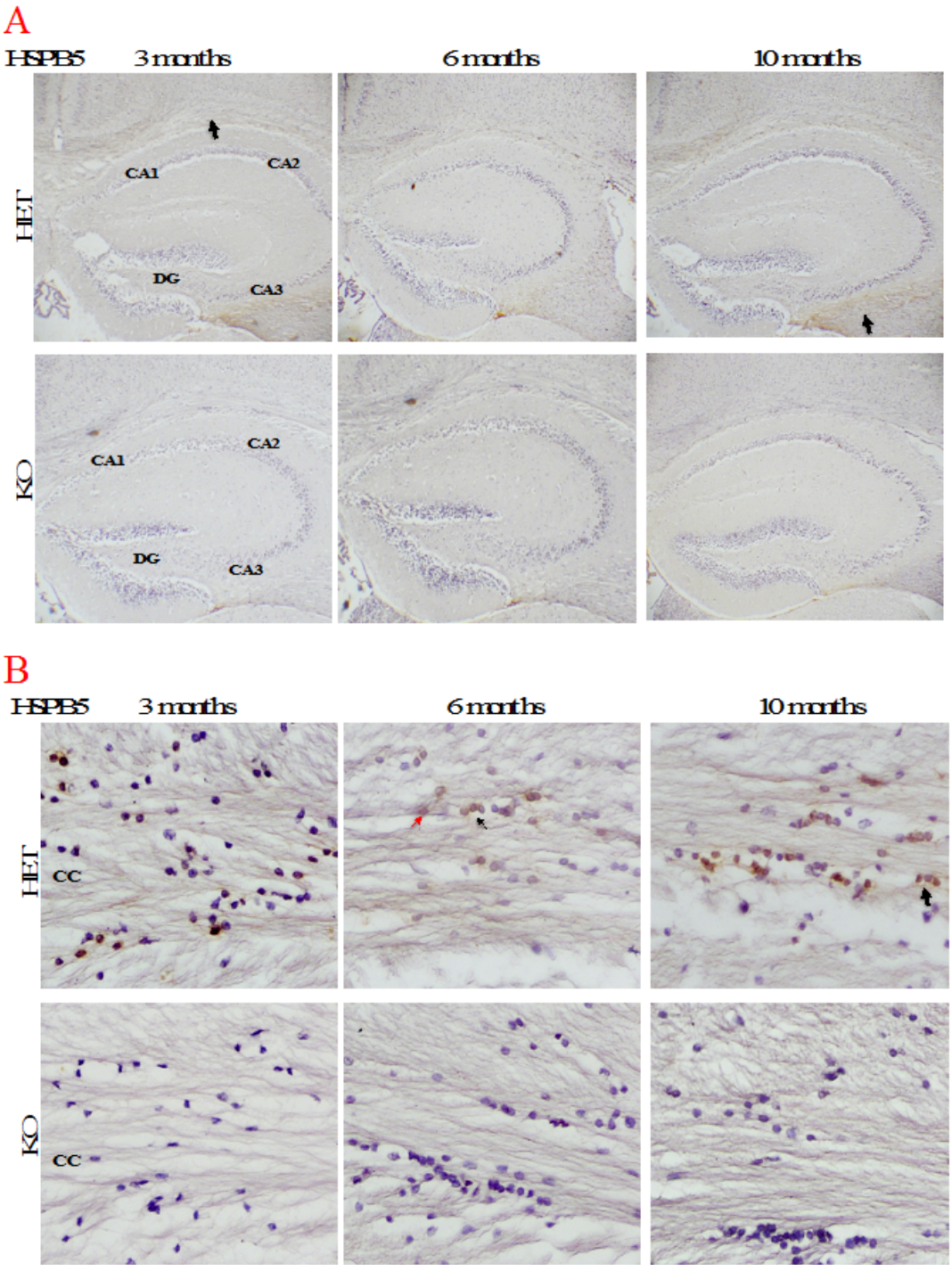

Figure 2.8 HSPB5 localisation in the hippocampus in 3, 6, and 10 month-old animals.

Sections stained with HSPB5 (brown staining) and haematoxylin (blue staining). (A) HSPB5 staining highlighting the CA1, CA2 CA3 and the DG. (B) HSPB5 staining highlighting the CC. For staining n=3 female mice/time point we used. Representative images are shown. Black arrows highlight localisation of HSPB5 in presumed oligodendrocyte cells. Red arrow shows HSPB5 staining in non-oligodendrocyte cell type. Abbreviation: CA1, Cornu Ammonis area 1; CA2, Cornu Ammonis area 2; CA3, Cornu Ammonis area 3; CC, Corpus callosum; DG, Dentate gyrus; HET, heterozygous; KO, knock out. Scale bars: (A) 250µm (B) 50µm.

2.4.2.4 Localisation of astrocytes in the hippocampus

Reactive gliosis, i.e., induced expression of astrocytes and microglia, is often indicative of neuronal dysfunction (Maragakis et al., 2006). Gliosis can precede or respond to degeneration.

In both HET and KO animals of all ages, the results show well organised, and non-overlapping distribution of astrocytes within the hippocampus (figure 2.9). The intensity of staining is comparable across the different ages and between genotypes, suggesting that state of activation in these astrocytes is similar.

2.4.2.5 Localisation of microglia in the hippocampus

Microglia also show nondescript staining in the corpus callosum (CC), stratum oriens (SOr) (figure 2.9) as well as other areas of the hippocampus (data not shown). The microglial staining is comparable between the HET and KO animals of all ages.

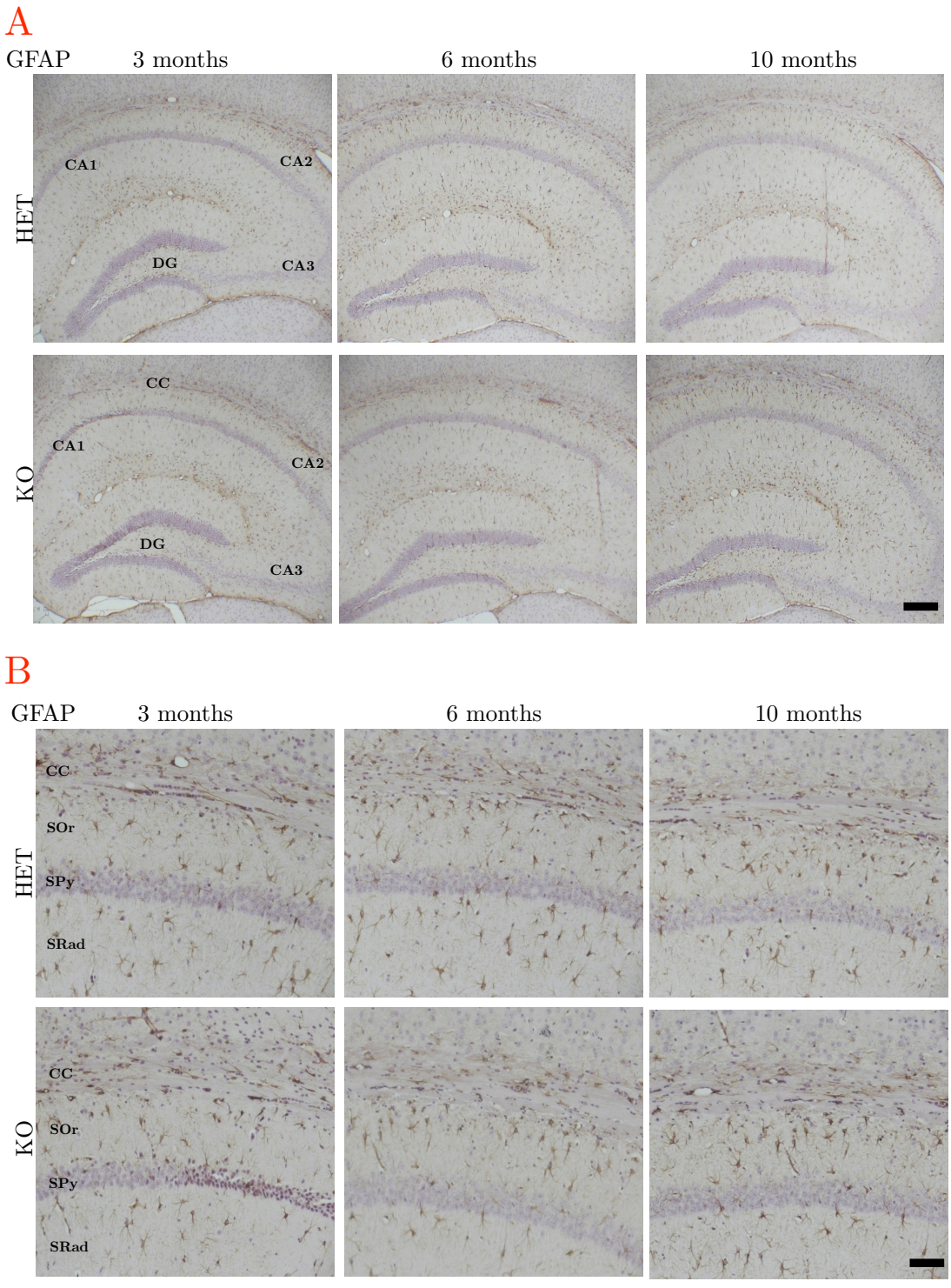

Figure 2.9 GFAP expression in the hippocampus in 3, 6, and 10 month-old animals.

Sections stained with GFAP (brown staining) and haematoxylin (blue staining). (A) GFAP staining highlighting the CA1, CA2 CA3 and the DG. (B) GFAP staining highlighting the CC, SOr, SPy and SRad. For staining n=3 female mice/time point we used. Representative images are shown. Abbreviation: CA1, Cornu Ammonis area 1; CA2, Cornu Ammonis area 2; CA3, Cornu Ammonis area 3; CC, Corpus callosum; DG, Dentate gyrus; HET, heterozygous; KO, knock out; SOr, Stratum oriens; SPy, Stratum pyramidale; SRad, Stratum radiatum. Scale bars: (A) 200µm (B) 50µm.

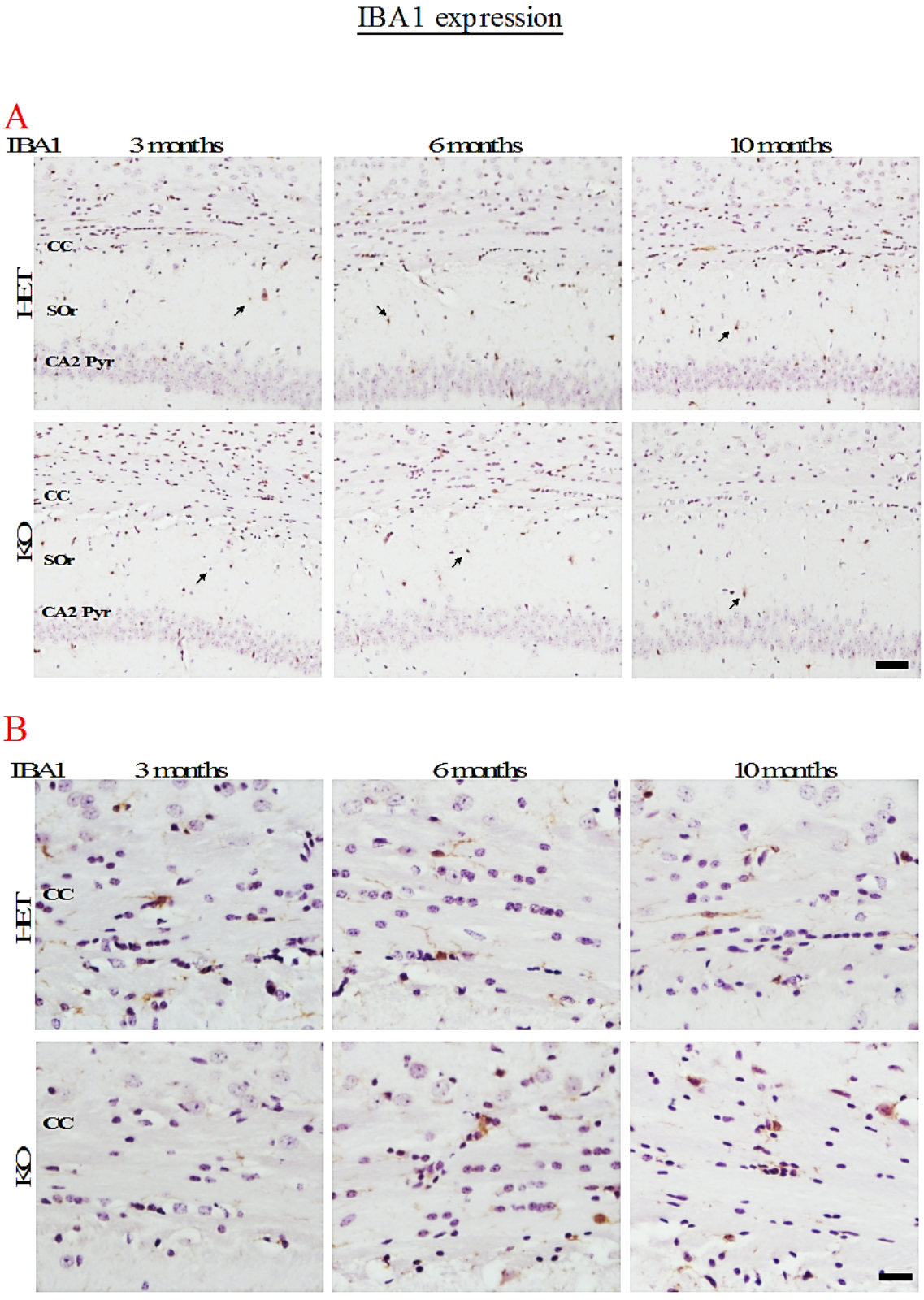

Figure 2.10 IBA1 expression in the hippocampus in 3, 6, and 10 month-old animals.

Sections stained with IBA1 (brown staining) and haematoxylin (blue staining). (A) IBA1 staining highlighting the CC, SOr, and the CA2 Pyr. (B) GFAP staining highlighting the CC, SOr, SPy and SRad. For staining involved n=3 female mice/time point were used. Representative images are shown. Abbreviation: CA2 Pyr, Cornu Ammonis area 2 pyramidale cells; CC, Corpus callosum; SOr, Stratum oriens; HET, heterozygous; KO, knock out. Scale bars (A) 100µm (B) 50µm.

2.5 Discussion

2.5.1 Functional characterisation of HSPB5 KO animals using biochemical expression and age-related phenotypes

Previous characterisation of HSPB5 KO mice using 129Sv mice strain, found that HSPB5 KO mice exhibited severe weakening muscles, lost significant weight, and developed hunched posture (kyphosis) from 40 weeks of age (10months) onwards (Brady et al., 2001). We investigated these phenotypes in our mice and found that on a C57Bl/6 background, HSPB5 KO mice were not phenotypically different from HSPB5 HET animals. The results also highlight possible gender differences in performance of behavioural tests. Although these differences were not significant, it is possible that such gender differences could skew and influence larger sets of data, as such, to eliminate confounding variables and reduce noise in the data, future experiments will be confined to one gender. Immunohistochemical analysis did not show any cellular and morphological difference between HET and KO animals.

2.5.2 HSPB5's potential role in oligodendrocytes

Characterisation of HSPB5 localisation showed HSPB5 to be enriched in the myelin fraction (figure 2.6). Immunohistochemistry supports this by showing HSPB5 to be localised in white-matter rich regions of the brain (figure 2.8). Our observations are supported by proteomic analysis that identifies HSPB5 as a myelin protein (Jahn et al., 2009), and immunohistochemistry further supports this by showing that HSPB5 colocalises with the major myelin protein 2',3'-Cyclic-nucleotide 3'-phosphodiesterase (CNP) (Quraishe, 2010). Co-localisation with CNP suggests that HSPB5 is localised in a sub-compartment of myelin known as non-compact myelin. Our results highlight that within myelin, HSPB5 is present in two pools- a cytoskeletal/ membrane-bound pool and a cytosolic pool (figure 2.6). The physiological role of two pools of HSPB5 is uncertain, however, as HSPB5 is induced by oligodendrocytes during heat-stress, its role is thought to be instrumental in oligodendrocyte function and myelin formation (Goldbaum et al., 2001). Even though our results do not support this, HSPB5's localisation in oligodendrocytes may still have undetected roles because oligodendrocytes are inherently vulnerable to protein misfolding and oxidative stress (see following section). Our

experiments may just not have been sensitive enough or effects may have been compensated (e.g. up regulation of other HSP's).

2.5.2.1 HSPB5 may have an important protein folding role in oligodendrocytes

Myelin is composed of 75% lipid and 25% protein (Jahn et al., 2009), however, formation of myelin is much more complicated than simple amalgamation of lipid and protein; the lipid portion of myelin is an intricate 2:2:1:1 balance of cholesterol, phospholipid, galactolipid and plasmalogen (Jahn et al., 2009). The protein portion is composed of at least 342 functionally distinct proteins that, together with the lipids, form functional domains that promote spiraling, lateral growth, and compaction of myelin for correct axonal insulation (Baumann et al., 2001). It is estimated that at peak myelination, an oligodendrocyte produces greater than 10 000 μm^2 of myelin per day (Pfeiffer et al., 1993), which, at maturity, equates to 100x the weight of the oligodendrocyte's cell body (Connor et al., 1996). Myelination therefore requires extensive lipid and protein sorting, trafficking and targeting, which makes oligodendrocytes vulnerable to the slightest aberrations in cytoskeleton organisation or protein quality control. The biosynthetic pathway of creating myelin is mediated by the endoplasmic reticulum (ER); in oligodendrocytes, it is thought that the operational capacity of the ER pathway is at full capacity and thus there is a bottleneck in protein production (Bradl et al., 1999; Bauer et al., 2002). This bottleneck means that the slightest changes in protein structure can disrupt the whole system, resulting in protein misfolding and several down-stream effects. HSPB5, being a molecular chaperone, is therefore likely to be an integral part of folding the vast quantities of proteins synthesised by oligodendrocytes. Given the extensive cytoskeletal network in oligodendrocytes and given HSPB5's cytoskeleton stabilising role, it is likely that HSPB5 also mediates an important cytoskeleton-stabilising role in oligodendrocytes (chapter 1). It is tempting to conclude that reduced expression of HSPB5 may impair oligodendrocytes and myelin production, however, as no studies have been carried out looking at the effect of reduced expression of HSPB5 on myelin ultrastructure, it is not possible to make such a conclusion.

2.5.2.2 HSPB5 may attenuate oxidative stress in oligodendrocytes

In addition to operational and logistic problems oligodendrocytes face, the cell type is also inherently vulnerable to oxidative stress due to the biosynthetic pathway of making and maintaining myelin; myelin synthesis requires myelin synthesising enzymes that use oxidised iron (Fe^{2+}) as a co-factor (Connor et al., 1996). Fe^{2+}, whilst important for myelin formation, is inherently unstable and thus is highly reactive with stable elements, a process that creates free radicals (Connor et al., 1996). Myelin synthesis also requires consumption of large amounts of oxygen and adenosine triphosphate (ATP) (McTigue et al., 2008). Increased oxygen consumption creates reactive oxygen species (ROS) and increased ATP generation leads to the formation of hydrogen peroxide- a ROS-creating reagent (McTigue et al., 2008). These attributes contribute to oligodendrocytes having the highest ROS concentration of any cell in the brain (Thorburne et al., 1996). Elevated ROS is detrimental to oligodendrocytes because, not only can it induce protein misfolding, but it is thought to contribute to lipid peroxidation and thus modification of myelin structure (Braughler et al., 1986). HSPB5 may therefore be present in oligodendrocytes to ameliorate ROS production and reduce lipid peroxidation.

This may occur through HSPB5 sequestering free-radical-producing Fe^{2+} ions. Direct interaction of HSPB5 with Fe^{2+} has not been shown *in situ*, however, HSPB5 has been shown to interact with other divalent metal ions, such as, oxidised Copper (Cu^{2+}) and Zinc (Zn^{2+}), via the α-crystallin domain (Mainz et al., 2012). Cu^{2+} and Zn^{2+}, like Fe^{2+}, are inherently unstable and thus highly reactive with stable elements, creating free radicals in the process. Interaction of HSPB5 with Cu^{2+} has been shown to effectively sequester the divalent metal ion and thus reduces ROS production and any associated oxidative stress (Prabhu et al., 2011). It is therefore conceivable that HSPB5 may interact with Fe^{2+} in a similar manner to reduce Fe^{2+}-mediated ROS production, which prevents lipid peroxidation. HSPB5 may therefore be expressed selectively in oligodendrocytes to ameliorate oxidative stress and maintain myelin structure and function.

It is clear that HSPB5's physiological expression in oligodendrocytes is likely to be of some evolutionary advantage, its reduced expression in R6/2 mice therefore raises some interesting questions as to the viability of oligodendrocytes and or integrity of myelin following this reduced expression.

2.5.3 HSPB5 role in other CNS cells

In silico microarray analysis of HSPB5 expression showed that microglia express almost 100fold more HSPB5 mRNA than B-cells and $CD4^+$ and $CD8^+$ T-cells (figure 2.6). It therefore appears that HSPB5 may play crucial roles in cells other than oligodendrocytes. Studies show HSPB5 to be induced in neurons and astrocytes during Alzheimer's, Parkinson's and Prions disease (Iwaki et al., 1992; Shinohara, 1993; Renkawek et al., 1994; Braak et al., 2001). During heat-stress, induction of HSPB5 is protective (Wettstein et al., 2012) and thus it is inferred to be protective during neurodegeneration (Clark et al., 2000; Sun et al., 2005c).

In astrocytes, HSPB5 is thought to modulate expression of pro-inflammatory cytokines (Shao et al., 2013); this notion is supported by a growing body of evidence that suggests that, extracellular to oligodendrocytes, HSPB5 modulates inflammatory processes (section 1.3.5). Proof of concept studies highlight that exogenous addition of HSPB5 by either intra peritoneal (i.p) or intra venous (i.v) methods, results in diminished production of pro-inflammatory mediators, decrease activation of immune cells, and improved prognosis in a variety of conditions from stroke to ischemia and multiple sclerosis (van Noort et al., 2010; Arac et al., 2011; Klopstein et al., 2012); it is thought that HSPB5 has the ability to modulated inflammation via an uncharacterised intracellular mechanism (Shao et al., 2013) and an extracellular mechanism comprised of actively binding onto pro-inflammatory mediators (Rothbard et al., 2012). Whilst HSPB5's pleiotropic nature offers several interesting avenues for investigation, the remainder of this thesis will investigate and expand on HSPB5's role as a modulator of the inflammatory response so as to shed light onto the consequences of HSP5's reduced expression in R6/2 animals.

2.5.4 Conclusion

In conclusion, this chapter highlights a selective white-matter expression of HSPB5 with a distinct sub-cellular compartmentalisation that we assume to be a cytosolic pool of HSPB5 as well as a pool of HSPB5 that is bound to some specialisation (likely cytoskeletal components). We identify that the deficiency in HSPB5 and the confound in HSPB2 expression in knockout animals does not result in significant confounding variable; as such, we can use the HSPB5 KO animals as a model for investigating the effects of reduced HSPB5 expression on inflammatory processes. We believe that the reported dysfunction observed in HSPB5 KO animals under a 129Sv background may be less severe in the C57bl background (discussed further in section 3.5).

3. CHARACTERISATION OF HSPB5 AS AN IMMUNE REGULATOR OF PERIPHERAL IMMUNE RESPONSE

As HSPB5 has been shown to have immune modulatory effects, this chapter is one of two chapters to investigate HSPB5's immune modulatory capacity. This chapter specifically investigates the immune modulatory capacity of HSPB5 in the periphery. *S. Typhimurium* is used in this experiment as it induces a robust innate and adaptive immune response.

3.1 Introduction

In the central nervous system (CNS), endogenous upregulation of HSPB5 is observed in both neurons and glia in several neurodegenerative conditions (Chapter 1). Studies investigating deficiency or overexpression of HSPB5 suggest that induction of HSPB5 is protective (Clark et al., 2000; Sun et al., 2005; Masilamoni et al., 2006; Arrigo et al., 2007; Steinman, 2008). As HSPB5 has several cellular roles (Chapter 1), the precise mechanism(s) by which it offers protection is not clear. Current thinking is that, as well as its other cellular roles, HSPB5 may also mediate crucial intracellular (Shao et al, 2013) and extracellular (Rothbard et al., 2012) anti-inflammatory roles. This notion is supported by proof of concept studies, which show that during experimental autoimmune encephalopathy (EAE) (Ousman et al., 2007; Rothbard et al., 2012) and also acute inflammatory condition, stroke (Arac et al., 2011), exogenously administered HSPB5 leads to dampened immune activation, reduced inflammatory molecules and improved disease prognosis.

These data highlight an increasing body of evidence that suggests HSPB5 to be a modulator of inflammation; however, as most of these investigations are conducted in models of multiple sclerosis, an autoimmune condition that is driven by T-cells, the autoimmune response observed here can hardly be described as the natural order of an immune response. Therefore, to investigate the immune modulatory capacity of HSPB5, studies need to be done using other disease models.

Firstly, we characterise the immune modulatory capacity of HSPB5 in the periphery by challenging HSPB5 deficient mice with Salmonellae. Salmonellae inoculation induces a non-autoimmune response that, unlike EAE or the conventional lipopolysaccharide (LPS) inoculation, has the capacity to activate both the innate and adaptive arms of the immune system (Mittrücker et al., 2000). As this model activates both components of the immune system, it should offer a comprehensive characterisation of HSPB5's capacity to modulate the immune system.

3.1.1 *Salmonellae* spp infection

Both humans and animals are affected by *Salmonella enterica* species and subspecies (spp) (Su et al., 2007). In humans, *Salmonella enterica* typhi (*S. typhi*) inoculation induces Typhoid fever (Parry et al., 2002). In mice, *S. typhi* is avirulent, instead, the subspecies *S. Typhimurium* leads to Typhoid fever-like disease (Santos et al., 2001). Regardless of species, Salmonellae have the capacity to activate both innate and adaptive arms of the immune system (Mittrücker et al., 2000).

3.1.2 Peripheral immune response to *S. Typhimurium*

3.1.2.1 Critical pathogenic events

In mice, the normal route of entry for *S. Typhimurium* is by oral ingestion. Once ingested, *S. Typhimurium* infiltrates M-cells that line the small intestine; infects resident macrophages and dendritic cells in gut associated lymphoid tissue (GALT); and terminates by infecting macrophages located in lymphoid organs, notably, the liver and spleen (Collins et al., 1974; Mittrücker et al., 2000; Sebastiani et al., 2002).

Experimentally, when *S. Typhimurium* is introduced by intraperitoneal (IP) injection, as was done in this study, bacteria directly enter the portal circulation from the peritoneum, which leads to accelerated and more potent lymphoid tissue infection (Collins, 1969). In the liver and spleen, regardless of oral or IP route, *S. Typhimurium* infects macrophages and initiates several successive rounds of intracellular multiplication, after which, cultures of *S. Typhimurium* extrude from the host cell and perpetuate the bacteria's life cycle (Mittrücker et al., 2000; Kirby et al., 2002). Over several days, bacterial titres in these tissue increase drastically, leading to an influx of immune cells that result in the physical enlargement of the liver (hepatomegaly) and spleen (splenomegaly) (Mastroeni et al., 2009).

3.1.2.2 Peripheral cytokine response

The liver and spleen remain enlarged for up to 42 days post-infection (Jackson et al., 2010), suggesting long-lasting prevalence of *S. Typhimurium*; however, if the bacterial load surpasses the lethal threshold of 10^8 bacteria in any one of the organs, animals become unable to overcome the infection due to sepsis and organ failure, which leads to animal death (Khan et al., 1998). To negate the increasing bacterial titre, tissue-resident macrophages, dendritic cells and natural killer cells mount a pro-inflammatory immune response characterised by significant induction of IL-12 (Mastroeni et al., 1996), TNF-α (Nauciel et al., 1992) and IFN-γ (Muotiala et al., 1990). These cytokines are imperative for successful elimination of *S. Typhimurium* because they activate the adaptive immune response (Mastroeni et al., 2009).

Activation of the adaptive immune response is important during *S. Typhimurium* infection because, *S. Typhimurium* is an intracellular pathogen; as a result, innate immune cells are inadequate at sterile elimination of *S. Typhimurium*. This is illustrated by studies on mice with significantly reduced T-cells, known as nude mice, which show that after *S. Typhimurium* infection, the nude mice were incapable of complete clearance of *S. Typhimurium,* succumbing to infection even though they mounted a robust innate immune response (Dougan et al., 2011).

T-cell activation is, therefore, important because it leads to activation of $CD4^+$ T-helper cells that over-express IL-12, TNF-α and IFN-γ, which promotes the activation of cytotoxic $CD8^+$ T-cells, natural killer cells, B-cells (Mastroeni et al., 2009) and enhances phagocytic behaviour from innate immune cells (Ibarra et al., 2009). The sustained over-expression of these cytokines is evident up to 21 days post-infection in the spleen and blood serum of infected animals (Pie et al., 1997; Püntener et al., 2012). Over a period of several weeks, the coordinated efforts of the innate and adaptive immune response reduce bacterial titre and overcome infection. See figure 3.1 for a time-line of key peripheral sites and inflammatory events to occur during *S. Typhimurium* infection.

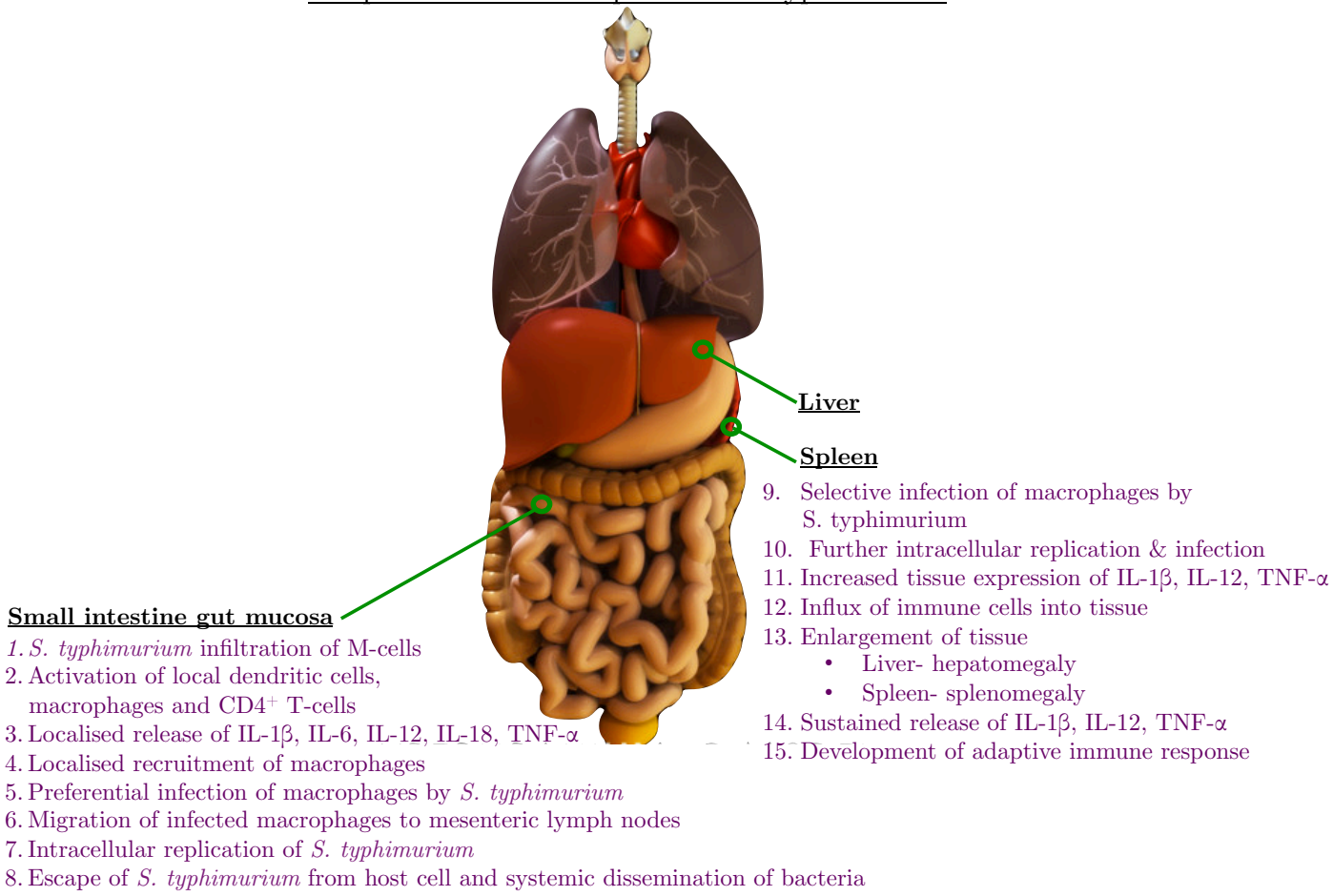

Figure 3.1 Anatomical representation of *S. Typhimurium* infection and the corresponding peripheral immune response.

The diagram shows the internal organs of a mouse and key anatomical sites, cells, and immune responses involved in the infiltration, propagation and elimination of *S. Typhimurium* following ingestion. Introduction of *S. Typhimurium* by intraperitoneal injection, as is often done experimentally, circumnavigates step 1-8 and instead involves the filtration of *S. Typhimurium* from the peritoneal cavity into lymphatic vessels, whereby *S. Typhimurium* is disseminated systemically.

3.1.3 CNS immune response to *S. Typhimurium*

Although the brain was historically thought to be immune privileged, recent accounts show that the peripheral immune system can, and does, communicate with the brain (Galea et al., 2007). It is, therefore, not surprising that following *S. Typhimurium* infection, an immune response is observed in the CNS (Püntener et al., 2012). The immune response is characterised by induction of microglia and pro-inflammatory cytokines IL-1β and IL-12. There are also acute behavioural changes such as piloerection, hunched posture, weight loss and burrowing deficits (Püntener et al., 2012), which are thought to be induced by cytokine signalling (Dantzer et al., 2007).

3.1.4 Summary

Figure 3.2 highlights the systemic and central events to occur during *S. Typhimurium* infection and provides context to our experimental mode. In summary, Salmonellae infection, with its capacity to activate both compartments of the immune response and induce quantifiable pathophysiological changes, provides a good basis to characterise the immune modulatory role of HSPB5.

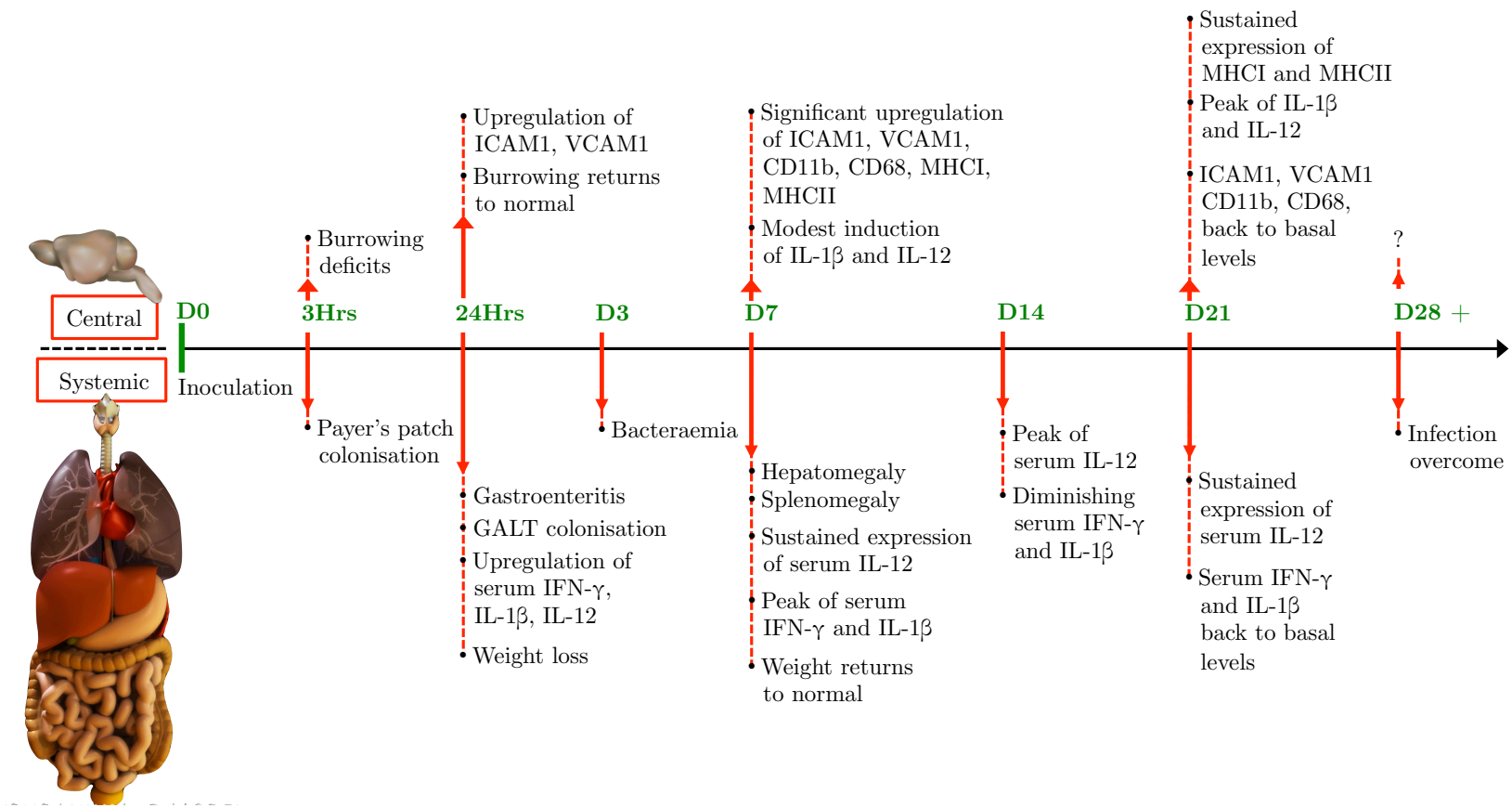

Figure 3.2 Time-course of cellular and molecular features associated with *S. typhimurium* infection. Diagram showing the summation of key events to occur during *S. typhimurium* infection, highlighting in particular, concurrent events in the periphery (systemic) and the brain (central). Information is as referenced in the text.

3.2 Aims

S. Typhimurium infection elicits a robust immune response with a well-defined cytokine and cellular profile in the periphery as well as the CNS. Our aim is to investigate whether HSPB5, or lack there-of, augments the inflammatory profile associated with *S. Typhimurium* infection.

S. Typhimurium infection leads to a robust peripheral and central immune response. As such, here, we use *S. Typhimurium* infection as a model to investigate the purported immune modulatory role(s) of HSPB5. Using wild type ($HSPB5^{+/+}$) and knockout ($HSPB5^{-/-}$) mice, we investigate differences, if any, observed in the peripheral and central immune response following challenge with *S. Typhimurium*.

As our work is hypothesis driven, we utilise key time-points in the *S. Typhimurium* infection timeline to investigate HSPB5's potential immune modulatory role; to investigate the immune response in the periphery, we measure serum cytokines at day 7, which as described previously, is when peak peripheral cytokines are observed (figure 3.2). The central immune response is measured at 21-days post infection, as this is the time-point at which the peak cytokine response has been observed in the brain. It is also apparent at this time-point that microglia may have an activated phenotype, as such, we investigate the cellular profile observed in the brain. Cytokine expression and cellular profile were investigated in the hippocampus and substantia nigra as we have previously shown that following systemic inflammation, the hippocampus shows robust immune activation (Cunningham et al., 2009), and there is also a robust immune activation in the substantia nigra (Brydon et al., 2008). We also investigate the substantia nigra because it has recently been reported to be an area that shows aberrant immune response following reduced expression of HSPB5 (Shao et al., 2013).

3.3 Materials and Methods

3.3.1 Animals and animal husbandry

8 weeks old female wild type ($HSPB5^{+/+}$), heterozygous ($HSPB5^{+/-}$) and knockout ($HSPB5^{-/-}$) C57Bl/6 littermate mice were obtained in-house (Biomedical Research Facility, University of Southampton). Mice were housed in groups of 5 in plastic cages with sawdust bedding for at least a week before testing. Mice were fed on an RM-1 Standard laboratory chow diet and had access to food and water *ad libitum*. The holding room was temperature controlled (21 – 23°C) with a 12hr:12hr light dark cycle (lights on at 07:00). Females were used due to lesser risk of aggressive outbreaks and to conform to most of the previous work done in the laboratory. All procedures were performed in accordance with the UK animals (Scientific Procedures) Act 1986 under personal license and ethical approval obtained from the University of Southampton and the UK Home Office.

3.3.2 Infection with *Salmonella typhimurium*

Control animals were given an intraperitoneal injection of saline; *S. Typhimurium* infected mice were given an intraperitoneal injection of 5.5 x 10^5 colony forming units (cfu) of live-attenuated *S. Typhimurium* strain SL3261. Mice were weighed daily over the course of the first week and bi-weekly thereafter to monitor gross weight loss (≥15% loss of the initial starting body weight results in termination of the experiment), in accordance with the Home Office license.

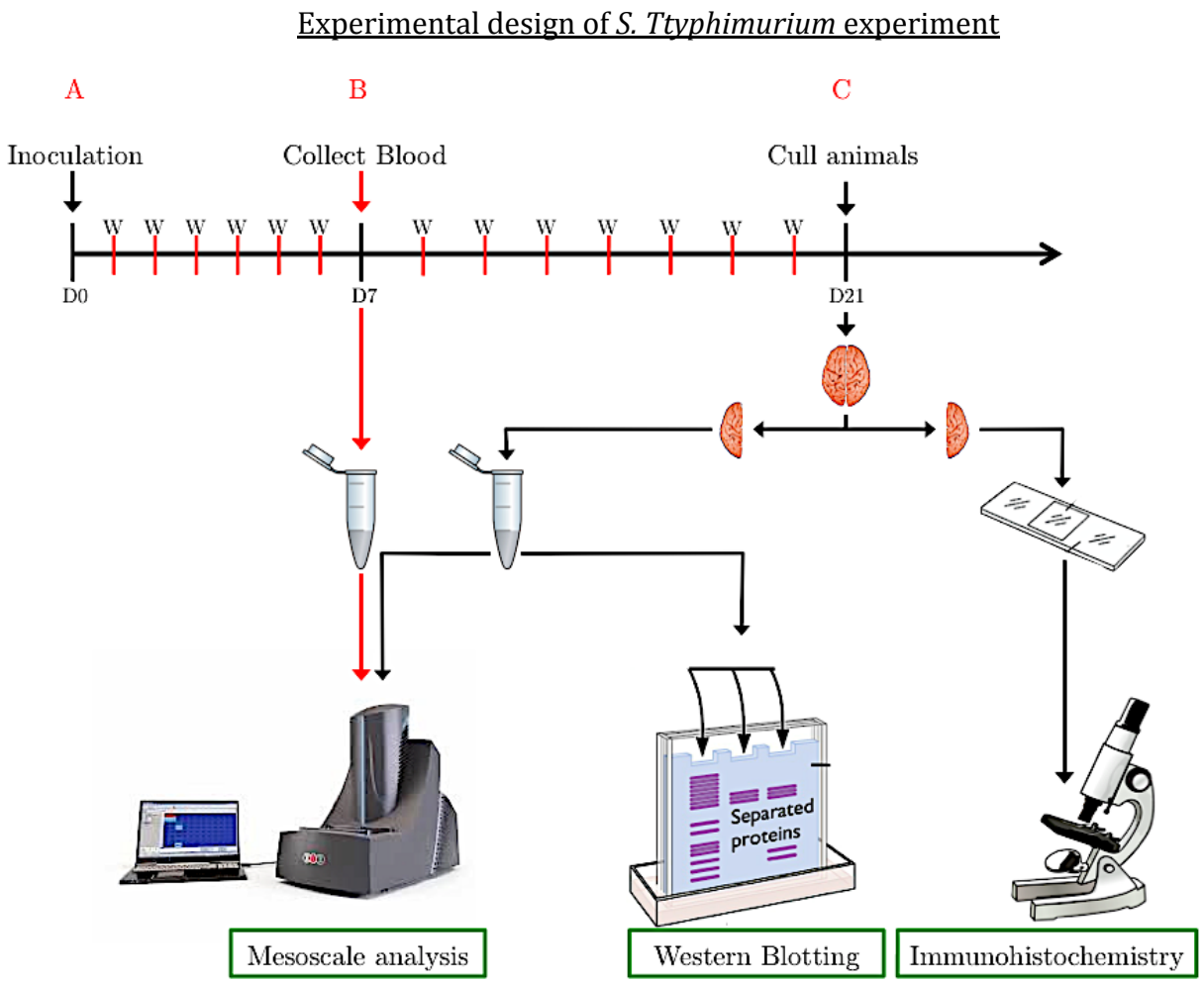

Figure 3.3 Time-course showing the experimental design of the *S. Typhimurium* experiment.
(A) Animals are either inoculated with *S. Typhimurium* or Saline. The weight of the mice was regularly monitored (W). (B) At day 7, blood was collected by tail-bleed method and cytokine levels were measured. (C) Animals were culled at day 21 and brains were collected. Half the brain was processed for cytokine and protein expression analysis, whilst the other half of the brain was processed for immunohistochemistry.

3.3.3 Tissue collection and processing

Tissue was collected at different time-points, as shown in figure 3.3, and processed as follows.

3.3.3.1 Blood serum

At day 7-post infection, approximately 500µl of blood was tail-bled from the mice and collected in 1.5ml eppendorfs. Samples were spun down at 5000rpm and the serum (supernatant) was collected and kept at -20°C until further use.

3.3.3.2 Brains

At the end of the experiment, animals were terminally anaesthetised with 10µl/g Pentobarbital (Sigma, UK). Mice were perfused with heparinised saline, but not fixed. The brain was removed and the two cerebral hemispheres were separated using a scalpel; half the brain was placed in a bijous and fixed in 10% formalin overnight at 4°C for immunohistochemistry processing (see section 3.3.4.1), whilst the other half was snap-frozen and stored at -20°C for biochemical analysis (see section 3.3.4.2).

3.3.4 Immunohistochemistry

Formalin-fixed brains were de-hydrated by immersion in a series of increasing concentration alcohols from 70% ethanol to 80%, 90%, 100% and, lastly, immersion into Histoclear (Sigma Aldrich, UK) (see table 3.1). This process was automated by a Leica-TP 1020 tissue processor (Leica Biosystems, UK). After dehydration, tissue was placed in plastic cassettes (Fisher Scientific, UK) and submerged in molten (40°C) paraffin wax (Polywax, UK) and allowed to solidify. Wax blocks were stored at room temperature. The wax-blocks were cut into 10µm sections on a Leica RM2255 rotary microtome (Leica Biosystems, UK) and tissue was floated on 40°C dH_2O in a tissue floatation bath (LAMB, UK). The resulting sections were mounted on SuperFrost™ microscope slides (Fisher Scientific, UK) and dried overnight at 37°C. Slides were stored at room temperature.

Treatment	Duration
70% ethanol	2 hours
70% ethanol	2 hours
80% ethanol	1 hour
90% ethanol	1 hour
Absolute ethanol I	1 hour
Absolute ethanol II	10 hours
Histoclear I	4 hours
Histoclear II	2 hours

Table 3.1 Automated settings for the dehydration of tissue using the Leica-TP 1020 tissue.

Treatment	Duration
Xylene I	10 minutes
Xylene II	10 minutes
100% ethanol	3 minutes
90% ethanol	3 minutes
80% ethanol	3 minutes
70% ethanol	3 minutes

Table 3.2 Tissue rehydration for immunohistochemistry.

1^{O} antibody	Species	Dilution	Incubation	Biotinylated antibody	Dilution
GFAP (Dako, US)	Mouse	1:5000	Over-night	Goat anti mouse-HRP	1:250
HSPB5 (Abcam, UK)		1:250			
IBA1 (Abcam, UK)		1:500			

Table 3.3 Primary and secondary antibodies used for immunohistochemistry analysis

3.3.4.1 Immunostaining and quantification

Sections were heated at 60°C for 30 minutes and then de-waxed in xylene (Fisher Scientific, UK). Sections were heated at 60°C for 30 minutes and then de-waxed in xylene (Fisher Scientific, UK) before being re-hydrated by immersion in a series of decreasing alcohol concentrations (see table 3.2). Endogenous peroxidase activity was blocked with a solution of 1% hydrogen peroxide (H_2O_2) and subsequent antigen retrieval was done by heating in citrate buffer (10mM citric acid (pH6)) in a 700W microwave for 5 minutes. Non-specific binding was prevented by incubating sections in goat, horse, or donkey serum (GIBCO life technologies, UK), depending on the host animal of the primary antibodies used. Sections were incubated with primary antibodies, as indicated: anti-glial fibrillary protein (mGFAP (Sigma Aldrich, UK) 1:1000), anti-ionised calcium-binding adapter molecule (mIBA1 (Abcam, UK) 1:500) and anti-alpha-B crystallin (mHSPB5 (Abcam, UK) 1:200) overnight (16-18hrs) at 4°C. Appropriate biotinylated secondary antibody ((Vector Laboratories, UK) 1:250) was applied for 1hr and then sections were incubated in ABC complex (Vector Laboratories, UK) for 45 minutes (see table 3.3). Location of antibody binding was determined by immersion in diaminobenzidine (DAB) solution (Sigma Aldrich, UK) with 1% hydrogen peroxide (H_2O_2) (Sigma Aldrich, UK). Sections were counterstained with Harris haematoxylin (VWR, UK) and de-hydrated by immersing in a series of increasing concentration alcohols and, lastly, by immersion into xylene (Fisher Scientific, UK). Coverslips were applied with Distrene-Plasticiser-Xylene (DPX) combined-mountant (VWR, UK). All images were taken using a Zeiss Axio Observer Z1 inverted microscope (Zeiss, UK).

3.3.5 Biochemistry

As the substantia nigra is in the mid-brain, the tissue between the brainstem and the hippocampus was collected in an eppendorf and snap-frozen. The hippocampus was micro-dissected from the mid-brain using the protocol described by Hagihara et al., (2009) and snap-frozen in an eppendorf. Tissue was weighed and diluted in 5 volumes (w/v) of TRIS buffer (150mM NaCl, 25mM Tris, 1% Triton X-100, complete protease inhibitor cocktail (Roche Diagnostics GmbH, Mannheim, Germany), pH7.2) and homogenised before being sub-aliquoted

into two portions; one for cytokine analysis using the mesoscale system and another for western blotting.

3.3.5.1 Cytokine analysis

Samples were centrifuged at 13 000 rpm for 30 minutes and supernatants were collected and assayed for total protein using a Bio-Rad D_C protein assay kit (Bio-Rad, UK). Cytokine levels were assessed using MSD multiplex kit (Meso Scale Discovery, Gaithersburg, MD, USA) for mouse pro-inflammatory cytokines (K15012B) as per manufacturer's instructions and read using a MESO™ QuickPlex SQ 120 reader and analysed with the accompanying Discovery Workbench® 4.0 software.

3.3.5.2 Western blot

For both mid-brain and hippocampal homogenates, total protein concentration was assessed using a Bio-Rad D_C protein assay kit (Bio-Rad, UK), as per manufacturer's instruction. All samples were diluted to a final concentration of 4mg/ml in 5x sample buffer (250mM TRIS-HCl (pH6.8), 10% SDS, 30% Glycerol, 5% β-mercapto-ethanol, 0.02% bromo-phenol blue) and run on a polyacrylamide gel composed of 5% stacking gel and 12.5% resolving gel in 1x Laemmli buffer (5mM TRIS (pH8.3), 192mM Glycine, 0.1% SDS) using the Bio-Rad protein gel system (Bio-Rad, UK). Equivalent loading was checked by coomassie staining (Sigma Aldrich, UK), as per manufacturer's instructions (see section 2.3.7). Coomassie membranes were scanned at 700nm using the Odyssey infrared imaging scanner (LiCOR, UK) and quantified using Odyssey software v1.2 (LiCOR, UK). Proteins were transferred to nitrocellulose membrane (Amersham, UK) overnight (16-18hrs) at 4°C in transfer buffer (1x Laemmli buffer, 20% (v/v) Methanol). Membranes were blocked with 4% non-fat milk (TESCO, UK) and incubated in primary antibodies: anti-glial fibrillary protein (mGFAP (Sigma Aldrich, UK) 1:5000) and anti-alpha-B crystallin (mHSPB5 (Abcam, UK) 1:500) overnight (16-18hrs) at 4°C (see table 3.4). Membranes were washed in TRIS-buffered saline with 0.05% tween (TBS-T) and secondary antibodies: anti-mouse or rabbit IRDye™ 680RD or IRDye™ 800CW (LiCOR, UK) were applied for 1hr. Membranes were visualised using the Odyssey infrared imaging scanner (LiCOR, UK), as per manufacturer's instructions.

Primary antibody	Originating species	Dilution	Secondary antibody	Dilution
CNP (Abcam, UK)		1:1000		
MBP (Abcam, UK)	Mouse	1:500	anti-mouse IR (Invitrogen, UK)	1:1000
HSPB5 (Abcam, UK)		1:500		

Table 3.4 Primary and secondary antibodies used for western blotting.

3.4 Results

3.4.1 Systemic effect of *S. Typhimurium* SL3261

3.4.1.1 Spleen size

Following *S. Typhimurium* infection, splenomegaly is apparent from 7 days post-infection (Püntener et al., 2012). Our results show that at 21 days post-infection, splenomegaly is still apparent with *S. Typhimurium*-infected animals (WT 0.65g ±0.18, HET 0.62g ±0.12g, and KO 0.74g ±0.09) showing significantly larger spleen size ($p<0.0001$) as compared to non-infected animals (WT 0.115g ±0.02, HET 0.12g ±0.006g, KO 0.12g ±0.01) (figure 3.4A, B). Genotype did not contribute significantly to any differences observed to spleen size ($p>0.05$).

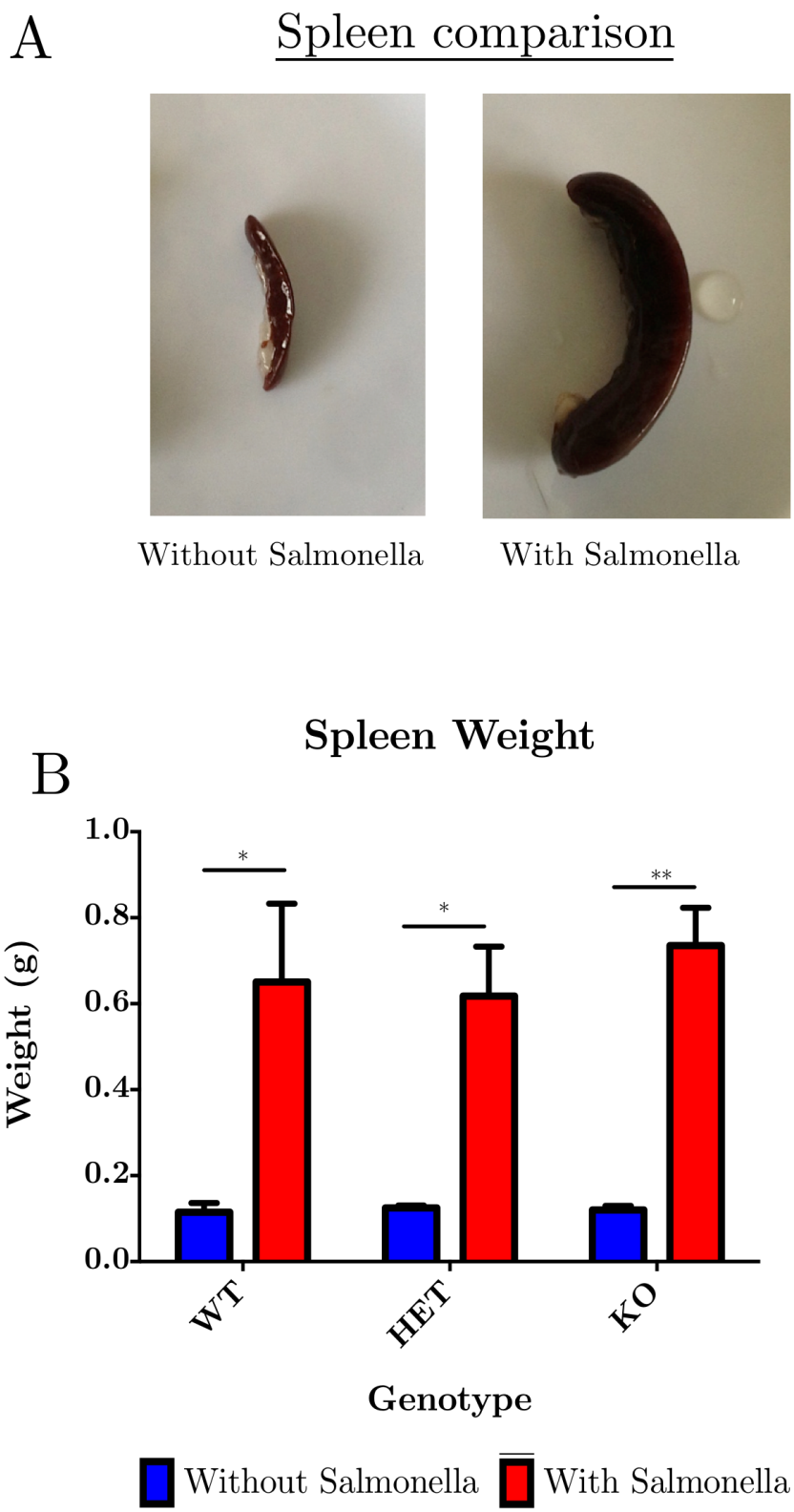

Figure 3.4 Spleen comparison of animals with or without *S. Typhimurium* SL3261 infection.

(A) Representative photographs of spleen size of naïve non-infected animals, "without Salmonella" and *S. Typhimurium*-infected mice, "with Salmonella". (B) Spleen weight change between animals with and without *S. Typhimurium* infection; significant difference between animals inoculated with *S. Typhimurium* and non-infected animals. No statistical difference in spleen weight between genotypes in both non-infected and infected animals. One-way ANOVA analysis with Tukey post-hoc analysis. Error bars represent SEM from 5 animals per time point. $P < 0.05$ (*), $P<(0.01$ (**).

3.4.1.2 Weight Change

Weight loss is often used as an indirect indicator for severity of infection as it is induced by pro-inflammatory cytokines (Langstein et al., 1991; Espat et al., 1994; McCarthy, 2000). Our results show that within the first 24hrs post-infection, infected WT mice had a net weight change of +2% (+0.6g ±2.5) whilst HET and KO infected mice had a net weight change of -0.05% (-0.02g ±6.2) and +0.2% (+0.04g ±3.6), respectively ($p>0.05$) (Figure 3.5B, D, F, H). At this stage of disease, genotype did not appear to affect weight loss; in fact, during the first week following *S. Typhimurium* inoculation, WT, HET and KO *S. Typhimurium*-infected animals gained weight to a comparable level as the non-infected control animals ($p>0.05$) (figure 3.5A, B).

WT *S. Typhimurium*-infected animals continued to gain weight at a comparable level to WT naïve animals for the duration of the experiment ($p>0.05$), however, for HET and KO *S. Typhimurium*-infected animals, from day 7 post-inoculation, they progressively lost weight at a rate of 0.27%/day and 0.38%/day, respectively (figure 3.5F, H). The difference in weight loss became significantly different from naïve controls ($p<0.05$) at day 15 and day 21 post-infection for KO and HET animals, respectively (figure 3.5F, H). Genotype appears to have significantly influenced weight loss in two ways: WT *S. Typhimurium*-infected animals did not lose weight whilst HET and KO *S. Typhimurium* animals lost significant weight. HET and KO naïve animals also gained weight at a slower rate than WT naïve animals ($p>0.05$ WT (0.88%/day ±0.14); HET (0.46%/day ±0.04), KO (0.39%/day ±0.03)).

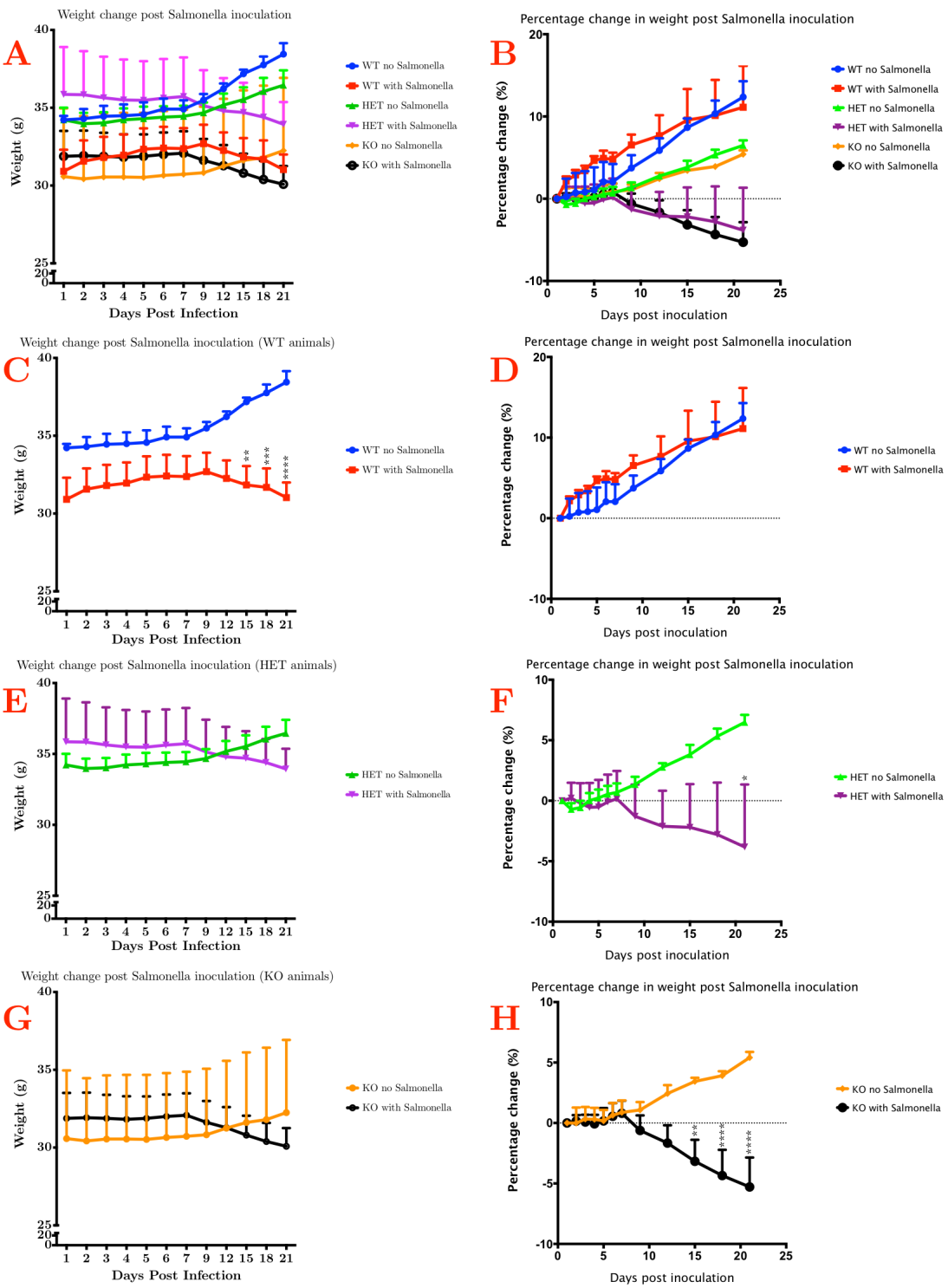

Figure 3.5 Analysis of weight following *S. Typhimurium* infection.
(A, C, E, G) Actual weight change in naïve non-infected mice and compared to *S. Typhimurium*-infected mice. (B, D, F, H) Percentage weight change as an expression of pre-inoculation weight in naïve non-infected mice and compared to *S. Typhimurium*-infected mice. (A, B) All genotypes. (C, D) WT animals. (E, F) HET animals. (G, H) KO animals. Two-way ANOVA analysis with Tukey post-hoc test. Error bars represent SEM for 5 animals. $P<0.05$ (*), $P<0.01$ (**), $P<0.001$ (***), $P<0.0001$ (****).

3.4.1.3 Peripheral cytokine profile

In EAE, HSPB5 KO animals have been shown to display exaggerated peripheral cytokine production (Ousman et al., 2007); we measured the peripheral cytokine response of WT, HET and KO animals following *S. Typhimurium* infection. We found that following *S. Typhimurium* infection, as compared to naïve control animals, WT *S. Typhimurium*-infected animals significantly induced serum cytokines IL-1β, IL-6, IL-10, IL-12, IFN-γ and TNF-α ($p<0.05$) (figure3.6A-F). HET and WT animals showed a comparable (if not less) but never more cytokine response (figure3.6A-F). Genetic differences were only apparent for IL-12p70 and TNF-α where WT *S. Typhimurium*-infected animals produced more cytokines than HET and KO animals ($p<0.05$).

For IL-1β, WT, HET and KO *S. Typhimurium*-infected animals show at least a 2-fold induction of IL-1β as compared to naïve controls ($p<0.05$) (figure 3.6A). There was no difference in the amount of IL-1β produced by the different genotypes ($p>0.05$ WT (13.6pg/ml ±3.3); HET (11.2pg/ml ±1.1), KO (10.1pg/ml ±1.2)).

IL-12, whose biologically active form is known as IL-12p70, was found significantly elevated in WT *S. Typhimurium*-infected animals as compared to naïve, non-infected control animals ($p<0.05$) (figure3.6B). HET and KO *S. Typhimurium*-infected animals did not show a significant induction of IL-12p70 ($p>0.05$). Genotype was seen to significantly influence the production of IL-12 ($p<0.05$ WT (130pg/ml ±23.6); HET (71pg/ml ±5.6), KO (59pg/ml ±6.6))

As compared to naïve, control animals, IFN-γ was found significantly upregulated in WT, HET and KO *S. Typhimurium*-infected animals ($p<0.001$) (figure3.6C). The induction was comparable between WT, HET, and KO *S. Typhimurium*-infected animals ($p>0.05$ WT (509pg/ml ±191); HET (342pg/ml ±71), KO (354pg/ml ±65)).

IL-6 showed significant upregulation in WT and KO *S. Typhimurium*-infected animals as compared to naïve control animals ($p<0.05$). HET *S. Typhimurium*-infected animals did not

show a significant upregulation ($p>0.05$). Genotype was not considered to significantly alter the induction of IL-6 ($p>0.05$ WT (251pg/ml ±51); HET (135pg/ml ±56), KO (149pg/ml ±54)).

IL-10, an anti-inflammatory cytokine that antagonises and modulates IFN-γ, showed significant induction in WT, HET and KO *S. Typhimurium*-infected animals as compared to naïve control animals ($p<0.05$) (figure 3.6E). Genotype did not significantly alter the induction of IL-10 ($p>0.05$ WT (110pg/ml ±19.6); HET (64pg/ml ±6.6), KO (73pg/ml ±11)).

WT *S. Typhimurium*-infected animals show a ≈ 23-fold induction of TNF-α as compared to naïve control mice ($p<0.05$) (figure 3.8F). In contrast, as compared to naïve control animals HET and KO *S. Typhimurium*-infected animals do not show significant induction of TNF-α. Genotype was considered to have significantly altered the induction of TNF-α ($p<0.05$ WT (18.6pg/ml ±2.8); HET (5.14pg/ml ±2.05), $p>0.05$, KO (6.52pg/ml ±3.38)).

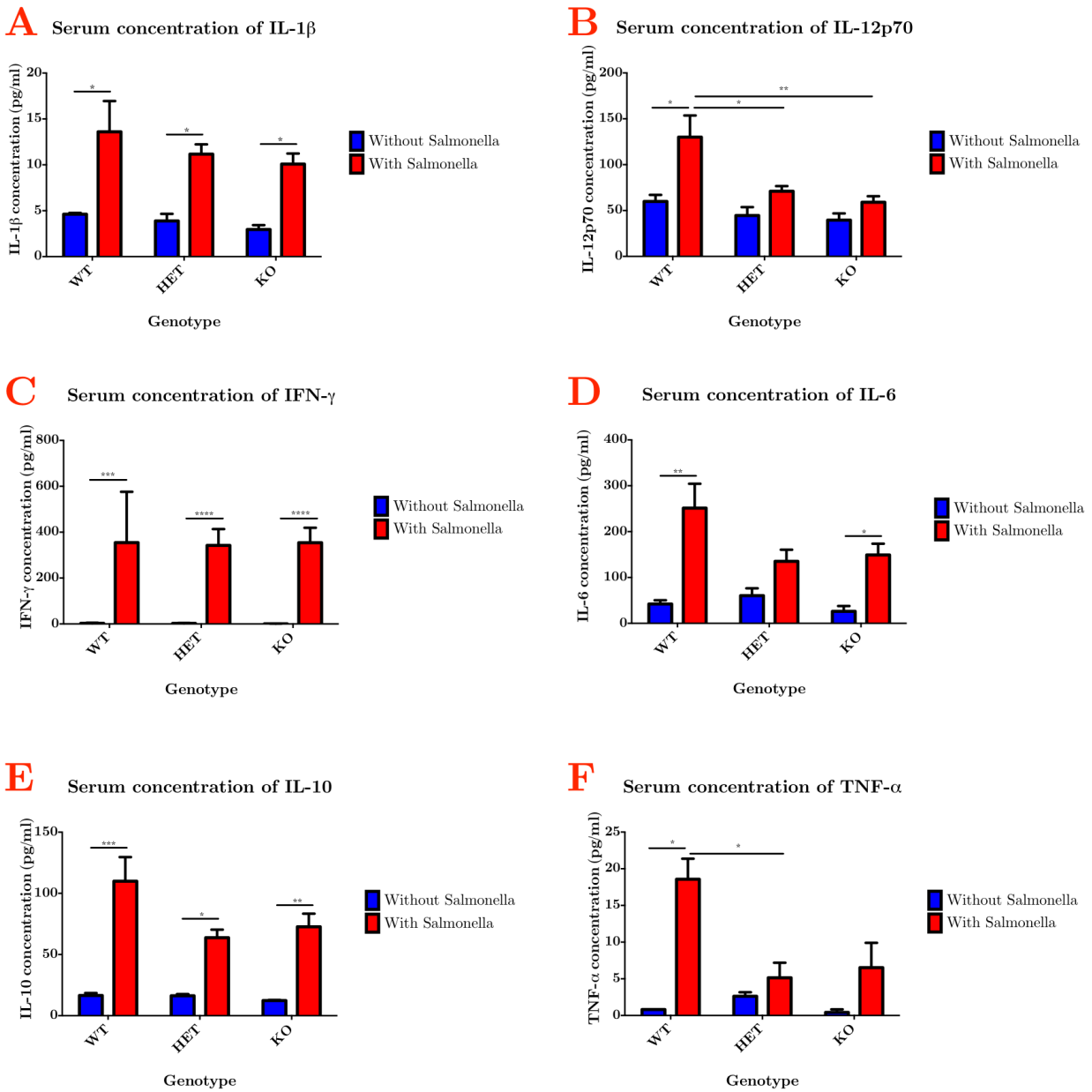

Figure 3.6 Serum cytokine levels at day 7-post *S. Typhimurium* SL3261 infection.

(A) Serum concentration of interleukin-1 beta (IL-1β). (B) Serum concentration of the biologically active form of interleukin-12 (IL-12p70). (C) Serum concentration of interferon-gamma (IFN-γ). (D) Serum concentration of interleukin-6 (IL-6). (E) Serum concentration of interleukin-10 (IL-10). (F) Serum concentration of tumour necrosis factor alpha (TNF-α). One-way ANOVA analysis with Tukey post-hoc analysis. Error bars represent SEM from 5 animals per time point. $P<0.05$ (*), $P<0.01$ (**), $P<0.001$ (***), $P<0.0001$ (****)

3.4.2 Central effects of *S. Typhimurium* SL3261

In the central nervous system, Ousman et al (2007) showed that deficiency in HSPB5 leads to increased astrocyte death and Shao et al (2013) further show that reduction in HSPB5 results in exaggerated release of IL-1β and marked induction of microglia in the substantia nigra. We investigated both the cellular and cytokine responses in the CNS following *S. Typhimurium* infection.

3.4.2.1 Central cytokine response

Using micro-dissected tissue to distinguish the cytokine response in different brain regions, we found that in this enriched tissue, the concentration of IL-12, IFN-γ, IL-6, IL-10 and TNF-α were found to be below the necessary threshold for detection by the mesoscale (data not shown). We did however find detectable levels of IL-1β in the hippocampus and midbrain.

In the hippocampus, as compared to naïve control animals, IL-1β was found upregulated in WT *S. Typhimurium*-infected mice ($p<0.05$) (figure 3.7A). HET and KO *S. Typhimurium*-infected animals did not mount a significant IL-1β response ($p>0.05$). Genotype did not significantly alter the production of IL-1β ($p>0.05$ WT (0.35pg/ml ±0.01); HET (0.14pg/ml ±0.06), KO (0.23pg/ml ±0.12)).

In the midbrain, as compared to naïve control animals, IL-1β was also upregulated in WT *S. Typhimurium*-infected animals ($p<0.01$) (figure 3.7B). HET and KO animals did not mount a response that was different from naïve controls ($p>0.05$). Genetic differences contributed to the difference in production of IL-1β between WT *S. Typhimurium*-infected and animals HET *S. Typhimurium*-infected animals ($p<0.05$ WT (0.95pg/ml ±0.09); HET (0.01pg/ml ±0.07)) but not KO *S. Typhimurium*-infected animals ($p>0.05$ WT (0.95pg/ml ±0.09); KO (0.44pg/ml ±0.19).

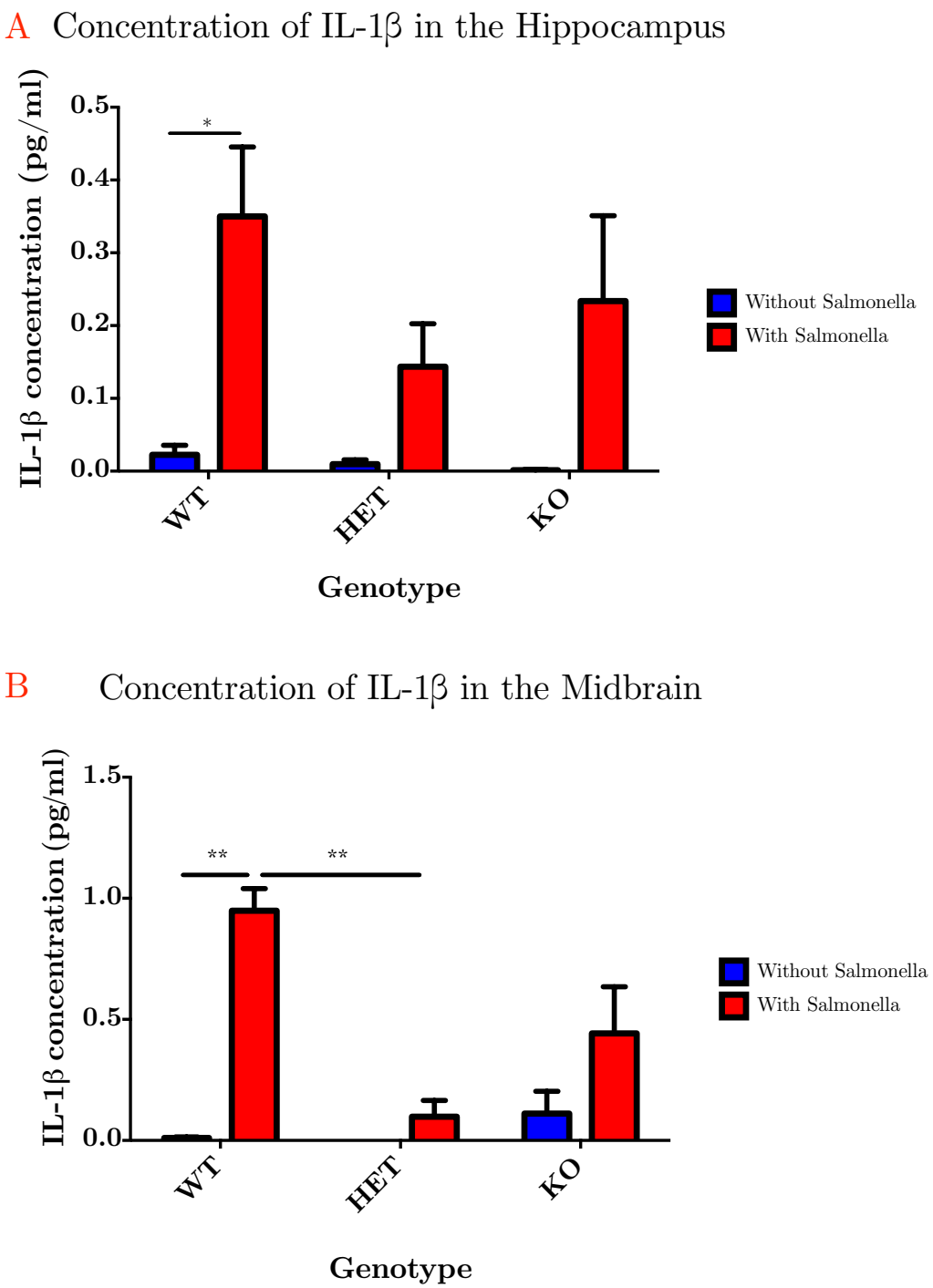

Figure 3.7 Central cytokine response to peripheral *S. typhimurium* infection at 21 days post-infection.
(A) IL-1β response in the hippocampus. (B) IL-1β response in the midbrain. Two-way ANOVA analysis with Tukey post-hoc analysis. Error bars represent SEM from 5 animals. $P<0.05$ (*), $P<0.01$ (**).

3.4.2.2 CNS cellular response

3.4.2.2.1 Astroglial response

In the hippocampus, GFAP analysis shows that at 21-days post-infection, the basal expression of GFAP appears to be different in KO naïve animals, as compared to WT and HET naïve animals, with naïve KO animals expressing less GFAP ($p<0.05$ WT (35.7pg/ml ±3.5), HET (37.8pg/ml ±7.5); KO (18.4pg/ml ±3.0)) (figure 3.8C). The number of GFAP-positive cells present at basal and during infection were seen in *S. Typhimurium*-infected animals is comparable to that observed in naïve animals ($p>0.05$) (figure 3.8A, B). Genotype did not influence the number of GFAP-positive cells.

In the substantia nigra, a significant upregulation of GFAP-positive cells is apparent in WT *S. Typhimurium*-infected animals ($p<0.01$) (figure 3.8D-E). The response mounted by HET and KO *S. Typhimurium*-infected animals was not significantly different to naïve controls ($p>0.05$). The number of GFAP-positive cells in the midbrain of WT *S. Typhimurium*-infected animals is considered significantly different from the number observed in HET and KO *S. Typhimurium*-infected animals ($p<0.01$).

3.4.2.2.2 Microglial response

Work by Püntener et al (2013) shows that at 21 days post *S. Typhimurium*-infection, the number of microglial in the brain is back to basal levels, althought they still exhibit an activated phenotype. Analysis of microglial activation at the same time-point following *S. Typhimurium* infection, shows that there is no significant increase of IBA1-postive cells in the hippocampus and substantia nigra of *S. Typhimurium*-infected animals as compared to naïve animals ($p>0.05$) (figure3.9A-D). Total IBA1 protein expression was not analysed.

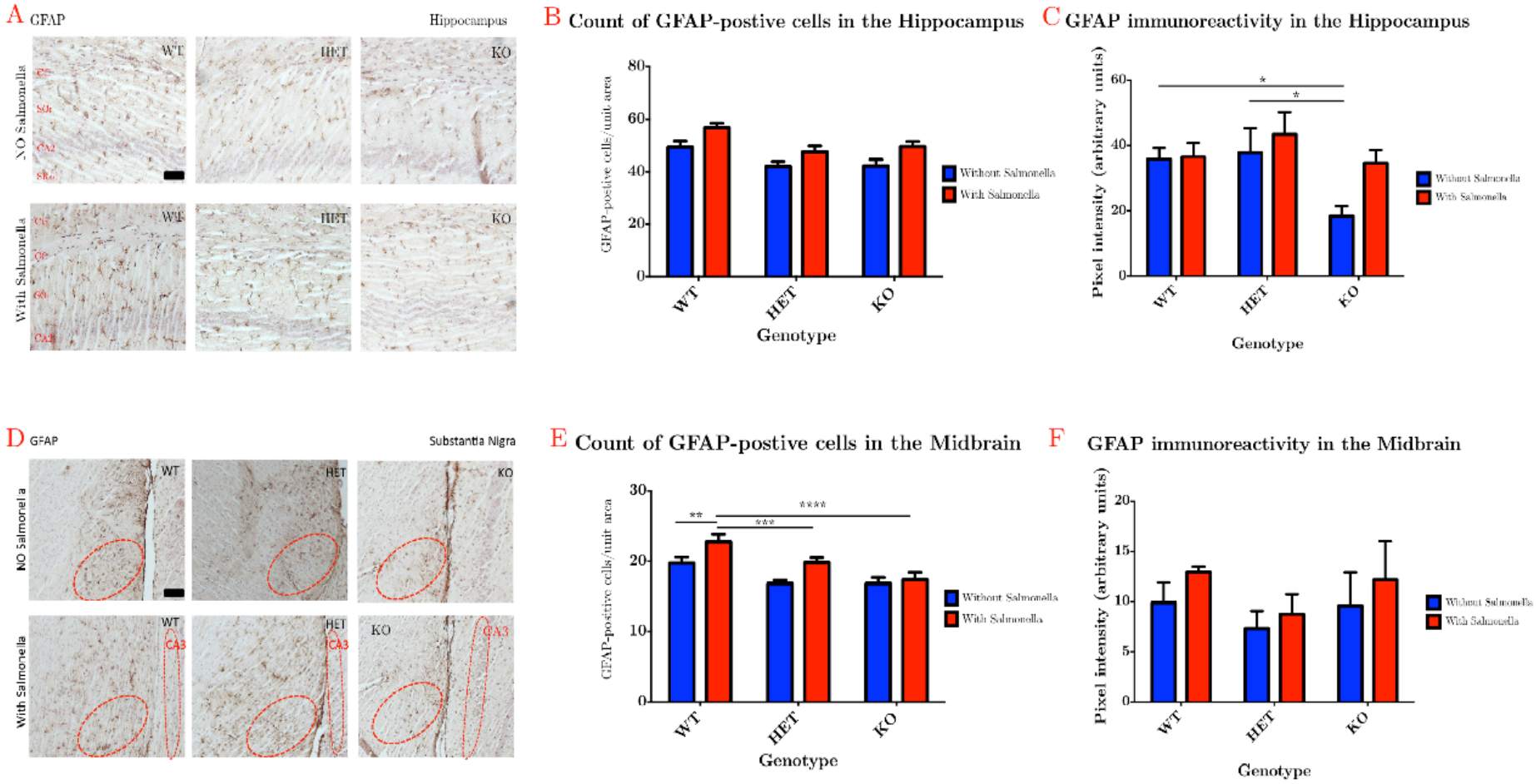

Figure 3.8 GFAP expression in the hippocampus and midbrain at 21 days post *S. typhimurium* infection.
(A, B, C) GFAP expression in the hippocampus, (D, E, F) GFAP expression in the substantia nigra. (A, D) immunohistochemistry analysis. (B, E), quantitative analysis of immunohistochemistry. (C, F), graphical representation of quantitative western blot. Representative images are shown. Scale bar = 50nm. One-way ANOVA analysis with Tukey post-hoc analysis. (B, E) Error bars represent SEM for n=3, 5 visual fields per animals. (C, F) Error bars represent SEM from 5 animals per time-point. P<0.05 (*), P<0.01 (**), P<0.001 (***), P<0.0001 (****). Scale bars: (A) 50μm, (B) 150μm.

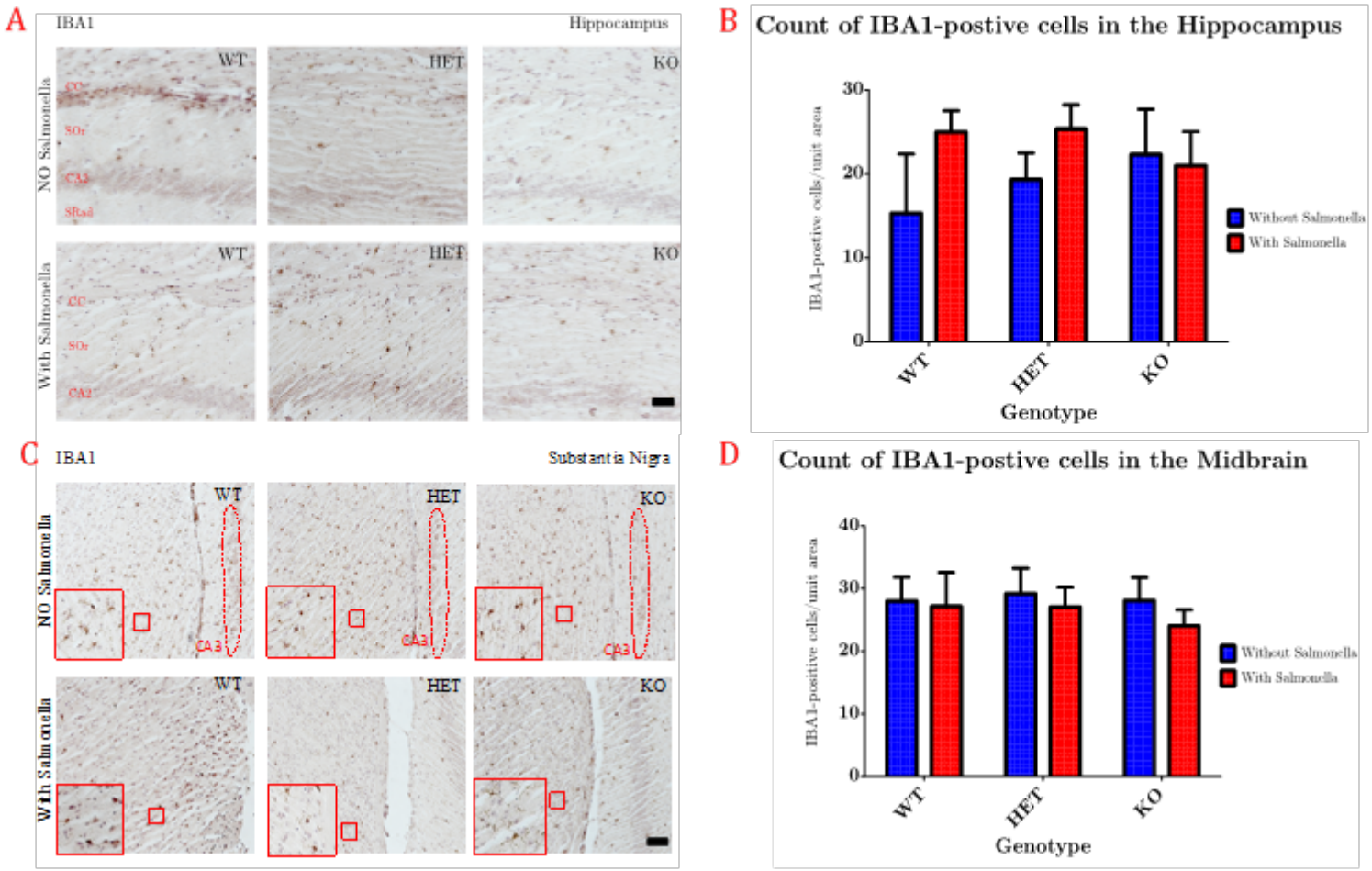

Figure 3.9 IBA1 expression in the hippocampus and midbrain at 21 days post *S. Typhimurium* infection.

(A and C) Immunohistochemistry image composite showing IBA1 immunoreactivity in the (A) hippocampus and (C) midbrain of naïve (no salmonella) and infected (with salmonella) animals. Representative images are shown. Scale bar = 50nm (B and D) Image analysis: number of IBA1-positive cells counted per unit area. (B) hippocampal and (D) midbrain cell counted IBA1-positive. One-way ANOVA analysis with Tukey post-hoc analysis. Error bars represent SEM for n=3, 5 visual fields per animal. Scale bars: (A) 50μm, (B) 100μm.

3.4.2.3 HSPB5 response to *S. Typhimurium*

We measured the HSPB5 response to *S. Typhimurium* because HSPB5 has recently been suggested to modulate astrocyte inflammatory action (Shao et al., 2013), moreover, it is often found upregulated in several neuro-inflammatory conditions.

3.4.2.3.1 HSPB5 expression

As is expected, basal expression of HSPB5 was most abundant in WT animals, which show a robust basal expression of HSPB5 (figure3.10A-D); in contrast, as compared to WT naïve animals, basal expression of HSPB5 in naïve HET animals was diminished by ≤ 50% ($p>0.05$) and naïve KO animals show no expression of HSPB5 in both the hippocampus and the midbrain. At 21 days post *S. Typhimurium* infection, the results show that as compared to naïve control animals, there is a significant induction of HSPB5 in the hippocampus of WT *S. Typhimurium*-infected animals ($p<0.0001$), but not in the hippocampus of HET and KO *S. Typhimurium*-infected animals ($p>0.05$) (figure 3.10A, B). Genotype is considered to have a significant effect on this response ($p<0.0001$ WT (5.6 AU ±0.8); HET (1.47 AU ±0.24), (KO 0AU)).

In the substantia nigra, basal expression of HSPB5 is apparent in WT animals but very diminished in naïve HET animals ($p>0.05$). As compared to naive animals, following *S. Typhimurium* infection, there is a trend towards upregulation of HSPB5 in WT and HET *S. Typhimurium*-infected animals, however the effect is not considered to be significantly different ($p>0.05$) (figure 3.10C, D). The response of WT *S. Typhimurium*-infected animals is considered significantly different to KO *S. Typhimurium*-infected animals ($p<0.05$ WT (3.34 AU ±1.1); (KO 0AU)).

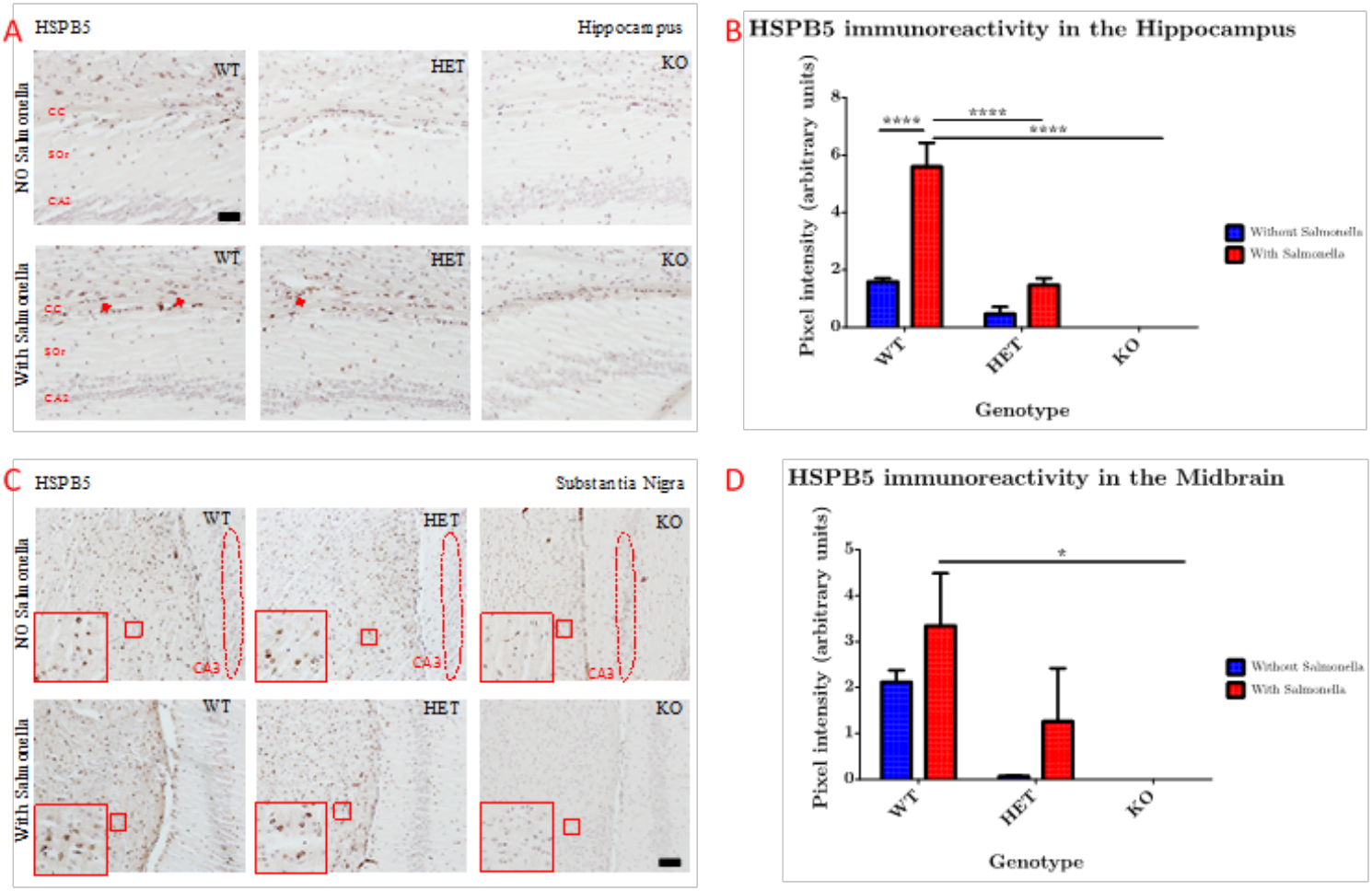

Figure 3.10 HSPB5 expression in the hippocampus and midbrain at 21 days post *S. Typhimurium* infection.

(A, B) HSPB5 expression in the hippocampus, (C, D) HSPB5 expression in the substantia nigra. (A, C) Immunohistochemistry analysis (B, D) Graphical representation of quantitative western blot. Representative images are shown. Scale bar = 50nm. One-way ANOVA analysis with Tukey post-hoc analysis. Error bars represent SEM from 5 animals per time-point. $P<0.05$ (*), $P<0.01$ (**), $P<0.001$ (***), $P<0.0001$ (****). Scale bars: (A) 50μm, (B) 150μm.

3.5 Discussion

The seminal paper by Ousman et al., (2007) suggested that HSPB5 acts as a negative modulator of inflammation; that is to say, HSPB5 acts as a molecular brake to dampen the inflammatory response. This conclusion is based on results by the group that show that in experimental autoimmune encephalopathy (EAE), a model of multiple sclerosis, as compared to WT mice, HSPB5 KO mice showed worse EAE disease progression, as illustrated by higher EAE score, increased splenocyte and lymph-node cell proliferation, significantly hyperactive macrophages and T-cells that contributed to significantly elevated expression of IL-12, TNF-α, IFN-γ and IL-17. HSPB5 KO mice also showed increased glial apoptosis and robust CNS inflammation as evidenced by upregulation of astrocyte and microglia staining. The group went further to show that intravenous injection of recombinant HSPB5 resulted in the amelioration of disease, suppression of immune cell activation and decreased production of cytokines. Ousman et al., suggested that HSPB5 was a negative modulator of inflammation. In our study, instead of using an autoimmune model of inflammation to characterise HSPB5's immune modulatory role, we utilised the *S. Typhimurium*-infection model of inflammation, which has been shown before to induce profound systemic and modest central immune activation (Püntener et al., 2012). To evaluate HSPB5's immune modulatory role, I will discuss and contrast each of the major observations made by Ousman et al in turn.

3.5.1 "Do HSPB5 KO mice show worse disease severity"?

Several assays exist to measure disease severity in mice. In the Ousman et al study, disease severity was measured by EAE clinical-sign scoring, which showed significantly higher scores, meaning worse disease progression, than WT mice. We used weight loss as an indicator of disease severity. Disease induced weight loss, referred specifically as cachexia, is, in part, caused by IL-1β, IL-6, or IFN-γ in conjunction with TNF-α (Langstein et al., 1991; Espat et al., 1994; McCarthy, 2000); these cytokines, especially TNF-α, show direct catabolic effect on skeletal muscle and adipose tissue, thereby inducing weight loss (Tracey et al., 1990; Reid & Li, 2001; Tisdale, 2008). Based on our results, *S. Typhimurium*-infected HET and KO mice lost the most

weight- a readout that suggests much worse severity of disease in these mice. This observation was, however, not substantiated, as we did not observe elevated IL-1β, IL-6, IFN-γ or TNF-α cytokine levels in HET and KO animals as compared to WT mice; in fact, as compared to WT *S. Typhimurium*-infected animals, HET and KO *S. Typhimurium*-infected animals expressed comparable, if not less, but never more, IL-1β, IL-6, IFN-γ and TNF-α. As cytokine expression cannot explain our observation, it is therefore likely that the observed weight loss in *S. Typhimurium*-infected HET and KO animals is due to a non-disease-related issue especially considering that naïve HET and KO animals show much reduced weight gain with age as compared to naïve WT mice. It would have, therefore, been useful to utilise other behavioural tests in our study, however this was not implemented as conventional behavioural tests such as burrowing showed transient behavioural deficit that resolved by 24hrs post-infection (Püntener et al., 2012) and we would not have been able to characterise the disease severity across the whole time-course of *S. Typhimurium* infection.

3.5.2 "Do HSPB5 KO mice show increased splenocyte and lymph node cell proliferation"?

Ousman *et al.* (2007) noted that during EAE, HSPB5 KO mice showed increased splenocyte and lymph node cell proliferation; that is to say, they observed an increase in the immune cells of the spleen and lymph nodes. As described earlier, splenomegaly, a condition that arises as due to an increase of $NK1.1^+$, $Gr1^+$ neutrophils, $CD4^+$ and $CD8^+$ T-cells in the spleen, is a key feature of *S. Typhimurium* infection (Jackson et al., 2010). We indirectly measured the extent of splenocyte proliferation by assessing differences in spleen sizes between WT, HET and KO animals. Our results provided evidence for no significant difference in the spleen size of naïve animals or *S. Typhimurium* infected animals. This would suggest that the extent of immune cells proliferation in these organs was comparable, providing supporting evidence that perhaps HSPB5 KO mice do not have an aberrant immune activation.

3.5.3 "Do HSPB5 KO mice show significantly hyperactive macrophages and T-cells that contributed to aberrant cytokine expression"?

As macrophages and T-cells are pivotal for the majority of systemic cytokines produced during *S. Typhimurium*-infection (Pie et al., 1997; Mittrücker & Kaufmann, 2000; Mittrücker et al., 2002), we indirectly measured the activation status of these cells by analysing their systemic cytokine output. Our results provided further support for lack of aberrant immune-cell activation as we showed equal to, if not less, expression of IL-1β, IL-12, IFN-γ TNF-α, IL-6 and IL-10 in KO as compared to WT *S. Typhimurium*-infected animals.

3.5.4 "Do HSPB5 KO mice show increased glial apoptosis and robust CNS inflammation as evidenced by upregulation of astrocyte and microglia staining"?

The peripheral immune system communicates with the central immune system via the inflammatory reflex arc (Dantzer & Kelley, 2007; Tracey, 2009). Previously, it has been shown that following systemic *S. Typhimurium* infection, there is a transient central immune activation that leads to an activated microglial phenotype that is still apparent even 21 days post *S. Typhimurium*-infection (Püntener et al., 2012). With regard to increased glial apoptosis, as we did not use the TUNEL assay, it is difficult make a conclusion, however, using immunohistochemistry and western blotting, we did not find any microglial differences between *S. Typhimurium*-infected WT and KO animals, which would suggest the lack of HSPB5 did not result in either loss or upregulation of microglia.

Immunohistochemical analysis of GFAP expression suggests some regional differences in GFAP expression, however these did not translate to total protein expression by western blot. Western blot analysis showed no significant differences in the expression of GFAP between *S. Typhimurium*-infected WT and KO animals, which, again, suggests that lack of HSPB5 did not result in either significant loss or upregulation of GFAP. There was, however, a significant reduction in the basal expression of GFAP in KO animals, which we attribute to as being an effect was likely induced because HSPB5 mediates an important role in the stabilisation of GFAP (Nicholl & Quinlan, 1994); lack of HSPB5 might have affected basal expression of

HSPB5. GFAP induction was however not affected following *S. Typhimurium* infection, which suggests that in HSPB5 KO animals a compensatory mechanism is enacted. HSPB8, which has been shown to share several cytoskeleton-stabilisation functions with HSPB5, is likely to have compensated for the GFAP stabilisation role of HSPB5 (Wettstein et al., 2012).

3.5.5 "Recombinant addition of HSPB5 by intravenous injection resulted in the amelioration of disease, suppression of immune cell activation and decreased production of cytokines"?

Our internal comparison acts to validate the notion that recombinant addition of HSPB5 results in amelioration of disease, suppression of immune-cell activation and decreased production of cytokines. It is thought that HSPB5 protective properties, suppression of immune-cell activation and decreased production of cytokines by direct serological binding to pro-inflammatory mediators (Rothbard et al., 2012).We showed, however, that although WT animals show a basal expression of HSPB5 that is ≈2fold and an induced response to *S. Typhimurium* that is ≈3fold to HET animals, they did not show significantly different suppression of immune-cell activation and/or decreased production of cytokines. Considering that KO animals have no HSPB5, the proposed benefits of HSPB5 expression did not show any dose response-related mechanism.

3.5.6 Conclusion

HSPB5 has wide ranging roles, from inhibition of apoptosis to negative regulation of gene transcription (see chapter 2). Whilst the evidence for HSPB5 modulating the immune response observed in EAE is clear, in our study, we did not observe significant immune modulation by HSPB5. Our model, the *S. Typhimurium*-infection model is a robust model to characterise peripheral immune activation. Although it also shows modest central immune activation, there are other models that can be used to characterise central immune activation; we will investigate the potential immune modulatory roles of HSPB5 in the CNS innate immune response in the next chapter.

4. CHARACTERISATION OF HSPB5 AS AN IMMUNE REGULATOR OF CNS INNATE IMMUNE RESPONSE

This chapter is the second of two chapters to characterise HSPB5's immune modulatory capacity. This chapter specifically investigates HSPB5's immune modulatory capacity in the CNS. The well-characterised ME7 Prion disease model is used to induce robust inflammation in the CNS.

4.4 Introduction

In chapter 3, we characterised the immune modulatory capacity of HSPB5 in the periphery. Contrary to suggestions from literature, we found that, following systemic infection, endogenous expression of HSPB5 did not dampen systemic inflammation or improve disease progression when compared to HSPB5 deficient animals. Furthermore, the associated immune response we observed in the CNS, suggested that, even here, endogenous expression of HSPB5 did not modulate inflammation.

We extend our investigation by specifically characterising the associated response mounted by CNS innate immune cells following immunogenic insult. This will provide further insight to HSPB5's capacity for immune modulation, but more importantly, this will clarify if the induction of HSPB5 that is observed in several neurodegenerative conditions has an influential immune modulatory role.

Current understanding of HSPB5's immune modulatory role stems from studies using animal models of multiple sclerosis (Ousman et al., 2007; Rothbard et al., 2012), ischemic optic neuropathy (Pangratz-Fuehrer et al., 2011), ischemia reperfusion (Velotta et al., 2011), and stroke (Arac et al., 2011). These models have one thing in common: significant neuro-inflammation.

In this chapter, we instead use the ME7 model of Prion disease, which is an animal model characterised by prominent neuro-inflammation as well as neurodegeneration. By challenging HSPB5 deficient mice with ME7 prion disease, we can investigate the immune modulatory capacity of HSPB5 on the innate immune cells of the brain and subsequent effect on neurodegeneration. As inflammation has been suggested to mediate a role in Huntington's disease, these findings will help elucidate the consequences of the selective down-regulation of HSPB5 observed in R6/2 mice (Zabel et al., 2002; Quraishe, 2010).

4.5.5 ME7 model of Prion disease

ME7 Prion, is just one of many mouse-specific Prion strains used to induce disease in naïve mice (chapter 1). This strain of Prion has been extensively characterised and shows well-defined, tractable and replicable pathophysiological features (Betmouni et al., 1996; 1999; Deacon et al., 2001; Guenther et al., 2001; Cunningham et al., 2003; Gray et al., 2006; 2009; Hilton et al., 2013). The pathophysiological features of ME7 Prion disease provide a sensitive assay by which researchers can dissect molecular, cellular and anatomical events that contribute to neurodegenerative pathology.

4.4.5.1 Pathophysiological events associated with ME7 Prion disease

Inoculation with ME7 Prion can be done by oral, intraperitoneal or intracranial routes; regardless of route, ME7 Prion pathology is observed in several brain regions (Bruce et al., 1991) but most extensively in the dorsal hippocampus (Cunningham et al., 2005a; Hilton et al., 2013). Hippocampal pathology correlates with disease progression and symptomatic behavioural changes (Deacon et al., 2001; 2002).

4.4.5.1.1 Hippocampal pathology

Pathology in the hippocampus occurs in a time-dependant fashion: it is characterised, firstly, by extensive extracellular deposition of abnormal Prion protein (PrP^{Sc}) and then followed by synaptic loss and neuronal death (Cunningham et al., 2003). These events are overlaid by robust innate immune cell activation (Betmouni et al., 1996; 1999). Refer to figure 4.1 for a timeline of disease progression, which can be summarised as follows: deposition of Prion protein occurs in the hippocampus from 8 weeks post-inoculation (Gray et al., 2009). Synaptic loss occurs soon after, from 12 weeks post-infection, and coincides with deficits in behaviour (Cunningham et al., 2003). Neuronal loss occurs from 18 weeks post-inoculation and is characterised by severe cognitive and motor behaviours deficits (Asuni et al., 2010). Typically, these symptoms culminate in animal death within 23-24 weeks post-infection.

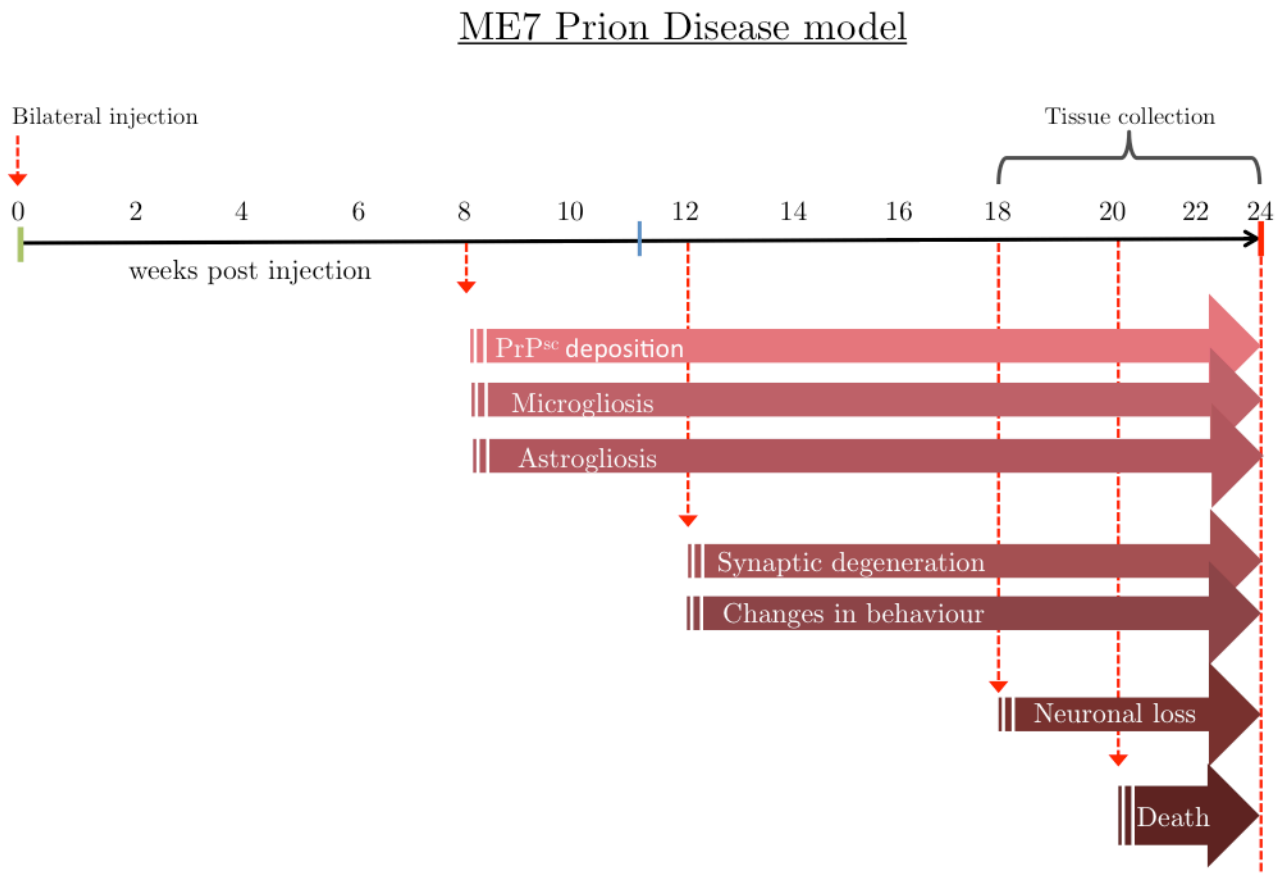

Figure 4.1 Summary of pathological events that occur during ME7 Prion Disease.
Bilateral hippocampal injections with either ME7 Prion brain homogenate (ME7) or normal naïve brain homogenate (NBH) are given to 8 week-old female mice. 8 weeks after inoculation with ME7 brain homogenate, extracellular deposition of proteinase K resistant prion (PrP^{Sc}) is apparent in the hippocampus. Microgliosis and astrogliosis are also apparent at this stage. At 12 weeks post prion inoculation the first evidence of synaptic degeneration is apparent. Significant changes in spontaneous behaviours become apparent. Neuronal loss occurs from 18 weeks post-inoculation onwards. Symptoms manifest in death between 20-24 weeks post-inoculation.

4.4.5.1.2 Immune response associated with ME7 Prion

Microglia and astrocytes, innate immune cells of the CNS (Ransohoff et al., 2012), show exquisite sensitivity to PrP^{Sc} deposition. Robust induction of these cells coincides with the earliest extracellular depositions of PrP^{Sc} (Betmouni et al., 1996; 1999; Aucouturier et al., 2000). Glial activation increases in a time-dependant fashion and is highly concentrated around PrP^{Sc} aggregates (Cunningham et al., 2003), suggesting that glia are responding to the aberrant protein aggregates.

4.4.5.1.2.1 Microglia

Early speculation suggested that the observed induction of microglia was detrimental because of the modest induction of pro-inflammatory cytokines IL-1β, IL-6, TNF-α (Betmouni et al., 1996). Subsequently, it has been shown that, as well as the afore mentioned cytokines, there is also, a much larger induction of anti-inflammatory cytokine TGFβ1 (Cunningham et al., 2002). TGFβ1 is associated with an atypical microglia phenotype (Perry et al., 2002) that contributes to phagocytic clearance of debris (Cunningham et al., 2005b; Teeling et al., 2007). Although atypical, the response of these microglia does not contribute to synaptic loss (Sisková et al., 2009).

4.4.5.1.2.2 Astrocytes

Little is known about the pathophysiological contribution of astrocytes during ME7 Prion disease, however; astrocytes show significant induction of GFAP (Asuni et al., 2013), a Type III intermediate filament, and selective upregulation of small heatshock proteins HSPB1, HSPB5, and HSPB8 (Quraishe, 2010). As GFAP is a Type III intermediate filament, the specific contribution of its upregulation during ME7 Prion disease is not clear, however, GFAP deficient astrocytes show less capacity to overcome acute CNS injuries (Pekny et al., 2004), therefore, induction of GFAP during Prion disease, as well as other conditions, is thought to be protective (Teismann et al., 2004).

Induction of HSPB5 in astrocytes is thought to suppress pro-inflammatory cytokine production and lead to reduced inflammation (Shao et al., 2013). HSPB1 and HSPB8 induction in astrocytes has not been characterised, however based on similar sequence homology to HSPB5, it is likely that these sHSPs, too, mediate a protective function.

4.4.5.2 Behavioural changes associated with ME7 prion disease

Impairment of several spontaneous behaviours, such as burrowing behaviour, develop concurrently with the synaptic loss in the hippocampus (Deacon et al., 2001; Guenther et al., 2001). Deficits progressively get worse with time, which correlates with hippocampal pathology (Deacon et al., 2002; Cunningham et al., 2003). By the time neuronal loss occurs, *ca.* 18weeks post inoculation, clinical symptoms become apparent: mice display significant affective, cognitive and motor behaviours deficits (Asuni et al., 2010). Two sensitive assays often used to discriminate pathological progression are burrowing behaviour and an open-field test that measures exploratory behaviour as a function of total distance travelled.

4.4.5.2.1 Burrowing behaviour

Mice exhibit an innate propensity to dig pellets out of a tube. This behaviour is hippocampal dependant (Deacon et al., 2002) and is referred to as burrowing. As compared to naïve control animals, ME7-inoculated mice show deficits in burrowing behaviour from 12 weeks post inoculation, which correlates with the beginning of synaptic loss. With time, burrowing progressively becomes worse (see figure 4.1).

4.4.5.2.2 Distance travelled

As an adjunct to burrowing behaviour, analysis of the distance travelled by ME7-inoculated mice shows that deficits in burrowing are not due to locomotor impairments (Cunningham et al., 2003); ME7-inoculated mice actually show increasing hyperactivity from 12 weeks post-infection. The neuro-biological basis of this behaviour is not fully understood, it is however, tractable and very replicable.

4.5 Aims

The pathophysiological features observed during ME7 prion inoculation are tractable, replicable and well defined. These features provide a sensitive assay to characterise molecular, cellular and behavioural features associated with neuro-inflammation and neurodegeneration in the CNS. By challenging HSPB5 deficient mice with ME7 Prion disease, we can investigate the influence of endogenous HSPB5 on the inflammatory process, especially in the context of neurodegeneration.

To characterise HSPB5's immune modulatory role in the CNS, we will inoculate HSPB5 deficient animals with ME7-prion and compare disease progression relative to animals that express HSPB5. We will investigate:

1. Behaviour deficits associated with ME7 inoculation. Behavioural analysis is a non-invasive mechanism we can use to provide a functional correlate to on-going neuropathology.
2. Cellular and molecular features associated with ME7-prion inoculation. We will characterise the extent of CNS immune-cell activation by analysing the upregulation of CNS immune cells and the cytokines expressed following ME7-inoculation.
3. Regional differences associated with ME7-prion inoculation. As basal expression of HSPB5 is noted in myelin and its upregulation is noted in astrocytes. We will characterise if there are regional pathology as due to HSPB5 deficiency.

4.6 Materials and methods

4.5.5 Animals and animal husbandry

8-weeks old female inbred mice, wild type ($HSPB5^{+/+}$), heterozygous ($HSPB5^{+/-}$) and knockout ($HSPB5^{-/-}$) littermates, were obtained in-house from the Biomedical Research Facility (University of Southampton). Mice were housed in groups of 3-5 in plastic cages all throughout the experiment. Mice were fed on an RM-1 Standard laboratory chow diet and had access to food and water *ad libitum*. The holding room was temperature controlled (21 – 23°C) with a 12hr:12hr light dark cycle (lights on at 07:00). Females were used to lessen risk of aggressive outbreaks and to conform to most of the previous work done in the laboratory. All procedures were preformed in accordance with the UK animals (Scientific Procedures) Act 1986 under personal license and ethical approval obtained from the University of Southampton and the UK Home Office.

4.5.6 Inoculation with ME7 prion homogenate

Mice were anaesthetised with a 2:1 combination of ketamine and xylazine at a dosage of 100µl/10g body weight. Full unconsciousness was tested for by pedal withdrawal reflex, following which, bilateral dorsal hippocampal injections with either ME7 prion homogenate (ME7) or normal brain homogenate (NBH) were given to the animals. The mice were mounted in a model-900 small animal stereotaxic frame (David Kopf Instruments, USA) and the scalp was cut open and skull exposed. Burr holes were drilled on either side at co-ordinates -2.0mm from Bregma, ±1.7mm bilateral, and -1.6mm deep. 1ul of either ME7 or NBH homogenate (10% w/v in sterile PBS) was injected using a 10ul Hamilton syringe (Sigma Aldrich, UK). The scalp was stitched together with grade 0.4 sutures (Ethicon, USA) and the mice were placed in a recovery chamber at 37^0C until full recovery. When full consciousness was regained,

4.6.7.3 Phenotype scoring

Phenotype scoring was used at the end-stage of disease (18 weeks) as a sensitive assay to try and supplement and distinguish findings from other assays. Phenotype scoring was adopted from the SHIRPA protocol (Rodgers 1997) and is used in several models of neurodegeneration specifically those with cerebellar dysfunction (Guyenet et al., 2010); to our knowledge, this is the first time this protocol has been used to characterise prion disease. All parameters were scored relative to severity of the phenotype to provide a quantitative comparison of phenotype.

4.6.7.3.1 Hind limb clasping

An assay of hind-limb clasping was used to measure muscle, lower motor neuron and spinocerebellar function (Rodgers 1997). Mice were suspended upside down from the tail for 20 seconds. If hind limbs were consistently splayed outwards, away from the abdomen, a normal reflex, the mice received a score of 0. If 1 limb was partially contracted towards the abdomen for more that 50% of the time, the animal scored 1. If 2 limbs were partially contracted towards the abdomen, they received a score of 2. If both hind limbs were completely contracted towards the abdomen, the animal received a score of 3. Scoring protocol can be observed in figure 4.1.

4.6.7.3.2 Ledge test

This assay was used to measure muscle, lower motor neuron and spinocerebellar function. Mice were individually placed on a ledge 10cm high. Mice instinctively try to lower themselves back onto a flat platform. Mice were scored on the following: successful lowering back onto platform, paws first, scored a 0; If footing was lost whilst on ledge, but otherwise successful lowering, mice received a score of 1; If the mice displayed an incapacity to balance and landed back on the platform awkwardly,

i.e. on their head, for example, they received a score of 2; lastly, if mice fell off the ledge completely, or did not move and stayed stationary, they received a score of 3.

4.6.7.3.3 Kyphosis test

Kyphosis is the dorsal curvature of the spine induced by loss of muscle tone in spinal muscles as secondary to neurodegeneration. Mice were placed on a flat surface and observed as they walked. If mice were able to walk with no persistent kyphosis, they received a score of 0. If mice exhibited mild kyphosis but could straighten their spine, they received a score of 1. If mice exhibited mild kyphosis and were unable to straighten their spine, they received a score of 2. Pronounced kyphosis and an inability to straighten their spine resulted in a score of 3.

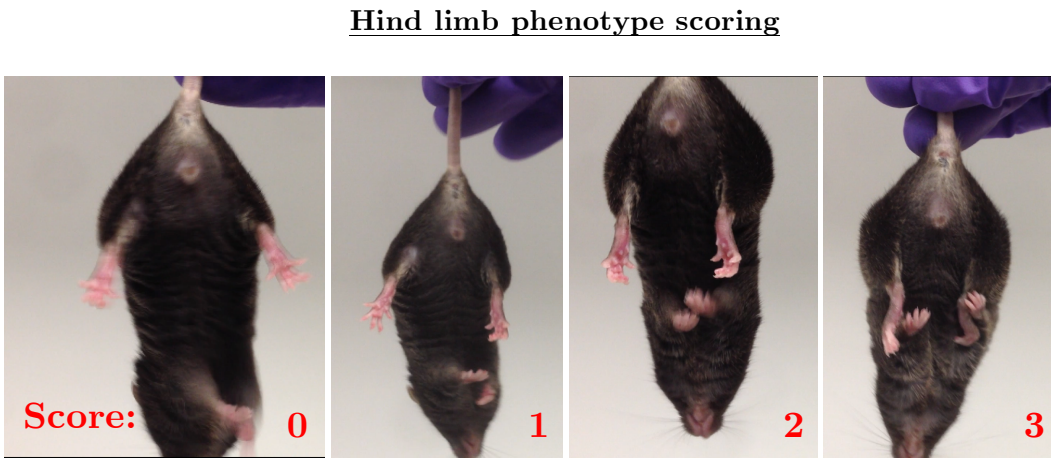

Figure 4.1 Hind limb phenotype scoring relative to severity of phenotype. 4 different mice showing the different phenotypes and how they are scored in the hind limb assay.

4.5.8 Tissue collection and processing

4.6.8.1 Terminal anaesthesia, perfusions and tissue fixation

At the end of the experiment, animals were terminally anaesthetised with 10µl/g Pentobarbital (Sigma Aldrich, UK). Mice were perfused with heparinised saline (0.9% saline containing 5000U/L heparin), but not fixed. The brain was removed and the two cerebral hemispheres were separated using a scalpel; half the brain was placed in a

bijous and fixed in 10% formalin overnight at 4°C for immunohistochemistry processing (section 4.3.5), whilst the other half was snap-frozen and stored at -20°C for biochemical analysis (section 4.3.6).

4.5.9 Immunohistochemistry

Formalin-fixed brains were de-hydrated by immersion in a series of increasing concentration alcohols and, lastly, by immersion into Histoclear (Sigma Aldrich, UK) (see table 4.1). Dehydration was carried out using a Leica-TP 1020 tissue processor (Leica Biosystems, UK). After dehydration, tissue was placed in plastic cassettes (Fisher Scientific, UK) and submerged in molten (40°C) paraffin wax (Polywax, UK) and allowed to solidify. Wax blocks were stored at room temperature. The wax-blocks were cut into 10µm sections on a Leica RM2255 rotary microtome (Leica Biosystems, UK) and tissue was floated on 40°C dH_2O in a tissue floatation bath (LAMB, UK). The resulting sections were mounted on SuperFrost™ microscope slides (Fisher Scientific, UK) and dried overnight at 37°C. Slides were stored at room temperature.

4.6.9.1 Immunostaining

Sections were heated at 60°C for 30 minutes and then de-waxed in xylene (Fisher Scientific, UK). Sections were re-hydrated by immersion in a series of decreasing concentration alcohols (see table 4.2). Sections to be stained for prion protein were autoclaved in distilled water for 15 minutes at 121°C and then microwaved for 5mins in 90% formic acid. Sections were subsequently rinsed in PBS. Endogenous peroxidase activity was blocked with a solution of 1% hydrogen peroxide (H_2O_2) and subsequent antigen retrieval was done for 5 minutes using citrate buffer (10mM citric acid (pH6)) in a 700W microwave. Non-specific binding was prevented by incubating sections in goat serum (GIBCO life technologies, UK). Sections were segregated using an ImmEdge™ hydrophobic barrier pen (Vector Labs, UK) and then incubated with primary antibodies: anti-glial fibrillary protein, mGFAP (1:1000) (Sigma Aldrich, UK); anti-prion protein, m6H4 (1:10000) (Prionics, Switzerland); anti-ionised

calcium-binding adapter molecule, mIBA1 (1:500) (Abcam, UK) and anti-alpha-B crystallin, mHSPB5 (1:200) (Abcam, UK) overnight (16-18hrs) at 4°C see table 4.1). Appropriate biotinylated secondary antibody ((Vector Laboratories, UK) 1:250) was applied for 1hr and then sections were incubated in ABC complex (Vector Laboratories, UK) for 45 minutes (see table 4.3). Location of antibody was determined by immersion in diaminobenzidine (DAB) solution with 1% hydrogen peroxide (H_2O_2) (Sigma Aldrich, UK). Sections were counterstained with Harris haematoxylin (VWR, UK) and de-hydrated by immersing in a series of increasing concentration alcohols and, lastly, by immersion into xylene (Fisher Scientific, UK) (reverse of table 4.2). Coverslips were applied with combined mountant DPX (Distrene, Plasticiser, Xylene) (VWR, UK). All images were taken using a Zeiss Axio Observer Z1 inverted microscope (Zeiss, UK).

4.6.9.1.1 Immunostaining quantification

Immunostaining was quantified using 3 animals from each condition; blind selection of 3 serial slides from each animal followed by analysis of 5 different microscopic fields from each slide. The number of cells positive for a particular immunogen were normalised to the number of haematoxylin positive cells within each region.

4.5.10 Biochemistry

The hippocampus was micro-dissected using the protocol described by (Hagihara et al., 2009) and snap-frozen in an eppendorf. The tissue was weighed and diluted in a 5x volume of TRIS buffer containing a complete protease inhibitor cocktail (Roche Diagnostics GmbH, Germany) and sub-aliquoted into two portions; one for cytokine analysis using quantitative polymerase chain reaction (qPCR) (section 4.3.6.1) and another for western blotting (section 4.3.6.2).

Treatment	Duration
70% ethanol	2 hours
70% ethanol	2 hours
80% ethanol	1 hour
90% ethanol	1 hour
Absolute ethanol I	1 hour
Absolute ethanol II	10 hours
Histoclear I	4 hours
Histoclear II	2 hours

Table 4.1 Automated settings for the dehydration of tissue

Treatment	Duration
Xylene I	10 minutes
Xylene II	10 minutes
100% ethanol	3 minutes
90% ethanol	3 minutes
80% ethanol	3 minutes
70% ethanol	3 minutes

Table 4.2 Tissue rehydration for immunohistochemistry.

1^{O} antibody	Species	Dilution	Incubation	Biotinylated antibody	Dilution
GFAP (Dako, US)	Mouse	1:5000	Over-night	Goat anti mouse-HRP	1:250
6H4 (Prionics, CH)		1:10000			
HSPB5 (Abcam, UK)		1:250			
IBA1 (Abcam, UK)		1:500			

Table 4.3 Primary and secondary antibodies used for immunohistochemistry analysis.

4.6.10.1 Quantitative PCR

4.6.10.1.1 RNA extraction and quantification

Hippocampal tissue diluted in a 5x volume of TRIS buffer (pH?) was obtained from the -80°C freezer. RNA was extracted from brain homogenate using Qiagen RNeasy Minikit (Qiagen, UK), according to manufacturer's instructions. To determine quality and quantity of RNA, total RNA content was analysed by NanoDrop spectrophotometer (Fisher Scientific, UK). Pure RNA has an A260/A280 ratio ≥2.0, purity of less than 1.9 was deemed insufficient for experimentation.

4.6.10.1.2 Complimentary DNA synthesis

For samples to be used as standard curves (WT NBH) 800ng of RNA was transcribed into cDNA and for the rest of the samples, 200ng of total RNA was reversed transcribed into cDNA using the iScript Select cDNA Synthesis kit (Bio-Rad, UK), as according to manufacturer's protocol. The reactions were incubated in a GeneAmp PCR System 9700 thermocycler (Applied Biosystems, UK) for 60 minutes at 42°C then 5 minutes at 85°C and stored at 4°C.

4.6.10.1.3 Quantitative real-time PCR

Samples to be used as standard curves were serially diluted, from neat, by a factor of 5, 4 times. All other samples were added neat and quantitative real-time PCR (rt-PCR) was performed by mixing cDNA with primers and iQ™ SYBR® Green (Bio-Rad, UK), as per manufacturer's instructions. Primers, sequences and melting temperatures are shown in Table 4.1. Reagents were incubated in a CHROMO 4 DNA engine thermocycler (Bio-Rad, UK). As SYBR® Green fluoresces when it binds to double stranded DNA, direct detection of amplified PCR products was monitored using provided Opticon Monitor Software v3.1.32. The cycling conditions used are documented in Appendix 4.1.

Cytokine	Primers	Tm
IL-1 (10µm) (Sigma Aldrich, UK)	Forward: 5' –TGTGTTTTCCTCCTTGCCTC- 3'	64.1^{O}C
	Reverse: 5' -CTGCCTAATGTCCCAAGA- 3'	63.9^{O}C
IL-6 (10µm) (Sigma Aldrich, UK)	Forward: 5' -TCCAGAAACCGCTATGAAGTTC-3'	64.1^{O}C
	Reverse: 5' -CACCAGCATCAGTCCCAAGA- 3'	66.4^{O}C
TNF-α (10µm) (Sigma Aldrich, UK)	Forward: 5' -CGAGGACAGCAAGGGCATA- 3'	63^{O}C
	Reverse: 5' -GCCACAAGCAGGAATGAGA- 3'	65.3^{O}C
GAPDH (10µm) (Sigma Aldrich, UK)	Forward: 5' -TGAACGGGAAGCTCACTGG- 3'	66.5^{O}C
	Reverse: 5' -TCCACCACCCTGTTGCTGTA- 3'	66.6^{O}C

Table 4.4: qPCR primers. Table showing primers, supplier, primer sequence and melting temperature (Tm) used for qPCR. Amplification efficiency of the primers is ≥95%.

4.6.10.1.4 GAPDH normalisation and quantification

All data obtained from rt-PCR was normalised to a non-changing reference gene, GAPDH, using the ΔC_T Method, whereby the base10 normalisation of the gene of interest is divided by base10 normalisation of GAPDH.

4.6.10.2 Western blot

Total protein concentration was assessed using a Bio-Rad D_C protein assay kit (Bio-Rad, UK), as per manufacturer's instruction. All samples were diluted to a final concentration of 4mg/ml in 5x sample buffer (250mM TRIS-HCl (pH6.8), 10% SDS, 30% Glycerol, 5% β-mercapto-ethanol, 0.02% bromo-phenol blue) and run on a polyacrylamide gel composed of 5% stacking gel and 12.5% resolving gel in 1x Laemmli buffer (5mM TRIS (pH8.3), 192mM Glycine, 0.1% SDS) using the Bio-Rad protein gel system (Bio-Rad, UK). Equivalent loading was checked by coomassie staining (Sigma Aldrich, UK), as per manufacturer's instructions (see section 2.3.7). Coomassie membranes were scanned at 700nm using the Odyssey infrared imaging scanner (LiCOR, UK) and quantified using Odyssey software v1.2 (LiCOR, UK).

Proteins were transferred to nitrocellulose membrane (Amersham, UK) overnight (16-18hrs) at 4°C in transfer buffer (1x Laemmli buffer, 20% (v/v) Methanol). Membranes were blocked with 4% non-fat milk (TESCO, UK) and incubated in primary antibodies: monoclonal anti-glial fibrillary protein, mGFAP (1:5000) (Sigma Aldrich, UK), monoclonal anti-prion protein, m6H4 (1:5000) (Prionics, Switzerland) and monoclonal anti-alpha-B crystallin, mHSPB5 (1:500) (Abcam, UK) overnight (16-18hrs) at 4°C (see table 4.5). In some laboratories, lysates to be probed with 6H4 antibody are subjected to proteinase K digestion; this step was not done in this experiment. Membranes were washed in TRIS-buffered saline with 0.05% tween (TBS-T) (pH7.2) and secondary antibodies: anti-mouse or rabbit IRDye™ 680RD or IRDye™ 800CW (LiCOR, UK) were applied for 1hr. Membranes were visualised using the Odyssey infrared imaging scanner (LiCOR, UK), as per manufacturer's instructions.

Primary antibody	Originating species	Dilution	Secondary antibody	Dilution
GFAP (Abcam, UK)		1:5000		
6H4 (Prionics, CH)	Mouse	1:5000	anti-mouse IR (Invitrogen, UK)	1:1000
HSPB5 (Abcam, UK)		1:500		

Table 4.5 Primary and secondary antibodies used for western blotting.

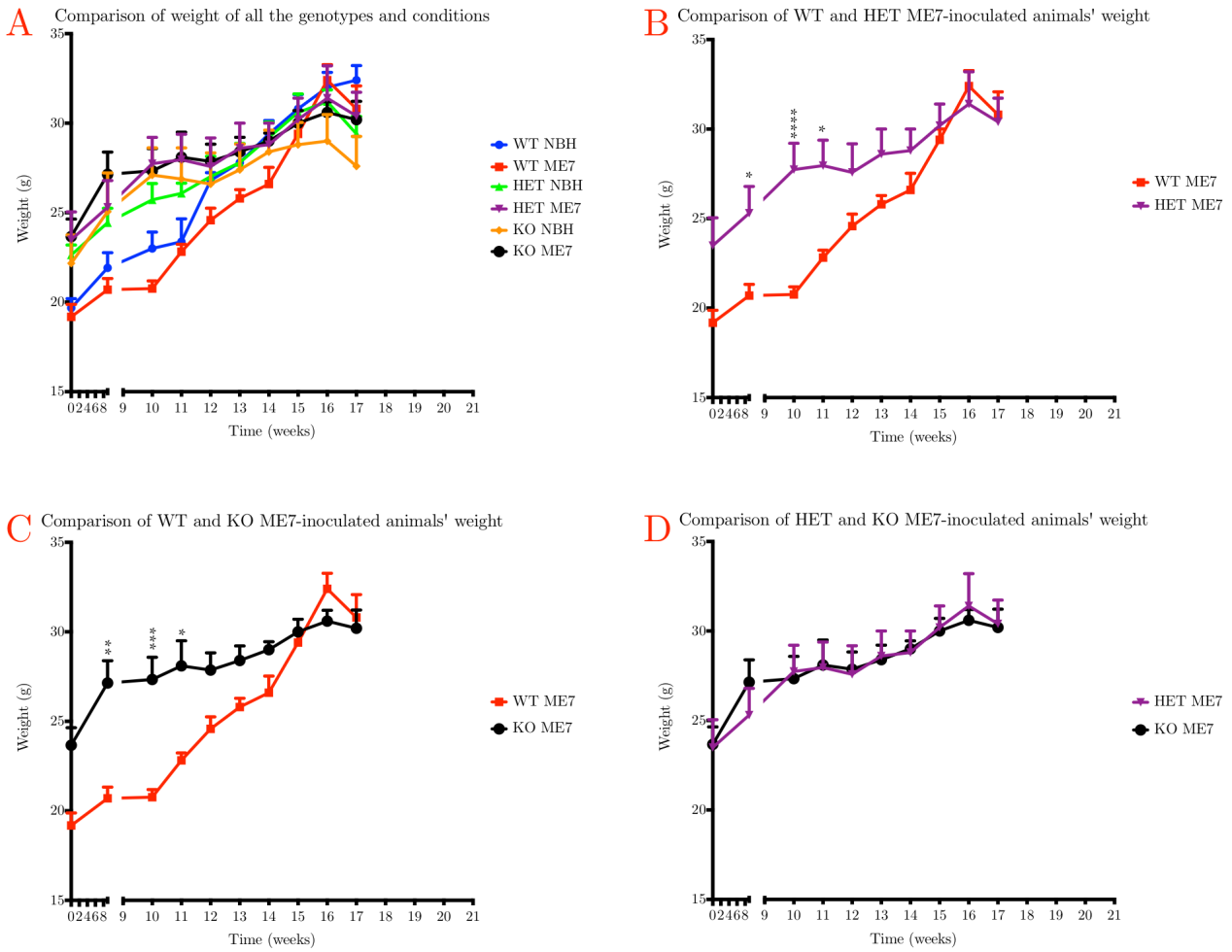

Figure 4.3 Characterisation of animal weight following ME7-prion inoculation. Graph showing weight measured from 8-21 weeks post inoculation.
(A) Change in weight for all animals in the cohort. (B) Comparison of change in weight between ME7-inoculated WT and HET animals. (C) Comparison of changes in weight between ME7-inoculated WT and KO animals. (D) Comparison of changes in weight between ME7-inoculated HET and KO animals. For each time-point, n=5 female mice. Two-way ANOVA analysis with Tukey post-hoc analysis was used. Error bars represent SEM from 5 animals per time point. $P < 0.05$ (*), $P<0.01$ (**), $P<0.001$ (***), $P<0.0001$ (****).

4.7.5.2 Burrowing behaviour

As compared to NBH-inoculated animals, burrowing behaviour showed progressive impairment in ME7-inoculated animals. Reduction in burrowing behaviour begins from 13 weeks post-inoculation for WT, HET and KO ME7-treated animals ($p>0.05$) (figure 4.4A) and shows significant deficit in WT and HET ME7-inoculated animals from 16-weeks post infection ($p<0.0001$) (figure 4.4B-C). ME7-inoculated KO animals show significant deficits from NBH-inoculated controls at 18-weeks post inoculation. The deficits in burrowing behaviour between WT, HET and KO ME7-inoculated animals was not statistically different ($p>0.05$).

4.7.5.3 Distance travelled (Open field behaviour)

The results show that whilst ME7-inoculated animals show deficits in burrowing behaviour (figure 4.4A-D), the deficits in burrowing are not due to shortcomings in ME7-inocuated animals' locomotor activity; ME7-inoculated animals actually show hyperactivity, i.e. increased exploratory behaviour, during open field-testing relative to NBH-inoculated animals (figure 4.5A-D).

As compared to naïve controls, WT and HET animals show significant hyperactivity from 12 weeks post-inoculation ($p<0.01$) (figure 4.5B-C) and KO animals show significant hyperactivity from 11 weeks post-inoculation ($p<0.0001$) (figure 4.5D). By 18 weeks post-inoculation, HET ME7 animals cover 68% more distance than WT ME7-inoculated animals ($p<0.0001$) and 40% more distance than KO ME7-inoculated animals ($p<0.01$).

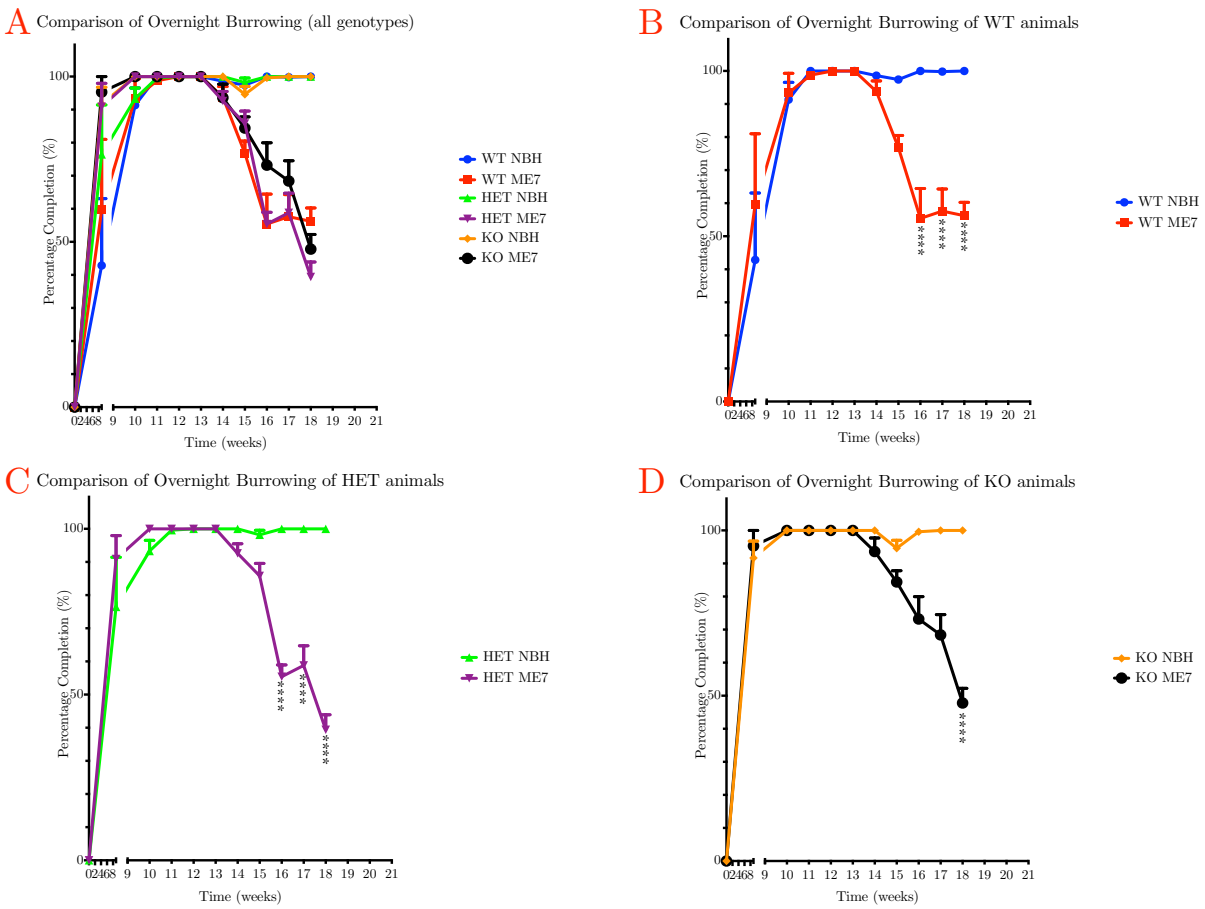

Figure 4.4 Characterisation of burrowing behaviour following ME7-inoculation. (A) Change in burrowing behaviour for all animals in the cohort. (B) Comparison of change in burrowing behaviour between WT NBH and ME7-inoculated animals. (C) Comparison of changes in burrowing behaviour between HET NBH and ME7-inoculated animals. (D) Comparison of changes in burrowing behaviour between KO NBH and ME7-inoculated animals. For each time-point, n=5 female mice. Two-way ANOVA analysis with Tukey post-hoc analysis was used. Error bars represent SEM from 5 animals per time point. $P < 0.05$ (*), $P<0.01$ (**), $P<0.001$ (***), $P<0.0001$ (****).

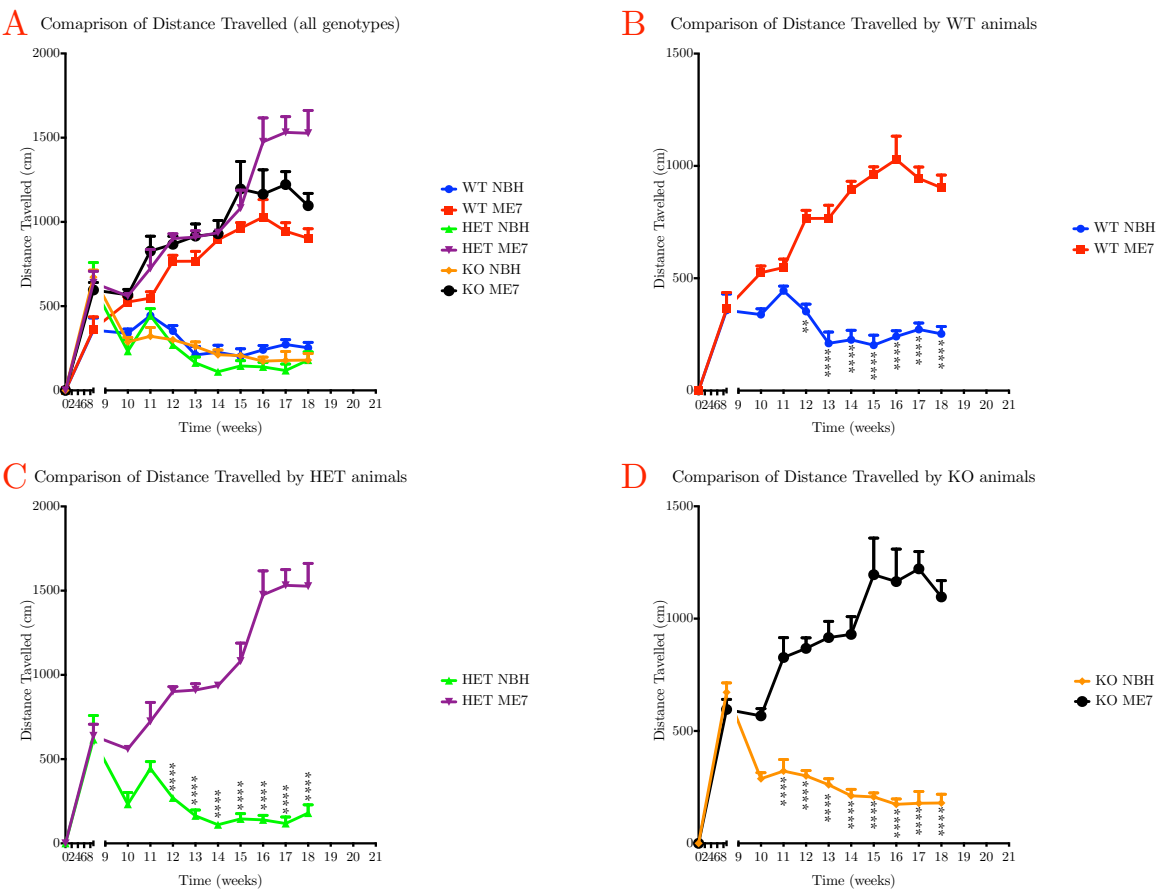

Figure 4.5 Characterisation of distance travelled during Open field Test following ME7 inoculation.

(A) Distance travelled for all animals in the cohort. (B) Comparison of distance travelled between WT NBH and ME7-inoculated animals. (C) Comparison of distance travelled between HET NBH and ME7-inoculated animals. (D) Comparison of distance travelled between KO NBH and ME7-inoculated animals. For each time-point, n=5 female mice. Two-way ANOVA analysis with Tukey post-hoc analysis was used. Error bars represent SEM from 5 animals per time point. $P < 0.05$ (*)
, $P<0.01$ (**), $P<0.001$ (***), $P<0.0001$ (****).

4.7.5.4 Behavioural analysis (cerebellum-dependant)

ME7 pathology is most pronounced in the hippocampus, however; thalamic and limbic regions, brainstem, cortex and the cerebellum are also affected (Cunningham et al., 2005a). To provide a more comprehensive characterisation of pathology, we extended our investigation to the cerebellum. Cerebellar dysfunction was investigated by scoring deficits in cerebellar-dependant tasks using a rapid and sensitive protocol for cerebellar dysfunction known as phenotype scoring (Guyenet et al., 2010). This protocol has been used successfully to discriminate cerebellar dysfunction in several conditions (Ditzler et al., 2003; Thomas et al., 2006; Chou et al., 2008).

4.7.5.4.1 Phenotype scoring

Measures include hind limb clasping, ledge test, and kyphosis (see Methods). Each measure is cerebellar dependent and is recorded on a scale of 0-3, with 0 resembling animals with no affective behaviour and 3 resembling those showing most affective phenotype. Measures may be analysed individually or for greater statistical power, combined into a composite phenotype score. As compared to NBH-inoculated controls, ME7-inoculated animals showed higher scores in all tests, signifying more cerebellar dysfunction in these animals (figure 4.6A-D).

4.7.5.4.1.1 Hind limb test

In the hind limb test, WT ME7-inoculated animals show the most impaired behaviour relative to NBH-control animals ($p<0.01$) (figure 4.6A). HET and KO ME7-inoculated animals show a trend towards affective scores ($p>0.05$). The scores of WT, HET and KO ME7-inoculated animals are not significantly different from each other ($p>0.05$).

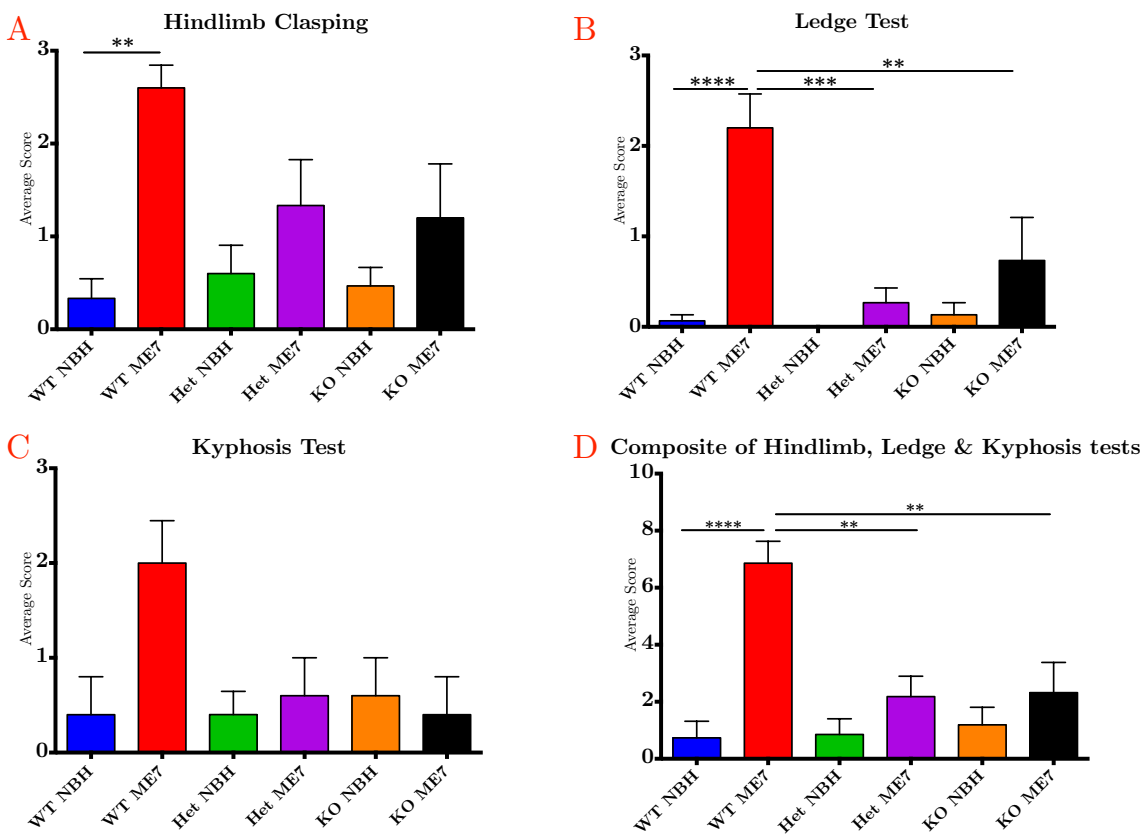

Figure 4.6 Characterisation of cerebellar dysfunction at 18 weeks post-inoculation.
(A) Hind limb clasping: test distinguishes difference in how mice splay their hind limbs when turned upside-down from the tail. (B) Ledge test: test measures balance and co-ordination. (C) Kyphosis test: test distinguishes hunched-back posture, an affective behaviour resulting from inability to coordinate muscular tone in the spine. (D) For added statistical power, composite of hind limb, ledge and kyphosis tests. Scoring: 0 denotes animals with no affective phenotype, 3 denotes animals with the most affective behaviour, thus signifying the most extensive cerebellar dysfunction. For each time-point, n=5 female mice. Two-way ANOVA analysis with Tukey post-hoc analysis was used. Error bars represent SEM from 5 animals per time point. $P < 0.05$ (*), $P<0.01$ (**), $P<0.001$ (***), $P<0.0001$ (****).

4.7.5.4.1.2 Ledge test

In the ledge test, a test of balance and coordination, WT ME7-inoculated animals showed severe deficits relative to NBH-inoculated control animals ($p<0.0001$) (figure 4.6B). WT ME7-inoculated animals were significantly more impaired in balancing and coordinating movement as compared to HET and KO ME7-inoculated animals ($p<0.01$). HET and KO ME7-inoculated animals did not show significantly different scores relative to NBH controls ($P>0.05$).

4.7.5.4.1.3 Kyphosis test

Kyphosis, a test for hunched posture, showed very low scores (i.e. no/little affective phenotype) for HET and KO ME7-inoculated animals as compared to NBH controls ($p>0.05$) (figure 4.6C). The test showed WT ME7-inoculated animals to have moderate kyphosis relative to NBH-inoculated controls ($p>0.05$). The kyphosis in WT ME7-inoculated animals is not significantly different to that observed in HET and KO ME7-inoculated animals ($p>0.05$).

4.7.5.4.1.4 Composite score

A composite of all 3 tests provides greater statistical power. The composite shows that out of all the genotypes, WT ME7-inoculated animals show the most severe cerebellar dysfunction relative to NBH controls ($p<0.0001$) as well as HET and KO ME7-inoculated animals ($p<0.01$) (figure 4.6D).

4.5.6 Molecular and cellular changes associated with ME7 Prion disease

ME7-inoculated animals show marked PrP^{Sc} accumulation in the limbic system, brainstem, cortex and cerebellum (Cunningham et al., 2005a). As some behavioural deficits are associated with hippocampal pathology, we characterised molecular and cellular changes in the hippocampus and also the overlying corpus callosum (CC). Here, our characterisation distinguishes two regions: the corpus callosum, for its richness in oligodendrocytes and the cortex, stratum oriens or stratum radiatum, for their abundance in astrocytes. The distinction is important as it investigates the effect of HSPB5 deficiency in two cells that express HSPB5.

4.7.6.1 PrP^{Sc} deposition

Immunohistochemical analysis shows ME7-inoculated animals with deposition of PrP^{Sc} within the dentate gyrus, with more sparse deposition apparent in the cortex, corpus callosum and stratum oriens of the mice; NBH-inoculated animals do not show deposition of PrP^{Sc} (figure 4.7A-B). Marked vacuolation (i.e. holes in the tissue), a key pathological hallmark of Prion disease, is also apparent in ME7-inoculated animals but not in NBH-inoculated animals (figure 4.7A-B).

Protein analysis confirms that the extent of PrP^{Sc} deposition is significantly different between NBH and ME7-inoculated animals ($p<0.0001$) (figure 4.7C), but not between ME7-inoculated WT, HET and KO animals ($p>0.05$) (figure 4.7C).

4.7.6.2 Microglia response

An analysis of the microglial response shows marked gliosis in the hippocampus of ME7-inoculated animals (figure 4.8A-C). Immunohistochemistry using IBA1 antibody highlights widespread microglial activation in all layers of the hippocampus for ME7-inoculated animals relative to NBH-inoculated animals (figure 4.8A). There are few microglia in the corpus callosum of NBH-inoculated animals, however, following ME7-inoculation, there is an activation of microglia in the corpus callosum (figure 4.8B).

Microglia count clarifies that as compared to NBH-inoculated controls, all ME7-inoculated animals, regardless of genotypes mounted a robust response ($p<0.05$) (figure 4.8C). As compared to NBH-inoculated controls, WT and HET ME7-inoculated animals mounted a ≥7-fold induction ($p<0.0001$) and KO ME7-inoculated animals mounted a ≥5-fold induction ($p<0.05$) of microglia. The capacity to activate microglia is not significantly different between ME7-inoculated WT, HET and KO animals ($p>0.05$).

Whilst immunohistochemical analysis is useful, it is not quantitative. Western blot analysis would be been very useful. We did not examine the immune-reactivity of microglia by western blot because it was difficult to optimise the IBA1 antibody for western blotting. FA11, a common microglial marker would have been a good alternative, but even this marker was difficult to optimise for western blott. Future experiments may aim to utilise CD68 or CD86 markers for western blotting.

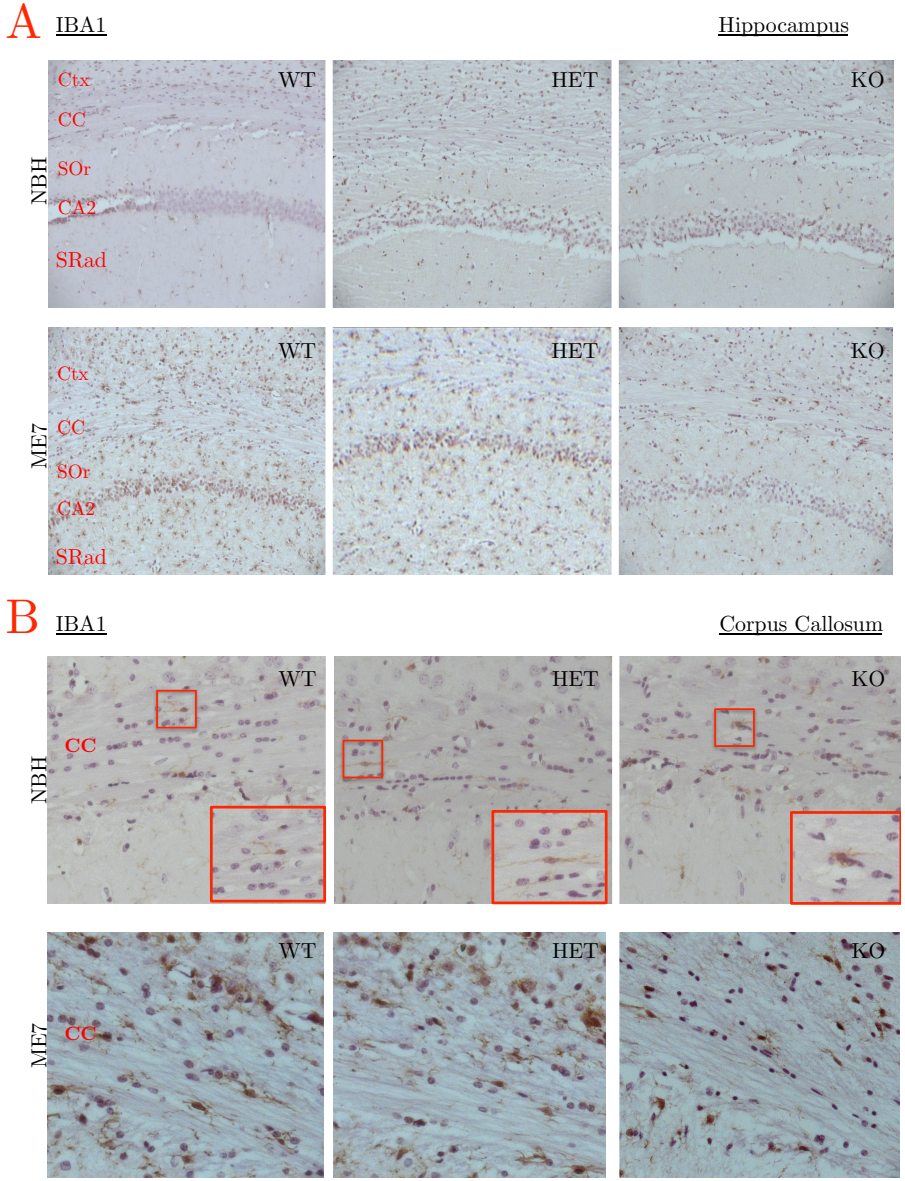

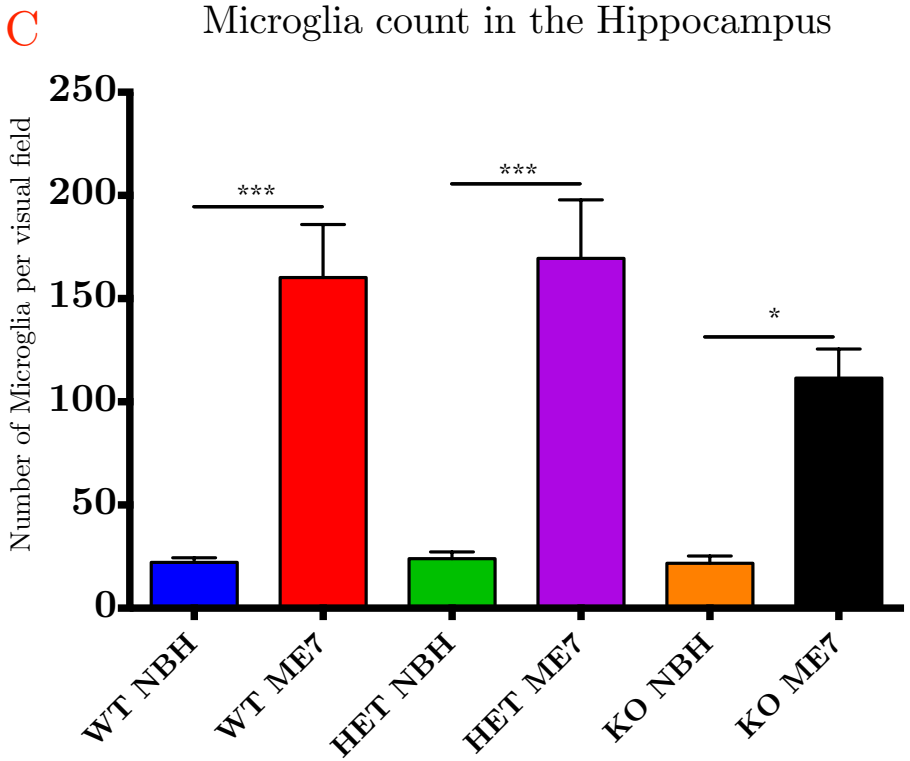

Figure 4.8 Microglial analysis in the hippocampus at end-stage of Prion disease.
Sections (A-B) Immunohistochemistry analysis. Sections stained with IBA1 antibody (brown staining) and haematoxylin (blue staining). (A) Overview of IBA1 expression in several layers of the hippocampus. (B) IBA1 expression in the corpus callosum (CC). Inserts highlight microglial morphology Representative images are shown. Phenotype analysis (C) was done with n=3 using 3 slides and 5 different visual fields each. Two-way ANOVA analysis with Tukey post-hoc analysis was used. $P < 0.05$ (*), $P<0.01$ (**), $P<0.001$ (***), $P<0.0001$ (****). Abbreviations: IBA1, ionised calcium-binding adaptor molecule 1; ME7, prion injected; NBH, normal brain homogenate injected; WT, wild type; HET, heterozygous; KO, knock-out; CA2, Cornu ammonis area 2; CC, Corpus callosum; Ctx, Cortex; SOr, Stratum oriens; SRad, Stratum radiatum. Scale bars: (A) 250μm, (B) 100μm.

4.7.6.3 Astroglial response

Astrocytes are readily detectable in all the layers of the hippocampus of NBH-inoculated animals (figure 4.9A-B). Following ME7-inoculation, there is widespread upregulation of GFAP in the cortex, corpus callosum, stratum oriens and stratum oriens of all ME7-inoculated animals (figure 4.9A-B). Protein analysis of hippocampal lysate confirms that relative to NBH-inoculated control animals, there is a significant upregulation of GFAP in ME7-inoculated WT, HET and KO animals ($p<0.01$) (figure 4.9C).

4.7.6.4 HSPB5 response

It has been previously shown that HSPB5, which shows basal expression in oligodendrocytes, is upregulated in astrocytes during ME7-prion disease. Our findings show that there is little HSPB5 staining in the cortex, stratum oriens and stratum radiatum in NBH-inoculated WT animals (figure 4.10A-B); the most significant HSPB5 staining is localised in the corpus callosum. Following ME7-inoculation, WT animals show a marked induction of HSPB5 in all regions of the hippocampus. Visually, HET animals show similar basal and induced pattern of HSPB5 expression as WT animals; KO animals show no expression of HSPB5 (figure 4.10A-B), which is as expected.

Protein analysis highlights that the basal expression of HSPB5 in HET and KO animals is significantly less than WT animals ($p<0.05$) (figure 4.10C). Following ME7-inoculation, relative to NBH-inoculated controls, WT animals mount the most significant response ($p<0.01$). HET and KO ME7-inoculated animals do not show a significant induction of HSPB5 following ME7-inoculation ($p>0.05$).

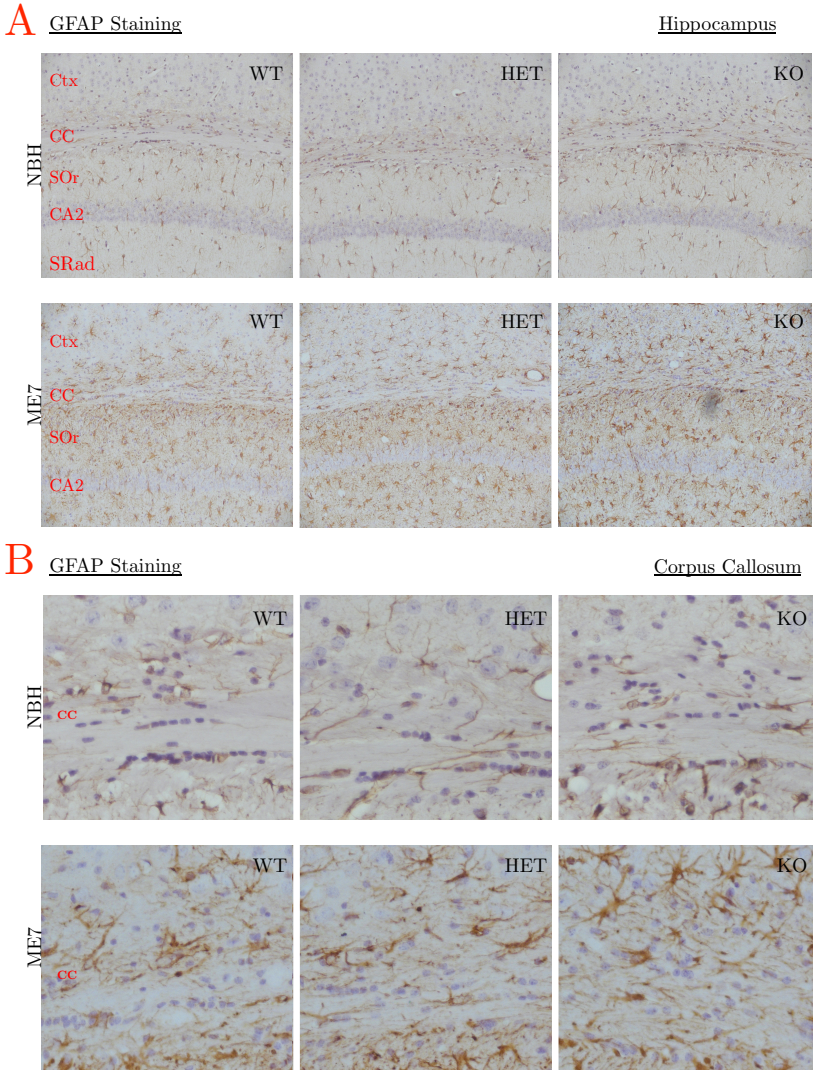

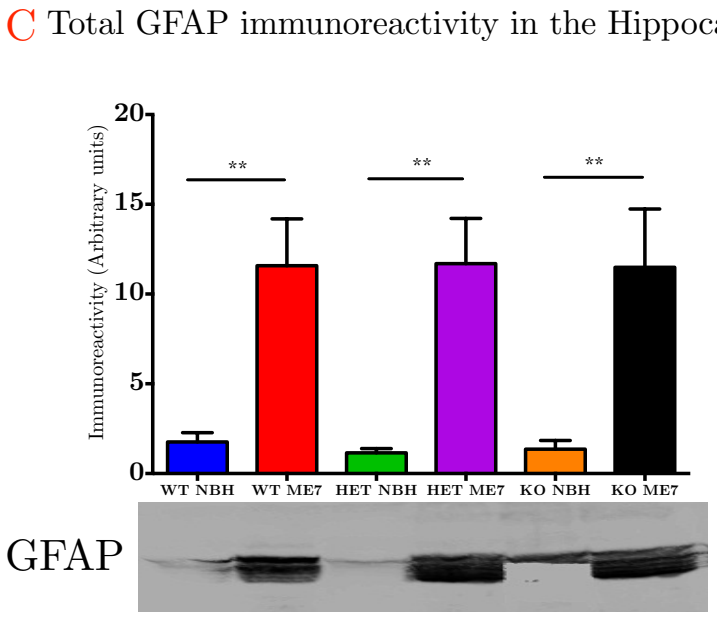

Figure 4.9 Astrocyte analysis in the hippocampus at end-stage of Prion disease.

Sections (A and B) stained with GFAP antibody (brown staining) and haematoxylin (blue staining). (A) Composite of GFAP expression localised in the Ctx, CC, SOr, CA2, and SRad. (B) Images showing GFAP immunoreactivity, focussing specifically on the CC. Representative images are shown. (C) Quantitative western blot showing GFAP immunoreactivity in the hippocampus. For western blot, n=5 female mice. Representative western blot is shown. 40μg protein loaded in each well; equal loading checked by coomassie staining (not shown). Two-way ANOVA analysis with Tukey post-hoc analysis was used. Abbreviations: GFAP, glial fibrillary protein; ME7, prion injected; NBH, normal brain homogenate injected; WT, wild type; HET, heterozygous; KO, knock-out; Ctx, cortex; CC, corpus callosum; SOr, stratum oriens; CA2, connu ammonis 2; SRad, stratum radiatum. Scale bars: (A) 250μm, (B) 100μm.

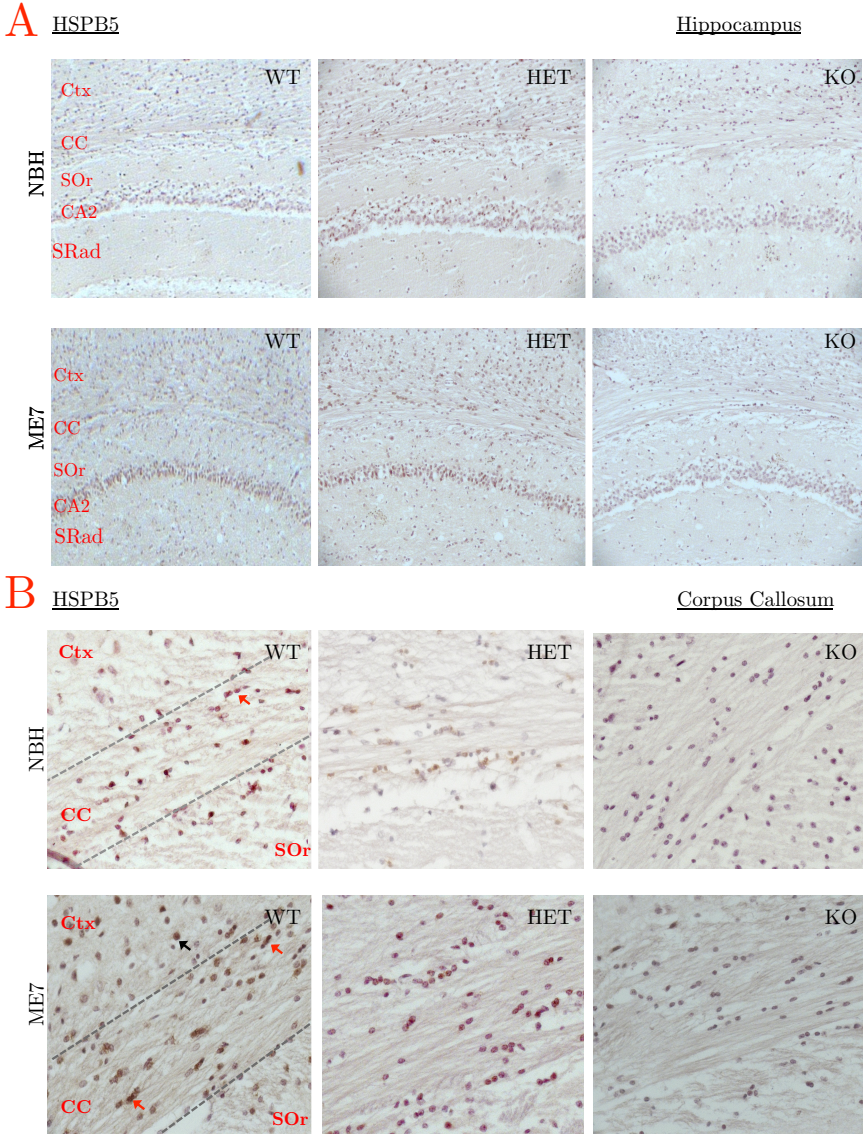

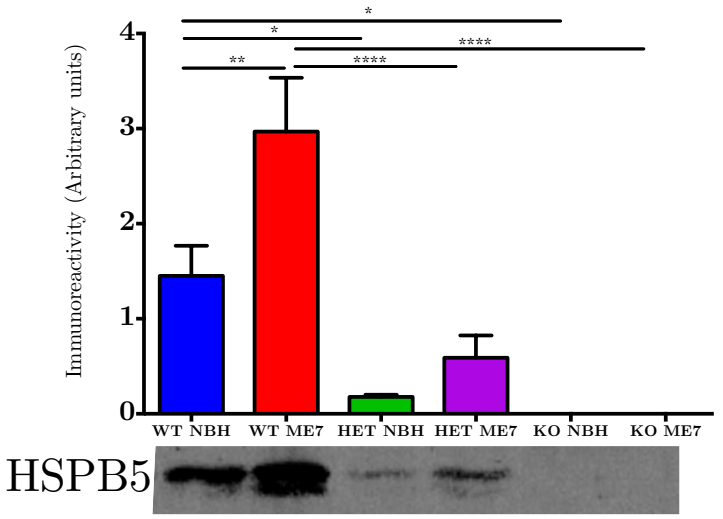

Figure 4.10 HSPB5 analysis in the hippocampus at end-stage of Prion disease.
Sections (A and B) stained with HSPB5 antibody (brown staining) and haematoxylin (blue staining). (A) Composite of HSPB5 expression localised in the Ctx, CC, SOr, CA2, and SRad. (B) Images showing HSPB5 immunoreactivity, focussing specifically on the CC. Representative images are shown. (C) Quantitative western blot showing HSPB5 immunoreactivity in the hippocampus. For western blot, n=5 female mice. Representative western blot is shown. 40µg protein loaded in each well; equal loading checked by coomassie staining (not shown). Two-way ANOVA analysis with Tukey post-hoc analysis was used. Abbreviations: HSPB5, small heat shock protein B5; ME7, prion injected; NBH, normal brain homogenate injected; WT, wild type; HET, heterozygous; KO, knock-out; Ctx, cortex; CC, corpus callosum; SOr, stratum oriens; CA2, connu ammonis 2; SRad, stratum radiatum. Scale bars: (A) 250µm, (B) 100µm.

4.7.6.5 Cytokine mRNA expression

Transcript levels of pro-inflammatory cytokines IL-1β, IL-6 and TNF-α were measured. In our lab, these cytokines have previously been shown to be elevated during ME7 Prion inoculation (Cunningham et al., 2005). Investigation of transcript levels of pro-inflammatory cytokines showed that, as compared to naïve, non-inoculated animals, ME7-inoculated animals induce cytokine transcript levels, regardless of genotype (figure 4.1); transcript levels of IL-1β were significantly upregulated in WT ($p<0.001$), HET ($p<0.01$) and KO ME7-inoculated animals ($p<0.0001$).

Transcript levels of IL-6 were also upregulated significantly in KO ME7-inoculated animals, showing a 2.3-fold induction ($p<0.01$) but not WT ME7-inoculated animals that showed a 1.5-fold induction ($p>0.05$) or HET ME7-inoculated animals that showed a 1.6-fold induction ($p>0.05$).

Transcript expression of TNF-α was significantly elevated in WT animals ($p<0.001$) and KO ME7-inoculated animals ($p<0.01$) but not in HET ME7-inoculated animals ($p>0.05$). Although the HET ME7-inoculated animals did not induce a significant amount of IL-6 and TNF-α mRNA in response to ME7 inoculation, their capacity of to induce cytokine was not statistically different from the WT and KO ME7 animals.

To conclude this experiment, it would have been useful to characterise the cytokine response using a mesoscale (similar to chapter 3) as this technique measures cytokine protein levels and is extremely sensitive. Unfortunately, a lack of funds hindered the use of the mesoscale.

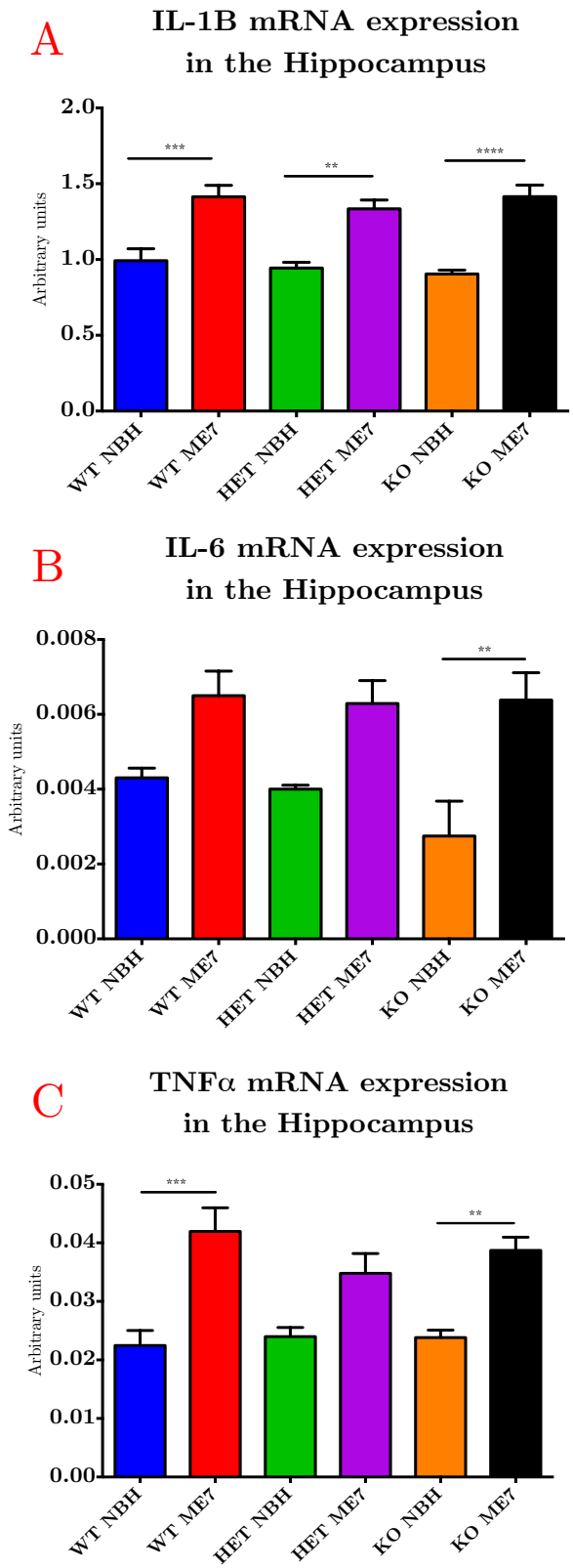

Figure 4.11 Transcriptional analysis of cytokine expression in the hippocampus following prion inoculation.
Transcriptional expression of (A) IL-1β, (B) IL-6, and (C) TNF-α in the hippocampus at 18 weeks post prion inoculation comparing inoculated animals to naïve animals. For all conditions, n=5 female mice. Two-way ANOVA analysis with Tukey post-hoc analysis was used. Error bars represent SEM from 5 animals per time point. $P < 0.05$ (*), $P<0.01$ (**), $P<0.001$ (***), $P<0.0001$ (****).

Discussion

HSPB5 is proposed to be a negative regulator of inflammation that may act as a molecular brake to dampen the inflammatory response (Masilamoni et al., 2006; Ousman et al., 2007). The study by Masilamoni et al., (2006) shows that intravenous administration of silver-nitrate to BALB/c mice results in GFAP upregulation, however, pre-treatment of the mice with recombinant HSPB5 blocked GFAP upregulation and resulted in lower levels of nitric oxide levels in the plasma, liver, neocortex and hippocampus. Ousman et al., (2007), on the other hand, using a model of experimental autoimmune encephalopathy (EAE) in 129/sv mice, showed that HSPB5 KO mice had worse progression of EAE, especially at the inductive (early) and progressive (late) stages. The mice also showed exaggerated activation of microglia with elevated levels of pro-inflammatory cytokines interleukin 2 (IL-2), interferon-gamma (IFN-γ), tumour necrosis factor- alpha (TNF-α) interleukin 12 (active form) (IL-12p40) and interleukin 17 (IL-17). Ousman et el., further showed that intravenous injection of recombinant HSPB5 results in suppression of inflammation and diminished production of pro-inflammatory cytokines IL-2, IFN-γ, TNF-α, IL-12p40, and IL-17. Several other studies have since shown immune modulatory roles of recombinant injection of HSPB5 in various conditions (van Noort et al., 2010; Arac et al., 2011; Klopstein et al., 2012). All these studies conclude that aside from being a molecular chaperone, HSPB5 is also a modulator of the inflammatory response. We have investigated this notion using a different paradigm of chronic inflammation, the Prion disease model, because this model has been extensively characterised in wild-type (WT) mice and shows distinct anatomical localisation, distinguished inflammatory response, synaptic changes, behavioural deficits, and lastly, neuronal loss and death (Betmouni et al., 1999; Deacon et al., 2001; Cunningham et al., 2003) -all of which can be used to elucidate if HSPB5 modulates the progression of chronic neurodegenerative disease.

Taken together, these results provide some evidence that during ME7 prion disease, HSPB5 does not modulate inflammatory processes and its deletion does not lead to exacerbated disease progression.

These results are somewhat surprising, especially considering the pleiotropic activities of HSPB5 (table 1.5). It would have been expected that WT animals, which have full complement of HSPB5, would have fared the best whilst KO animals would have fared the worst. The question therefore stands, why did HSPB5 KO mice, in our hands, not display a heightened inflammatory response and or worsened disease progression? Several explanations stand to reason to explain our results.

a) Genetic differences between mice strains

As mentioned previously in chapter 3, the mice used by Masilamoni et al., are BALB/c, whilst those used in the EAE study by Ousman et al., are 129/sv. In our study, we have used C57Bl/6 mice. It is well documented that different mice strains have different genetic compositions and display divergent phenotypes, as reviewed by Yoshiki & Moriwaki (2006) and Sellers et al., (2012). These divergent phenotypes extend to different physiological, neurobiological and behavioural traits as exemplified by significantly different inflammatory profiles -even to the same stimulus (Mills et al., 1999; Soudi et al., 2013), different disease progression/outcome (Rowland et al., 1992; Swihart et al., 1995; Peng et al., 2011) as well as different behavioural phenotypes (Crawley et al., 1997; Crawley, 2007). Whilst studies involving different strains can offer foundations for identifying specific genes involved in disease, here, the comparison of results obtained from different strains has confounded the issue as to whether HSPB5 is a modulator of the inflammatory response. It is therefore likely that in our hands, HSPB5 KO mice did not recapitulate findings from other laboratories and show an exaggerated immune response because of underlying differences of mice strains. If the genetic background of the mice does not influence the result in anyway, the next point will explain why we likely did not observe an exaggerated immune response.

b) HSPB5 is a regulator of inflammation

HSPB5 is known to mediate several pleiotropic activities. The protein partners that interact with HSPB5 (table 1.5) to mediate these diverse functions are known as the HSPB5's interactome and their (potential) interactions have been mapped out (figure 4.12) and are continually being updated. To date, only 2 of HSPB5's interaction partners are known to be involved in inflammatory processes- β2 microglobulin and IKKβ, see table 1.5. The interaction of HSPB5 with β2 microglobulin is strictly ex vivo and has not been shown to occur physiologically and therefore is unlikely to contribute to HSPB5's inflammatory in vivo role. The interaction of HSPB5 with IKKB as shown by Adhikari et al (2011), on the other hand, shows HSPB5 interacting with IKKB, a key protein in the NFkB pathway. The NFkB pathway mediates part of the cellular response to cytokine signalling and other stimuli (Perkins, 2007). The authors of this study came to the conclusion that in myoblast, HSPB5 abrogates TNF-α toxicity by associating with IKKB leading to downstream upregulation of pro-survival protein Bcl-2. The inflammation modulatory role of HSPB5 in this situation is not directly through modulating cytokines and or immune-cell proliferation, as has been previously suggested, but instead, HSPB5's modulatory role is through increasing the anti-apoptotic capacity of cells. Using this paradigm, it could be postulated that lack of HSPB5 results in less ability of cells to overcome cytokine-mediated cytotoxicity and could potentially explain why in the Ousman (2007) study, HSPB5 KO mice, which had elevated cytokine levels, appeared to have worsened progression of disease. Adhikari's postulate does not, however, explain why HSPB5 KO mice show elevated cytokine levels in the first place and or why cytokine levels diminished following recombinant supplementation of HSPB5 to EAE mice. However, an explanation for why HSPB5 KO mice appear to have fared better in our study is outline in the next bullet point.

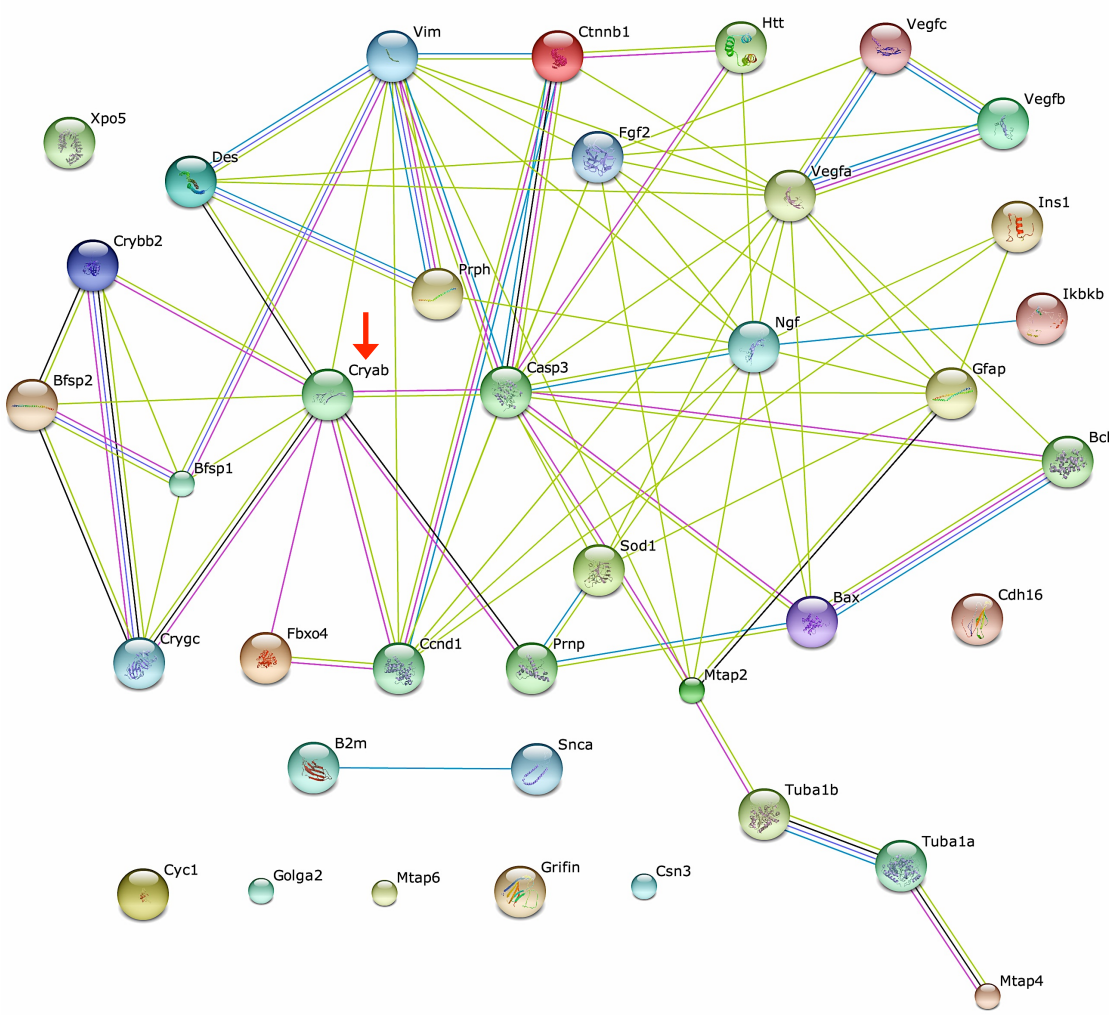

Figure 4.2 Proposed interactome network of HSPB5.

STRING database network (http://string-db.org/) showing experimentally and literature derived direct and indirect protein interaction and associations of HSPB5 (Cryab). Lines show interactions and associations of various proteins. Gene names and associated protein names: B2M, β2 microglobulin; Bax, Bax; Bcl2l1, Bcl-xs; Bfsp1, Filensin; Bfsp2, Phakinin; Casp3, Caspase-3; Ccnd1, Cyclin D1; Cdh16, Cadherin-16; Cryab, HSPB5; Crybb2, B2 crystallin; Crygc, γ-C crystallin; Csn3, K Casein; Ctnnb1, Catenin; Cyc1, Cyclin D1; Des, Desmin; Fbxo4, FBXO4; Fgf2, FGF2; Gfap, GFAP; Golga2, GM130; Grifin, GRIFIN; Htt, Htt; Ikbkb, IKKB; Ins1, Insulin; Mtap2, MAPs; Ngf, NGF; Prnp, Prion protein; Prph, Peripherin; Snca, α-synuclein; Sod1, SOD1; Tuba1a; Tubulin Vegfa, VEGF; Vim, Vimentin.

c) HSPB5 redundancy may lead to compensatory mechanisms

As a protective mechanism, cells have mechanisms that compensate for loss of gene function (Zhang, 2003; 2012), however it is important to note that not all gene redundancies are compensated. As HSPB5 has been shown to have prenatal developmental roles (Christians et al., 2003; Kida et al., 2010; Chaerkady et al., 2011; Tian et al., 2013) the fact that the HSPB5 KO mice are viable and show very little phenotypic differences to WT mice (Brady et al., 2001) may infer that other proteins have compensated for HSPB5's role. This concept is not altogether alien especially considering that small heatshock proteins routinely mediate function through assembly in large oligomeric structures with other small heatshock proteins through an evolutionarily conserved alpha-crystallin domain (Arrigo et al., 2007). The intimate relationship of HSPB5 with other sHSPs could mean that loss of HSPB5 results in compensation from the other interaction partners. This notion is supported by studies, for example, which show that knocking out HSPB4, an sHSP, results in upregulation of α, β and γ crystallin sHSPs (Xi et al., 2003). Table 4.6 shows the possible interaction of each sHSP, and as is evident, it is conceivable that compensation occurs after gene loss. It would have been useful to investigate the immune-reactivity of the other sHSPs that are expressed in the CNS- HSPB1, HSPB6 and HSPB8. Future experiments should prioritise this.

d) ME7 titre may have been too low to induce full constellation of symptoms

Overt weight-loss is a prototypical symptom of ME7 prion disease (Betmouni et al., 1999). As our results do not show evidence of weight loss, it has been suggested that perhaps the concentration of our inocula were not very high. Low ME7 titre could mean that inoculated animals did not mount the most robust response to ME7 and therefore we did not adequately test HSPB5's immune modulatory role. Although this cannot be ruled out, our other observations following ME7 innoculation (PrP deposition, robust astrogliosis and microgliosis, hyperactivity and decreased burrowing activity) are suggestive that the innocula was effective and conducive to investigate HSPB5's immune modulatory role.

4.5.3 Conclusion

Although HSPB5 appears to have immune modulatory roles in various studies, our findings using HSPB5 KO mice and a well characterised model of innate immune inflammation in the CNS do not recapitulate these findings. It is possible that our results don't support literature because of differences in methodologies. It is also possible that HSPB5 modulates inflammation via a mechanisms that we did not measure: whilst we measured immune cell upregulation and cytokine levels, it is possible that HSPB5 may instead prompt cells to be more resistant to cytokine-induced cytotoxic stress. Lastly, it is also possible that prenatal knocking out of HSPB5 results in compensation from other small heatshock proteins, which then results in a superlative protective effect; however, as other studies (using 129Sv mice) do not appear to show this compensatory measure, this conclusion is difficult to justify.

sHSP	Interaction partner(s)	References
HSPB1	HSPB5	(Fu & Liang, 2003)
	HSPB6	(Mymrikov et al., 2012)
	HSPB8	(Sun et al., 2004)
HSBP2	HSPB3	(Sugiyama et al., 2000)
	HSPB6	(Mymrikov et al., 2012)
	HSPB8	(Sun et al., 2004)
HSPB3	HSPB2	(Sugiyama et al., 2000)
	HSPB8	(Fontaine et al., 2005)
HSPB4	HSPB5	(Skouri-Panet et al., 2012)
HSPB5	HSPB1	(Fu & Liang, 2003)
	HSPB4	(Groenen et al., 1994)
	HSPB6,	(Mymrikov et al., 2012)
	HSPB8	(Mymrikov et al., 2012)
HSPB6	HSPB1	(Mymrikov et al., 2012)
	HSPB2	(Mymrikov et al., 2012)
	HSPB5	(Mymrikov et al., 2012)
	HSPB8	(Fontaine et al., 2005)
HSPB7	HSPB8	(Sun et al., 2004)
HSPB8	HSPB1	(Sun et al., 2004)
	HSPB2	(Sun et al., 2004)
	HSPB3	(Fontaine et al., 2005)
	HSPB5	(Mymrikov et al., 2012)
	HSPB6	(Fontaine et al., 2005)
	HSPB7	(Sun et al., 2004)

Table 4.6 Table showing the diverse range of oligomeric partners of small heatshock proteins.

The diverse range of oligomeric partners than can interact with a given small heatshock protein may offer options to gene redundancy.

5. CHARACTERISATION OF HSPB5 RESPONSE DURING HUNTINGTON'S DISEASE

Reduced expression of HSPB5 has been observed in the R6/2 animal model of Huntington's disease. This chapter investigates whether this reduced expression is also observed in human disease.

5.1 Introduction

Previous work on R6/2 animals highlights a selective and progressive reduced expression of HSPB5 in the striatum, frontal cortex, and cerebellum of diseased animals (chapter 1). The reduced expression of HSPB5 is observed as early as 4weeks into disease progression, and by end-stage of disease, there is as much as an 80% reduction of the sHSP (Quraishe, 2010). Reduced expression of HSPB5 is observed within areas that show significant pathology in both R6/2 animals (Zhang et al., 2010; Rattray et al., 2013) as well as in HD (Vonsattel et al., 1985; Vonsattel, 2008); HSPB5 reduction may therefore contribute to pathology or be a result of pathology.

Thus-far, this thesis has investigated the influence of HSPB5 on inflammatory processes and has shown that, in C57Bl/6 mice, reduced expression of HSPB5 does not appear to influence the innate inflammatory response in the periphery (chapter 3) and the CNS (chapter 4). It is not clear however, whether the reduced expression of HSPB5 contributes to pathology in the R6/2 animal model of HD; we had imagined that perhaps the reduced expression of HSPB5 contributes to the exaggerated immune activation that has previously been reported during HD (Ellrichmann et al., 2013). Some insight to this question will likely come from work currently underway in the Muchowski lab (Muchowski P.J., U.C.S.F) where they have crossed R6/2 animals with HSPB5 KO mice and are monitoring disease progression. This thesis will instead conclude with a comparative investigation into HSPB5 expression during the animal model of HD and human HD post-mortem tissue.

Given HSPB5's constitutive localisation in oligodendrocytes (see chapter 2), we believe the comparison between R6/2 and HD findings to be important because reduced expression of HSPB5 may provide an explanation for the pre-symptomatic white-matter changes that are observed in both R6/2 animals (Park et al., 2010) and HD patients (Bartzokis et al., 2007; Dumas et al., 2012). It is thus of interest to probe whether the reduced expression of HSPB5 observed in R6/2 animals is also observed in HD.

This following section provides background on the distribution and extent of neuropathological changes occurring during HD and contrasts them to R6/2 pathology (summarised table 5.1).

5.1.1 Huntington's disease

Huntington's disease is characterised by significant atrophy of an area of the basal ganglia known as the striatum (chapter 1). Atrophy of the striatum is caused by significant death of medium spiny neurons of the caudate nucleus and the putamen (areas of the striatum). Whilst the most significant atrophy is observed in the striatum, progressive atrophy is also noted in the substantia nigra (Spargo et al., 1993), cerebral cortex (Vonsattel, 2008), hippocampus (Spargo et al., 1993), cerebellum (Jeste et al., 1984), hypothalamus and thalamus (Kremer, 1992; Heinsen et al., 1999). The areas in HD that are affected by neurodegeneration are mirrored in animal models of HD, except that in R6/2 mice, anatomical atrophy is not accompanied by neuronal loss (Zhang et al., 2010; Aggarwal et al., 2012; Rattray et al., 2013).

In humans, disease progression can be classified by the extent of striatal atrophy present in post-mortem tissue and assigned a grade from 0-4 (summarised in table 5.1) (Vonsattel et al., 1985). On this scale, grade-0 tissue is described as having no overt changes in brain cyto-architecture, although individuals exhibit some clinical (behavioural) symptoms of disease. Grade 1-3 tissue shows continued atrophy of the striatum and at advanced stages, increasing non-striatal brain atrophy (Vonsattel et al., 1985). During these stages, tissue also shows progressive and extensive gliosis for both astrocytes and microglia (Myers et al., 1991; Vonsattel et al., 1998; Ellrichmann et al., 2013). Grade-4 tissue is characterised by extreme atrophy of the striatum and other non-striatal regions (Vonsattel et al., 1985) (summarised in figure 5.1). Due to comorbidities, HD carriers can die during any one of the 4 grades of disease, which is somewhat different from animal models that tend to live till end-stage.

Human HD		R6/2 HD	
Grade0 (<1%)	Macroscopic: No gross change (1,6)	**Early-stage (0-3weeks)**	Macroscopic: No gross change (3,5)
	Some WM changes (2)		WM changes (4)
	Microscopic: 30-50% loss of striatal neurons (1,6)		Microscopic: No neuronal loss (5)
	No gliosis (1,6)		No gliosis (5)
Grade1 (4%)	Behaviour: Some clinical traits (1)		Behaviour: No changes (5)
Grade2 (16%)	Macroscopic: Gross changes in -Striatum (1,6)	**Mid-stage (4-9weeks)**	Macroscopic: Gross changes in -Striatum (3,5)
	Some changes in -Cortex (1,6)		-Cortex (5)
	-Hippocampus (1,6)		-Hippocampus (3,5)
	-Corpus callosum (1,6)		-Corpus callosum (5)
Grade3 (52%)	Microscopic: Continued loss of striatal neurons (1,6)		Microscopic: No neuronal loss (5)
	Robust gliosis (6,7)		No gliosis (5)
	Behaviour: overt clinical traits (1)		Behaviour: Motor deficits (5)
Grade4 (27%)	Macroscopic: Extensive changes in -Striatal regions (1,6)	**Late-stage (10weeks+)**	Macroscopic: Continued changes of -Striatum (3,5)
	- other regions (1,6)		-Cortex (5)
	Microscopic: Extensive loss of striatal neurons (1,6)		-Hippocampus (3,5)
			-Corpus callosum (5)
	Extensive gliosis (7)		Microscopic: No neuronal loss (5)
	Behaviour: penetrant clinical trait (1,6)		No gliosis (5)
			Behaviour: Motor deficits (5)

Table 5.1 Comparison of pathophysiological features in humans and R6/2 mice.
Human pathology classified from Grade 0-4, depending on severity of striatal atrophy; the animal correlate is shown in direct apposition to the human grade. R6/2 early-stage disease is correlated to Grade 0 and 1 human HD, whilst mid-stage R6/2 pathology is homologous to human grade 2 and 3. Late-stage R6/2 pathology is correlated to Grade 4 human HD tissue. References 1 (Vonsattel et al., 1985); 2 (Dumas et al., 2012); 3 (Zhang et al., 2010); 4 (Park et al., 2010); 5 (Rattray et al., 2013); 6 (Vonsattel, 2008); 7 (Vonsattel et al., 1998).

5.1.2 R6/2 model

Unlike human pathology, disease progression in R6/2 animals is not measured by striatal pathology; instead, it is measured as a function of time: the longer an animal survives post-natally (in days/weeks), with most animals surviving till en-stage of disease. As a result, to measure the extent of pathology, animals have to be sacrificed at given time-points. Pathology can be broadly described as proceeding in 3 stages: early-stage (<3weeks), mid-stage (4-9weeks) and late-stage (10weeks+) (Li et al., 2005). Early-stage disease is characterised by no overt changes in the brain cyto-architecture and no behavioural changes (Vonsattel, 2008). As with HD, mid-stage R6/2 pathology shows wide-spread changes in the striatum, cortex, hippocampus and corpus callosum (Zhang et al., 2010; Rattray et al., 2013) and increasing deficits in motor activity (Carter et al., 1999; Aggarwal et al., 2012). Late stage of disease is defined by extended atrophy of striatal and non-striatal brain regions accompanied by increasingly worse motor deficits (Zhang et al., 2010; Rattray et al., 2013). It is therefore evident that there are some similarities between HD and R6/2 pathology.

5.1.2.1 Neuropathological limitations of the R6/2 animal model

There are however, some key differences in disease progression between humans and R6/2 mice: key pathological hallmarks observed during HD are progressive neuronal loss (Vonsattel, 2008) and gliosis (Vonsattel et al., 1998); these observations are not observed in R6/2 mice (Mangiarini et al., 1996; Schilling et al., 1999; Turmaine et al., 2000). As gross neuronal loss is not observed during the progression of R6/2 animal model (Mangiarini et al., 1996; Turmaine et al., 2000; Rattray et al., 2013), the atrophy of several brain regions is thought to be caused by shrinkage of neuronal cell bodies and processes (Turmaine et al., 2000). Wide-spread gliosis is also not observed in the R6/2 animal model (Rattray et al., 2013). These observations constitute crucial differences between the pathophysiology of HD in mice and humans and highlight how animal models of disease are far from perfect. None-the-less, for now, the pathology observed in R6/2 mice is considered robust and replicable and can inform on human disease (Rubinsztein, 2002; Beal et al., 2004; Vonsattel, 2008).

5.1.3 Heatshock protein expression in R6/2 animals

Immuno-blotting shows high expression of HSPB5 in the striatum, frontal cortex and cerebellum of mice (Quraishe, 2010). Reduced expression of HSPB5 is observed in these regions in R6/2 animals from mid-stage of disease (4weeks+), with significant and progressive reduced expression as time progresses (Zabel et al., 2002; Quraishe, 2010). Analysis of the other sHSPs that are expressed in the CNS (table 1.2) shows no significant reduction of these sHSPs in the striatum, frontal cortex or cerebellum (Quraishe, 2010), leaving very interesting questions about why and how HSPB5 is selectively reduced.

Quraishe et al., (2010) highlighted that the reduced expression of HSPB5 was only observed at the protein level rather than the transcript level. Although HSP40 and HSP70 have been shown to be sequestered in aggregates (Stenoien et al., 1999; Wyttenbach et al., 2000; Hay et al., 2004), dot blot analysis suggests that the reduced expression of HSPB5 is not due to sequestration (Quraishe, 2010). It is therefore likely that mHTT may reduce HSPB5 expression by increasing the turn-over of HSPB5. Given the important homeostatic roles mediated by HSPB5, the reduced expression of HSPB5 may not only be a sign of pathology but may also contribute to pathology. Hence the question: how transferrable are findings from R6/2 animals to HD?

5.2 Aims

Although the animal models thus-far available to study HD do not produce the full constellation of clinical, neuroanatomical and neuropathological changes observed in HD, for now, they are the best models we have and understanding their translation capacity to human disease is paramount. This chapter will therefore aim to evaluate the extent to which the reduced expression of HSPB5 in R6/2 animals is mimicked in HD post-mortem tissue. This analysis will be valuable for understanding whether HSPB5 is implicated in HD pathology.

Our investigations of human tissue will be informed by findings from R6/2 animals: HSPB5 expression in HD tissue will be investigated in the frontal cortex and the cerebellum (striatum was not provided by the Brain Bank), areas that showed high constitutive expression of HSPB5 and significant reduction in R6/2 tissue. Based on similar neuropathological changes at these stages of disease, grade-2 human HD tissue will loosely be associated with mid-stage R6/2 tissue and grade-4 human HD tissue will be associated with end-stage R6/2 pathology, thereby allowing somewhat of a temporal analysis of HSPB5 expression during HD progression.

To aid our characterisation, HSP70, CNP and GFAP expression will also be investigated. HSP70 will be characterised because together with HSP40, it is the only other HSP known to show reduced expression during R6/2 disease progression (Hay et al., 2004); its characterisation here will therefore provide an independent measure as to whether there is a gross reduction of HSPs during HD. CNP, a myelin protein, will also be characterised because white-matter changes are widely observed during HD (Bartzokis et al., 2007). As HSPB5 is expressed in white-matter (see chapter 2), CNP will act to determine whether reduced expression of HSPB5 is linked to white-matter changes. Astrogliosis and induced expression of HSPB5 are often coincidental in several diseases (Iwaki et al., 1992; Renkawek et al., 1992; 1994), as such, we also characterise GFAP immunoreactivity to inform us on whether there is an overt gliosis so as to account for variables that can influence HSPB5 immunoreactivity.

5.3 Materials and methods

5.3.1 Animal tissue

Animal tissue collection was done by Quraishe, S (University of Southampton, UK) as described (Quraishe, 2010). 9 week (mid-stage) and 17 week (end-stage) cerebellar and cortical tissue was stored in -80°C storage. For experimentation, tissue obtained from -80°C storage was processed as according to section 5.3.3.

5.3.2 Human tissue

Grade 2 and grade 4 HD cerebellar and frontal cortex post-mortem tissue (12 Huntington's Disease case and 12 Controls) was obtained from the New Zealand Human Brain Bank courtesy of Professor RLM Faull (University of Auckland, New Zealand) and stored at -80°C. Acquisition of the tissue was done under strict terms of the New Zealand Human Tissue Act (2008) and its use in the UK was only carried out after ethical approval (University of Southampton Human Subjects Ethics Committee). Where possible the cerebellar and cortical tissue at each stage were sourced from the same individual. Aside from the anatomical designation distinguishing Frontal cortex from Cerebellum, the Brain Bank did not provide us with details of sample composition (i.e. proportion of the tissue that was grey matter and white-matter). To overcome this, some of our data will be normalised to CNP immunoreactivity (see section 5.3.3.2). CAG-repeat data was not provided upon request and in some cases, post-mortem delay (PM delay) was also not provided by the Brain bank.

5.3.2.1 Participants

Cerebellar and frontal cortex tissue was provided from 12 post-mortem individuals. Individual data (i.e. age, sex, post-mortem (PM) delay and CAG repeats), for each participant (anonymised). A summary of group demographics is provided in table 5.2-5.5.

Cerebellum				
	Control group		HD group (Grade 2)	
	Mean	Range	Mean	Range
Age (yrs.)	65.8 ±7.8	57 - 78	63 ±9.7	47 - 74
CAG (repeats)	-	-	-	-
PM delay (hrs.)	12.9 ±4.9	7.5 - 19	13.5 ±9.07	4 - 29
n number	6 Male		6 Male	

Table 5.2 Table showing age and post mortem delay (PM delay) of tissue collection of 6 control and 6 Stage 2 HD cases (cerebellum). No CAG repeats data was not provided by Brain bank.

Cerebellum				
	Control group		HD group (Grade 4)	
	Mean	Range	Mean	Range
Age (yrs.)	52 ±13	41 - 66	54 ±8.8	44 - 65
CAG (repeats)	-	-	-	-
PM delay (hrs.)	-	-	-	-
n number	3 Male: 3 Female		3 Male: 3 Female	

Table 5.3 Table showing age of 6 control and 6 Stage 4 HD cases (cerebellum). No CAG repeats data or PM data was not provided by Brain bank.

Frontal Cortex				
	Control group		HD group (Grade 2)	
	Mean	Range	Mean	Range
Age (yrs.)	68 ±7.1	62 - 78	64.2 ±10	47 - 74
CAG (repeats)	-	-	-	-
PM delay (hrs.)	13 ±5.3	7.5 - 19	10 ±5.5	4 - 16
n number	6 Male		6 Male	

Table 5.4 Table showing age and post mortem delay (PM delay) of tissue collection of 6 control and 6 Stage 2 HD cases (frontal cortex). No CAG repeats data was not provided by Brain bank.

Frontal Cortex				
	Control group		HD group (Grade 4)	
	Mean	Range	Mean	Range
Age (yrs.)	52 ±13	41 - 66	54 ±8.8	44 - 65
CAG (repeats)	-	-	-	-
PM delay (hrs.)	-	-	-	-
n number	3 Male: 3 Female		3 Male: 3 Female	

Table 5.5 Table showing age of 6 control and 6 Stage 4 HD cases (frontal cortex). No CAG repeat data or PM delay data was provided by the Brain bank.

5.3.3 Biochemistry

Tissue was weighed and diluted in a 1:2 volume of 2% SDS containing a complete protease inhibitor cocktail (Roche Diagnostics GmbH, Germany). Total protein concentration was assessed using a Bio-Rad D_C protein assay kit (Bio-Rad, UK), as per manufacturer's instruction. All samples were diluted to a final concentration of 4mg/ml in 5x sample buffer (250mM TRIS-HCl (pH6.8), 10% SDS, 30% Glycerol, 5% β-mercapto-ethanol, 0.02% bromo-phenol blue) and run on a polyacrylamide gel composed of 5% stacking gel and 12.5% resolving gel in 1x Laemmli buffer (5mM TRIS (pH8.3), 192mM Glycine, 0.1% SDS) using the Bio-Rad protein gel system (Bio-Rad, UK). Equivalent loading was checked by coomassie staining (Sigma Aldrich, UK), as per manufacturer's instructions.

5.3.3.1 Protein transfer and immuno-blotting

Proteins were transferred to nitrocellulose membrane (Amersham, UK) overnight (16-18hrs) at 4°C in transfer buffer (1x Laemmli buffer, 20% (v/v) Methanol). Nitrocellulose membranes were blocked with 4% non-fat milk (TESCO, UK) and incubated in primary antibodies overnight (16-18hrs) (table 5.6). Membranes were washed in TRIS-buffered saline with 0.05% tween (TBS-T) (pH7.2) and incubated in secondary antibodies for 1hr (table 5.6). Membranes were visualised using the Odyssey infrared imaging scanner (LiCOR, UK), as per manufacturer's instructions.

Primary antibody	Originating species	Dilution	Secondary antibody	Dilution
CNP (Abcam, UK)	Mouse	1:1000	anti-mouse IR (Invitrogen, UK)	1:1000
GFAP (Dako, US)		1:5000		
HSPB5 (Abcam, UK)		1:500		
HSP70 (Abcam, UK)		1:1000		

Table 5.6 Primary and secondary antibodies used to analyse R6/2 and human HD tissue.

5.3.3.2 Normalisation, quantification and statistical analysis

Immunoreactivity was measured by quantifying pixel intensity using Odyssey software v1.2 (LiCOR, UK). The immunoreactivity observed on each nitrocellulose membrane was normalised to counterpart coomassie gels that were loaded and run concurrently (see figure 5.1 for illustration of normalisation procedure). Values and graphs were compiled and statistically analysed using GraphPad Prism v6 (GraphPad Software, US). Data was statistically analysed using an unpaired T-test and as the sample sizes were very small, Welch's correction was applied to the data in order to take into account differences in standard deviation.

As the white/grey-matter composition of the tissue was not specified by the Brain Bank, we checked the composition of the tissue by normalising some of the data with major myelin protein, CNP. See figure 5.4.

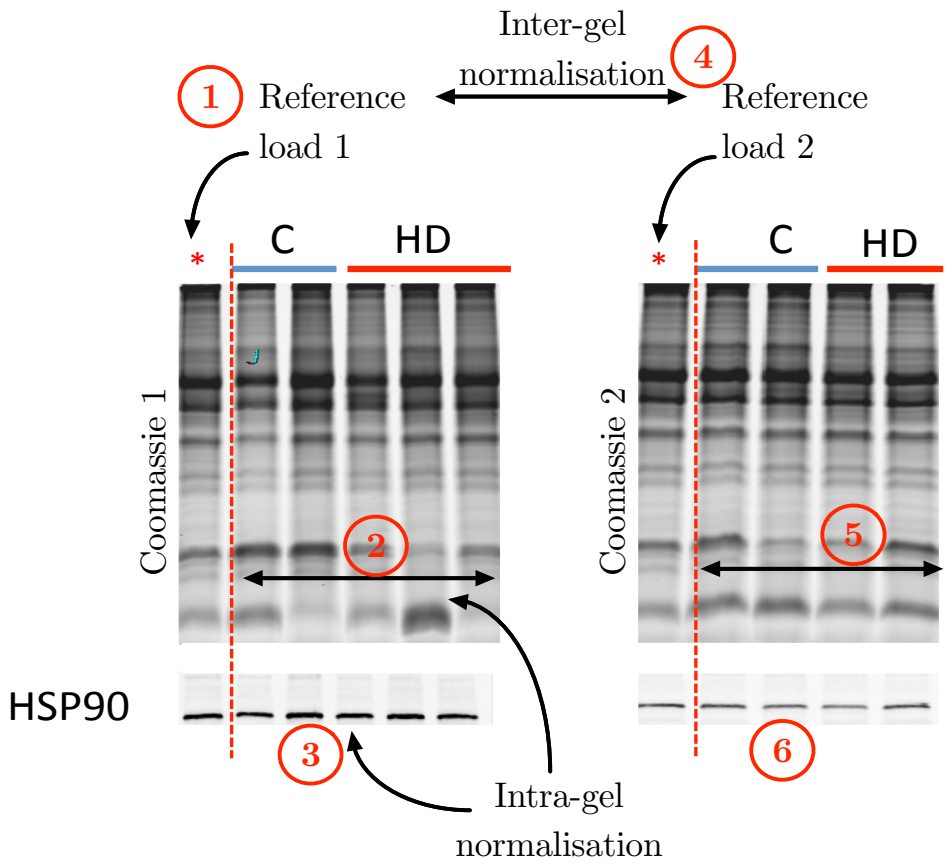

	Coomassie intensity	Normalised intensities	Multiplication factor	HSP90 Immunoreactivity	Normalised intensity
Reference Load	51	1	1	4	4
C1	55	1.078431373	0.927272727	4	3.709090909
C2	44	0.862745098	1.159090909	7	8.113636364
HD 1	66	1.294117647	0.772727273	6	4.636363636
HD2	58	1.137254902	0.879310345	7	6.155172414
HD3	68	1.333333333	0.75	6	4.5

Figure 5.1 Western-blotting normalisation procedure.
All samples were loaded in parallel: one gel was for coomassie staining and the other for immuno-blotting; on these gels, analysis was internally controlled by loading control samples (C) and Huntington's disease (HD) samples on the same gel. Due to the large number of samples, loading had to be split to several gels. To normalise loading within gels and between gels, the following procedure was done: (1) on each gel, 40µg of the same reference sample was loaded first and acted as a Reference Loading sample for intra-gel and inter-gel normalisation. Subsequently, 40µg of experimental samples was then loaded (2) Following gel electrophoresis, equivalent protein loading of all samples was checked by coomassie staining: immunoreactivity of all the samples was measured (see table, coomassie intensity) and division of the immunoreactivity values of experimental samples with reference load shows whether samples are under or over-loaded (see table, normalised intensities). Based on under or over-loading of coomassie gels, (3) immuno-blots are normalised by multiplying immuno-blot immuno-reactivity by the normalisation factor (see table, multiplication factor, HSP90 immunoreactivity and normalised intensity). (4) Inter-gel normalisation was done by comparing the coomassie intensity of Reference Load 1 with that of Reference Load 2. Once normalised, steps (5) and (6) follow the same procedure as the initial intra-gel normalisation (see steps 2 and 3).

5.4 Results

5.4.1 Expression of HSPB5 during R6/2 HD

To confirm the previously observed reduced expression of HSPB5 in R6/2 animals, we repeated the experiment and found a significant reduced expression of HSPB5 in the cerebellum and frontal cortex during disease progression (figure 5.2 and 5.3). In the cerebellum, there was a 74% reduction of HSPB5 expression at mid-stage (9 weeks) of disease ($p<0.05$) (figure 5.2A,B); the reduction proceeded further still to 89% by end-stage (17-weeks) of disease ($p<0.05$) (figure 5.2C,D).

In the frontal cortex, there is no reduction in HSPB5 expression at mid-stage (9 weeks) of disease (figure 5.3A,B), however, by end-stage (17 weeks) of disease, HSPB5 expression is reduced by 82% as compared to wild type animals ($p<0.05$)(figure 5.3C,D). Both observations support previous investigations in the R6/2 mouse model (Zabel et al., 2002; Quraishe, 2010).

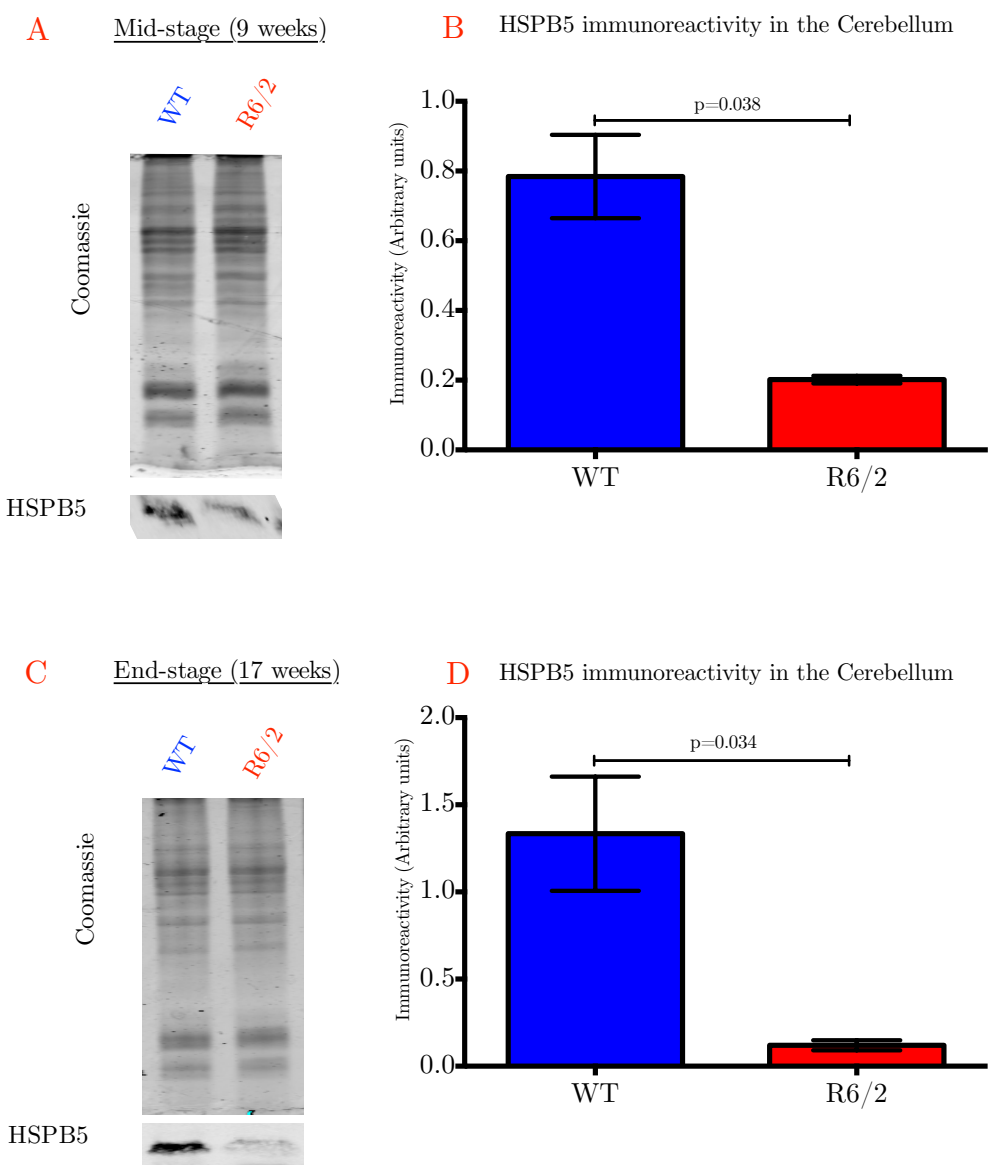

Figure 5.2 HSPB5 immunoreactivity in R6/2 cerebellar tissue.
Representative coomassie and western blots for HSPB5 immunoreactivity at (A) mid-stage (9-weeks) and (C) late-stage (17-weeks) of disease. Equivalent protein loading was checked and normalised by coomassie staining. Graphical representation of HSPB5 immunoreactivity at (B) mid-stage (9-weeks) and (D) late-stage (17-weeks) of disease; blue bars represent wild type (WT) animals and red bars represent R6/2 animals. Error bars represent SEM, n=5. Unpaired T-test with Welch's correction used to analyse data; significant difference indicated by $p<0.05$.

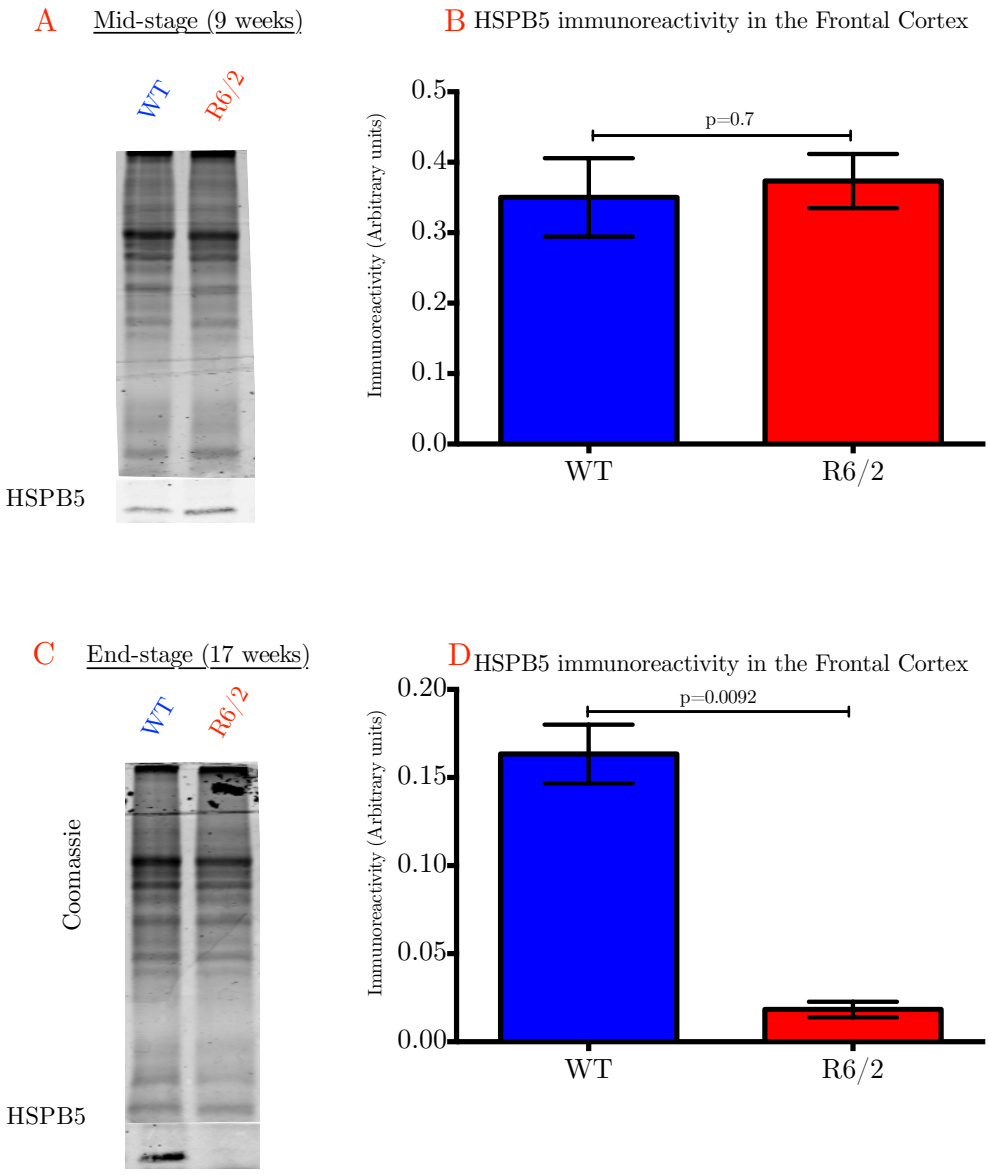

Figure 5.3 HSPB5 immunoreactivity in R6/2 frontal cortex tissue.
Representative coomassie and western blots for HSPB5 immunoreactivity at (A) mid-stage (9-weeks) and (C) late-stage (17-weeks) of disease. Equivalent protein loading was checked and normalised by coomassie staining. Graphical representation of HSPB5 immunoreactivity at (B) mid-stage (9-weeks) and (D) late-stage (17-weeks) of disease; blue bars represent wild type (WT) animals and red bars represent R6/2 animals. Error bars represent SEM, n=5. Unpaired T-test with Welch's correction used to analyse data; significant difference indicated by $p<0.05$.

5.4.2 Expression of HSPB5 during human HD

Firstly, analysis of human data shown considerable individual differences in immunoreactivity for all the markers measured. We postulated that this may be due to the human tissue containing different compositions of grey/white-matter, which would influence the results. We therefore decided to check the grey/white-matter composition of our tissue by normalising HSPB5 to CNP expression. AS both these proteins are expressed in myelin, the resulting ratio between the two shows the relative grey/white-matter composition of the tissue. Provided that the ratios between control subjects and HD cases are not significantly different, we can use subsequent data with confidence that the tissue has similar composition.

For cerebellar tissue stage 2 HD cases showed a HSPB5:CNP ratio of 1.22±0.42:1 and controls had a ration of 0.78±0.24:1; these ratios were not significantly different ($p>0.05$) (figure 5.4A). The grey/white-matter comparison between the HD cases and controls is therefore considered to be comparable. Stage 4 cerebellar tissue and control tissue also showed comparable HSPB5:CNP ratios; stage 4 HD cases, 0.3±0.06:1 and controls 0.37±0.13 ($p>0.05$) (figure 5.4B).As compared to controls, the HSPB5:CNP ratios of frontal cortex tissue from stage 2 and stage 4 HD cases was also comparable to controls ($p>0.05$)(figure 5.4C,D). These results highlight that the individual differences observed for different markers (see supplementary figure S5.2) are not due to tissue having significantly different grey/white-matter composition. As the grey/white-matter composition of the tissue is comparable, we can therefore use the data we obtained as is.

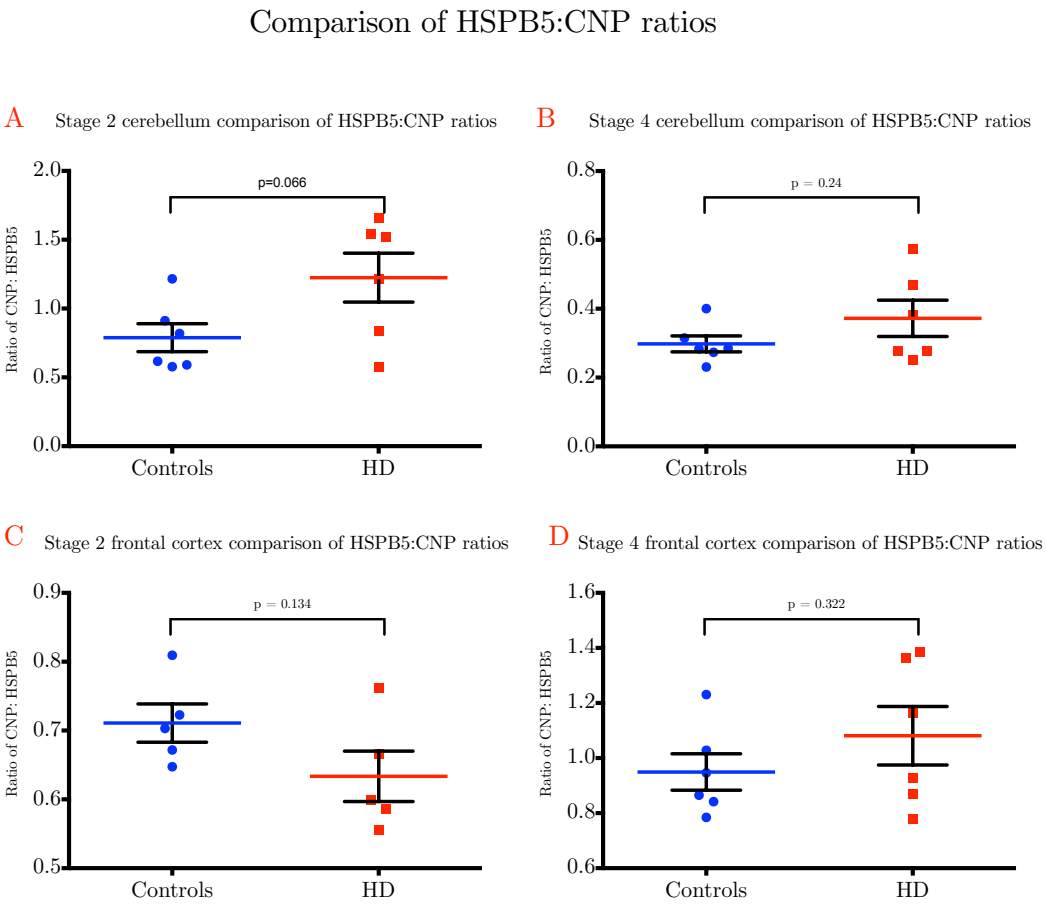

Figure 5.4 Normalisation of HSPB5 expression to CNP. Normalisation to check whether the tissue grey/white-matter composition in comparable.

(A) Comparison of CNP:HSPB5 ratios in the cerebellum between controls and stage 2 HD tissue. (B) Comparison of CNP:HSPB5 ratios in the cerebellum between controls and stage 4 HD tissue. (C) Comparison of CNP:HSPB5 ratios in the frontal cortex between controls and stage 2 HD tissue. (D) Comparison of CNP:HSPB5 ratios in the frontal cortex between controls and stage 4 HD tissue. Blue data-points represent controls and red data-points represent HD cases. Error bars represent SEM, n=6. Unpaired T-test with Welch's correction used to analyse data; significant difference indicated by $p<0.05$.

In grade-2 cerebellar tissue, protein analysis of HSP70, GFAP, CNP and HSPB5 shows that there are no differences in the immunoreactivity of these markers between control individuals and HD cases ($p>0.05$) (figure 5.5 A-E). The expression of HSP70, GFAP and HSPB5 is unchanged even in grade-4 HD tissue ($p>0.05$); CNP however appears to be significantly reduced in the grade-4 cerebellar HD tissue (figure 5.5F-J). The reduced expression of CNP may reflect white-matter changes that are observed during HD. The results from the cerebellum therefore show that there is no reduction of HSP70 and HSPB5, which is contrary to results from R6/2 animals (Zabel et al., 2002; Hay et al., 2004; Quraishe, 2010). The results also show that in the cerebellum, there is no astrogliosis in grade 2 and grade 4 tissue.

Protein analysis of grade-2 frontal cortex tissue shows that this tissue is characterised by an induction of HSP70 and GFAP ($p<0.05$) (figure 5.6A-C); the induction is still maintained in grade-4 HD tissue ($p<0.05$) (figure 5.6F-H). As compared to controls, CNP and HSPB5 are unchanged ($p>0.05$) in grade-2 (figure 5.6A,C-D) and grade-4 (figure 5.6F,I-J) frontal cortex tissue.

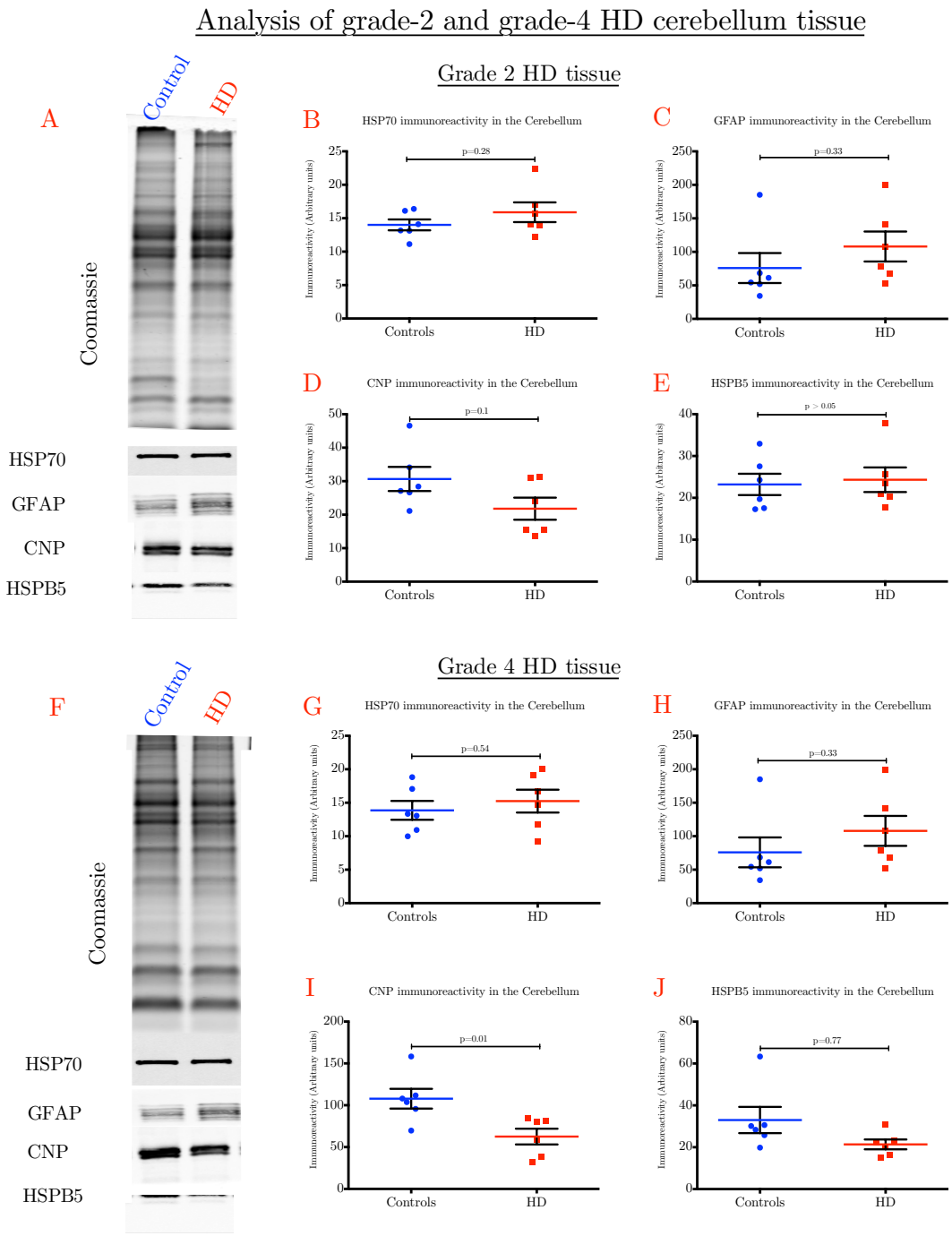

Figure 5.5 Immuno-blotting analysis of cerebellar tissue from grade 2 and grade 4 HD tissue.

A-E, Grade 2 cerebellar tissue; F-J, Grade 4 cerebellar tissue. (A,F) Representative coomassie and immuno-blots HSP70, GFAP, CNP and HSPB5. Graphical representation of immunoreactivity for HSP70 (B,G), GFAP (C,H), CNP (D,I) and HSPB5 (E,J). Blue data-points represent controls and red data-points represent HD cases. Error bars represent SEM, n=6. Unpaired T-test with Welch's correction used to analyse data; significant difference indicated by $p<0.05$.

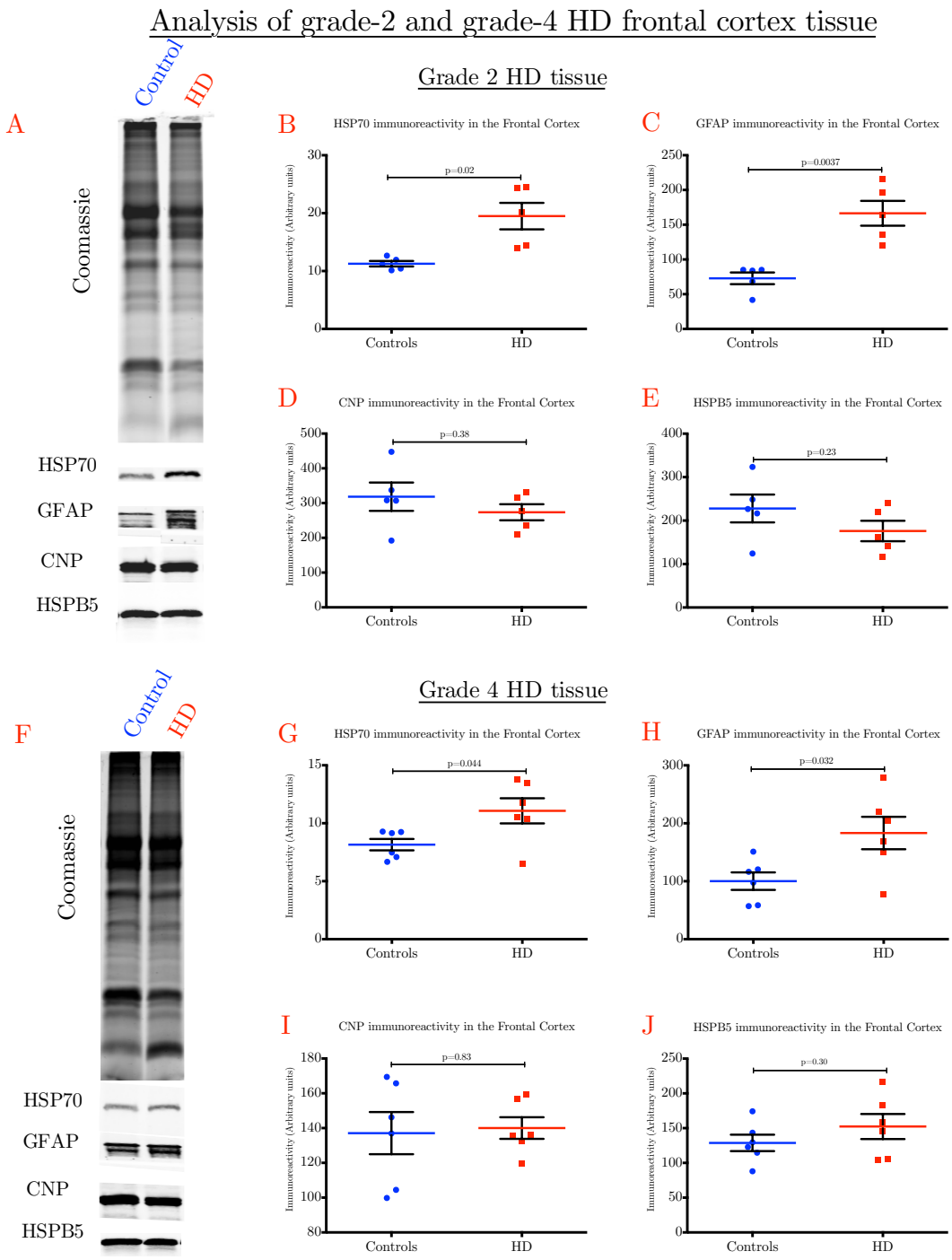

Figure 5.6 Immuno-blotting analysis of grade 2 and grade 4 frontal cortex HD tissue. A-E, Grade 2 frontal cortex tissue; F-J, Grade 4 frontal cortex tissue. (A,F) Representative coomassie and immuno-blots HSP70, GFAP, CNP and HSPB5. Graphical representation of immunoreactivity for HSP70 (B,G), GFAP (C,H), CNP (D,I) and HSPB5 (E,J). Blue data-points represent controls and red data-points represent HD cases. Error bars represent SEM, n=6. Unpaired T-test with Welch's correction used to analyse data; significant difference indicated by $p<0.05$.

5.5 Discussion

Studies in R6/2 mice have shown a significant reduced expression of HSPB5 (Zabel et al., 2002; Quraishe, 2010), HSP40 and HSP70 (Hay et al., 2004). This chapter provides the first comparative study investigating the expression of HSPB5 during HD. Our results show comparable expression of HSPB5 in the cerebellum of frontal cortex of HD cases with control cases (figure 5.5-5.6). Results from R6/2 animals predicted reduced expression of HSPB5 in disease cases (figure 5.2-5.3) (Zabel et al., 2002; Quraishe, 2010). Evidently, the finding from R6/2 animals is asynchronous with findings from human tissue. The potential reason(s) why this may be the case is discussed below in section 5.5.1.

We also investigated HSP70 expression in HD cases and found that in the cerebellum, expression of HSP70 was comparable to control tissue (figure 5.5). The likely reason why no changes in HSP70 expression was noticed in the cerebellar tissue is discussed below in section 5.5.1. In the frontal cortex however, there was a significant induction of HSP70 (figure 5.5); this observation is contrary to findings from R6/2 animals that show significantly reduced expression of HSP70 during disease progression (Hay et al., 2004). To our knowledge, this is the first characterisation of HSP70 expression in HD tissue. Several in vitro models show the induction of HSP70 to supress toxicity of mutant polyQ proteins (Warrick et al., 1999; Jana et al., 2000), however, in vivo experiments where R6/2 animals were bred with HSP70 over-expressing mice show that over-expression of HSP70 did not have an effect on disease progression in the transgenic offspring (Hansson et al., 2003). It is therefore uncertain whether the induction of HSP70 in HD cases confers significant protection.

As CNP is a major constituent of myelin, analysis of CNP expression in the cerebellum and frontal cortex (figure 5.5C and 5.6C) suggests that there were no gross changes in myelin structure in HD cases. As an increasing body of evidence that show white-matter changes to be some of the earliest changes observed during HD (Ciarmiello et al., 2006; Bartzokis et al., 2007), It is apparent from our findings that characterisation of CNP expression alone does not accurately depict the ultrastructural changes that are observed by the advanced

techniques, magnetic resonance imaging (MRI) that were used by Ciarmiello et al., (2006) and Bartokis et al., (2007). As our characterisation of CNP does not tell us anything about the ultrastructure of myelin, the only conclusion we can make is that CNP expression appears unchanged.

Analysis of GFAP expression in the cerebellum and the frontal cortex aimed to discern whether or not gliosis was apparent in HD cases. This was considered an important distinction because induction of HSPB5 is coincidental with astrogliosis in several conditions (Iwaki et al., 1992; Renkawek et al., 1992; 1994). We found no induction of HSPB5 in both grade-2 and grade-4 cerebellar tissue (figure 5.5B) (see section 5.5.1 for likely explanation). In the frontal cortex, grade-2 and grade-4 tissue showed a marked induction of GFAP. This is suggestive of a gliosis and is in keeping with wider literature that shows astroglial activation and proliferation in HD patients (Vonsattel, 2008). As astrogliosis is not observed in R6/2 animals (Rattray et al., 2013) and considering that induction of HSPB5 is often coincidental with astrogliosis, it is therefore apparent that the robust induction of GFAP in human tissue may therefore have masked reduction in HSPB5 expression as due to a relative increased induction of HSPB5 in astrocytes. Immunohistochemical studies to confirm HSPB5 localisation in HD tissue would have been useful and would have shed some light as to whether astrogliosis counter-acts reduced expression of HSPB5.

Our results challenge the prevailing assumption that molecular results obtained from established animal models extrapolate and translate to human disease. The reason why results from R6/2 animals did not correlate with HD tissue is likely to be because the R6/2 model is not an accurate model for HD. This statement is justified by that whilst neuronal loss (Vonsattel, 2008) and astrogliosis (Vonsattel et al., 1998) are observed in HD tissue, they are not observed in R6/2 tissue (Mangiarini et al., 1996; Schilling et al., 1999; Turmaine et al., 2000). In addition, the cerebellar pathology that is observed in R6/2 animals (Zhang et al., 2010), has not been reported in HD tissue; this disparity may thus explain why the induction of HSP70 and GFAP that is observed in frontal cortex tissue was not observed in cerebellar tissue.

It could therefore be argued that our findings do not mimic those obtained from R6/2 animals because the R6/2 animal model is not a good model for HD, instead; based on that the cerebellar pathology that is observed in R6/2 animals (Zhang et al., 2010) is also observed in juvenile-onset HD (Vonsattel et al., 1998), one could argue that the R6/2 disease model is a better model for juvenile-onset HD (see below) than it does adult-onset HD (which is the tissue that we analysed).

5.5.1 R6/2 mice as a model for juvenile-onset HD

R6/2 mice have about 150 or more CAG repeats that are expressed at 75% of endogenous levels (Mangiarini et al., 1996). As a result of this, disease progression is rapid in terms of behavioural changes, brain pathology and age of death. R6/2 mice have therefore become an easy and relatively inexpensive model that has become extensively characterised to inform pathophysiology of human HD (Li et al., 2005). I would argue however that the mechanistic nature of R6/2 HD makes the condition akin to juvenile-onset HD rather than adult-onset HD. The distinction between juvenile-onset HD and adult-onset HD is important to note because juvenile-onset HD differs from adult-onset HD in terms of disease onset, duration, neurological and behavioural symptoms (Nance et al., 2001). I argue that the R6/2 model is akin to juvenile-inset HD because R6/2 mice express 150 polyglutamine repeats; this large number of polyglutamine repeats result in a condition where disease onset, duration and pathophysiology correlate significantly with juvenile-onset HD. Considering that the average life-expectancy of a mouse is ≈ 2yrs (94weeks) (Yuan et al., 2009) and yet R6/2 mice expressing 150 polyglutamine repeats die between 15-20weeks of age (Li et al., 2005). This drastic reduction in life-expectancy is homologous to the drastic reduction in life-expectancy observed in juvenile-onset HD (average life-expectancy of humans is ≈ 83yrs and yet individuals with juvenile-onset HD show disease before the age of 20 and die soon afterwards (Nance et al., 2001)). In contrast, adult-onset HD is characterised by onset of disease ≈ 35-50yrs and death occurring ≈ 15-20years after onset. It should therefore be clear that the accelerated disease progression observed in R6/2 animals is reminiscent of juvenile-onset HD. R6/1 mice, which have later onset and slower progression of disease, may provide a more faithful model for human adult-onset HD.

5.5.2 Use animal models expressing full length mHTT

Whilst the use of R6/2 and R6/2 animals is very economical, due to accelerated experimental time-course, it should also be note that these model only express exon 1 of the mHTT gene. As they do not express the full protein, it is highly likely that any results we obtain from these models will always be unable to be reciprocated in humans. To better characterise the similarities of animals models with human disease, it would be beneficial to use animal models that express full length mHTT such as YAC and BAC models; it would be very interesting to investigate if there is a reduced expression of HSPB5 in these models. Given the results we obtained from humans, it is unlikely there will be a reduced expression of HSPB5. None-the-less, YAC and BAC models are likely to show symptoms and clinical manifestations that are more faithful to human disease- albeit at a more protracted time-course and thus more expensive to the experimenter.

5.5.3 Conclusion

It is apparent from our comparative study that the results obtained from animal models, whilst useful, have to be extrapolated with caution to human conditions. Better animal models with a more faithful constellation of clinical, neuroanatomical and neuropathological changes to HD is needed. This is highlighted by that a recent meta-analysis of animal studies that are published in high-impact journals (Cell, Nature and Science) shows that only 1/3 of studies actually translated to humans and of these, only 1/10 show potential for therapeutic advantage (van der Worp et al., 2010). Cumulatively, what is becoming clearer is that characterisation of complex human disease using a single mechanistic animal models (such as R6/2 mice), is likely not going to capture and recapitulate all the necessary pathophysiological hallmarks of disease thus lessening therapeutic exploitability.

6. GENERAL DISCUSSION

As there is a selective reduced expression of HSPB5 during the R6/2 animal model of Huntington's disease (chapter 1), this thesis aimed to characterise the influence of that reduction. Whilst reduced expression of HSPB5 has been shown *in vitro* to sensitise cells to oxidative stress, cytoskeletal destabilisation and apoptotic death (see chapter 1.3), a growing body of *in vivo* characterisation shows that reduced expression of HSPB5 results in increased immune-cell proliferation and activation of $CD3^+$, $CD4^+$, $CD8^+$, γδ T-cells and microglia as well as significantly increased production of pro-inflammatory cytokines (see chapter 1.4). *In vivo*, these exaggerated inflammatory properties have been shown to exacerbate progression of multiple sclerosis (MS), the animal models of MS as well as stroke (chapter 1.4). Furthermore, recombinant addition of HSPB5 to animal models of MS and stroke, results in better disease prognosis as due to reduce immune cell activation and reduced cytokine production. These findings have been taken to be suggestive of HSPB5 acting as a potent immune modulator. Given that exaggerated inflammation has been implicated as a driver of several neurodegenerative conditions (González-Scarano et al., 1999), including HD (Ellrichmann et al., 2013), the aim of this thesis was to investigate the impact of reduced HSPB5 expression on peripheral (chapter 3) and central (chapter 4) inflammatory processes, in order to inform whether the reduced expression of HSPB5 observed in R6/2 animals is pathological. The thesis concluded by comparing whether reduced expression of HSPB5 was observed in HD.

Our initial experiments highlighted that knocking out HSPB5 did not have any adverse effect on basal behavioural and cellular and morphological aspects of CNS innate immune cells of knockout mice (chapter 2). We later showed that following *S. typhimurium* infection, HSPB5 deficient animals did not show an exaggerated immune response or worsened disease progression (chapter 3.3); instead they showed comparable immune response and disease progression to wild type animals. These results were contrary to findings from literature, which showed HSPB5 deficient animals to have exaggerated peripheral immune-cell activation and exaggerated levels of peripheral cytokines.

In chapter 4, we used the prion disease model to dissect HSPB5's influence on innate inflammatory processes in the CNS. Over the years, the prion disease model has been extensively characterised and provides a well-characterised, robust and tractable method to investigate neurodegenerative processes. Similar to results from chapter 3, our investigations into HSPB5's influence on the central innate immune response did not indicate negative consequences for HSPB5-deficient animals (chapter 4.3).

Our results therefore do not support findings observed in animal models of MS or stroke. These results were unexpected and somewhat surprising, not in the least because of HSPB5's immune modulatory role but due to HSPB5's other wide-ranging roles. As mentioned before, reduced expression of HSPB5 has been shown to sensitise cells to oxidative stress, cytoskeletal destabilisation and apoptotic death, as such, we would have expected HSPB5 KO animals to be significantly impaired in most of our experiments. The reason why our findings do not support literature are two-fold: the gene-knockout model we used may have resulted in redundancy and compensation, and the strain differences between experiments may have mediated a great role in the results we obtained.

Redundancy and compensation

Given that sHSPs share 22%-65% sequence homology (NCBI, basic local alignment search tool (BLAST) (Altschul et al., 1997)) and that the functional capacity of sHSPs is mediated through making large oligomeric complexes of between 15-50 subunits (chapter 1), it is conceivable that compensation can occur if there is a redundancy. This is highlighted, for example, by a study that shows that whilst HSPB5 has potent immune modulatory roles in 129sv mice, I.V addition of any 1 of 7 other sHSPs (HSPB1, HSPB2, HSPB3, HSPB4, HSPB6, HSPB7 or HSPB8) also result in therapeutic effect (although not to the same extent as HSPB5) (Kurnellas et al., 2012). These data are indicative of how similar sequence homology allows sHSPs the capacity to mediate over-lapping roles and compensate for extreme redundancies- such as those observed in KO animals. We therefore argue that perhaps a better approach to investigating the effect of reduced

expression of HSPB5 would have been to use an inducible gene knockout model, where experimenters can reduce gene expression as and when needed via molecular switch. Such methods exist and involve a variety of techniques, including adenovirus-mediated targeted DNA recombination (Wang et al., 1996) and inducible gene targeting using the cre/lox system (Sauer, 1998). Due to the gradual and incremental nature of these systems on gene loss, we believe them to be more likely to produce cellular effects that are synonymous with physiological reduced expression of a gene.

Strain differences

We also believe that the disparity between our results and those from literature may have been due to genetic difference between mice strains. Genetic differences between mice strains influence an animal's responses to antigen, the calibre of the immune response and the susceptibility of mice to autoimmune conditions (Sellers et al., 2012). C57Bl/6 mice, for example, the mice that were used in our experiments, demonstrate a Th1-type bias to pathogens, whilst other strains, such as Balb/c mice display a Th-2 bias to pathogens (Mills et al., 2000). Data suggests that the mice that were used in both the MS studies (Ousman et al., 2007) and the stroke studies (Arac et al., 2011) exhibit a greater Th-1 phenotype than C57Bl/6 mice, as 129sv mice express the Slc11a1 gene and C57Bl/6 mice do not (Fortier et al., 2005; Caron et al., 2006; Stober et al., 2007). The Slc11a1 gene influences expression of major histocompatibility complex II (MHCII) and antigen presenting function of microphages and dendritic cells (Stober et al., 2007); gene expression profiling shows that 129sv mice have a significant up-regulation of pro-inflammatory cytokines followed by a gradual increase in immunoglobulin transcripts as compared to mice that lack the Slc11a1 gene (Caron et al., 2006). These results go to explain why C57Bl/6 mice are more susceptible to *S. Enteritidis* and *Mycobacterium*, whereas 129sv mice are more resistant to these organisms (Fortier et al., 2005; Caron et al., 2006). These data highlight how genetic differences between mice strains can influence the immune response mounted by mice and could explain why we did not observe the expected aberrant immune response in HSPB5 KO animals.

The thesis concluded with a comparison of R6/2 findings with HD tissue and showed that although there is a reduced expression of HSPB5 in R6/2 animals, this reduced expression is not mirrored in human disease. It is likely that we did not replicate our findings from R6/2 animals in humans because the R6/2 model is not an accurate representation of the human disease. As mentioned in chapter 5.5, the length of CAG repeats that are expressed by R6/2 animals makes the condition more synonymous to juvenile onset HD rather than adult onset HD, as such, the molecular events underpinning the condition are also likely to be different.

6.1 Future direction

Whilst our characterisation of HSPB5's immune modulatory role did not show deficiency of HSPB5 to result in pathology, for future experiments it would be useful to breed HSPB5 KO animals with R6/2 animals and investigate whether deficiency in HSPB5 results in exaggerated disease progression. Given the similarities of R6/2 animals disease pathology and juvenile onset HD, it would also be interesting to investigate whether the observed reduced expression of HSPB5 observed in R6/2 animals is replicated in juvenile onset HD cases. Perhaps more importantly, however, it is our suggestion that future experiments that aim to be extrapolated to humans should be done in animals expressing the full length of mHTT rather than only exon 1. This approach whilst more protracted, and therefore expensive, is likely to have better fidelity to human disease and therefore more likely to offer real insights/therapeutic intervention.

REFERENCES

Adhikari, A. S., Singh, B. N., Rao, K. S., & Rao, C. M. (2011). αB-crystallin, a small heat shock protein, modulates NF-κB activity in a phosphorylation-dependent manner and protects muscle myoblasts from TNF-α induced cytotoxicity. Biochimica et biophysica acta, 1813(8), 1532–42. doi:10.1016/j.bbamcr.2011.04.009

Aggarwal, M., Duan, W., Hou, Z., Rakesh, N., Peng, Q., Ross, C. A., … Zhang, J. (2012). Spatiotemporal mapping of brain atrophy in mouse models of Huntington's disease using longitudinal in vivo magnetic resonance imaging. NeuroImage, 60(4), 2086–95. doi:10.1016/j.neuroimage.2012.01.141

Altschul, S. F., Madden, T. L., Schäffer, A. A., Zhang, J., Zhang, Z., Miller, W., & Lipman, D. J. (1997). Gapped BLAST and PSI-BLAST: a new generation of protein database search programs. Nucleic acids research, 25(17), 3389–402.

Aquino, D. A., Capello, E., Weisstein, J., Sanders, V., Lopez, C., Tourtellotte, W. W., … Norton, W. T. (1997). Multiple sclerosis: altered expression of 70- and 27-kDa heat shock proteins in lesions and myelin. Journal of neuropathology and experimental neurology, 56(6), 664–72.

Arac, A., Brownell, S. E., Rothbard, J. B., Chen, C., Ko, R. M., Pereira, M. P., … Steinberg, G. K. (2011). Systemic augmentation of alphaB-crystallin provides therapeutic benefit twelve hours post-stroke onset via immune modulation. Proceedings of the National Academy of Sciences of the United States of America, 108(32), 13287–92. doi:10.1073/pnas.1107368108

Armstrong, C. L., Krueger-Naug, A. M., Currie, R. W., & Hawkes, R. (2001). Constitutive expression of heat shock protein HSP25 in the central nervous system of the developing and adult mouse. The Journal of Comparative Neurology, 434(3), 262–274. doi:10.1002/cne.1176

Arrigo, A.-P. (2007). Anti-apoptotic, Tumorigenic and Metastatic Potential of Hsp27 (HspB1) and αB-crystallin (HspB5): Emerging Targets for the Development of New Anti-Cancer Therapeutic Strategies. In S. K. Calderwood, M. Y. Sherman, & D. R. Ciocca (Eds.), Heat Shock Proteins in Cancer (Vol. 2, pp. 73 – 92). Dordrecht: Springer Netherlands. doi:10.1007/978-1-4020-6401-2

Arrigo, A.-P. (2013). Human small heat shock proteins: protein interactomes of homo- and hetero-oligomeric complexes: an update. FEBS letters, 587(13), 1959–69. doi:10.1016/j.febslet.2013.05.011

Arrigo, A.-P., Simon, S., Gibert, B., Kretz-Remy, C., Nivon, M., Czekalla, A., … Vicart, P. (2007). Hsp27 (HspB1) and alphaB-crystallin (HspB5) as therapeutic

targets. FEBS letters, 581(19), 3665–74. doi:10.1016/j.febslet.2007.04.033

Arrigo, A.-P., Virot, S., Chaufour, S., Firdaus, W., Kretz-Remy, C., & Diaz-Latoud, C. (2005). Hsp27 consolidates intracellular redox homeostasis by upholding glutathione in its reduced form and by decreasing iron intracellular levels. Antioxidants & redox signaling, 7(3-4), 414–22. doi:10.1089/ars.2005.7.414

Asuni, A. A., Gray, B., Bailey, J., Skipp, P., Perry, V. H., & O'Connor, V. (2013). Analysis of the hippocampal proteome in ME7 prion disease reveals a predominant astrocytic signature and highlights the brain-restricted production of clusterin in chronic neurodegeneration. The Journal of biological chemistry. doi:10.1074/jbc.M113.502690

Asuni, A. A., Hilton, K., Siskova, Z., Lunnon, K., Reynolds, R., Perry, V. H., & O'Connor, V. (2010). Alpha-synuclein deficiency in the C57BL/6JOlaHsd strain does not modify disease progression in the ME7-model of prion disease. Neuroscience, 165(3), 662–74. doi:10.1016/j.neuroscience.2009.10.047

Aucouturier, P., Carp, R. I., Carnaud, C., & Wisniewski, T. (2000). Prion diseases and the immune system. Clinical immunology (Orlando, Fla.), 96(2), 79–85. doi:10.1006/clim.2000.4875

Bartzokis, G., Lu, P. H., Tishler, T. a, Fong, S. M., Oluwadara, B., Finn, J. P., … Perlman, S. (2007). Myelin breakdown and iron changes in Huntington's disease: pathogenesis and treatment implications. Neurochemical research, 32(10), 1655–64. doi:10.1007/s11064-007-9352-7

Basha, E., O'Neill, H., & Vierling, E. (2012). Small heat shock proteins and α-crystallins: dynamic proteins with flexible functions. Trends in biochemical sciences, 37(3), 106–17. doi:10.1016/j.tibs.2011.11.005

Bauer, J., Bradl, M., Klein, M., Leisser, M., Deckwerth, T. L., Wekerle, H., & Lassmann, H. (2002). Endoplasmic reticulum stress in PLP-overexpressing transgenic rats: gray matter oligodendrocytes are more vulnerable than white matter oligodendrocytes. Journal of neuropathology and experimental neurology, 61(1), 12–22.

Baumann, N., & Pham-Dinh, D. (2001). Biology of oligodendrocyte and myelin in the mammalian central nervous system. Physiological reviews, 81(2), 871–927.

Beal, M. F., & Ferrante, R. J. (2004). Experimental therapeutics in transgenic mouse models of Huntington's disease. Nature reviews. Neuroscience, 5(5), 373–84. doi:10.1038/nrn1386

Benndorf, R., Hayess, K., Ryazantsev, S., Wieske, M., Behlke, J., & Lutsch, G. (1994). Phosphorylation and supramolecular organization of murine small heat shock protein HSP25 abolish its actin polymerization-inhibiting activity. The Journal of biological chemistry, 269(32), 20780–4.

Betmouni, S., & Perry, V. H. (1999b). The acute inflammatory response in CNS following injection of prion brain homogenate or normal brain homogenate. Neuropathology and applied neurobiology, 25(1), 20–8.

Betmouni, S., Deacon, R. M. J., Rawlins, J. N. P., & Perry, V. H. (1999a). Behavioral consequences of prion disease targeted to the hippocampus in a mouse model of scrapie. Psychobiology, 27(1), 63–71. doi:10.3758/BF03332100

Betmouni, S., Perry, V. H., & Gordon, J. L. (1996). Evidence for an early inflammatory response in the central nervous system of mice with scrapie. Neuroscience, 74(1), 1–5. doi:10.1016/0306-4522(96)00212-6

Bidmon, H.-J., Görg, B., Palomero-Gallagher, N., Behne, F., Lahl, R., Pannek, H. W., … Zilles, K. (2004). Heat shock protein-27 is upregulated in the temporal cortex of patients with epilepsy. Epilepsia, 45(12), 1549–59. doi:10.1111/j.0013-9580.2004.14904.x

Björkdahl, C., Sjögren, M. J., Zhou, X., Concha, H., Avila, J., Winblad, B., & Pei, J.-J. (2008). Small heat shock proteins Hsp27 or alphaB-crystallin and the protein components of neurofibrillary tangles: tau and neurofilaments. Journal of neuroscience research, 86(6), 1343–52. doi:10.1002/jnr.21589

Boelens, W. C., Croes, Y., & de Jong, W. W. (2001). Interaction between αB-crystallin and the human 20S proteasomal subunit C8/α7. Biochimica et Biophysica Acta (BBA) - Protein Structure and Molecular Enzymology, 1544(1-2), 311–319. doi:10.1016/S0167-4838(00)00243-0

Braak, H., Tredici, K., Sandmann-Keil, D., Rüb, U., & Schultz, C. (2001). Nerve cells expressing heat-shock proteins in Parkinson's disease. Acta Neuropathologica, 102(5), 449–454. doi:10.1007/s004010100395

Bradl, M., Bauer, J., Inomata, T., Zielasek, J., Nave, K. A., Toyka, K., … Wekerle, H. (1999). Transgenic Lewis rats overexpressing the proteolipid protein gene: myelin degeneration and its effect on T cell-mediated experimental autoimmune encephalomyelitis. Acta neuropathologica, 97(6), 595–606.

Brady, J. P., Garland, D. L., Green, D. E., Tamm, E. R., Giblin, F. J., & Wawrousek, E. F. (2001). AlphaB-crystallin in lens development and muscle integrity: a gene knockout approach. Investigative ophthalmology & visual science, 42(12), 2924–34.

Brady, J. P., Garland, D., Duglas-Tabor, Y., Robison, W. G., Groome, A., & Wawrousek, E. F. (1997). Targeted disruption of the mouse alpha A-crystallin gene induces cataract and cytoplasmic inclusion bodies containing the small heat shock protein alpha B-crystallin. Proceedings of the National Academy of Sciences of the United States of America, 94(3), 884–9.

Braughler, J. M., Duncan, L. A., & Chase, R. L. (1986). The involvement of iron in lipid peroxidation. Importance of ferric to ferrous ratios in initiation. The Journal of biological chemistry, 261(22), 10282–9.

Brocchieri, L., Conway de Macario, E., & Macario, A. J. L. (2008). hsp70 genes in the human genome: Conservation and differentiation patterns predict a wide array of overlapping and specialized functions. BMC evolutionary biology, 8, 19. doi:10.1186/1471-2148-8-19

Brown, P., Preece, M., Brandel, J. P., Sato, T., McShane, L., Zerr, I., … Collins, S. J. (2000). Iatrogenic Creutzfeldt-Jakob disease at the millennium. Neurology, 55(8), 1075–81.

Bruce, M. E., McConnell, I., Fraser, H., & Dickinson, A. G. (1991). The disease characteristics of different strains of scrapie in Sinc congenic mouse lines: implications for the nature of the agent and host control of pathogenesis. The Journal of general virology, 72 (Pt 3), 595–603.

Bruinsma, I. B., Bruggink, K. A., Kinast, K., Versleijen, A. A. M., Segers-Nolten, I. M. J., Subramaniam, V., … Verbeek, M. M. (2011). Inhibition of α-synuclein aggregation by small heat shock proteins. Proteins, 79(10), 2956–67. doi:10.1002/prot.23152

Brydon, L., Harrison, N. A., Walker, C., Steptoe, A., & Critchley, H. D. (2008). Peripheral inflammation is associated with altered substantia nigra activity and psychomotor slowing in humans. Biological psychiatry, 63(11), 1022–9. doi:10.1016/j.biopsych.2007.12.007

Caron, J., Larivière, L., Nacache, M., Tam, M., Stevenson, M. M., McKerly, C., … Malo, D. (2006). Influence of Slc11a1 on the outcome of Salmonella enterica serovar Enteritidis infection in mice is associated with Th polarization. Infection and immunity, 74(5), 2787–802. doi:10.1128/IAI.74.5.2787-2802.2006

Carra, S., Seguin, S. J., & Landry, J. (2008). HspB8 and Bag3: a new chaperone complex targeting misfolded proteins to macroautophagy. Autophagy, 4(2), 237–9.

Carter, R. J., Lione, L. A., Humby, T., Mangiarini, L., Mahal, A., Bates, G. P., … Morton, A. J. (1999). Characterization of Progressive Motor Deficits in Mice Transgenic for the Human Huntington's Disease Mutation. J. Neurosci., 19(8), 3248–3257.

Cattaneo, E., Zuccato, C., & Tartari, M. (2005). Normal huntingtin function: an alternative approach to Huntington's disease. Nature reviews. Neuroscience, 6(12), 919–30. doi:10.1038/nrn1806

Caughey, B. (2003). Prion protein conversions: insight into mechanisms, TSE transmission barriers and strains. British Medical Bulletin, 66(1), 109–120. doi:10.1093/bmb/66.1.109

Cerghet, M., Skoff, R. P., Bessert, D., Zhang, Z., Mullins, C., & Ghandour, M. S. (2006). Proliferation and death of oligodendrocytes and myelin proteins are differentially regulated in male and female rodents. The

Journal of neuroscience : the official journal of the Society for Neuroscience, 26(5), 1439–47. doi:10.1523/JNEUROSCI.2219-05.2006

Chabas, D., Baranzini, S. E., Mitchell, D., Bernard, C. C., Rittling, S. R., Denhardt, D. T., … Steinman, L. (2001). The influence of the proinflammatory cytokine, osteopontin, on autoimmune demyelinating disease. Science (New York, N.Y.), 294(5547), 1731–5. doi:10.1126/science.1062960

Chaerkady, R., Letzen, B., Renuse, S., Sahasrabuddhe, N. A., Kumar, P., All, A. H., … Kerr, C. L. (2011). Quantitative temporal proteomic analysis of human embryonic stem cell differentiation into oligodendrocyte progenitor cells. Proteomics, 11(20), 4007–20. doi:10.1002/pmic.201100107

Chang, W.-H., Cemal, C. K., Hsu, Y.-H., Kuo, C.-L., Nukina, N., Chang, M.-H., … Hsieh, M. (2005). Dynamic expression of Hsp27 in the presence of mutant ataxin-3. Biochemical and biophysical research communications, 336(1), 258–67. doi:10.1016/j.bbrc.2005.08.065

Chou, A.-H., Yeh, T.-H., Ouyang, P., Chen, Y.-L., Chen, S.-Y., & Wang, H.-L. (2008). Polyglutamine-expanded ataxin-3 causes cerebellar dysfunction of SCA3 transgenic mice by inducing transcriptional dysregulation. Neurobiology of Disease, 31(1), 89–101.

Christians, E. S., Zhou, Q., Renard, J., & Benjamin, I. J. (2003). Heat shock proteins in mammalian development. Seminars in Cell & Developmental Biology, 14(5), 283–290.

Ciarmiello, A., Cannella, M., Lastoria, S., Simonelli, M., Frati, L., Rubinsztein, D. C., & Squitieri, F. (2006). Brain white-matter volume loss and glucose hypometabolism precede the clinical symptoms of Huntington's disease. Journal of nuclear medicine : official publication, Society of Nuclear Medicine, 47(2), 215–22.

Ciocca, D. R., Arrigo, A. P., & Calderwood, S. K. (2013). Heat shock proteins and heat shock factor 1 in carcinogenesis and tumor development: an update. Archives of toxicology, 87(1), 19–48. doi:10.1007/s00204-012-0918-z

Clark, J. I., & Muchowski, P. J. (2000). Small heat-shock proteins and their potential role in human disease. Current opinion in structural biology, 10(1), 52–9.

Collinge, J. (2005). Molecular neurology of prion disease. Journal of neurology, neurosurgery, and psychiatry, 76(7), 906–19. doi:10.1136/jnnp.2004.048660

Collins, F. M. (1969). Effect of specific immune mouse serum on the growth of Salmonella enteritidis in nonvaccinated mice challenged by various routes. Journal of bacteriology, 97(2), 667–75.

Collins, F. M., & Carter, P. B. (1974). Cellular immunity in enteric disease. The American journal of clinical nutrition, 27(12), 1424–33.

Connor, J. R., & Menzies, S. L. (1996). Relationship of iron to oligodendrocytes and myelination. Glia, 17(2), 83–93. doi:10.1002/(SICI)1098-

1136(199606)17:2<83::AID-GLIA1>3.0.CO;2-7

Craig, E. A., Huang, R., Aron, A., & Andrew, A. (2006). The diverse roles of J-proteins, the obligate Hsp70 co-chaperone. In S. G. Amara, E. Bamberg, S. Grinstein, S. C. Hebert, R. Jahn, W. J. Lederer, … M. Schweiger (Eds.), Reviews of Physiology, Biochemistry and Pharmacology. Berlin, Heidelberg: Springer Berlin Heidelberg. doi:10.1007/978-3-540-33146-9

Crawley, J. N. (2007). What's Wrong With My Mouse: Behavioral Phenotyping of Transgenic and Knockout Mice (p. 544). Wiley-Liss.

Crawley, J. N., Belknap, J. K., Collins, A., Crabbe, J. C., Frankel, W., Henderson, N., … Paylor, R. (1997). Behavioral phenotypes of inbred mouse strains: implications and recommendations for molecular studies. Psychopharmacology, 132(2), 107–24.

Csermely, P., Schnaider, T., Soti, C., Prohászka, Z., & Nardai, G. (1998). The 90-kDa molecular chaperone family: structure, function, and clinical applications. A comprehensive review. Pharmacology & therapeutics, 79(2), 129–68.

Cunningham, C., Boche, D., & Perry, V. H. (2002). Transforming growth factor beta1, the dominant cytokine in murine prion disease: influence on inflammatory cytokine synthesis and alteration of vascular extracellular matrix. Neuropathology and applied neurobiology, 28(2), 107–19.

Cunningham, C., Campion, S., Lunnon, K., Murray, C. L., Woods, J. F. C., Deacon, R. M. J., … Perry, V. H. (2009). Systemic inflammation induces acute behavioral and cognitive changes and accelerates neurodegenerative disease. Biological psychiatry, 65(4), 304–12. doi:10.1016/j.biopsych.2008.07.024

Cunningham, C., Deacon, R. M. J., Chan, K., Boche, D., Rawlins, J. N. P., & Perry, V. H. (2005a). Neuropathologically distinct prion strains give rise to similar temporal profiles of behavioral deficits. Neurobiology of Disease, 18(2), 258–269.

Cunningham, C., Deacon, R. M. J., Chan, K., Boche, D., Rawlins, J. N. P., & Perry, V. H. (2005b). Neuropathologically distinct prion strains give rise to similar temporal profiles of behavioral deficits. Neurobiology of disease, 18(2), 258–69. doi:10.1016/j.nbd.2004.08.015

Cunningham, C., Deacon, R., Wells, H., Boche, D., Waters, S., Diniz, C. P., … Perry, V. H. (2003). Synaptic changes characterize early behavioural signs in the ME7 model of murine prion disease. The European journal of neuroscience, 17(10), 2147–55.

Dabir, D. V, Trojanowski, J. Q., Richter-Landsberg, C., Lee, V. M.-Y., & Forman, M. S. (2004). Expression of the small heat-shock protein alphaB-crystallin in tauopathies with glial pathology. The American journal of pathology, 164(1), 155–66.

Dantzer, R., & Kelley, K. W. (2007). Twenty years of research on cytokine-induced sickness behavior. Brain, behavior, and immunity, 21(2), 153–60. doi:10.1016/j.bbi.2006.09.006

De Keyser, J., Sulter, G., & Luiten, P. G. (1999). Clinical trials with neuroprotective drugs in acute ischaemic stroke: are we doing the right thing? Trends in neurosciences, 22(12), 535–40.

Deacon, R. M., Croucher, A., & Rawlins, J. N. P. (2002). Hippocampal cytotoxic lesion effects on species-typical behaviours in mice. Behavioural brain research, 132(2), 203–13.

Deacon, R. M., Raley, J. M., Perry, V. H., & Rawlins, J. N. (2001). Burrowing into prion disease. Neuroreport, 12(9), 2053–7.

Del Vecchio, P. J., MacElroy, K. S., Rosser, M. P., & Church, R. L. (1984). Association of alpha-crystallin with actin in cultured lens cells. Current eye research, 3(10), 1213–9.

Den Engelsman, J., Keijsers, V., de Jong, W. W., & Boelens, W. C. (2003). The small heat-shock protein alpha B-crystallin promotes FBX4-dependent ubiquitination. The Journal of biological chemistry, 278(7), 4699–704. doi:10.1074/jbc.M211403200

Ditzler, S., Stoeck, J., LeBlanc, M., Kooperberg, C., Hansen, S., Coppin, L., & Olson, J. M. (2003). A Rapid Neurobehavioral Assessment Reveals that FK506 Delays Symptom Onset in R6/2 Huntington's Disease Mice. Preclinica Research Articles, 1(3), 115–126.

Djabali, K., de Néchaud, B., Landon, F., & Portier, M. M. (1997). AlphaB-crystallin interacts with intermediate filaments in response to stress. Journal of cell science, 110 (Pt 2, 2759–69.

Djabali, K., Piron, G., de Néchaud, B., & Portier, M. M. (1999). alphaB-crystallin interacts with cytoplasmic intermediate filament bundles during mitosis. Experimental cell research, 253(2), 649–62. doi:10.1006/excr.1999.4679

Dobson, C. M. (2004). Principles of protein folding, misfolding and aggregation. Seminars in Cell & Developmental Biology, 15(1), 3–16.

Dobson, C. M., & Karplus, M. (1999). The fundamentals of protein folding: bringing together theory and experiment. Current opinion in structural biology, 9(1), 92–101.

Dougan, G., John, V., Palmer, S., & Mastroeni, P. (2011). Immunity to salmonellosis. Immunological reviews, 240(1), 196–210. doi:10.1111/j.1600-065X.2010.00999.x

Doyle, S. M., & Wickner, S. (2009). Hsp104 and ClpB: protein disaggregating machines. Trends in biochemical sciences, 34(1), 40–8. doi:10.1016/j.tibs.2008.09.010

Doyle, S. M., Genest, O., & Wickner, S. (2013). Protein rescue from aggregates by powerful molecular chaperone machines. Nature reviews. Molecular cell biology, 14(10), 617–29. doi:10.1038/nrm3660

Dumas, E. M., van den Bogaard, S. J. A., Ruber, M. E., Reilman, R. R., Stout, J. C., Craufurd, D., … Roos, R. A. C. (2012). Early changes in white matter pathways of the sensorimotor cortex in premanifest Huntington's disease. Human brain mapping, 33(1), 203–12. doi:10.1002/hbm.21205

Echeverria, P. C., & Picard, D. (2010). Molecular chaperones, essential partners of steroid hormone receptors for activity and mobility. Biochimica et biophysica acta, 1803(6), 641–9. doi:10.1016/j.bbamcr.2009.11.012

Ehrnsperger, M., Gräber, S., Gaestel, M., & Buchner, J. (1997). Binding of non-native protein to Hsp25 during heat shock creates a reservoir of folding intermediates for reactivation. The EMBO journal, 16(2), 221–9. doi:10.1093/emboj/16.2.221

Ellis, R. J. (2006). Molecular chaperones: assisting assembly in addition to folding. Trends in biochemical sciences, 31(7), 395–401. doi:10.1016/j.tibs.2006.05.001

Ellis, R. J. (2011). Protein Aggregation: Opposing Effects of Chaperones and Crowding. In A. Wyttenbach & V. O'Connor (Eds.), Folding the Synapse (pp. 9–34). Boston, MA: Springer US. doi:10.1007/978-1-4419-7061-9

Ellis, R. J., & Minton, A. P. (2006). Protein aggregation in crowded environments. Biological chemistry, 387(5), 485–97. doi:10.1515/BC.2006.064

Ellrichmann, G., Reick, C., Saft, C., & Linker, R. A. (2013). The role of the immune system in Huntington's disease. Clinical & developmental immunology, 2013, 541259. doi:10.1155/2013/541259

Espat, N. J., Copeland, E. M., & Moldawer, L. L. (1994). Tumor necrosis factor and cachexia: a current perspective. Surgical oncology, 3(5), 255–62.

Fanelli, M. A., Montt-Guevara, M., Diblasi, A. M., Gago, F. E., Tello, O., Cuello-Carrión, F. D., … Ciocca, D. R. (2008). P-cadherin and beta-catenin are useful prognostic markers in breast cancer patients; beta-catenin interacts with heat shock protein Hsp27. Cell stress & chaperones, 13(2), 207–20. doi:10.1007/s12192-007-0007-z

Fontaine, J.-M., Sun, X., Benndorf, R., & Welsh, M. J. (2005). Interactions of HSP22 (HSPB8) with HSP20, alphaB-crystallin, and HSPB3. Biochemical and biophysical research communications, 337(3), 1006–11. doi:10.1016/j.bbrc.2005.09.148

Fortier, A., Min-Oo, G., Forbes, J., Lam-Yuk-Tseung, S., & Gros, P. (2005). Single gene effects in mouse models of host: pathogen interactions. Journal of leukocyte biology, 77(6), 868–77. doi:10.1189/jlb.1004616

Fu, L., & Liang, J. J.-N. (2003). Enhanced stability of alpha B-crystallin in the presence of small heat shock protein Hsp27. Biochemical and biophysical research communications, 302(4), 710–4.

Galea, I., Bechmann, I., & Perry, V. H. (2007). What is immune privilege (not)? Trends in immunology, 28(1), 12–8. doi:10.1016/j.it.2006.11.004

Ganea, E. (2001). Chaperone-like activity of alpha-crystallin and other small heat

shock proteins. Current protein & peptide science, 2(3), 205–25.

Gangalum, R. K., Atanasov, I. C., Zhou, Z. H., & Bhat, S. P. (2011). AlphaB-crystallin is found in detergent-resistant membrane microdomains and is secreted via exosomes from human retinal pigment epithelial cells. The Journal of biological chemistry, 286(5), 3261–9. doi:10.1074/jbc.M110.160135

Ghosh, J. G., Houck, S. A., & Clark, J. I. (2007a). Interactive sequences in the stress protein and molecular chaperone human alphaB crystallin recognize and modulate the assembly of filaments. The international journal of biochemistry & cell biology, 39(10), 1804–15. doi:10.1016/j.biocel.2007.04.027

Ghosh, J. G., Houck, S. A., & Clark, J. I. (2008). Interactive sequences in the molecular chaperone, human alphaB crystallin modulate the fibrillation of amyloidogenic proteins. The international journal of biochemistry & cell biology, 40(5), 954–67. doi:10.1016/j.biocel.2007.10.035

Ghosh, J. G., Shenoy, A. K., & Clark, J. I. (2007b). Interactions between important regulatory proteins and human alphaB crystallin. Biochemistry, 46(21), 6308–17. doi:10.1021/bi700149h

Goldbaum, O., & Richter-Landsberg, C. (2001). Stress proteins in oligodendrocytes: differential effects of heat shock and oxidative stress. Journal of Neurochemistry, 78(6), 1233–1242.

González-Scarano, F., & Baltuch, G. (1999). Microglia as mediators of inflammatory and degenerative diseases. Annual review of neuroscience, 22, 219–40. doi:10.1146/annurev.neuro.22.1.219

Gopalakrishnan, S., & Takemoto, L. (1992). Binding of actin to lens alpha crystallins. Current eye research, 11(9), 929–33.

Gray, B. C., Siskova, Z., Perry, V. H., & O'Connor, V. (2009). Selective presynaptic degeneration in the synaptopathy associated with ME7-induced hippocampal pathology. Neurobiology of disease, 35(1), 63–74. doi:10.1016/j.nbd.2009.04.001

Gray, Skipp, P., O'Connor, V. M., & Perry, V. H. (2006). Increased expression of glial fibrillary acidic protein fragments and mu-calpain activation within the hippocampus of prion-infected mice. Biochemical Society transactions, 34(Pt 1), 51–4. doi:10.1042/BST0340051

Green, D. R. (2011). Means to an End: Apoptosis and Other Cell Death Mechanisms. (D. R. Green, Ed.) (p. 220). Cold Spring Harbor Laboratory Press.

Groenen, P. J., Merck, K. B., de Jong, W. W., & Bloemendal, H. (1994). Structure and modifications of the junior chaperone alpha-crystallin. From lens transparency to molecular pathology. European journal of biochemistry / FEBS, 225(1), 1–19.

Guenther, K., Deacon, R. M., Perry, V. H., & Rawlins, J. N. (2001). Early behavioural

changes in scrapie-affected mice and the influence of dapsone. The European journal of neuroscience, 14(2), 401–9.

Gusev, N. B., Bogatcheva, N. V, & Marston, S. B. (2002). Structure and properties of small heat shock proteins (sHsp) and their interaction with cytoskeleton proteins. Biochemistry. Biokhimiĭa, 67(5), 511–9.

Guyenet, S. J., Furrer, S. A., Damian, V. M., Baughan, T. D., La Spada, A. R., & Garden, G. A. (2010). A simple composite phenotype scoring system for evaluating mouse models of cerebellar ataxia. Journal of visualized experiments : JoVE, (39). doi:10.3791/1787

Hagemann, T. L., Boelens, W. C., Wawrousek, E. F., & Messing, A. (2009). Suppression of GFAP toxicity by alphaB-crystallin in mouse models of Alexander disease. Human molecular genetics, 18(7), 1190–9. doi:10.1093/hmg/ddp013

Hagihara, H., Toyama, K., Yamasaki, N., & Miyakawa, T. (2009). Dissection of hippocampal dentate gyrus from adult mouse. Journal of visualized experiments : JoVE, (33), e1543. doi:10.3791/1543

Halliday, G. M., McRitchie, D. A., Macdonald, V., Double, K. L., Trent, R. J., & McCusker, E. (1998). Regional specificity of brain atrophy in Huntington's disease. Experimental neurology, 154(2), 663–72. doi:10.1006/exnr.1998.6919

Han, M. H., Hwang, S.-I., Roy, D. B., Lundgren, D. H., Price, J. V, Ousman, S. S., … Steinman, L. (2008). Proteomic analysis of active multiple sclerosis lesions reveals therapeutic targets. Nature, 451(7182), 1076–81. doi:10.1038/nature06559

Hansson, O., Nylandsted, J., Castilho, R. F., Leist, M., Jäättelä, M., & Brundin, P. (2003). Overexpression of heat shock protein 70 in R6/2 Huntington's disease mice has only modest effects on disease progression. Brain research, 970(1-2), 47–57.

Haslbeck, M., & Buchner, J. (2002). Small Stress Proteins. (A.-P. Arrigo & W. E. G. Müller, Eds.) (Vol. 28, pp. 37–59). Berlin, Heidelberg: Springer Berlin Heidelberg. doi:10.1007/978-3-642-56348-5

Hatters, D. M., Lindner, R. A., Carver, J. A., & Howlett, G. J. (2001). The molecular chaperone, alpha-crystallin, inhibits amyloid formation by apolipoprotein C-II. The Journal of biological chemistry, 276(36), 33755–61. doi:10.1074/jbc.M105285200

Hay, D. G., Sathasivam, K., Tobaben, S., Stahl, B., Marber, M., Mestril, R., … Bates, G. P. (2004). Progressive decrease in chaperone protein levels in a mouse model of Huntington's disease and induction of stress proteins as a therapeutic approach. Human molecular genetics, 13(13), 1389–405. doi:10.1093/hmg/ddh144

Head, M. W., Corbin, E., & Goldman, J. E. (1993). Overexpression and abnormal modification of the stress proteins alpha B-crystallin and HSP27 in Alexander disease. The American journal of pathology, 143(6), 1743–

53.

Heinsen, H., Rüb, U., Bauer, M., Ulmar, G., Bethke, B., Schüler, M., … Schmitz, C. (1999). Nerve cell loss in the thalamic mediodorsal nucleus in Huntington's disease. Acta neuropathologica, 97(6), 613–22.

Hightower, L. E., & Guidon, P. T. (1989). Selective release from cultured mammalian cells of heat-shock (stress) proteins that resemble glia-axon transfer proteins. Journal of cellular physiology, 138(2), 257–66. doi:10.1002/jcp.1041380206

Hilton, K. J., Cunningham, C., Reynolds, R. A., & Perry, V. H. (2013). Early Hippocampal Synaptic Loss Precedes Neuronal Loss and Associates with Early Behavioural Deficits in Three Distinct Strains of Prion Disease. PloS one, 8(6), e68062. doi:10.1371/journal.pone.0068062

Horwich, A. (2002). Protein aggregation in disease: a role for folding intermediates forming specific multimeric interactions. The Journal of clinical investigation, 110(9), 1221–32. doi:10.1172/JCI16781

Horwitz, J. (1992). Alpha-crystallin can function as a molecular chaperone. Proceedings of the National Academy of Sciences, 89(21), 10449–10453. doi:10.1073/pnas.89.21.10449

Hu, W.-F., Gong, L., Cao, Z., Ma, H., Ji, W., Deng, M., … Li, D. W.-C. (2012). αA- and αB-crystallins interact with caspase-3 and Bax to guard mouse lens development. Current molecular medicine, 12(2), 177–87.

Ibarra, J. A., & Steele-Mortimer, O. (2009). Salmonella--the ultimate insider. Salmonella virulence factors that modulate intracellular survival. Cellular microbiology, 11(11), 1579–86. doi:10.1111/j.1462-5822.2009.01368.x

Irobi, J., Van Impe, K., Seeman, P., Jordanova, A., Dierick, I., Verpoorten, N., … Timmerman, V. (2004). Hot-spot residue in small heat-shock protein 22 causes distal motor neuropathy. Nature genetics, 36(6), 597–601. doi:10.1038/ng1328

Iwaki, T., Iwaki, A., Tateishi, J., Sakaki, Y., & Goldman, J. E. (1993). Alpha B-crystallin and 27-kd heat shock protein are regulated by stress conditions in the central nervous system and accumulate in Rosenthal fibers. The American journal of pathology, 143(2), 487–95.

Iwaki, T., Kume-Iwaki, A., Liem, R. K., & Goldman, J. E. (1989). Alpha B-crystallin is expressed in non-lenticular tissues and accumulates in Alexander's disease brain. Cell, 57(1), 71–8.

Iwaki, T., Wisniewski, T., Iwaki, a, Corbin, E., Tomokane, N., Tateishi, J., & Goldman, J. E. (1992). Accumulation of alpha B-crystallin in central nervous system glia and neurons in pathologic conditions. The American journal of pathology, 140(2), 345–56.

Jack, C. R., Lexa, F. J., Trowjanowski, J. Q., Braffman, B. H., & Atlas, S. W. (2009). Normal Aging, Dementia, and Neurodegenerative Disease. In Magnetic Resonance Imaging of the Brain and Spine (4th ed., pp. 1026 – 1088).

Lippincott Williams & Wilkins.

Jackson, A., Nanton, M. R., O'Donnell, H., Akue, A. D., & McSorley, S. J. (2010). Innate immune activation during Salmonella infection initiates extramedullary erythropoiesis and splenomegaly. Journal of immunology (Baltimore, Md.: 1950), 185(10), 6198–204. doi:10.4049/jimmunol.1001198

Jahn, O., Tenzer, S., & Werner, H. B. (2009). Myelin proteomics: molecular anatomy of an insulating sheath. Molecular neurobiology, 40(1), 55–72. doi:10.1007/s12035-009-8071-2

Jakob, U., Gaestel, M., Engel, K., & Buchner, J. (1993). Small heat shock proteins are molecular chaperones. J. Biol. Chem., 268(3), 1517–1520.

Jana, N. R., Tanaka, M., Wang, G. h, & Nukina, N. (2000). Polyglutamine length-dependent interaction of Hsp40 and Hsp70 family chaperones with truncated N-terminal huntingtin: their role in suppression of aggregation and cellular toxicity. Human molecular genetics, 9(13), 2009–18.

Jeste, D. V, Barban, L., & Parisi, J. (1984). Reduced Purkinje cell density in Huntington's disease. Experimental neurology, 85(1), 78–86.

Johnston, J. A., Ward, C. L., & Kopito, R. R. (1998). Aggresomes: a cellular response to misfolded proteins. The Journal of cell biology, 143(7), 1883–98.

Kampinga, H. H., Hageman, J., Vos, M. J., Kubota, H., Tanguay, R. M., Bruford, E. A., … Hightower, L. E. (2009). Guidelines for the nomenclature of the human heat shock proteins. Cell stress & chaperones, 14(1), 105–11. doi:10.1007/s12192-008-0068-7

Kamradt, M. C., Chen, F., & Cryns, V. L. (2001a). The small heat shock protein alpha B-crystallin negatively regulates cytochrome c- and caspase-8-dependent activation of caspase-3 by inhibiting its autoproteolytic maturation. The Journal of biological chemistry, 276(19), 16059–63. doi:10.1074/jbc.C100107200

Kamradt, M. C., Chen, F., & Cryns, V. L. (2001b). The small heat shock protein alpha B-crystallin negatively regulates cytochrome c- and caspase-8-dependent activation of caspase-3 by inhibiting its autoproteolytic maturation. The Journal of biological chemistry, 276(19), 16059–63. doi:10.1074/jbc.C100107200

Kamradt, M. C., Lu, M., Werner, M. E., Kwan, T., Chen, F., Strohecker, A., … Cryns, V. L. (2005). The small heat shock protein alpha B-crystallin is a novel inhibitor of TRAIL-induced apoptosis that suppresses the activation of caspase-3. The Journal of biological chemistry, 280(12), 11059–66. doi:10.1074/jbc.M413382200

Kappé, G., Boelens, W. C., & de Jong, W. W. (2010). Why proteins without an alpha-crystallin domain should not be included in the human small heat shock protein family HSPB. Cell stress & chaperones, 15(4), 457–

61. doi:10.1007/s12192-009-0155-4

Kato, K., Hasegawa, K., Goto, S., & Inaguma, Y. (1994). Dissociation as a result of phosphorylation of an aggregated form of the small stress protein, hsp27. The Journal of biological chemistry, 269(15), 11274–8.

Kato, S., Hirano, A., Umahara, T., Kato, M., Herz, F., & Ohama, E. (1992). Comparative immunohistochemical study on the expression of alpha B crystallin, ubiquitin and stress-response protein 27 in ballooned neurons in various disorders. Neuropathology and applied neurobiology, 18(4), 335–40.

Khan, S. a, Everest, P., Servos, S., Foxwell, N., Zähringer, U., Brade, H., … Maskell, D. J. (1998). A lethal role for lipid A in Salmonella infections. Molecular microbiology, 29(2), 571–9.

Kida, E., Wierzba-Bobrowicz, T., Palminiello, S., Kaur, K., Jarzabek, K., Walus, M., … Golabek, A. A. (2010). Molecular chaperone alphaB-crystallin is expressed in the human fetal telencephalon at midgestation by a subset of progenitor cells. Journal of neuropathology and experimental neurology, 69(7), 745–59. doi:10.1097/NEN.0b013e3181e5f515

Kim, T., & Pfeiffer, S. E. (2000). Myelin glycosphingolipid/cholesterol-enriched microdomains selectively sequester the non-compact myelin proteins CNP and MOG. Journal of neurocytology, 28(4-5), 281–93.

Kim, Y.-S., Randolph, T. W., Stevens, F. J., & Carpenter, J. F. (2002). Kinetics and energetics of assembly, nucleation, and growth of aggregates and fibrils for an amyloidogenic protein. Insights into transition states from pressure, temperature, and co-solute studies. The Journal of biological chemistry, 277(30), 27240–6. doi:10.1074/jbc.M202492200

Kirbach, B. B., & Golenhofen, N. (2011). Differential expression and induction of small heat shock proteins in rat brain and cultured hippocampal neurons. Journal of neuroscience research, 89(2), 162–75. doi:10.1002/jnr.22536

Kirby, A. C., Yrlid, U., & Wick, M. J. (2002). The innate immune response differs in primary and secondary Salmonella infection. Journal of immunology (Baltimore, Md. : 1950), 169(8), 4450–9.

Klemenz, R., Frohli, E., Steiger, R. H., Schafer, R., & Aoyama, A. (1991). Alpha B-crystallin is a small heat shock protein. Proceedings of the National Academy of Sciences, 88(9), 3652–3656. doi:10.1073/pnas.88.9.3652

Klopstein, A., Santos-Nogueira, E., Francos-Quijorna, I., Redensek, A., David, S., Navarro, X., & López-Vales, R. (2012). Beneficial effects of αB-crystallin in spinal cord contusion injury. The Journal of neuroscience : the official journal of the Society for Neuroscience, 32(42), 14478–88. doi:10.1523/JNEUROSCI.0923-12.2012

Kremer, H. P. (1992). The hypothalamic lateral tuberal nucleus: normal anatomy and changes in neurological diseases. Progress in brain research, 93, 249–61.

Kurnellas, M. P., Brownell, S. E., Su, L., Malkovskiy, A. V, Rajadas, J., Dolganov, G., … Rothbard, J. B. (2012). Chaperone activity of small heat shock proteins underlies therapeutic efficacy in experimental autoimmune encephalomyelitis. The Journal of biological chemistry, 287(43), 36423–34. doi:10.1074/jbc.M112.371229

Lambert, H., Charette, S. J., Bernier, A. F., Guimond, A., & Landry, J. (1999). HSP27 Multimerization Mediated by Phosphorylation-sensitive Intermolecular Interactions at the Amino Terminus. J. Biol. Chem., 274(14), 9378–9385.

Langbehn, D. R., Brinkman, R. R., Falush, D., Paulsen, J. S., & Hayden, M. R. (2004). A new model for prediction of the age of onset and penetrance for Huntington's disease based on CAG length. Clinical genetics, 65(4), 267–77. doi:10.1111/j.1399-0004.2004.00241.x

Langstein, H. N., Doherty, G. M., Fraker, D. L., Buresh, C. M., & Norton, J. A. (1991). The Roles of {gamma}-Interferon and Tumor Necrosis Factor {alpha} in an Experimental Rat Model of Cancer Cachexia. Cancer Res., 51(9), 2302–2306.

Li, J. Y., Popovic, N., & Brundin, P. (2005). The use of the R6 transgenic mouse models of Huntington's disease in attempts to develop novel therapeutic strategies. NeuroRx : the journal of the American Society for Experimental NeuroTherapeutics, 2(3), 447–64. doi:10.1602/neurorx.2.3.447

Liang, P., & MacRae, T. H. (1997). Molecular chaperones and the cytoskeleton. Journal of cell science, 110 (Pt 1, 1431–40.

Lin, D. I., Barbash, O., Kumar, K. G. S., Weber, J. D., Harper, J. W., Klein-Szanto, A. J. P., … Diehl, J. A. (2006). Phosphorylation-dependent ubiquitination of cyclin D1 by the SCF(FBX4-alphaB crystallin) complex. Molecular cell, 24(3), 355–66. doi:10.1016/j.molcel.2006.09.007

Lindquist, S. (1986). The heat-shock response. Annual review of biochemistry, 55, 1151–91. doi:10.1146/annurev.bi.55.070186.005443

Lindquist, S., & Craig, E. A. (1988). The heat-shock proteins. Annual review of genetics, 22, 631–77. doi:10.1146/annurev.ge.22.120188.003215

Liu, S., Li, J., Tao, Y., & Xiao, X. (2007). Small heat shock protein alphaB-crystallin binds to p53 to sequester its translocation to mitochondria during hydrogen peroxide-induced apoptosis. Biochemical and biophysical research communications, 354(1), 109–14. doi:10.1016/j.bbrc.2006.12.152

Lowe, J., Errington, D. R., Lennox, G., Pike, I., Spendlove, I., Landon, M., & Mayer, R. J. (1992a). Ballooned neurons in several neurodegenerative diseases and stroke contain alpha B crystallin. Neuropathology and applied neurobiology, 18(4), 341–50. doi:10.1111/j.1365-2990.1992.tb00796.x

Lowe, J., Landon, M., Pike, I., Spendlove, I., McDermott, H., & Mayer, R. J. (1990).

Dementia with beta-amyloid deposition: involvement of alpha B-crystallin supports two main diseases. Lancet, 336(8713), 515–6.

Lowe, J., McDermott, H., Pike, I., Spendlove, I., Landon, M., & Mayer, R. J. (1992b). alpha B crystallin expression in non-lenticular tissues and selective presence in ubiquitinated inclusion bodies in human disease. The Journal of pathology, 166(1), 61–8. doi:10.1002/path.1711660110

Mainz, A., Bardiaux, B., Kuppler, F., Multhaup, G., Felli, I. C., Pierattelli, R., & Reif, B. (2012). Structural and mechanistic implications of metal binding in the small heat-shock protein αB-crystallin. The Journal of biological chemistry, 287(2), 1128–38. doi:10.1074/jbc.M111.309047

Mairesse, N., Horman, S., Mosselmans, R., & Galand, P. (1996). Antisense inhibition of the 27 kDa heat shock protein production affects growth rate and cytoskeletal organization in MCF-7 cells. Cell biology international, 20(3), 205–12. doi:10.1006/cbir.1996.0025

Mambula, S. S., Stevenson, M. A., Ogawa, K., & Calderwood, S. K. (2007). Mechanisms for Hsp70 secretion: crossing membranes without a leader. Methods (San Diego, Calif.), 43(3), 168–75. doi:10.1016/j.ymeth.2007.06.009

Mangiarini, L., Sathasivam, K., Seller, M., Cozens, B., Harper, A., Hetherington, C., … Bates, G. P. (1996). Exon 1 of the HD gene with an expanded CAG repeat is sufficient to cause a progressive neurological phenotype in transgenic mice. Cell, 87(3), 493–506.

Mao, Y. W., Xiang, H., Wang, J., Korsmeyer, S., Reddan, J., & Li, D. W. (2001). Human bcl-2 gene attenuates the ability of rabbit lens epithelial cells against H2O2-induced apoptosis through down-regulation of the alpha B-crystallin gene. The Journal of biological chemistry, 276(46), 43435–45. doi:10.1074/jbc.M102195200

Mao, Y.-W., Liu, J.-P., Xiang, H., & Li, D. W.-C. (2004). Human alphaA- and alphaB-crystallins bind to Bax and Bcl-X(S) to sequester their translocation during staurosporine-induced apoptosis. Cell death and differentiation, 11(5), 512–26. doi:10.1038/sj.cdd.4401384

Maragakis, N. J., & Rothstein, J. D. (2006). Mechanisms of Disease: astrocytes in neurodegenerative disease. Nature clinical practice. Neurology, 2(12), 679–89. doi:10.1038/ncpneuro0355

Masilamoni, J. G., Jesudason, E. P., Baben, B., Jebaraj, C. E., Dhandayuthapani, S., & Jayakumar, R. (2006). Molecular chaperone α-crystallin prevents detrimental effects of neuroinflammation. Biochimica et Biophysica Acta (BBA) - Molecular Basis of Disease, 1762(3), 284–293.

Mastroeni, P., Grant, A., Restif, O., & Maskell, D. (2009). A dynamic view of the spread and intracellular distribution of Salmonella enterica. Nature reviews. Microbiology, 7(1), 73–80. doi:10.1038/nrmicro2034

Mastroeni, P., Harrison, J. A., Chabalgoity, J. A., & Hormaeche, C. E. (1996). Effect of interleukin 12 neutralization on host resistance and gamma

interferon production in mouse typhoid. Infection and immunity, 64(1), 189–96.

Maxwell, R. (2010). Deaths from Neurodegenerative Diseases in England, 2002 to 2008. NEoLCIN Bulletin. National End of Life Care Intelligence Network.

Mayer, M. P., & Bukau, B. (2005). Hsp70 chaperones: cellular functions and molecular mechanism. Cellular and molecular life sciences : CMLS, 62(6), 670–84. doi:10.1007/s00018-004-4464-6

McCarthy, D. O. (2000). Tumor necrosis factor alpha and interleukin-6 have differential effects on food intake and gastric emptying in fasted rats. Research in nursing & health, 23(3), 222–8.

McMurray, C. T. (2000). Neurodegeneration: diseases of the cytoskeleton? Cell death and differentiation, 7(10), 861–5. doi:10.1038/sj.cdd.4400764

McTigue, D. M., & Tripathi, R. B. (2008). The life, death, and replacement of oligodendrocytes in the adult CNS. Journal of neurochemistry, 107(1), 1–19. doi:10.1111/j.1471-4159.2008.05570.x

Mills, C. D., Kincaid, K., Alt, J. M., Heilman, M. J., & Hill, A. M. (2000). M-1/M-2 Macrophages and the Th1/Th2 Paradigm. The Journal of Immunology, 164(12), 6166–6173. doi:10.4049/jimmunol.164.12.6166

Mills, J. C., Stone, N. L., & Pittman, R. N. (1999). Extranuclear apoptosis. The role of the cytoplasm in the execution phase. The Journal of cell biology, 146(4), 703–8.

Minami, M., Mizutani, T., Kawanishi, R., Suzuki, Y., & Mori, H. (2003). Neuronal expression of alphaB crystallin in cerebral infarction. Acta neuropathologica, 105(6), 549–54. doi:10.1007/s00401-003-0679-0

Mittrücker, H. W., & Kaufmann, S. H. (2000). Immune response to infection with Salmonella typhimurium in mice. Journal of leukocyte biology, 67(4), 457–63.

Mittrücker, H., Köhler, A., & Kaufmann, S. H. E. (2002). Characterization of the murine T-lymphocyte response to Salmonella enterica serovar Typhimurium infection. Infection and immunity, 70(1), 199–203. doi:10.1128/IAI.70.1.199

Morimoto, R. I., & Santoro, M. G. (1998). Stress-inducible responses and heat shock proteins: new pharmacologic targets for cytoprotection. Nature biotechnology, 16(9), 833–8. doi:10.1038/nbt0998-833

Moriyama, H., Edskes, H. K., & Wickner, R. B. (2000). [URE3] Prion Propagation in Saccharomyces cerevisiae: Requirement for Chaperone Hsp104 and Curing by Overexpressed Chaperone Ydj1p. Molecular and Cellular Biology, 20(23), 8916–8922. doi:10.1128/MCB.20.23.8916-8922.2000

Mounier, N., & Arrigo, A.-P. (2002). Actin cytoskeleton and small heat shock proteins: how do they interact? Cell stress & chaperones, 7(2), 167–76.

Muchowski, P. J., & Wacker, J. L. (2005). Modulation of neurodegeneration by molecular chaperones. Nature reviews. Neuroscience, 6(1), 11–22.

doi:10.1038/nrn1587

Mudher, A., & Lovestone, S. (2002). Alzheimer's disease-do tauists and baptists finally shake hands? Trends in neurosciences, 25(1), 22–6.

Muotiala, A., & Mäkelä, P. H. (1990). The role of IFN-gamma in murine Salmonella typhimurium infection. Microbial pathogenesis, 8(2), 135–41.

Myers, R. H., Vonsattel, J. P., Paskevich, P. A., Kiely, D. K., Stevens, T. J., Cupples, L. A., … Bird, E. D. (1991). Decreased neuronal and increased oligodendroglial densities in Huntington's disease caudate nucleus. Journal of neuropathology and experimental neurology, 50(6), 729–42.

Mymrikov, E. V, Seit-Nebi, A. S., & Gusev, N. B. (2012). Heterooligomeric complexes of human small heat shock proteins. Cell stress & chaperones, 17(2), 157–69. doi:10.1007/s12192-011-0296-0

Nance, M. A., & Myers, R. H. (2001). Juvenile onset Huntington's disease--clinical and research perspectives. Mental retardation and developmental disabilities research reviews, 7(3), 153–7. doi:10.1002/mrdd.1022

Nataf, S. (2009). Neuroinflammation responses and neurodegeneration in multiple sclerosis. Revue neurologique, 165(12), 1023–8. doi:10.1016/j.neurol.2009.09.012

Nauciel, C., & Espinasse-Maes, F. (1992). Role of gamma interferon and tumor necrosis factor alpha in resistance to Salmonella typhimurium infection. Infection and immunity, 60(2), 450–4.

Nicholl, I. D., & Quinlan, R. A. (1994). Chaperone activity of alpha-crystallins modulates intermediate filament assembly. The EMBO journal, 13(4), 945–53.

Ohto-Fujita, E., Fujita, Y., & Atomi, Y. (2007). Analysis of the alphaB-crystallin domain responsible for inhibiting tubulin aggregation. Cell stress & chaperones, 12(2), 163–71.

Ousman, S. S., Tomooka, B. H., van Noort, J. M., Wawrousek, E. F., O'Connor, K. C., Hafler, D. a, … Steinman, L. (2007a). Protective and therapeutic role for alphaB-crystallin in autoimmune demyelination. Nature, 448(7152), 474–9. doi:10.1038/nature05935

Ousman, S. S., Tomooka, B. H., van Noort, J. M., Wawrousek, E. F., O'Connor, K. C., Hafler, D. A., … Steinman, L. (2007b). Protective and therapeutic role for alphaB-crystallin in autoimmune demyelination. Nature, 448(7152), 474–9. doi:10.1038/nature05935

Outeiro, T. F., & Tetzlaff, J. (2007). Mechanisms of disease II: cellular protein quality control. Seminars in pediatric neurology, 14(1), 15–25. doi:10.1016/j.spen.2006.11.005

Pangratz-Fuehrer, S., Kaur, K., Ousman, S. S., Steinman, L., & Liao, Y. J. (2011). Functional rescue of experimental ischemic optic neuropathy with αB-crystallin. Eye (London, England), 25(6), 809–17. doi:10.1038/eye.2011.42

Park, L., Howland, D., Schaeffer, E., Yrjänheikki, J. M., & Puoliväli, J. (2010).

Characterization of White Matter Defects in R6 / 2 Mouse Model of Huntington ' s Disease by Diffusion Tensor MRI and Tract-Based Spatial Statistics, (2001), 9112.

Parry, C. M., Hien, T. T., Dougan, G., White, N. J., & Farrar, J. J. (2002). Typhoid fever. The New England journal of medicine, 347(22), 1770–82. doi:10.1056/NEJMra020201

Patel, A. R., Ritzel, R., McCullough, L. D., & Liu, F. (2013). Microglia and ischemic stroke: a double-edged sword. International journal of physiology, pathophysiology and pharmacology, 5(2), 73–90.

Pekny, M., & Pekna, M. (2004). Astrocyte intermediate filaments in CNS pathologies and regeneration. The Journal of pathology, 204(4), 428–37. doi:10.1002/path.1645

Peng, H., Yang, X.-P., Carretero, O. A., Nakagawa, P., D'Ambrosio, M., Leung, P., … Rhaleb, N.-E. (2011). Angiotensin II-induced dilated cardiomyopathy in Balb/c but not C57BL/6J mice. Experimental physiology, 96(8), 756–64. doi:10.1113/expphysiol.2011.057612

Perkins, N. D. (2007). Integrating cell-signalling pathways with NF-kappaB and IKK function. Nature reviews. Molecular cell biology, 8(1), 49–62. doi:10.1038/nrm2083

Perng, M., Cairns, L., van den IJssel, P., Prescott, A., Hutcheson, A., & Quinlan, R. (1999). Intermediate filament interactions can be altered by HSP27 and alphaB-crystallin. J. Cell Sci., 112(13), 2099–2112.

Perry, V. H., Cunningham, C., & Boche, D. (2002). Atypical inflammation in the central nervous system in prion disease. Current opinion in neurology, 15(3), 349–54.

Perutz, M. F. (1992). Protein Structure: New Approaches to Disease and Therapy. W.H. Freeman and Co.

Pfeiffer, S. E., Warrington, a E., & Bansal, R. (1993). The oligodendrocyte and its many cellular processes. Trends in cell biology, 3(6), 191–7.

Piao, C.-S., Kim, S.-W., Kim, J.-B., & Lee, J.-K. (2005). Co-induction of alphaB-crystallin and MAPKAPK-2 in astrocytes in the penumbra after transient focal cerebral ischemia. Experimental brain research, 163(4), 421–9. doi:10.1007/s00221-004-2197-2

Pie, S., Truffa-Bachi, P., Pla, M., & Nauciel, C. (1997). Th1 response in Salmonella typhimurium-infected mice with a high or low rate of bacterial clearance. Infection and immunity, 65(11), 4509–14.

Plumier, J. C., Hopkins, D. A., Robertson, H. A., & Currie, R. W. (1997). Constitutive expression of the 27-kDa heat shock protein (Hsp27) in sensory and motor neurons of the rat nervous system. The Journal of comparative neurology, 384(3), 409–28.

Prabhu, S., Srinivas, V., Ramakrishna, T., Raman, B., & Rao, C. M. (2011). Inhibition of Cu2+-mediated generation of reactive oxygen species by the small heat shock protein αB-crystallin: the relative contributions of

the N- and C-terminal domains. Free radical biology & medicine, 51(3), 755–62. doi:10.1016/j.freeradbiomed.2011.05.021

Prusiner, S. B. (2001). Shattuck lecture--neurodegenerative diseases and prions. The New England journal of medicine, 344(20), 1516–26. doi:10.1056/NEJM200105173442006

Püntener, U., Booth, S. G., Perry, V. H., & Teeling, J. L. (2012). Long-term impact of systemic bacterial infection on the cerebral vasculature and microglia. Journal of neuroinflammation, 9, 146. doi:10.1186/1742-2094-9-146

Quraishe, S. (2010, April 2). The sHsp expression signature in the brain and modulation in models of chronic neurodegeneration.

Ranford, J. C., Coates, A. R. M., & Henderson, B. (2004). Chaperonins are cell-signalling proteins: the unfolding biology of molecular chaperones. Expert Reviews in Molecular Medicine, 2(08), 1–17. doi:10.1017/S1462399400002015

Ransohoff, R. M., & Brown, M. A. (2012). Innate immunity in the central nervous system. The Journal of clinical investigation, 122(4), 1164–71. doi:10.1172/JCI58644

Rattray, I., Smith, E., Gale, R., Matsumoto, K., Bates, G. P., & Modo, M. (2013). Correlations of behavioral deficits with brain pathology assessed through longitudinal MRI and histopathology in the R6/2 mouse model of HD. PloS one, 8(4), e60012. doi:10.1371/journal.pone.0060012

Reid, M., & Li, Y.-P. (2001). Tumor necrosis factor-alpha and muscle wasting: a cellular perspective. Respiratory Research, 2(5), 269–272. doi:10.1186/rr67

Renkawek, K., Bosman, G. J., & de Jong, W. W. (1994a). Expression of small heat-shock protein hsp 27 in reactive gliosis in Alzheimer disease and other types of dementia. Acta neuropathologica, 87(5), 511–9.

Renkawek, K., Jong, W. W., Merck, K. B., Frenken, C. W. G. M., Workum, F. P. A., & Bosman, G. J. C. G. M. (1992). aB-Crystallin is present in reactive glia in Creutzfeldt-Jakob disease. Acta Neuropathologica, 83(3), 324–327. doi:10.1007/BF00296796

Renkawek, K., Stege, G. J., & Bosman, G. J. (1999). Dementia, gliosis and expression of the small heat shock proteins hsp27 and alpha B-crystallin in Parkinson's disease. Neuroreport, 10(11), 2273–6.

Renkawek, K., Voorter, C. E. M., Bosman, G. J. C. G. M., Workum, F. P. A., & Jong, W. W. (1994b). Expression of aB-crystallin in Alzheimer's disease. Acta Neuropathologica, 87(2), 155–160. doi:10.1007/BF00296185

Robertson, A. L., Headey, S. J., Saunders, H. M., Ecroyd, H., Scanlon, M. J., Carver, J. a, & Bottomley, S. P. (2010). Small heat-shock proteins interact with a flanking domain to suppress polyglutamine aggregation. Proceedings of the National Academy of Sciences of the United States of America, 107(23), 10424–9. doi:10.1073/pnas.0914773107

Romanova, N. V, & Chernoff, Y. O. (2009). Hsp104 and prion propagation. Protein

and peptide letters, 16(6), 598–605.

Ross, C. A., & Tabrizi, S. J. (2011). Huntington's disease: from molecular pathogenesis to clinical treatment. Lancet neurology, 10(1), 83–98. doi:10.1016/S1474-4422(10)70245-3

Rothbard, J. B., Kurnellas, M. P., Brownell, S., Adams, C. M., Su, L., Axtell, R. C., … Steinman, L. (2012). Therapeutic effects of systemic administration of chaperone αB-crystallin associated with binding proinflammatory plasma proteins. The Journal of biological chemistry, 287(13), 9708–21. doi:10.1074/jbc.M111.337691

Rothbard, J. B., Zhao, X., Sharpe, O., Strohman, M. J., Kurnellas, M., Mellins, E. D., … Steinman, L. (2011). Chaperone activity of α B-crystallin is responsible for its incorrect assignment as an autoantigen in multiple sclerosis. Journal of immunology (Baltimore, Md. : 1950), 186(7), 4263–8. doi:10.4049/jimmunol.1003934

Rowland, E. C., Lozykowski, M. G., & McCormick, T. S. (1992). Differential cardiac histopathology in inbred mouse strains chronically infected with Trypanosoma cruzi. The Journal of parasitology, 78(6), 1059–66.

Rubinsztein, D. C. (2002). Lessons from animal models of Huntington's disease. Trends in Genetics, 18(4), 202–209. doi:10.1016/S0168-9525(01)02625-7

Sajjad, M. U., Samson, B., & Wyttenbach, a. (2010). Heat shock proteins: therapeutic drug targets for chronic neurodegeneration? Current pharmaceutical biotechnology, 11(2), 198–215.

Santos, R. L., Zhang, S., Tsolis, R. M., Kingsley, R. A., Adams, L. G., & Bäumler, A. J. (2001). Animal models of Salmonella infections: enteritis versus typhoid fever. Microbes and infection / Institut Pasteur, 3(14-15), 1335–44.

Sauer, B. (1998). Inducible gene targeting in mice using the Cre/lox system. Methods (San Diego, Calif.), 14(4), 381–92. doi:10.1006/meth.1998.0593

Schilling, G., Becher, M. W., Sharp, A. H., Jinnah, H. A., Duan, K., Kotzuk, J. A., … Borchelt, D. R. (1999). Intranuclear inclusions and neuritic aggregates in transgenic mice expressing a mutant N-terminal fragment of huntingtin. Human molecular genetics, 8(3), 397–407.

Sebastiani, G., Blais, V., Sancho, V., Vogel, S. N., Stevenson, M. M., Gros, P., … Malo, D. (2002). Host immune response to Salmonella enterica serovar Typhimurium infection in mice derived from wild strains. Infection and immunity, 70(4), 1997–2009.

Selkoe, D. J., & Lansbury, P. J. (1999). Alzheimer's Disease Is the Most Common Neurodegenerative Disorder. In G. J. Siegel, B. W. Agrannof, & R. W. Albers (Eds.), Basic Neurochemistry: Molecular, Cellular and Medical Aspects (6th ed.). Lippincott-Raven.

Sellers, R. S., Clifford, C. B., Treuting, P. M., & Brayton, C. (2012). Immunological

variation between inbred laboratory mouse strains: points to consider in phenotyping genetically immunomodified mice. Veterinary pathology, 49(1), 32–43. doi:10.1177/0300985811429314

Shammas, S. L., Waudby, C. A., Wang, S., Buell, A. K., Knowles, T. P. J., Ecroyd, H., … Meehan, S. (2011). Binding of the molecular chaperone αB-crystallin to Aβ amyloid fibrils inhibits fibril elongation. Biophysical journal, 101(7), 1681–9. doi:10.1016/j.bpj.2011.07.056

Shao, J., & Diamond, M. I. (2007). Polyglutamine diseases: emerging concepts in pathogenesis and therapy. Human molecular genetics, 16 Spec No, R115–23. doi:10.1093/hmg/ddm213

Shao, W., Zhang, S., Tang, M., Zhang, X., Zhou, Z., Yin, Y., … Zhou, J. (2013). Suppression of neuroinflammation by astrocytic dopamine D2 receptors via αB-crystallin. Nature, 494(7435), 90–4. doi:10.1038/nature11748

Shinohara, H. (1993). a B crystallin and HSP28 are enhanced in the cerebral cortex of patients with Alzheimer ' s disease, 119, 203–208.

Simon, S., Dimitrova, V., Gibert, B., Virot, S., Mounier, N., Nivon, M., … Arrigo, A.-P. (2013). Analysis of the dominant effects mediated by wild type or R120G mutant of αB-crystallin (HspB5) towards Hsp27 (HspB1). PloS one, 8(8), e70545. doi:10.1371/journal.pone.0070545

Singh, B. N., Rao, K. S., Ramakrishna, T., Rangaraj, N., & Rao, C. M. (2007). Association of alphaB-crystallin, a small heat shock protein, with actin: role in modulating actin filament dynamics in vivo. Journal of molecular biology, 366(3), 756–67. doi:10.1016/j.jmb.2006.12.012

Sisková, Z., Page, A., O'Connor, V., & Perry, V. H. (2009). Degenerating synaptic boutons in prion disease: microglia activation without synaptic stripping. The American journal of pathology, 175(4), 1610–21. doi:10.2353/ajpath.2009.090372

Skouri-Panet, F., Michiel, M., Férard, C., Duprat, E., & Finet, S. (2012). Structural and functional specificity of small heat shock protein HspB1 and HspB4, two cellular partners of HspB5: role of the in vitro hetero-complex formation in chaperone activity. Biochimie, 94(4), 975–84. doi:10.1016/j.biochi.2011.12.018

Soto, C., Estrada, L., & Castilla, J. (2006). Amyloids, prions and the inherent infectious nature of misfolded protein aggregates. Trends in biochemical sciences, 31(3), 150–5. doi:10.1016/j.tibs.2006.01.002

Soudi, S., Zavaran-Hosseini, A., Muhammad Hassan, Z., Soleimani, M., Jamshidi Adegani, F., & Hashemi, S. M. (2013). Comparative study of the effect of LPS on the function of BALB/c and C57BL/6 peritoneal macrophages. Cell journal, 15(1), 45–54.

Spargo, E., Everall, I. P., & Lantos, P. L. (1993). Neuronal loss in the hippocampus in Huntington's disease: a comparison with HIV infection. Journal of neurology, neurosurgery, and psychiatry, 56(5), 487–91.

Steinman, L. (2008). New targets for treatment of multiple sclerosis. Journal of the neurological sciences, 274(1-2), 1–4. doi:10.1016/j.jns.2008.06.040

Stenoien, D. L., Cummings, C. J., Adams, H. P., Mancini, M. G., Patel, K., DeMartino, G. N., … Mancini, M. A. (1999). Polyglutamine-expanded androgen receptors form aggregates that sequester heat shock proteins, proteasome components and SRC-1, and are suppressed by the HDJ-2 chaperone. Human molecular genetics, 8(5), 731–41.

Stober, C. B., Brode, S., White, J. K., Popoff, J.-F., & Blackwell, J. M. (2007). Slc11a1, formerly Nramp1, is expressed in dendritic cells and influences major histocompatibility complex class II expression and antigen-presenting cell function. Infection and immunity, 75(10), 5059–67. doi:10.1128/IAI.00153-07

Su, A. I., Wiltshire, T., Batalov, S., Lapp, H., Ching, K. A., Block, D., … Hogenesch, J. B. (2004). A gene atlas of the mouse and human protein-encoding transcriptomes. Proceedings of the National Academy of Sciences of the United States of America, 101(16), 6062–7. doi:10.1073/pnas.0400782101

Su, L.-H., & Chiu, C.-H. (2007). Salmonella: clinical importance and evolution of nomenclature. Chang Gung medical journal, 30(3), 210–9.

Sugiyama, Y., Suzuki, A., Kishikawa, M., Akutsu, R., Hirose, T., Waye, M. M., … Ohno, S. (2000). Muscle develops a specific form of small heat shock protein complex composed of MKBP/HSPB2 and HSPB3 during myogenic differentiation. The Journal of biological chemistry, 275(2), 1095–104.

Sun, G., Guo, M., Shen, A., Mei, F., Peng, X., Gong, R., … Xiao, G. (2005a). Bovine PrPC directly interacts with alphaB-crystalline. FEBS letters, 579(24), 5419–24. doi:10.1016/j.febslet.2005.08.065

Sun, Guo, M., Shen, A., Mei, F., Peng, X., Gong, R., … Xiao, G. (2005b). Bovine PrPC directly interacts with alphaB-crystalline. FEBS letters, 579(24), 5419–24. doi:10.1016/j.febslet.2005.08.065

Sun, X., Fontaine, J.-M., Rest, J. S., Shelden, E. A., Welsh, M. J., & Benndorf, R. (2004). Interaction of human HSP22 (HSPB8) with other small heat shock proteins. The Journal of biological chemistry, 279(4), 2394–402. doi:10.1074/jbc.M311324200

Sun, Y., & MacRae, T. H. (2005c). The small heat shock proteins and their role in human disease. The FEBS journal, 272(11), 2613–27. doi:10.1111/j.1742-4658.2005.04708.x

Swihart, K., Fruth, U., Messmer, N., Hug, K., Behin, R., Huang, S., … Louis, J. A. (1995). Mice from a genetically resistant background lacking the interferon gamma receptor are susceptible to infection with Leishmania major but mount a polarized T helper cell 1-type CD4+ T cell response. The Journal of experimental medicine, 181(3), 961–71.

Tallot, P., Grongnet, J. F., & David, J. C. (2003). Dual perinatal and developmental

expression of the small heat shock proteins [FC12]aB-crystallin and Hsp27 in different tissues of the developing piglet. Biology of the neonate, 83(4), 281–8. doi:69488

Teeling, J. L., Felton, L. M., Deacon, R. M. J., Cunningham, C., Rawlins, J. N. P., & Perry, V. H. (2007). Sub-pyrogenic systemic inflammation impacts on brain and behavior, independent of cytokines. Brain, behavior, and immunity, 21(6), 836–50. doi:10.1016/j.bbi.2007.01.012

Teismann, P., & Schulz, J. B. (2004). Cellular pathology of Parkinson's disease: astrocytes, microglia and inflammation. Cell and tissue research, 318(1), 149–61. doi:10.1007/s00441-004-0944-0

Thedieck, C., Kalbacher, H., Kratzer, U., Lammers, R., Stevanovic, S., & Klein, G. (2008). alpha B-crystallin is a cytoplasmic interaction partner of the kidney-specific cadherin-16. Journal of molecular biology, 378(1), 145–53. doi:10.1016/j.jmb.2008.02.008

Thomas, P. S., Fraley, G. S., Damian, V., Damien, V., Woodke, L. B., Zapata, F., … La Spada, A. R. (2006). Loss of endogenous androgen receptor protein accelerates motor neuron degeneration and accentuates androgen insensitivity in a mouse model of X-linked spinal and bulbar muscular atrophy. Human molecular genetics, 15(14), 2225–38. doi:10.1093/hmg/ddl148

Thompson, C. B. (1995). Apoptosis in the pathogenesis and treatment of disease. Science (New York, N.Y.), 267(5203), 1456–62.

Thorburne, S. K., & Juurlink, B. H. (1996). Low glutathione and high iron govern the susceptibility of oligodendroglial precursors to oxidative stress. Journal of neurochemistry, 67(3), 1014–22.

Tian, X.-C., Wang, Q.-Y., Li, D.-D., Wang, S.-T., Yang, Z.-Q., Guo, B., & Yue, Z.-P. (2013). Differential expression and regulation of Cryab in mouse uterus during preimplantation period. Reproduction (Cambridge, England), 145(6), 577–85. doi:10.1530/REP-13-0042

Tisdale, M. J. (2008). Catabolic mediators of cancer cachexia. Current opinion in supportive and palliative care, 2(4), 256–61.

Tobin, A. J., & Signer, E. R. (2000). Huntington's disease: the challenge for cell biologists. Trends in cell biology, 10(12), 531–6.

Todd, T. W., & Lim, J. (2013). Aggregation formation in the polyglutamine diseases: protection at a cost? Molecules and cells, 36(3), 185–94. doi:10.1007/s10059-013-0167-x

Tortosa, R., Vidal, E., Costa, C., Alamillo, E., Torres, J. M., Ferrer, I., & Pumarola, M. (2008). Stress response in the central nervous system of a transgenic mouse model of bovine spongiform encephalopathy. Veterinary journal (London, England : 1997), 178(1), 126–9. doi:10.1016/j.tvjl.2007.06.002

Tracey, K. J. (2009). Reflex control of immunity. Nature reviews. Immunology, 9(6), 418–28. doi:10.1038/nri2566

Tracey, K. J., Morgello, S., Koplin, B., Fahey, T. J., Fox, J., Aledo, A., … Cerami, A. (1990). Metabolic effects of cachectin/tumor necrosis factor are modified by site of production. Cachectin/tumor necrosis factor-secreting tumor in skeletal muscle induces chronic cachexia, while implantation in brain induces predominantly acute anorexia. The Journal of clinical investigation, 86(6), 2014–24. doi:10.1172/JCI114937

Turmaine, M., Raza, A., Mahal, A., Mangiarini, L., Bates, G. P., & Davies, S. W. (2000). Nonapoptotic neurodegeneration in a transgenic mouse model of Huntington's disease. Proceedings of the National Academy of Sciences of the United States of America, 97(14), 8093–7. doi:10.1073/pnas.110078997

Van der Worp, H. B., Howells, D. W., Sena, E. S., Porritt, M. J., Rewell, S., O'Collins, V., & Macleod, M. R. (2010). Can animal models of disease reliably inform human studies? PLoS medicine, 7(3), e1000245. doi:10.1371/journal.pmed.1000245

Van Noort, J. M., Bsibsi, M., Gerritsen, W. H., van der Valk, P., Bajramovic, J. J., Steinman, L., & Amor, S. (2010). Alphab-crystallin is a target for adaptive immune responses and a trigger of innate responses in preactive multiple sclerosis lesions. Journal of neuropathology and experimental neurology, 69(7), 694–703. doi:10.1097/NEN.0b013e3181e4939c

Van Noort, J. M., van Sechel, A. C., Bajramovic, J. J., el Ouagmiri, M., Polman, C. H., Lassmann, H., & Ravid, R. (1995). The small heat-shock protein alpha B-crystallin as candidate autoantigen in multiple sclerosis. Nature, 375(6534), 798–801. doi:10.1038/375798a0

Vega, V. L., Rodríguez-Silva, M., Frey, T., Gehrmann, M., Diaz, J. C., Steinem, C., … De Maio, A. (2008). Hsp70 translocates into the plasma membrane after stress and is released into the extracellular environment in a membrane-associated form that activates macrophages. Journal of immunology (Baltimore, Md. : 1950), 180(6), 4299–307.

Velotta, J. B., Kimura, N., Chang, S. H., Chung, J., Itoh, S., Rothbard, J., … Fischbein, M. P. (2011). αB-crystallin improves murine cardiac function and attenuates apoptosis in human endothelial cells exposed to ischemia-reperfusion. The Annals of thoracic surgery, 91(6), 1907–13. doi:10.1016/j.athoracsur.2011.02.072

Verbeek, R., van Dongen, H., Wawrousek, E. F., Amor, S., & van Noort, J. M. (2007). Induction of EAE by T cells specific for alpha B-crystallin depends on prior viral infection in the CNS. International immunology, 19(3), 277–85. doi:10.1093/intimm/dxl144

Verschuure, P., Tatard, C., Boelens, W. C., Grongnet, J.-F., & David, J. C. (2003). Expression of small heat shock proteins HspB2, HspB8, Hsp20 and cvHsp in different tissues of the perinatal developing pig. European

journal of cell biology, 82(10), 523–30. doi:10.1078/0171-9335-00337

Vicart, P., Caron, A., Guicheney, P., Li, Z., Prévost, M. C., Faure, A., … Fardeau, M. (1998). A missense mutation in the alphaB-crystallin chaperone gene causes a desmin-related myopathy. Nature genetics, 20(1), 92–5. doi:10.1038/1765

Vidal, E., Acín, C., Foradada, L., Monzón, M., Márquez, M., Monleón, E., … Bolea, R. (2008). Immunohistochemical characterisation of classical scrapie neuropathology in sheep. Journal of comparative pathology, 141(2-3), 135–46. doi:10.1016/j.jcpa.2009.04.002

Vleminckx, V., Van Damme, P., Goffin, K., Delye, H., Van Den Bosch, L., & Robberecht, W. (2002). Upregulation of HSP27 in a transgenic model of ALS. Journal of neuropathology and experimental neurology, 61(11), 968–74.

Vonsattel, J. P. G. (2008). Huntington disease models and human neuropathology: similarities and differences. Acta neuropathologica, 115(1), 55–69. doi:10.1007/s00401-007-0306-6

Vonsattel, J. P., & DiFiglia, M. (1998). Huntington disease. Journal of neuropathology and experimental neurology, 57(5), 369–84.

Vonsattel, J. P., Myers, R. H., Stevens, T. J., Ferrante, R. J., Bird, E. D., & Richardson, E. P. (1985). Neuropathological classification of Huntington's disease. Journal of neuropathology and experimental neurology, 44(6), 559–77.

Vos, M. J., Zijlstra, M. P., Carra, S., Sibon, O. C. M., & Kampinga, H. H. (2011). Small heat shock proteins, protein degradation and protein aggregation diseases. Autophagy, 7(1), 101–3.

Vos, M. J., Zijlstra, M. P., Kanon, B., van Waarde-Verhagen, M. a W. H., Brunt, E. R. P., Oosterveld-Hut, H. M. J., … Kampinga, H. H. (2010). HSPB7 is the most potent polyQ aggregation suppressor within the HSPB family of molecular chaperones. Human molecular genetics, 19(23), 4677–93. doi:10.1093/hmg/ddq398

Wang, J., Martin, E., Gonzales, V., Borchelt, D. R., & Lee, M. K. (2008). Differential regulation of small heat shock proteins in transgenic mouse models of neurodegenerative diseases. Neurobiology of aging, 29(4), 586–97. doi:10.1016/j.neurobiolaging.2006.11.009

Wang, K., & Spector, A. (1996a). alpha-crystallin stabilizes actin filaments and prevents cytochalasin-induced depolymerization in a phosphorylation-dependent manner. European journal of biochemistry / FEBS, 242(1), 56–66.

Wang, X., Osinska, H., Klevitsky, R., Gerdes, A. M., Nieman, M., Lorenz, J., … Robbins, J. (2001). Expression of R120G-alphaB-crystallin causes aberrant desmin and alphaB-crystallin aggregation and cardiomyopathy in mice. Circulation research, 89(1), 84–91.

Wang, Y., Krushel, L. A., & Edelman, G. M. (1996b). Targeted DNA recombination in vivo using an adenovirus carrying the cre recombinase gene.

Proceedings of the National Academy of Sciences of the United States of America, 93(9), 3932–6.

Warrick, J. M., Chan, H. Y., Gray-Board, G. L., Chai, Y., Paulson, H. L., & Bonini, N. M. (1999). Suppression of polyglutamine-mediated neurodegeneration in Drosophila by the molecular chaperone HSP70. Nature genetics, 23(4), 425–8. doi:10.1038/70532

Wenk, G. L. (2003). Neuropathologic changes in Alzheimer's disease. The Journal of clinical psychiatry, 64 Suppl 9, 7–10.

Wettstein, G., Bellaye, P. S., Micheau, O., & Bonniaud, P. (2012). Small heat shock proteins and the cytoskeleton: an essential interplay for cell integrity? The international journal of biochemistry & cell biology, 44(10), 1680–6. doi:10.1016/j.biocel.2012.05.024

Wilhelmus, M. M. M., Boelens, W. C., Otte-Höller, I., Kamps, B., de Waal, R. M. W., & Verbeek, M. M. (2006a). Small heat shock proteins inhibit amyloid-beta protein aggregation and cerebrovascular amyloid-beta protein toxicity. Brain research, 1089(1), 67–78. doi:10.1016/j.brainres.2006.03.058

Wilhelmus, M. M. M., Otte-Höller, I., Wesseling, P., de Waal, R. M. W., Boelens, W. C., & Verbeek, M. M. (2006b). Specific association of small heat shock proteins with the pathological hallmarks of Alzheimer's disease brains. Neuropathology and applied neurobiology, 32(2), 119–30. doi:10.1111/j.1365-2990.2006.00689.x

Wood, P. L. (1995). Microglia as a unique cellular target in the treatment of stroke: potential neurotoxic mediators produced by activated microglia. Neurological research, 17(4), 242–8.

Wyttenbach, A., Carmichael, J., Swartz, J., Furlong, R. A., Narain, Y., Rankin, J., & Rubinsztein, D. C. (2000). Effects of heat shock, heat shock protein 40 (HDJ-2), and proteasome inhibition on protein aggregation in cellular models of Huntington's disease. Proceedings of the National Academy of Sciences of the United States of America, 97(6), 2898–903.

Xi, J., Farjo, R., Yoshida, S., Kern, T. S., Swaroop, A., & Andley, U. P. (2003). A comprehensive analysis of the expression of crystallins in mouse retina. Molecular vision, 9, 410–9.

Yerbury, J. J., Gower, D., Vanags, L., Roberts, K., Lee, J. A., & Ecroyd, H. (2013). The small heat shock proteins αB-crystallin and Hsp27 suppress SOD1 aggregation in vitro. Cell stress & chaperones, 18(2), 251–7. doi:10.1007/s12192-012-0371-1

Yoshiki, A., & Moriwaki, K. (2006). Mouse phenome research: implications of genetic background. ILAR journal / National Research Council, Institute of Laboratory Animal Resources, 47(2), 94–102.

Young, J. C., Moarefi, I., & Hartl, F. U. (2001). Hsp90: a specialized but essential protein-folding tool. The Journal of cell biology, 154(2), 267–73.

Yuan, R., Tsaih, S.-W., Petkova, S. B., Marin de Evsikova, C., Xing, S., Marion, M. A., … Paigen, B. (2009). Aging in inbred strains of mice: study design and

interim report on median lifespans and circulating IGF1 levels. Aging cell, 8(3), 277–87. doi:10.1111/j.1474-9726.2009.00478.x

Zabel, C., Chamrad, D. C., Priller, J., Woodman, B., Meyer, H. E., Bates, G. P., & Klose, J. (2002). Alterations in the mouse and human proteome caused by Huntington's disease. Molecular & cellular proteomics : MCP, 1(5), 366–75.

Zhang, J. (2003). Evolution by gene duplication: an update. Trends in Ecology & Evolution, 18(6), 292–298.

Zhang, J. (2012). Genetic redundancies and their evolutionary maintenance. Advances in experimental medicine and biology, 751, 279–300. doi:10.1007/978-1-4614-3567-9_13

Zhang, J., Peng, Q., Li, Q., Jahanshad, N., Hou, Z., Jiang, M., … Duan, W. (2010). Longitudinal characterization of brain atrophy of a Huntington's disease mouse model by automated morphological analyses of magnetic resonance images. NeuroImage, 49(3), 2340–51. doi:10.1016/j.neuroimage.2009.10.027

Zhang, Y., Huang, L., Zhang, J., Moskophidis, D., & Mivechi, N. F. (2002). Targeted disruption of hsf1 leads to lack of thermotolerance and defines tissue-specific regulation for stress-inducible Hsp molecular chaperones. Journal of cellular biochemistry, 86(2), 376–93. doi:10.1002/jcb.10232

Zhao, L. N., Long, H., Mu, Y., & Chew, L. Y. (2012). The Toxicity of Amyloid β Oligomers. International journal of molecular sciences, 13(6), 7303–27. doi:10.3390/ijms13067303

Zourlidou, A., Payne Smith, M. D., & Latchman, D. S. (2004). HSP27 but not HSP70 has a potent protective effect against alpha-synuclein-induced cell death in mammalian neuronal cells. Journal of neurochemistry, 88(6), 1439–48.